UNIVERSITÉ DU QUÉBEC

THÈSE

PRÉSENTÉ À

L'UNIVERSITÉ DU QUÉBEC À CHICOUTIMI

COMME EXIGENCE PARTIELLE

DU PhD EN SCIENCES APPLIQUÉES

PAR

JUNSUO LIU

PÉTROGENÈSE DES ROCHES ALCALINES MAFIQUES D'ÂGE MÉSO-CÉNOZOÏQUE DANS LES PROVINCES DE HUNAN ET GUANGXI, CHINE SEPTENTRIONALE

AOÛT 1992

Bibliothèque
Paul-Émile-Boulet

UQAC
Université du Québec
à Chicoutimi

Mise en garde/Advice

Afin de rendre accessible au plus grand nombre le résultat des travaux de recherche menés par ses étudiants gradués et dans l'esprit des règles qui régissent le dépôt et la diffusion des mémoires et thèses produits dans cette Institution, **l'Université du Québec à Chicoutimi (UQAC)** est fière de rendre accessible une version complète et gratuite de cette œuvre.

Motivated by a desire to make the results of its graduate students' research accessible to all, and in accordance with the rules governing the acceptation and diffusion of dissertations and theses in this Institution, the **Université du Québec à Chicoutimi (UQAC)** is proud to make a complete version of this work available at no cost to the reader.

L'auteur conserve néanmoins la propriété du droit d'auteur qui protège ce mémoire ou cette thèse. Ni le mémoire ou la thèse ni des extraits substantiels de ceux-ci ne peuvent être imprimés ou autrement reproduits sans son autorisation.

The author retains ownership of the copyright of this dissertation or thesis. Neither the dissertation or thesis, nor substantial extracts from it, may be printed or otherwise reproduced without the author's permission.

PETROGENESIS OF THE MESOZOIC-CENOZOIC MAFIC ALKALINE SUBVOLCANIC ROCKS IN HUNAN-GUANGXI PROVINCES, SOUTHERN CHINA

LIU JUNSUO, 1992

A Thesis submitted in conformity with the requirements for the
Degree of Doctor of Philosophy in the
Université du Québec à Chicoutimi
and
the Institute of Geochemistry, Academia Sinica.

ABSTRACT

PETROGENESIS OF MESOZOIC-CENOZOIC MAFIC ALKALINE ROCKS IN HUNAN-GUANGXI PROVINCES, SOUTHERN CHINA

Junsuo Liu

Mesozoic-Cenozoic mafic alkaline rocks are exposed widely in the form of subvolcanic dykes and diatremes in the area of southern Hunan and Guangxi Provinces in southern China. These subvolcanic rocks occur about 1000 km to the west of the eastern Chinese coast, and, therefore, are called the inland subvolcanic belt to distinguish them from the alkaline mafic rocks of the Circum-Pacific coastal belt. These inland rocks can be divided into basanites, trachybasalts (alkaline basaltic affinity), and lamproitic rocks.

The basanites and trachybasalts are Cenozoic magmatic products (51-28 Ma). They are relatively Fe rich, with a #Mg < 66. The basanites have high MgO (9-10 wt%) and Ni (~ 200 ppm) contents, and carry numerous small mantle-derived peridotite xenoliths. This indicates that the basanites have experienced little differentiation. The trachybasalts have wider MgO (5.5-8.4 wt%) and Ni (163-251 ppm) variations, much lower CaO (6.5-7.3 wt%) and Sc (~13 ppm) contents than the basanites; but Al_2O_3 is quite high (~15 wt%). These variations in composition may be due to fractional crystallization of calcium clinopyroxene. The basanites and trachybasalts have very similar incompatible element contents and have highly enriched and differentiated spidergrams. La, Nb, Ta, K, U, Th and Ba are 100-130 times enriched relative to the primitive mantle, that is 2-3 times more than in most island-arc or ocean-island alkaline basaltic rocks. These trace element distribution patterns are similar to that of rift-related Kenya basanite. An important characteristic of the trace element enrichment patterns of the basanites and trachybasalts is that the LILEs (Ba, Th, U) are at about the same level or slightly lower than the La. This is difficult to explain by partial melting of a primitive mantle source. By the same argument, zone refining may be excluded also. Furthermore, the low #Mg feature does not agree with a primitive mantle peridotite source either. However, most mantle amphiboles have similar #Mg as the basanites and trachybasalts. Amphibole-veined mantle peridotite xenoliths are often carried by alkaline volcanic rocks. Such veined peridotite are often also enriched in incompatible trace elements. So partial melting of amphibole-veined peridotite might have generated the basanites and trachybasalts.

The lamproites are Mesozoic products (~ 132-135 Ma). They are very rich in MgO (15.5-16.9 wt%) and CaO (11-14 wt%), low in Al_2O_3 (8.1-8.8 wt%). K/Na and K/Al ratios are much higher than the basanites

and trachybasalts. These rocks are more enriched and differentiated in incompatible elements than the basanites and trachybasalts: Ba is 210-450 times more than in primitive mantle; La has a similar level as that in the basanites; the HREEs contents are only about half as much as those of the basanites. Such highly enriched trace element chemistry, especially the LILEs, require an extremely small degree of partial melting, if a primitive mantle source is assumed. Crustal contamination can explain the strong enrichment of incompatible trace elements; but it can not explain the high MgO, low Al_2O_3 contents at the same time. This high MgO (~16 wt%) low Al_2O_3 (<9 wt%) character suggests that the lamproites come from a source depleted in basaltic components. The HREE depletion in the lamproites relative to the basanites may indicate either garnet retention or garnet loss in the source prior to lamproite generation. The lamproites also have large negative Ta-Nb and Zr-Hf-Ti anomalies on their spidergram, indicating the involvement of ancient subducted materials. All these arguments suggest that source metasomatism is needed to generate the lamproites.

The basanites and trachybasalts are closely related with the lamproites in space. They share some common chemical traits too: their REE patterns are similar in trend and level. Though lamproitic magmatism is traditionally treated as an event totally unrelated with alkaline basaltic magmatism, the K/Na distribution among mafic alkaline rocks challenges this thought. On the K/Na - $(La/Yb)_N$ logarithmic plot, almost all mantle-derived magmatic rocks are projected on a linear band, and K/Na increase is proportional to REE differentiation. This is interpreted to indicate that K/Na and REE differentiations are related. Closely related with this differentiation process is the MgO - Al_2O_3 negative correlation trend defined by average alkaline basaltic rock, mafic lamprophyres, lamproites and average kimberlite. These two trends can not be explained by partial melting and/or crustal contamination process alone. A metasomatic process in the source could generate the two trends.

In summary, the major conclusions of this work are (1) the basanites and trachybasalts are believed to have formed from an amphibole-veined, incompatible element enriched lherzolite source. Partial melting was initiated by the Cenozoic continental rifting in eastern China. (2) the lamproites are post-orogenic magmatic product formed after the continent collision in early Mesozoic. The source of the lamproites is thought to be a phlogopite peridotite with a high K/Na ratio, which had been depleted in basaltic components and then selectively enriched in K and incompatible trace elements by metasomatism. This phlogopite peridotite zone was located in the garnet peridotite region, below the amphibole peridotite source of the basanites. (3) the phlogopite peridotite zone and the shallower amphibole peridotite zone are infered to form a double-layered metasomatic structure in the lithospheric mantle, which was formed at different pressures by progressive mantle metasomatism caused by metasomatic agent coming from the depth.

RÉSUMÉ

PÉTROGENÈSE des ROCHES ALCALINES MAFIQUES d'ÂGE MÉSO-CÉNOZOÏQUE dans les PRPOVINCES de HUNAN et GUANGXI, CHINE SEPTENTRIONALE

Junsuo Liu

Des roches alcalines mafiques du Méso-Cénozoique affleurent sous forme de dykes subvolcaniques et de diatrèmes dans les provinces de Guangxi et de Hunan de la Chine septentrionale. Ces roches, localisées approximativement à 1000 km de la côte est de la Chine, constituent une zone interne continentale distincte de l'importante zone volcanique côtière du pacifique. Les roches de la zone interne sont divisées en deux grands groupes. Le premier groupe comprend des roches d'affinité lamproïtique et le deuxième, des basanites et des trachybasaltes. Des basaltes olivines alcalins ont été reportés dans la zone interne mais aucun n'a été échantillonné.

Les basanites et les trachybasaltes sont d'âge cénozoïque (51-28 Ma). Ils sont relativement riches en fer et leur Mg# < 66. Les basanites ont des contenus en MgO (9-10 % poids) et en Ni (~ 200 ppm) élevés et contiennent des xénolithes ultramafiques centimétriques du manteau supérieur. Ceci indique un faible degré de différenciation pour les basanites. Comparés aux basanites, les trachybasaltes montrent: un étalement des concentrations plus important du MgO (5.5-6.4 % poids) et du Ni (163-251 ppm), des concentrations plus faibles en CaO (6.5-7.3%) et en Sc (~ 13 ppm) et plus élevées en Al_2O_3 (~ 15%). Ceci atteste probablement de la cristallisation d'un clinopyroxène riche en calcium. Les basanites et trachybasaltes montrent des diagrammes arachnides similaires, fortement enrichis en éléments en traces traces incompatibles. Les élements suivants de ces roches: La, Nb, Ta, K, Th et Ba, montrent des enrichissements de l'ordre de 100 à 130 fois par rapport au manteau primitif et de 2 à 3 fois par rapport à celui des basaltes des îles en arc et des îles océaniques. Les patrons de distribution des éléments en traces sont comparables à ceux des basanites du Kenya associées au rift de l'Afrique de l'est. Une des caractéristiques importante des patrons basanites et des trachybasaltes est que l'enrichissement en éléments lithophiles à grand rayon ionique "LILE" (Ba, Th, U) est similaire, ou sensiblement plus bas que celui du La. Conséquemment, ces patrons sont difficilement explicables par une fusion partielle d'une source mantellique primitive ou encore par affinage de zone. Ceci est consistant avec le Mg# qui est trop élevé dans ces roches pour impliquer une telle source. Cependant, la majorité des amphiboles mantelliques ont des Mg# similaires à celui des basanites et des trachybasaltes. Or, dans les roches alcalines volcaniques il est fréquent de trouver des xénolithes mantelliques veinés par des

amphiboles et ceux-ci sont souvent enrichis en éléments en traces incompatibles. Donc, la peridotite veinée d'amphiboles représente probablement la source des basanites et des trachybasalts.

Les lamproïtes, d'âge mésozoïque (~ 132-135 Ma), sont trés riches en MgO (15.5-16.9 % poids) et CaO (11-14 % poids), pauvres en Al_2O_3 (8.1-8.8 % poids) et les ratios K/Na et K/Al sont beaucoup plus élevés que ceux des basanites et des trachybasaltes. Les teneurs en éléments incompatibles de ces roches sont également plus élevées que celles des basanites et des trachybasaltes et le degré de différenciation de ces éléments est plus fort. C'est ainsi que la teneur en Ba atteint 210-450 fois celle du manteau primitif, que le La est au même niveau que dans les basanites et que les valeurs en terres rares lourdes "HREE" sont la moitié de celles des basanites. Un tel enrichissement en éléments en traces, en particulier les "LILE", élimine un manteau primitif comme source. Une contamination crustale peut expliquer le fort enrichissement en éléments traces mais pas le haut contenu en MgO couplé avec une faible valeur en Al_2O_3 et doit être également rejetée. Le trés haut Mg# de ces roches indique une source appauvrie en composants basaltiques. La déplétion marquée en "HREE" dans les lamproites comparée aux basanites peut indiquer soit une rétention de grenat à la source soit une perte de grenat dans celle-ci antérieurement à la formation des lamproites. Par ailleurs, les lamproïtes montrent des anomalies marquées en Ta-Nb et Zr-Hf-Ti sur les diagrammes arachnides. Ces anomalies, typiques du magmatisme des zones de convergence, sont possiblement des indices de l'existence de reliques de matériaux provenant d'une ancienne zone de Benioff sous la région considérée. Les arguments ci-dessus indiquent que la source des lamproites aurait été métasomatisée.

Spatialement, les basanites et les trachybasaltes sont étroitement assoçiés avec les lamproïtes. Ils partagent aussi certains traits géochimiques communs: les patrons de "REE" sont similaires aussi bien au niveau de la forme des patrons que des teneurs. Bien que le magmatisme lamproïtique soit traditionnellement considéré comme indépendant du magmatisme dont dérive les basanites et les trachybasaltes, la distribution des rapports K/Na dans les roches mafiques alcalines remet ceci en question. C'est ainsi que sur le diagramme logarithmique K/Na vs $(La/Nb)_N$ l'ensemble des roches mafiques d'origine mantellique se distribue selon un couloir rectilinéaire ou l'augmentation du ratio K/Na est proportionnel à la différenciation des "REE". Ceci indique que la différenciation des "REE" et du rapport K/Na résultent de processus pétrogénétiques reliés. De la même façon, les roches moyennes suivantes: les basaltes alcalins, les lamprophyres mafiques, les lamproïtes et les kimberlites montrent une corrélation négative entre le MgO et l'Al_2O_3. Cette lignée évolutive peut être reliée aux mêmes processus pétrogénétiques. Le processus d'une fusion partielle d'un pyrolite, seule ou combinée avec de la contamination crustale, ne permet pas d'expliquer les lignées évolutives précitées. Un processus d'une différenciation de la source par un métasomatisme du matériau mantellique peut expliquer les lignées évolutives.

En résumé, les conclusions de ce travail sont: (1) les basanites et les trachybasaltes sont vraisemblablement formés à partir d'un manteau lherzolitique veinés d'amphiboles et enrichit en éléments incompatibles. La fusion partielle de la source est provoquée par un rift contintal Cénozoïque dans la région orientale de la Chine et les roches sont probablement une extension vers le continent de la province basaltique cotière du pacifique. (2) les lamproïtes sont les produits d'un magmatisme post-collisionnel au Mésozoïque. Ils dérivent d'une péridotite à phlogopite avec un haut ratio K/Na, appauvrie en composants basaltiques et enrichie sélectivement en potassium et en éléments incompatibles par métasomatisme. La zone à péridotite à phlogopite se trouve au niveau des péridotites à grenat en dessous des péridotites à amphibole qui est la source des trachybasaltes et des basanites. (3) Les zones à péridotite à phlogopite et à péridotite à amphibole forment une structure métasomatique à double couche causée, à différentes pressions, par un métasomatisme progressif résultant d'agents métasomatiques venant de plus profond dans le manteau.

ACKNOWLEDGEMENTS

This study is sponsored by the Canadian International Development Agency (CIDA) under the joint project between the Institute of Geochemistry, Academia Sinica (IGAS) and the Université du Québec à Chicoutimi. This joint project is managed by the Association of Universities and Colleges of Canada (AUCC). I wish to show my special gratitude to CIDA, AUCC, Dr. Jayanta Guha, the director of the project at UQAC and Dr. Guangchi Tu, the director of the project in IGAS.

I am especially grateful to Dr. Gérard Woussen and Dr. Sarah-Jane Barnes for their helpful advise, patient reading and correction of the thesis. Without them, the thesis may not have been possible. I would like to give my thanks to Dr. Michael Higgins at UQAC and Prof. Xiande Xie at the Guangzhou Branch, Academia Sinica for their help and advise during my thesis work. I am also grateful to Prof. Hongsen Xie at the Institute of Geochemistry, Academia Sinica for his help during the field work and for some of the analyses.

I would also like to thank Dr. Don Francis at McGill University for his advise and his generosity for allowing the use of his geochemical data analyses software. My sincere gratitude goes to Dr. Huan-zhang Lu, Dr. Jacques Carignan, Dr. Edward Chown, Dr. Alain Rouleau, Dr. Pierre Cousineau and Dr. Edward D. Sawyer for their help during my study and thesis work. A special thanks also goes to all personnel members of Sciences de la Terre and those working in the Library of UQAC for their help and services during my study at UQAC.

TABLE OF CONTENTS

List of figures

List of plates

List of tables

CHAPTER I

INTRODUCTION

Tholeiitic to alkaline volcanic and subvolcanic rocks of mafic to ultramafic composition occur extensively in southern and eastern China from the late Mesozoic to recent times (the last recorded eruption was in 1721). They can be divided into two major belts: (1) the Cenozoic tholeiitic to alkaline coastal volcanic belt which is exposed along the eastern coast and comprises about 95% of these rocks, and (2) the Mesozoic-Cenozoic alkaline inland volcanic/subvolcanic belt (Fig.1.1). This work is focused on the inland subvolcanic rocks.

1.1 MANTLE-DERIVED VOLCANIC ROCKS

Mafic volcanic rocks are the most voluminous mantle-derived volcanic products which provide us with natural indirect and as well as direct mantle samples that yield information on physical conditions and processes in the upper mantle and lower crust. Study of mantle-derived volcanic rocks not only enables us to understand better the geochemical characteristics of the upper mantle, and its formation and evolution; but to acquire some insights about the composition, formation and evolution of the Earth and other terrestrial planets in the solar system. Studies of mantle-derived volcanic and subvolcanic rocks generally involve characterization of the chemical compositions of their sources, processes of their formation and of their later evolution. These processes are controlled by tectonic settings. Therefore, a fundamental step in the study of mantle-derived volcanic and subvolcanic rocks is to distinguish their chemical characteristics inherited from the source from those acquired during later evolution (Wilson, 1989). With the aid of trace element and isotope studies of mantle-derived volcanic-subvolcanic rocks,

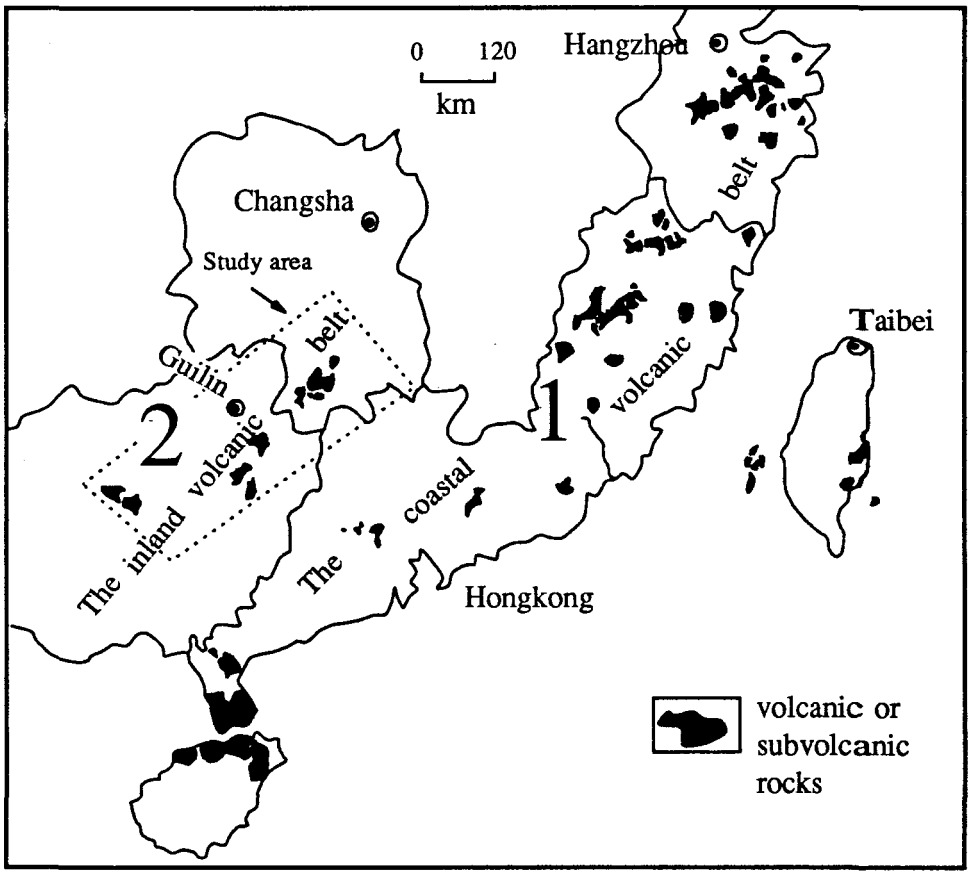

Fig. 1.1 A sketch map showing the two volcanic/subvolcanic belts in southern China. The areas of the outcrops are exaggerated for clarity (Modified after Zhang & Cong, 1987).

it is possible to characterize (1) the composition of the source (i.e. to consider whether it was depleted or enriched prior to melting); (2) the degree and mechanism of partial melting; (3) the residual phases. Before considering these source effects it is necessary to study the evolution processes such as magma-mixing, wall-rock assimilation and fractional crystallization.

There is now a consensus that primary basaltic and alkaline mafic magmas were formed by partial melting process in the mantle (Bowen, 1928; Yoder & Tilley, 1962; Ito & Kennedy, 1967; Kushiro, et at., 1968; Frey, etal., 1978; Green, 1970, 1980; Jaques & Green, 1980; Takahashi & Kushiro, 1983) mainly at plate boundaries or weak structural zones (Wilson, 1989) and that later processes produce wide composition spectrum of magmas in a particular tectonic environment (O'Hara, 1968; O'Hara & Mathews, 1981; De Paolo, 1981; Turner & Campbell, 1986; Maalfe & Johnston, 1986; Marsh, 1989; Wetzel, et al., 1989). Thus recognizing primary magmas is the key to characterizing their source chemistry. Generally, basaltic primary magmas are thought to have high #Mg, Ni and Cr contents, and are formed in the mantle. The compositions of the magmas depend on the source chemistry, degree and mechanism of partial melting: factors which vary with tectonic environment (Wilson, 1989). Present day volcanic activity occurs in four major tectonic settings: mid-ocean-ridges (MOR), island-arcs and active continental margins (IA & ACM), oceanic islands (OI) and continental rift areas (CR). Each of these environments has a different source feature: magmas erupted in MOR zone have a depleted asthenosphere source (known as the MORB source); OI basaltic rocks have a MORB source mixed with primitive mantle patches (plumes), and some of these patches are enriched with recycled old crustal materials; magmas of IA&ACM setting have as their source a mixture of a MORB source, subducted materials, OI type mantle plume, enriched subcontinental lithosphere and probably recycled old crustal materials; for the CR rocks, a strongly enriched subcontinental lithosphere source is responsible (Sun, 1984, Wilson, 1989). None of these sources is homogeneous in terms of isotopes (Zindler & Hart, 1986).

It is a common practice to analyze the geological settings of ancient magmatism by comparing them with present day magmatism of known tectonic settings (Wilson, 1989).

1.2 MAFIC VOLCANIC ROCKS IN CHINA

In southeastern China, a continental collision occurred during the early Mesozoic resulting in the Huanan terrane overthrusting onto the Yangtze foreland (Hsü et al., 1990). The continuing reaction between the two collided continents in the Mesozoic after the collision caused intensive S-type granite plutonism in the Huanan terrane in a compressional environment (Fig. 1.2*). At the same time, voluminous intermediate volcanic rocks were formed with terrigenous clastics in a foreland basin at the southeastern margin of the Huanan terrane. Near the end of the Mesozoic (around 85 Ma) the tectonic regime of the whole area of eastern China became extensional, forming many NNE rifts and horsts by rifting (È & Zhao, 1987; Taylor and Hayes, 1980). Accompanying the rifting, tholeiitic and alkaline volcanic/subvolcanic activity took place along NNE faults or around NNE-extended grabens, resulting in the extensively distributed Cenozoic volcanic rocks in eastern China, which is a part of the circum-Pacific volcanic belt (Fig. 1.3, Zhang & Cong, 1987).

Cenozoic volcanic activity in eastern China can be divided into three time periods: Early Tertiary (80-25 Ma), late Tertiary (25-2 Ma) and Quaternary (2 Ma or later). Early Tertiary volcanic products are dominated by tholeiitic basalts and are limited to the vicinity of the grabens. Late Tertiary volcanism is most extensive; volcanism occurred everywhere across the area of eastern China. At some locations, tholeiitic basalts dominate; at others alkaline basalts are important along with some peralkaline rocks. Quaternary volcanism is less extensive and of limited extent; rocks of this period are mainly alkaline. In some places, only basanites, nephelinites and trachybasalts were developed (È & Zhao, 1987).

---

* In Fig. 1.2 & 2.1 and in the text referencing these figures, a lithospheric fault is a fault that cuts through the crust into the upper mantle; a basement fault cuts the sedimentary strata and the basement but not the upper mantle; a crustal fault cuts only the sedimentary strata.

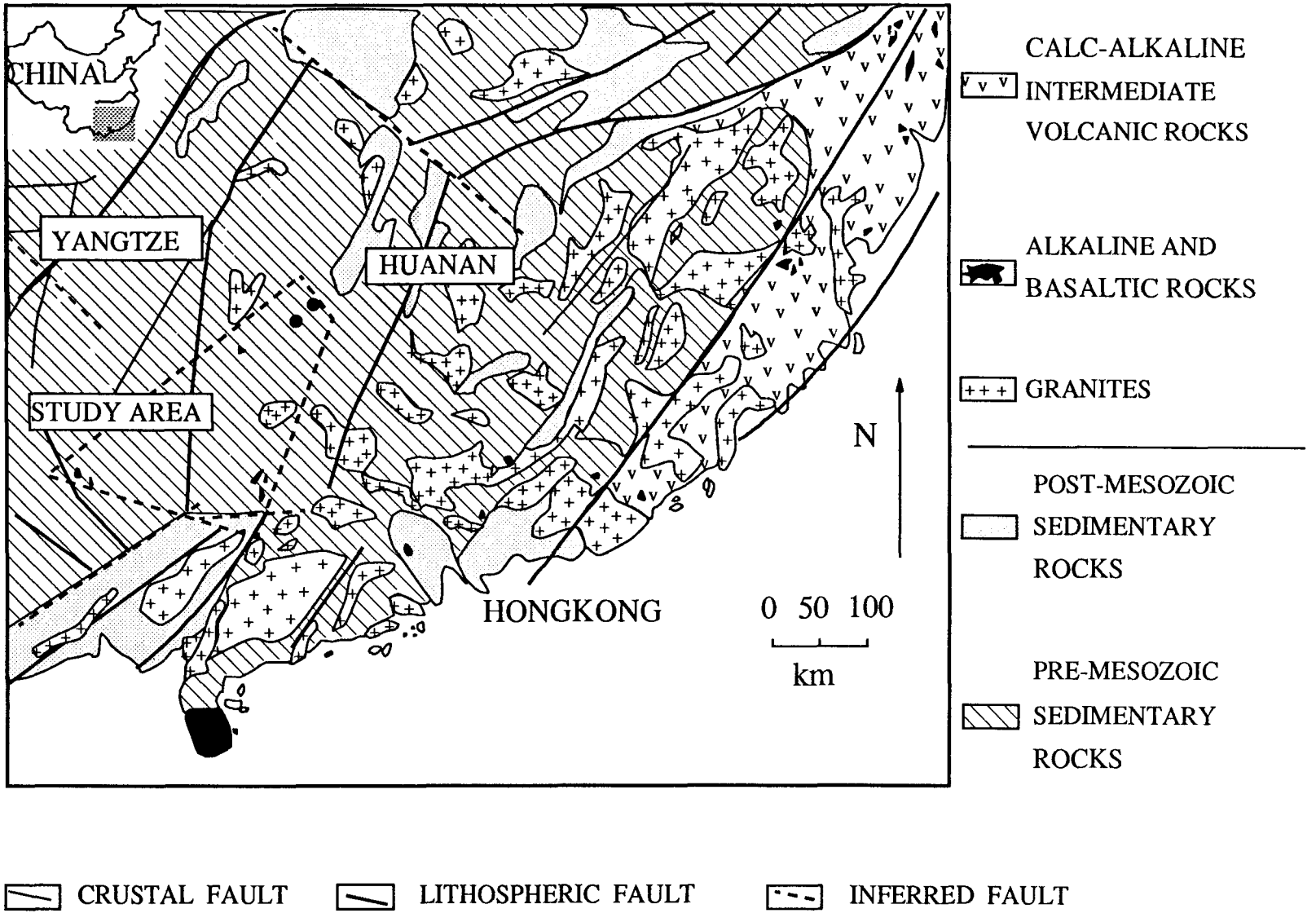

Fig. 1.2 Geologic map of southeastern China showing the tectonic settings and the distributions of the Meso-Cenozoic volcanic rocks and Mesozoic granites (Modified after Zhang, 1986).

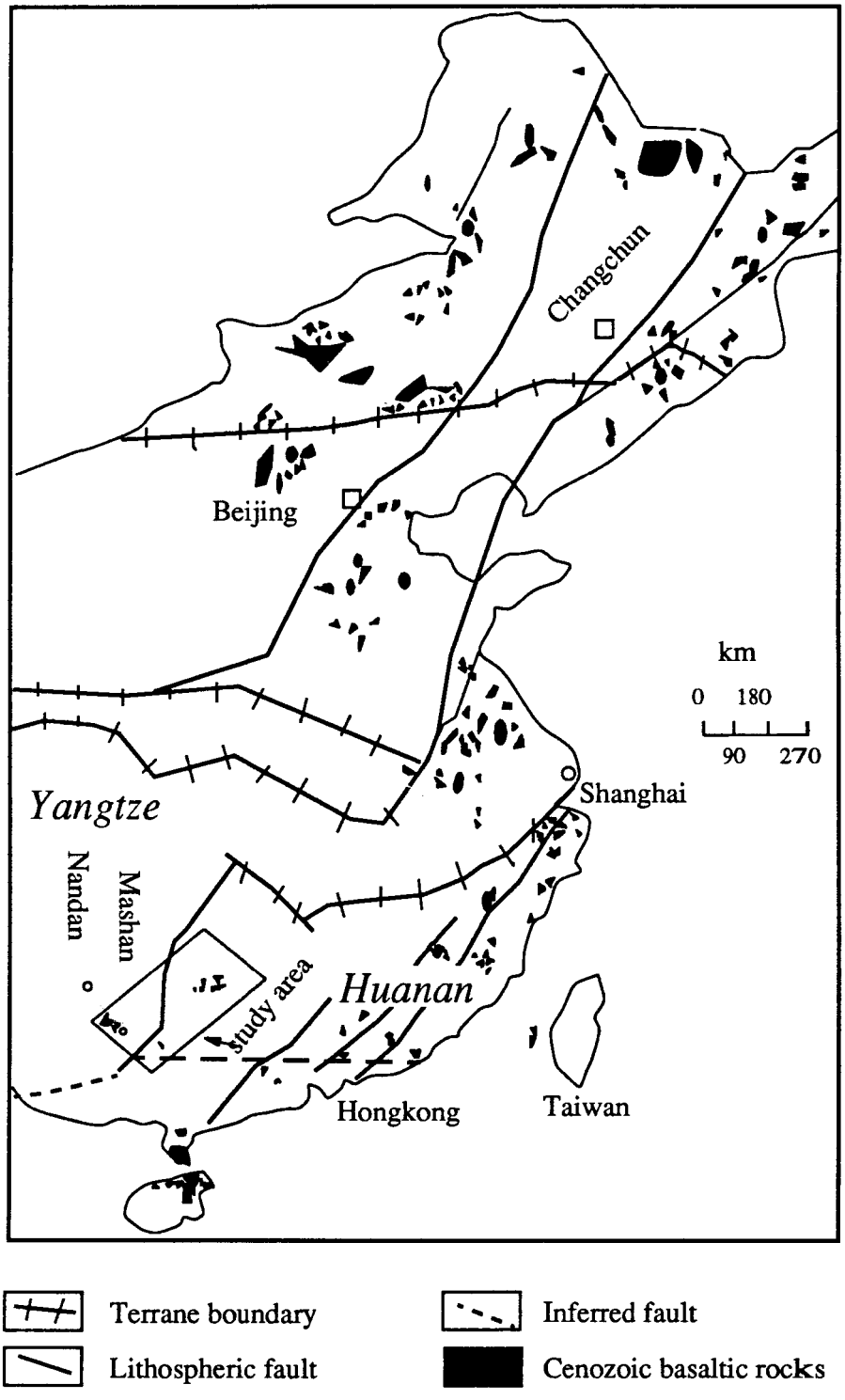

Fig. 1.3 A sketch map showing the rift regime and the distribution of Cenozoic volcanic rocks in eastern China (modified after E & Zhao, 1987)

As mentioned earlier, in the southern part of the eastern China volcanic province, two volcanic/subvolcanic belts are recognized: the coastal belt and the inland belt. The inland belt consists only of highly alkaline subvolcanic rocks: basanite-trachybasalts and olivine lamproites. These two types of rocks are very different in chemical composition, texture and mineralogy. The coastal and the inland belts are both important examples of the Mesozoic-Cenozoic lithospheric processes in southeastern China.

1.3 PREVIOUS STUDIES OF THE VOLCANIC ROCKS

In the last decade, the basalts and xenoliths from the coastal belt have been the subject of quite comprehensive studies of their petrography, chemistry, and petrogenesis. Before 1980, the major work was of descriptive petrology and geochemistry (Shen & Pan, 1951; Zhao, 1956; Zheng et al., 1978; Cong, et al., 1979). During the 1980s, "The crust and upper mantle formation and evolution of the marginal Pacific Ocean belt of China" was proposed as a Chinese national program. Studies of the basaltic rocks and their xenoliths from the coastal area were carried out, and numerous publications appeared (e.g. Sun & Lai, 1980; Zhou & Chen, 1981; Huang et al., 1982; Zhou, et al., 1982; Zhou & Armstrong, 1982; Zhang & Cong, 1983, 1984, 1987; Cao & Zhu, 1987; Hekinian, et al., 1989). Mineralogy, chemistry and Sr isotopic properties of the basalts and their source regions are quite well understood, though mantle structure and heterogeneity remain open for further study. It is generally accepted that the coastal volcanic rocks were formed in a continental rifting environment (Zhang & Cong, 1987).

In contrast, however, the subvolcanic rocks and xenoliths from the inland belt have received little attention in the past. Only a preliminary survey report is available (Liu, 1980, 1982). These inland subvolcanic rocks are more alkaline than most of the coastal rocks. They are exposed in the inner area of the continent, about 1000 km west of the coast, located in a collision mélange belt to the east of an ancient suture zone recognized recently (Hsü et al., 1987, 1988, 1989, 1990). These inland rocks are mainly subvolcanic.

They were reported to fall into two dyke groups: eastern group and western group (Liu, 1980). The eastern group is located along a major NNE fault (Daoxian-Pingnan faults in Fig. 2.1). Dykes in this group were intruded in NNE and NS subfracture systems, at the intersection of these fractures, diatremes were formed. The western group of dykes is distributed along a NW major fault (Nandan-Mashan fault). Rocks in the eastern group were described by Liu (1980) as olivine basalts, basanites and limburgites; rocks in the western group include only basanites and limburgites (Liu, 1980). The olivine basalts have 5-10% olivine and minor augite phenocrysts. They contain plagioclase (25-50%), augite (20-50%) and glasses (5-65%) in their groundmass. The basanites are composed of 40-50% augite or titanoaugite, and 40-50% plagioclase. They may also contain 5-8% olivine phenocrysts and 10-15% analcime. The limburgites were described to have 8-18% olivine and minor augite or titanoaugite phenocrysts. The groundmass of these limburgites is composed of augite or titanoaugite and brown glass, and minor amounts of mica, magnetite, magnesian spinel and analcime. These limburgites may also have plagioclase in their groundmass making them transitional to basanites. In Liu's (1980) report, these rocks were classified on the basis of their petrography. However, no chemical classification, which is more suitable than a petrographic classification for these fine grained subvolcanic rocks, was available. Besides, the term 'limburgite' was used in the report in a very broad sense, including olivine-rich, plagioclase-free rocks in the eastern group and plagioclase-bearing rocks in the western group. The high alkali content (Table 4 in Liu 1984) of the reported olivine basalts should qualify them as alkaline basalts.

In this study, we did not find any limburgites or olivine basalts. Instead, we found lamproites, basanites and trachybasalts. Evidently, a more precise and clear classification is needed for the inland rocks. The geochemical study of these rocks is of great importance in understanding the chemistry of the source of these rocks and for addressing questions related to mantle processes, lithosphere structure and ancient tectonic environment in the region of southern China. What are the common chemical characteristics of these inland subvolcanic rocks and their sources? How did they acquire these characteristics? Do they

differ in origin from those rocks in the coastal area? Do these inland subvolcanic rocks have something to do with ancient subduction which had been in the area? Questions like these need to be addressed and are helpful to understand the geology of the area of southern China.

1.4 RESULTS OF THIS STUDY

Fifty two samples of the alkaline rocks and their xenoliths were collected during a 5 week field trip. A hundred and three thin sections of these samples have been prepared and examined using a polarising microscope. Thirty fresher samples of the collection were analyzed for their major oxides. Twenty four alkaline rock samples (7 lamproites, 8 basanites,9 trachybasalts) were also analyzed for their rare earth elements, trace elements and platinum-group elements. About 40 olivine analyses were made in the alkaline rocks and in their mantle peridotite xenoliths at McGill University using a CAMECA microprobe; 34 analyses of pyroxene; 22 analyses of phlogopite in the Huzhiyan lamproites; 18 analyses of the analcime in the lamproites; 16 analyses of K-feldspar in the lamproites; 12 analyses of the plagioclase in the basanites and in the trachybasalts; 9 analyses of opaque minerals from all the three alkaline rock types.

In this thesis, the following work has been carried out. (1) A thorough petrographic study and description were done for each rock type. Based on the petrography the collected rocks are divided into two petrographic series: plagioclase-bearing series which are further classified as trachybasalts and basanites, and plagioclase-free series which is classified as lamproite by its mineralogy. (2) Major oxide chemical characteristics are explored with Harker-type and Pearce-type diagrams. A linear composition array defined by the plagioclase-bearing rocks was found and is discussed. In alkaline rocks in general a negative correlation between Al_2O_3 and MgO is observed and discussed. (3) Close affinity of the plagioclase-bearing rocks to eastern Africa rift basanites is revealed by trace elements on Thompson spidergrams for the alkaline rocks. The patterns of the lamproites

on the spidergrams suggest clearly the existence of an ancient subduction zone in the study area, which is hotly debated among structural geologists working for the region (Hsü, et al., 1988, 1989, 1990, Gupta 1989; Rodgers, 1989). (4) A logarithmic correlation between K/Na and $(La/Yb)_N$ is found among the alkaline rocks in the study area from the basanites to the lamproites. The trend is actually shared by almost all mantle-derived alkaline rocks. (5) Continental rift-related magmatism is suggested for the basanites and trachybasalts in this study, the same conclusion had been reached for rocks in the coastal belt; the lamproites, however, have a different origin, they are post-orogenic magmatic products related to the early Mesozoic collisional orogenesis in the region. For both the lamproites and the basanites and trachybasalts, a metasomatized mantle source is needed. (6) A two-layer metasomatic model is proposed for the lithosphere. The difference between the metasomatized sources for the lamproites and for the basanite-trachybasalts is that they represent different examples of a pressure-controlled metasomatic process: the lamproites originated at greater depths, from the phlogopite metasomatic zone; the basanite-trachybasalts originate from the shallower amphibole metasomatic zone.

CHAPTER II

REGIONAL GEOLOGY

2.1 REGIONAL GEOLOGY

The study area is located in southwestern Hunan and northern Guangxi Provinces, southern China. The major strata that crop out in this area are upper Palaeozoic shaly carbonates and lower Palaeozoic flysch. Proterozoic clastic rocks outcrop in the northwest, and Cenozoic unconsolidated sediments are distributed throughout the lowland area caused by extensional faulting (Fig. 2.1).

In southern China, marine sedimentary rocks formed before the early Mesozoic. From the Jurassic on, sedimentary rocks are terrigenous red clastics and unconsolidated sediments limited to some NNE narrow basins.

2.2 REGIONAL TECTONICS

The tectonics of southern China has been a subject of debate for some time. Basically, there are two major tectonic units or terranes: Yangtze and Huanan, separated by lithospheric fault zone (Fig. 1.2). By invoking a thrust model, Hsü et al (1990) interpreted that the southern China area was an ocean (Banxi Ocean) bounded by two separate continents (Yangtze and Huanan) during pre-Mesozoic time. A pre-Devonian accretionary prism was formed on the northwestern active margin of the Huanan continent (the Proterozoic clastics and lower Palaeozoic flysch in Fig. 1.2). During the early Devonian, the margin became inactive and carbonate rocks were deposited unconformably on top of the accretionary prism (the lower Palaeozoic carbonate in Fig. 1.2). The ocean

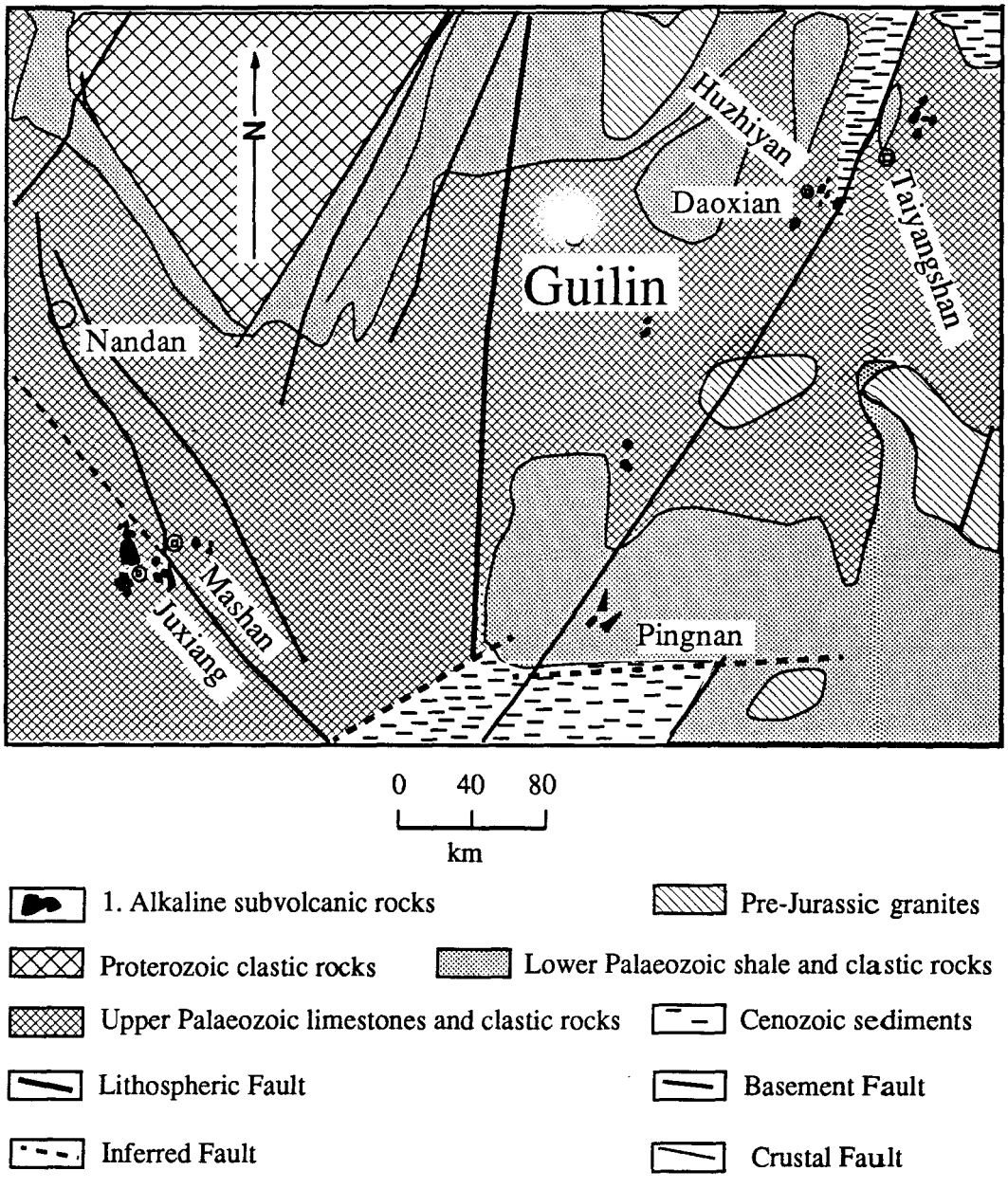

Fig. 2.1 Geologic map of the study area showing the two alkaline rock groups in the inland subvolcanic rock belt (modified after Liu, 1982).

was closed in late Triassic and Huanan terrane was overthrust onto the Yangtze continent. As a result of this collision, S-type granites were formed in Huanan during Mesozoic. Then in late Mesozoic the Huanan terrane which had been connected with the Yangtze terrane was overthrust in turn by another microcontinent further to the southeast, the Dongnanya (southeastern Asia) continent. This process is shown in a cartoon in Fig. 2.2.

The long compressional geohistory of southern China characterized by ocean-continent or continent-continent interaction ended by late Mesozoic, and a whole unified eastern Chinese continent was formed. Since then, the tectonic regime in the whole eastern China area changed from compressional to extensional, and rifting began turning the area into rifts and horsts. Cenozoic alkaline mafic volcanism developed in this area as a result of the rifting.

2.3 SETTING OF THE ALKALINE MAFIC ROCKS

There are about 500 subvolcanic bodies in southwestern Hunan and northern Guangxi Provinces (the inland belt) along the suture zone between Huanan and Yangtze continents (the Huanan cover zone in Fig. 2.2c). Most were intruded into Palaeozoic flysch or carbonate formations; others into Cretaceous sandstones. They can be divided into two groups: the eastern group and the western group (Fig. 2.1, Liu, 1980). Rocks in the eastern group are distributed along a major NNE fault (Daoxian-Pingle fault) from Ningyuan through Daoxian (Hunan Province) to Pingle (Guangxi Province). They are located in the NNE and NS secondary fractures as dykes generally several meters wide, or at the intersections of these two fractures as diatremes of a few to over ten thousands square meters (Liu, 1982). The western group are distributed on both sides of a NW major fault zone (Nandan-Mashan fault), especially at the intersections of two secondary NW and NE fractures. They occur generally as small diatremes of 50 by 60 to 200 by 150 meters (Liu, 1982). Alkaline rocks and their xenoliths have been collected for this study from two

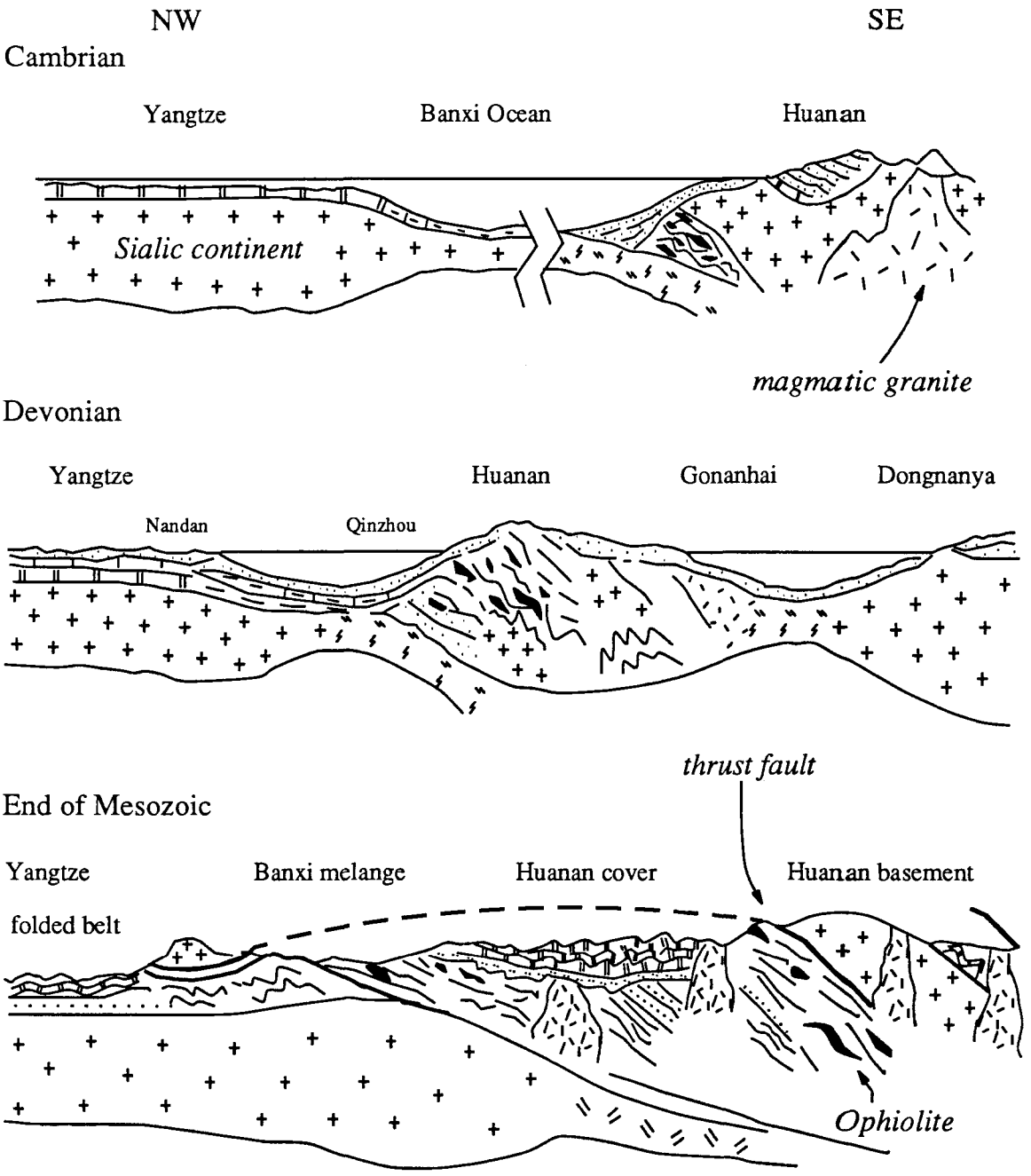

Fig. 2.2 Synthesized sections across the Fig. 1.2 from the NW to SE showing schematically the tectonic evolution of South China (After Hsü et al, 1990).

Cambrian: Existence of the Banxi ocean which separate the Yangtze and Huanan continents. Active subduction. Devonian: Closure of the Banxi ocean and the subduction was almost finished. Late Mesozoic: Continental collision phase. Cenozoic: Rifting phase, see Fig. 1.2 and 1.3

major places (Taiyangshan and Huzhiyan) in the eastern group, and from one place (Juxiang) in the western group.

None of the rocks collected for this study have been dated; but an available K-Ar age of a 'limburgite' from Huzhiyan is 132-135 Ma, and available K-Ar ages for alkaline rocks in the western group are 51-28 Ma (Liu, 1982).

CHAPTER III

PETROGRAPHY and MINERALOGY

3.1 INTRODUCTION

The alkaline rocks collected for this study fall into two petrographic categories: one with plagioclase, the other without plagioclase. The plagioclase-bearing rocks can be further divided into two major types: trachybasalts which are from Taiyangshan (the eastern group) and basanites which characterize the western group. Non-plagioclase bearing rocks from Huzhiyan (eastern group) were classified as 'limburgite' by Liu (1982); but are classified, based on modal mineralogy, as lamproite or more precisely madupitic olivine lamproites in this study using the terminology of Mitchell (1985).

All silicate minerals in these rocks were analyzed at McGill University using a CAMECA electron microprobe with these conditions: operating potential 15 kV, beam-current 7.4-8 μA, beam size 5-10 μm (depending on minerals), 25-50 second counting times. The analyses were corrected by ZAF procedure. Opaque minerals were analyzed by EDS method using the same microprobe.

3.2 NON-PLAGIOCLASE BEARING ROCKS

3.2.1 Texture and Mineralogy

3.2.1.1 Lamproites

According to Mitchell (1985), *"lamproite is a group of ultramafic rocks characterized by the presence of widely varying modal amounts of titanian Al-poor phlogopite, titanian tetraferrophlogopite, potassian titanian richterite, forsteritic olivine,*

diopside, sanidine and leucite as the major phases. Minor and accessory phases include enstatite, pridereite, apatite, wadeite, magnesiochromite, ilmenite, shcherbakovite, armalcolite, perovskite and jeppeite. Analcime is common as a secondary mineral replacing leucite and/or sanidine... It is particularly important to note that the presence of leucite is not essential in order that a rock to be considered as a member of the lamproite clan". The Huzhiyan potassic rocks are classified here as madupitic olivine lamproite, because of their special mineralogy described below and of their whole rock chemistry which will be discussed later in Chapter 4.

The Huzhiyan rocks consist of euhedral, subhedral and irregular olivine megacrysts (0.05-2 mm, 20-25%), subhedral poikilitic phlogopite (1-3 mm, 10-15%), clinopyroxene phenocryst (0.2-0.5 mm, 1-2%), fine euhedral clinopyroxene (0.02-0.1 mm, 35-40%), anhedral alkali feldspar (0.02-0.05 mm, 5-10%), glassy subhedral to anhedral analcime (about 0.02 mm, 15-20%), and minor apatite, magnesioilmenite, and ulvöspinel (less than 1%, see Table 3.1 for the compositions of these opaque minerals). These rocks are porphyritic and highly inhomogeneous (plate 1): olivine megacrysts, large elongated poikilitic phlogopite crystals (containing smaller clinopyroxene) and elongated patches enriched in alkali feldspar and diopside (2-phase pockets) are mixed with a normal matrix composed of thin prismatic clinopyroxene and interstitial analcime (plate 1b).

The olivine megacrysts include phenocrysts and xenocrysts. The xenocrysts are irregular olivine fragments which are thought to came from the fragments of mantle xenoliths and which have undergone deformation as indicated by their undulatary extinction (plate 2). These xenocrysts represent about 30% of the total olivine megacrysts. The phenocrysts are euhedral, some of them are skeletal (plate 3). The olivine phenocrysts are slightly altered, some have a phlogopite rim formed around their margins (plate 4).

The clinopyroxenes in normal matrix and in the 2-phase pockets have different textures: those in normal matrix are thin prisms; crystals in the 2-phase pockets are well

Table 3.1. Composition of opaque minerals from the inland alkaline rocks (EDS data)
(IL-ilmenite, SP-spinel, Lh-lherzolite)
(BSP1, BSP2, BIL3, LhSP in the sample Bas4; TBSP in TB5; LamIL, LamSp in Lam4)

	BSP1	BSP2	BIL3	TBSP	LhSP	LamIL1	LamIl2
MgO	2.70	2.97	3.82	1.57	20.31	8.89	21.04
Cr_2O_3	0.28	0.14	0.31	0.68	19.24	1.51	14.57
Al_2O_3	1.96	2.26	0.10	1.91	50.15	0.29	54.15
TiO_2	23.96	25.17	54.10	26.47	0.19	55.25	0.13
Fe_2O_3	19.69	19.21	-	14.35	-	-	-
FeO	50.44	49.22	40.99	51.65	9.38	33.28	9.51
MnO	0.97	1.03	0.69	1.48	0.34	0.62	0.39
V_2O_3	-	-	-	1.88	-	-	-
Total	99.99	100.00	100.01	100.00	99.61	99.84	99.79
O	0.000	4.000	3.000	4.000	4.000	3.000	4.000
Mg^{+2}	0.148	0.161	0.140	0.086	0.807	0.313	0.821
Cr^{+3}	0.008	0.004	0.006	0.020	0.405	0.028	0.301
Al^{+3}	0.085	0.097	0.003	0.083	1.574	0.008	1.670
Ti^{+4}	0.661	0.687	0.997	0.731	0.004	0.981	0.003
Fe^{+3}	0.543	0.525	0.000	0.397	0.000	0.000	0.000
Fe^{+2}	1.547	1.495	0.840	1.587	0.209	0.657	0.208
Mn^{+2}	0.030	0.032	0.014	0.046	0.008	0.012	0.009
V^{+3}	-	-	-	-	-	-	-
T Metal	3.021	3.000	1.999	2.996	3.006	2.000	3.012

Note: Fe_2O_3 was not analyzed. The Fe_2O_3 contents of BSP1 and BSP2 are calculated using a Fe^{+3}/Fe^{+2} ratio of 0.26 to fit the spinel formula. The Fe_2O_3 content of sample TBSP is calculated for the same reason using a Fe^{+3}/Fe^{+2} ratio 0.2.

developed euhedral crystals, larger than those in the matrix (plate 1b). The phlogopites are mainly poikilitic crystals enclosing clinopyroxene (plate 5). These poikilitic phlogopite crystals can be divided into two shape groups: one consists of very long blades (the length is usually more than 5 times the width), the other consists of less elongated, subhedral to anhedral crystals. The phlogopite blades and the 2-phase pockets are distributed in a regular pattern. The long poikilitic phlogopite blades are distributed along three linear fracture zones, and the 2-phase pockets are parallel to one of these linear zones (plate 6). This textural pattern is interpreted to have formed during the late stage of magma solidification, when a fracture system developed and the residual liquid filled and crystallized long poikilitic phlogopite and 2-phase pockets enriched in feldspar and clinopyroxene. A preferential orientation of clinopyroxene in normal groundmass and in the 2-phase pocket areas indicates there was a flow in the magma when it crystallized. Beside poikilitic phlogopite and phlogopite rims upon some olivine megacrysts, a chain of blue-green mica along a fracture is observed.

The analcimes appear as subhedral to round interstitial grains between thin euhedral clinopyroxenes in the groundmass (plate 7a) or as irregular crystals gathering around phlogopite phenocrysts (plate 7b), some analcime crystals contain small crystals of other minerals. Because of their anhedral shape and isotropic optics, the analcimes in the Huzhiyan rocks are easily to be mistaken as glasses. This may be why the rocks were originally classified as 'limburgite'.

3.2.2 Mineral Chemistry

3.2.2.1 Olivine

The olivine, which appears only as megacrysts in the Huzhiyan lamproite, is highly magnesium-rich, ranging in composition from $Fo_{89.8}$ to $Fo_{95.1}$ with an average Fo_{93} (Fig. 3.1, Table 3.2). Olivine phenocrysts with such high Fo content are typical of all lamproites from around the world (Bergman, 1987; Mitchell, 1985a). NiO content of the

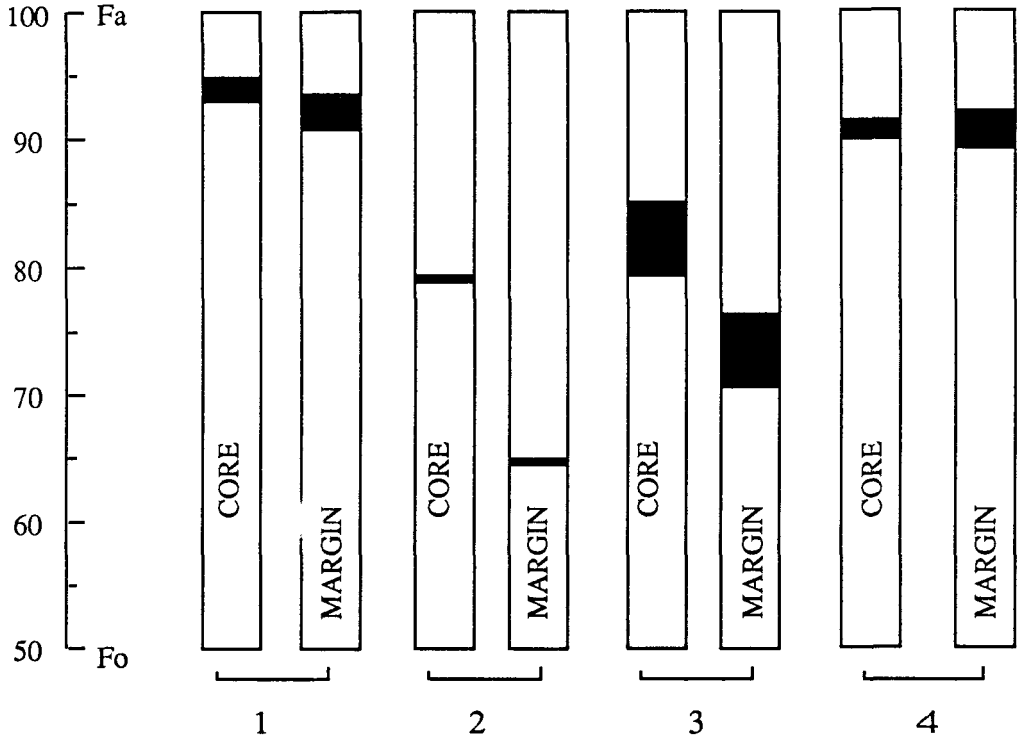

Black areas stand for compositional range

1. Phenocryst olivines in the lamproites
2. Phenocryst olivines in the trachybasalts
3. Phenocryst olivines in the basanites
4. Xenocryst olivines in the trachybasalts and basanites

Fig. 3.1 The range of compositions of the olivine megacrysts in the alkaline rocks from the inland subvolcanic belt of southern China.

Table 3.2. Chemical composition of olivine megacrysts in lamproites (Lam4) (c--core of a crystal, m--margin of the crystal; p--phenocryst, x--xenocryst)

	OLp1c	OLp1m	OLp2c	OLp2m	OLp3c	OLp3m	OLx1c	OLx1m
SiO_2	41.38	40.79	42.14	41.38	42.35	42.33	41.76	42.18
MgO	50.65	49.33	50.08	47.4	51.14	49.32	51.08	50.67
FeO	5.74	7.06	6.02	9.37	4.61	6.91	4.96	5.58
MnO	0.14	0.12	0.14	0.23	0.09	0.15	0.12	0.13
CaO	0.24	0.12	0.08	0.16	0.07	0.16	0.07	0.1
NiO	0.32	0.22	0.27	0.2	0.32	0.08	0.22	0.28
Total	98.51	97.8	98.86	98.78	98.65	99.05	98.29	99.08
Cations Based on 4 Oxygen Atoms								
Si	1.011	1.011	1.025	1.023	1.025	1.030	1.017	1.022
Mg	1.845	1.822	1.817	1.747	1.846	1.790	1.856	1.831
Fe^{+2}	0.117	0.146	0.122	0.194	0.093	0.141	0.101	0.113
Mn	0.003	0.003	0.003	0.005	0.002	0.003	0.002	0.003
Ca	0.006	0.003	0.002	0.004	0.002	0.004	0.002	0.003
Ni	0.006	0.004	0.005	0.004	0.006	0.002	0.004	0.005
T Metal	1.978	1.979	1.950	1.954	1.949	1.939	1.965	1.955
Percentage of End Members								
Fa	6.1	7.53	6.44	10.18	4.86	7.43	5.27	5.93
Fo	93.9	92.47	93.56	89.82	95.11	92.57	94.73	94.07

olivine ranges from 0.08-0.32%, CaO 0.07-0.24%. Compared to lherzolite olivine (Table 3.3), the lamproite olivine is higher in MgO (Fig. 3.2) and CaO, and lower in NiO. With respect to phenocryst olivine from the other two types of the alkaline rocks (Table 3.4 & 3.5) in the region, the lamproite olivine has higher MgO and NiO, and lower CaO. Phenocrystic olivine in the lamproite is slightly zoned. The cores are rich in Fo and NiO (Fig. 3.1).

3.2.2.2 Clinopyroxene

As mentioned above, the clinopyroxenes in the lamproites are divided into two textural types: the thin prismatic crystal in the 'normal groundmass' and large euhedral crystals in the 2-phase pockets. Both types are diopside (Fig. 3.3) with CaO ranging from 22.73% to 24.84%, MgO 11.95-17.47% (Table 3.6). The clinopyroxenes in the 'normal groundmass' have a relatively narrow range of composition. Their Al_2O_3 contents range from 1.72 to 4.13% (Table 3.6, sample 6-11), Cr_2O_3 0.07-0.23%, Na_2O 0.21-0.34%. These clinopyroxenes are different from those in other lamproites from around the world in having higher Al_2O_3 (Bergman, 1987; Fig. 3.4), from the diopside megacrysts in mafic lamprophyre or in alkali basaltic rocks in having lower Al_2O_3 (Bergman, 1987), from the diopsides in the lherzolite xenoliths in having lower Cr_2O_3 (see Tables 3.6 & 3.7), and from the diopsidic megacrysts in kimberlite (Mitchell, 1985) in having lower Na_2O.

In contrast to the clinopyroxenes in normal groundmass, the clinopyroxenes in the pockets vary greatly, especially in the Al_2O_3 content: smaller euhedral diopside near the margins or in narrow parts of the pockets are poor in Cr_2O_3 (0.01-0.11%), and very poor in Al_2O_3 (0.12-0.91) (Table 3.6, sample 1-4), typical for clinopyroxenes in lamproites from around the world (Fig. 3.4; Mitchell, 1985; Bergman, 1987), and also similar to microphenocryst and groundmass clinopyroxenes in kimberlite (Mitchell, 1986); the large euhedral prisms of clinopyroxene in the wide parts of the 2-phase pockets (Table 3.6, sample 5), have much higher Al_2O_3 (6.64-7.86%), FeO (6.66-7.05%), and TiO_2 (0.5-

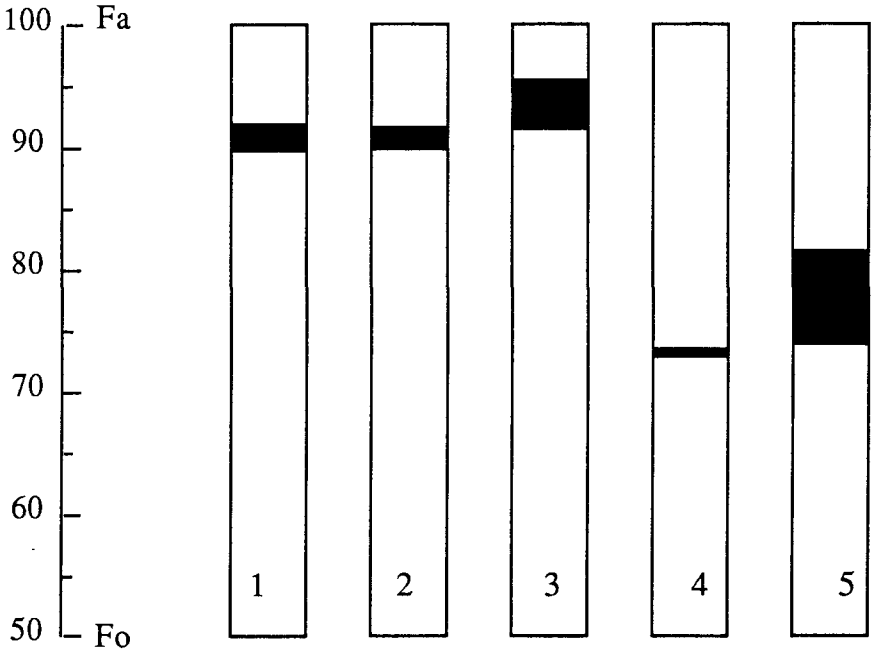

Black areas stand for compositional range

1. Xenocryst olivines in the basanites and trachybasalts
2. Olivines in the mantle lherzolite
3. Phenocryst olivines in the lamproites
4. Phenocryst olivines in the trachybasalts
5. Phenocryst olivines in the basanites

Fig. 3.2 Comparison of composition between the olivines in the lamproites, trachybasalts, basanites, and lherzolites from the inland subvolcanic rock belt of southern China.

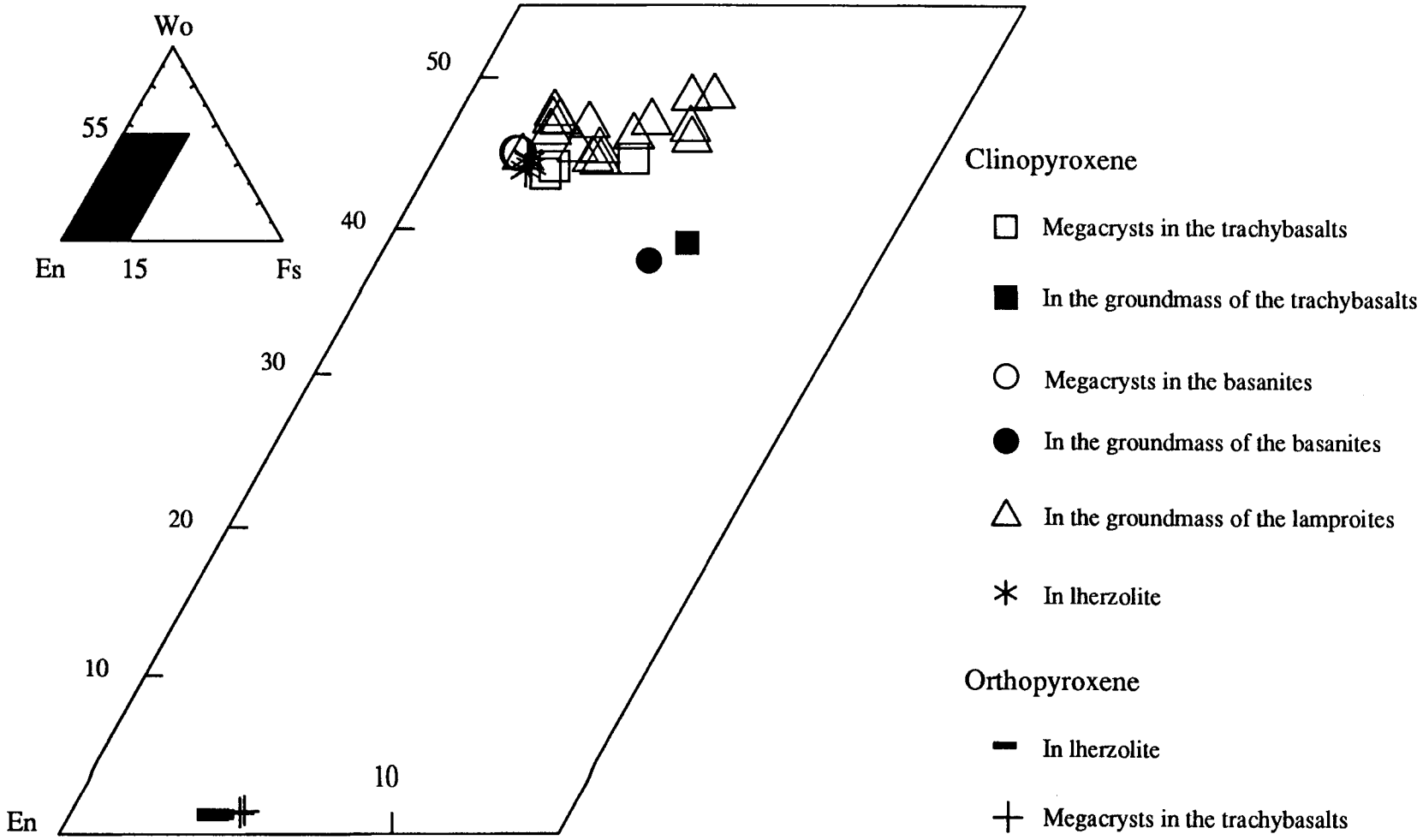

Fig. 3.3 Quadrilateral diagram showing the variation in composition of the pyroxenes in the alkaline rocks from the inland subvolcanic belt in southern China.

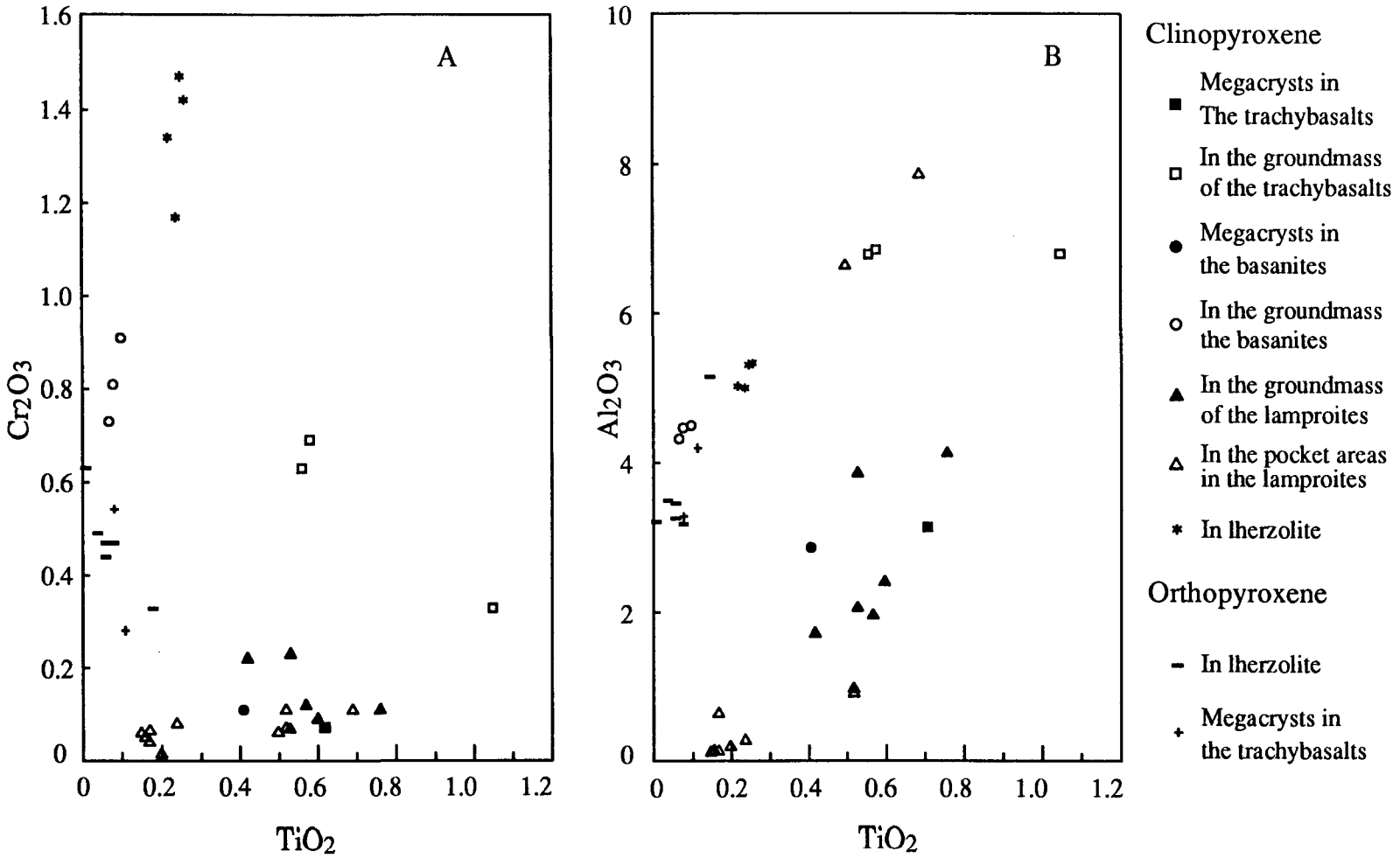

Fig. 3.4 TiO_2 - Cr_2O_3 (A) and TiO_2 - Al_2O_3 (B) plots showing the range in composition of the clinopyroxenes in the alkaline rocks from the inland subvolcanic belt of southern China.

Table 3.3. Chemical composition of olivines in mantle lherzolites
(sample 1, 2, 3 from a xenolith in TB1; 4,5,6 in TB6; c--core, m--margin)

	Lh1c	Lh1m	Lh2c	Lh2m	Lh3	Lh4	Lh5	Lh6
SiO_2	40.62	40.8	40.56	40.87	39.65	40.25	40.26	40.60
MgO	48.78	48.94	48.74	49.48	48.51	48.17	48.53	48.82
FeO	8.39	8.33	8.27	8.33	9.85	9.81	10.09	10.05
MnO	0.09	0.11	0.11	0.09	0.12	0.15	0.13	0.20
CaO	0.05	0.09	0.05	0.06	0.09	0.05	0.06	0.05
NiO	0.31	0.35	0.32	0.34	0.36	0.34	0.38	0.01
Total	98.24	98.61	98.04	99.1	98.58	98.75	99.45	99.74
Cations Based on 4 Oxygen Atoms								
Si	1.007	1.007	1.007	1.004	0.989	1.000	0.995	0.999
Mg	1.803	1.802	1.804	1.812	1.804	1.785	1.789	1.790
Fe^{+2}	0.174	0.172	0.172	0.171	0.205	0.204	0.209	0.207
Mn	0.002	0.002	0.002	0.002	0.003	0.003	0.003	0.004
Ca	0.001	0.002	0.001	0.002	0.002	0.001	0.002	0.001
Ni	0.006	0.007	0.006	0.007	0.007	0.007	0.008	0.000
T Metal	1.986	1.985	1.986	1.993	2.022	2.000	2.009	2.003
Percentage of End Members								
Fo	90.83	90.86	90.91	90.98	89.70	89.64	89.47	89.46
Fa	9.17	9.14	9.09	9.02	10.30	10.36	10.53	10.54

Table 3.4. Chemical composition of olivine megacrysts in basanites (Sample Bas4) (OL--Olivine, p--phenocryst, x--xenocryst, c--core of a crystal, m--margin of a crystal)

	OLp1c	OLp1m	OLp2c	OLp2m	OLp3c	OLp3m	OLx1c	OLx1m
SiO_2	39.59	38.48	38.33	37.86	39.67	38.04	40.53	40.18
MgO	44.7	40.53	39.88	34.69	44.94	36.79	49.26	48.68
FeO	14.6	19.78	20.64	26.47	14.12	24.03	8.84	9.28
MnO	0.2	0.31	0.27	0.48	0.16	0.4	0.11	0.09
CaO	0.26	0.31	0.3	0.42	0.25	0.4	0.05	0.06
NiO	0.23	0.15	0.13	0.1	0.2	0.12	0.34	0.35
Total	99.59	99.55	99.55	100.02	99.33	99.78	99.13	98.64
Cations Based on 4 Oxygen Atoms								
Si	0.998	0.995	0.995	1.006	1.000	1.002	0.999	0.997
Mg	1.680	1.563	1.544	1.375	1.689	1.445	1.810	1.802
Fe^{+2}	0.308	0.428	0.448	0.588	0.298	0.529	0.182	0.193
Mn	0.004	0.007	0.006	0.011	0.003	0.009	0.002	0.002
Ca	0.007	0.009	0.008	0.012	0.007	0.011	0.001	0.002
Ni	0.005	0.003	0.003	0.002	0.004	0.003	0.007	0.007
T Metal	2.004	2.009	2.009	1.988	2.001	1.997	2.003	2.005
Percentage of End Members								
Fo	84.13	78.12	77.16	69.56	84.7	72.76	90.45	89.93
Fa	15.87	21.88	22.84	30.44	15.3	27.24	9.55	10.07

Table 3.5. Chemical composition of olivine megacrysts in trachybasalts (Sample TB5) (OL--Olivine, p--phenocryst, x--xenocryst, c--core of a crystal, m--margin of a crystal)

	OLp1c	OLp1m	OLp2c	OLp2m	OLx1c	OLx1m	OLx2c	OLx2m
SiO_2	39.02	37.28	38.81	37.2	40.11	40.14	40.5	40.64
MgO	41.7	31.59	41.9	32.93	49.27	45.88	49.72	49.7
FeO	18.35	30.01	18.2	29.14	8.79	11.3	8.32	8.62
MnO	0.29	0.54	0.27	0.61	0.09	0.14	0.09	0.12
CaO	0.16	0.34	0.2	0.33	0.07	0.06	0.06	0.06
NiO	0.22	0.07	0.22	0.09	0.35	0.33	0.34	0.36
Total	99.7	99.82	99.59	100.29	98.67	97.85	99.04	99.49
Cations Based on 4 Oxygen Atoms								
Si	0.999	1.010	0.996	1.000	0.994	1.012	0.997	0.997
Mg	1.593	1.276	1.603	1.320	1.820	1.725	1.825	1.818
Fe^{+2}	0.393	0.680	0.390	0.655	0.182	0.238	0.171	0.177
Mn	0.006	0.012	0.006	0.014	0.002	0.003	0.002	0.002
Ca	0.004	0.010	0.005	0.010	0.002	0.002	0.002	0.002
Ni	0.005	0.002	0.005	0.002	0.007	0.007	0.007	0.007
T Metal	2.001	1.980	2.009	2.000	2.013	1.975	2.006	2.006
Percentage of End Members								
Fo	79.3	64.76	79.99	66.3	90.51	87.44	91.02	90.69
Fa	20.7	35.24	20.01	33.7	9.49	12.56	8.98	9.31

Table 3.6. Composition of clinopyroxenes in the Huzhiyan lamproites (Lam4), (#)--# averaged (sample 1-5 in pocket area, 6-11 in groundmass; c--core, m--margin)

	Cpx1c (2)	Cpx1m	Cpx2c	Cpx2m	Cpx3c	Cpx3m	Cpx4c	Cpx4m
SiO_2	53.76	52.53	54.45	54.39	54.18	51.80	54.90	54.52
TiO_2	0.17	0.52	0.15	0.16	0.24	0.52	0.17	0.20
Cr_2O_3	0.07	0.11	0.06	0.05	0.08	0.07	0.04	0.01
Al_2O_3	0.64	0.91	0.12	0.14	0.28	0.97	0.13	0.19
FeO	2.83	7.26	2.75	2.99	3.99	7.54	2.67	3.03
MnO	0.07	0.24	0.09	0.04	0.18	0.23	0.08	0.06
MgO	17.47	13.31	16.34	16.71	15.56	13.36	16.39	16.26
CaO	23.12	23.55	24.30	24.20	24.03	23.10	24.84	24.35
Na_2O	0.24	0.56	0.29	0.31	0.34	0.62	0.25	0.35
Total	98.37	98.99	98.55	98.99	98.88	98.21	99.47	98.97
Number of Ions Calculated Based on 6 Oxygen Atoms								
Si	1.985	1.976	2.011	2.002	2.006	1.968	2.010	2.008
Ti^{+4}	0.005	0.015	0.004	0.004	0.007	0.015	0.005	0.006
Cr^{+3}	0.002	0.003	0.002	0.001	0.002	0.002	0.001	0.000
Al	0.028	0.040	0.005	0.006	0.012	0.043	0.006	0.008
Fe^{+2}	0.087	0.228	0.085	0.092	0.124	0.240	0.082	0.093
Mn	0.002	0.008	0.003	0.001	0.006	0.007	0.002	0.002
Mg	0.962	0.746	0.900	0.917	0.859	0.756	0.894	0.892
Ca	0.915	0.949	0.962	0.954	0.953	0.940	0.974	0.961
Na	0.017	0.041	0.021	0.022	0.024	0.046	0.018	0.025
Percentage of End Members (unnormalized to 100%)								
Fs	4.83	12.91	4.70	5.00	6.96	13.46	4.56	5.17
En	48.09	37.32	44.98	45.84	42.93	37.82	44.71	44.62
Wo	45.74	47.47	48.08	47.72	47.66	47.01	48.71	48.04
Jadeite	1.7	4.1	2.1	2.2	2.4	4.6	1.8	2.5

Table 3.6. Continued

	Cpx5c (2)	Cpx5m (2)	Cpx6	Cpx7	Cpx8 (3)	Cpx9 (6)	Cpx10 (3)	Cpx11 (6)
SiO_2	47.99	46.08	51.84	50.60	51.54	52.45	51.70	50.66
TiO_2	0.50	0.69	0.42	0.76	0.60	0.57	0.53	0.53
Cr_2O_3	0.06	0.11	0.22	0.11	0.09	0.12	0.23	0.07
Al_2O_3	6.64	7.86	1.72	4.13	2.41	1.96	2.06	3.86
FeO	6.66	7.05	3.87	5.52	4.88	4.67	4.47	5.52
MnO	0.09	0.09	0.10	0.09	0.13	0.10	0.14	0.11
MgO	12.61	11.95	15.96	14.02	16.06	15.97	15.80	14.66
CaO	24.03	23.72	22.99	23.78	23.19	23.61	22.73	23.48
Na_2O	0.22	0.24	0.21	0.34	0.26	0.32	0.26	0.25
Total	98.80	97.79	97.33	99.35	99.16	99.77	97.92	99.14
Number of Ions Calculated Based on 6 Oxygen Atoms								
Si	1.812	1.765	1.949	1.884	1.914	1.933	1.937	1.888
Ti^{+4}	0.014	0.020	0.012	0.021	0.017	0.016	0.015	0.015
Cr^{+3}	0.002	0.003	0.007	0.003	0.003	0.003	0.007	0.002
Al	0.295	0.355	0.076	0.181	0.105	0.085	0.091	0.170
Fe^{+2}	0.210	0.226	0.122	0.172	0.152	0.144	0.140	0.172
Mn	0.003	0.003	0.003	0.003	0.004	0.003	0.004	0.003
Mg	0.710	0.682	0.895	0.778	0.889	0.877	0.882	0.814
Ca	0.972	0.973	0.926	0.948	0.923	0.932	0.913	0.938
Na	0.016	0.018	0.015	0.025	0.019	0.023	0.019	0.018
Percentage of End Members (unnormalized to 100%)								
Fs	11.72	12.93	7.14	10.33	9.04	8.54	8.35	9.8
En	35.48	34.11	44.73	38.90	44.45	43.87	44.12	40.72
Wo	48.60	48.67	46.31	47.42	46.13	46.62	45.63	46.88
Jadeite	1.9	1.8	1.6	1.8	1.5	2.5	1.9	2.3

Table 3.7. Composition of clinopyroxenes in mantle lherzolite (a xenolith in TB1)

	CpxLh1	CpxLh2	CpxLh3	CpxLh4
SiO_2	52.31	52.37	51.86	51.79
TiO_2	0.25	0.24	0.22	0.26
Cr_2O_3	1.47	1.17	1.34	1.42
Al_2O_3	5.31	5.00	5.02	5.33
FeO	2.41	2.44	2.28	2.48
MnO	0.03	0.02	0.08	0.10
MgO	15.68	15.74	15.79	15.74
CaO	20.24	20.83	20.99	20.63
Na_2O	1.36	1.32	1.21	1.34
Total	99.06	99.13	98.79	99.09
Number of Ions Calculated Based on 6 Oxygen Atoms				
Si	1.907	1.911	1.901	1.894
Ti^{+4}	0.007	0.007	0.006	0.007
Cr^{+3}	0.042	0.034	0.039	0.041
Al	0.228	0.215	0.217	0.230
Fe^{+2}	0.073	0.074	0.070	0.076
Mn	0.001	0.001	0.002	0.003
Mg	0.852	0.856	0.863	0.858
Ca	0.791	0.814	0.824	0.808
Na	0.096	0.093	0.086	0.095
Percentage of End Members (unnormalized to 100%)				
Fs	4.2	4.3	4.1	4.5
En	42.6	42.8	43.1	42.9
Wo	39.5	40.7	41.2	40.4
Jadeite	9.6	9.3	8.6	9.5

0.69%), but lower MgO (11.95-12.6%). These high FeO an Al_2O_3 diopsides contain some $Ca(Al,Ti)AlSiO_6$ molecular. Textural relations (see discussions in the previous section) indicate that these high FeO and Al_2O_3 diopsides crystallized at the latest stage in the fractures. The diopsides in the 2-phase pockets are usually strongly zoned in composition. FeO increases toward the margins (Table 3.6, where c stands for core, m for margin).

3.2.2.3 Phlogopite

The subhedral poikilitic groundmass phlogopites have very similar compositions to the elongated bladed crystals along linear weak zones. Both of them are very Mg-rich, with a Mg number (#Mg) greater than 0.8 (Table 3.8). They fall within the field of the phlogopites from ultramafic rocks on the $Mg - (Fe^{+2}+Mn) - (Ti+Fe^{+3}+Al^{vi})$ diagram (Fig. 3.5, Engel & Engel, 1960). But unlike phlogopites from almost all other rock types, these lamproite phlogopites have very high BaO (0.62-3.42%; Fig. 3.6). While the TiO_2 (1.24-2.93%), and FeO (7.15-9.22%) contents are comparable to those of lamproite phlogopites from around the world (Fig. 3.7), the Al_2O_3 content is generally higher than that of phlogopites in most other lamproites (Bergman, 1987; Mitchell, 1985). They are not Al-deficient in the tetrahedral site in their structure as normal lamproite phlogopites are. Actually, in their Al_2O_3, BaO and K_2O contents, these phlogopites are very similar to some phlogopites in the diamondiferous kimberlites from Orroroo, south Australia (Smith et al., 1984). One non-poikilitic blue-green mica crystal has much higher iron (FeO_T 21.6%, Table 3.8, sample 14), and is similar in color and in shape to the non-poikilitic mica chain along a fracture (see the previous section). This non-poikilitic mica could be an exotic later phase.

3.2.2.4 Analcime

The round anhedral analcimes in the groundmass and irregular aggregates around some phlogopites have similar compositions. They are MgO+FeO (0.75-5.37%) rich, and

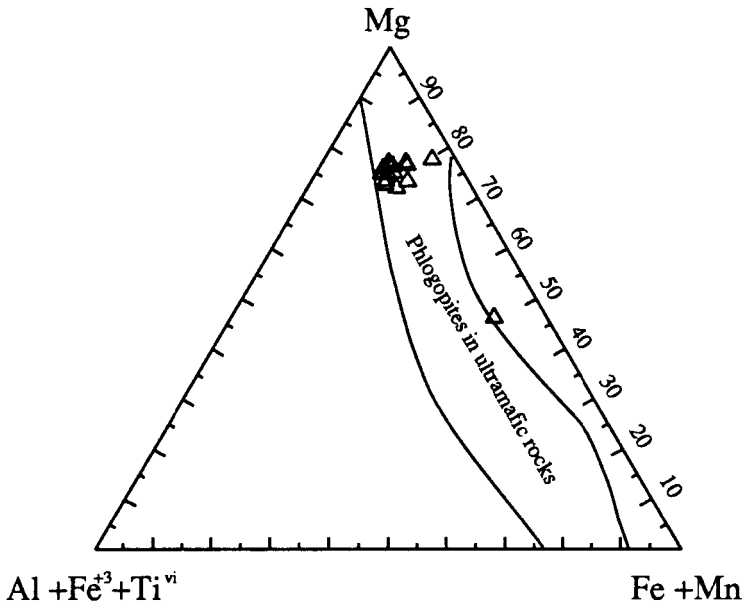

Fig. 3.5 Distribution of cations in the octahedral site in the crystal structure for the phlogopites in the Huzhiyan lamproites (Modified after Engel & Engel, 1960).

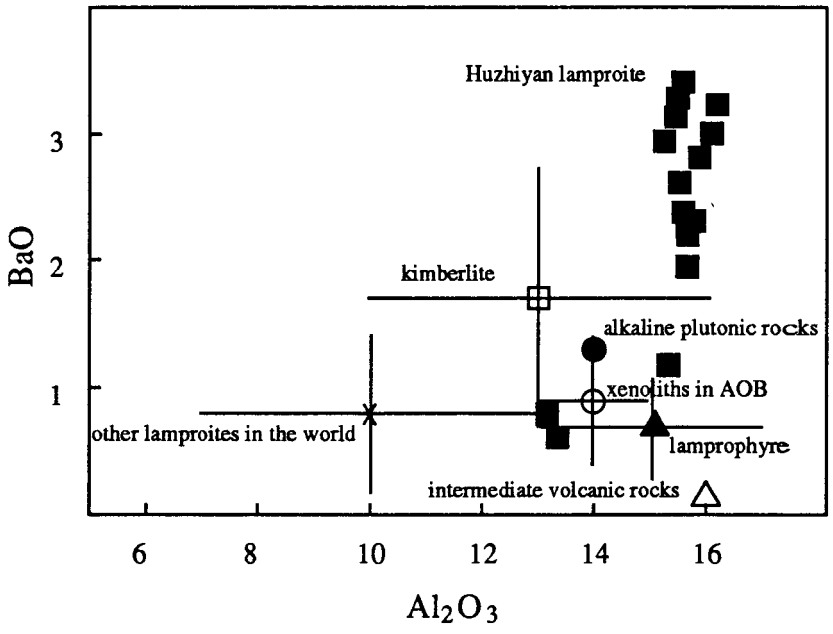

Fig. 3.6 BaO - Al_2O_3 plot showing the high BaO character of the Huzhiyan phlogopites compared to phlogopites in other igneous rocks from around the world (Data source: Bergman, 1987).

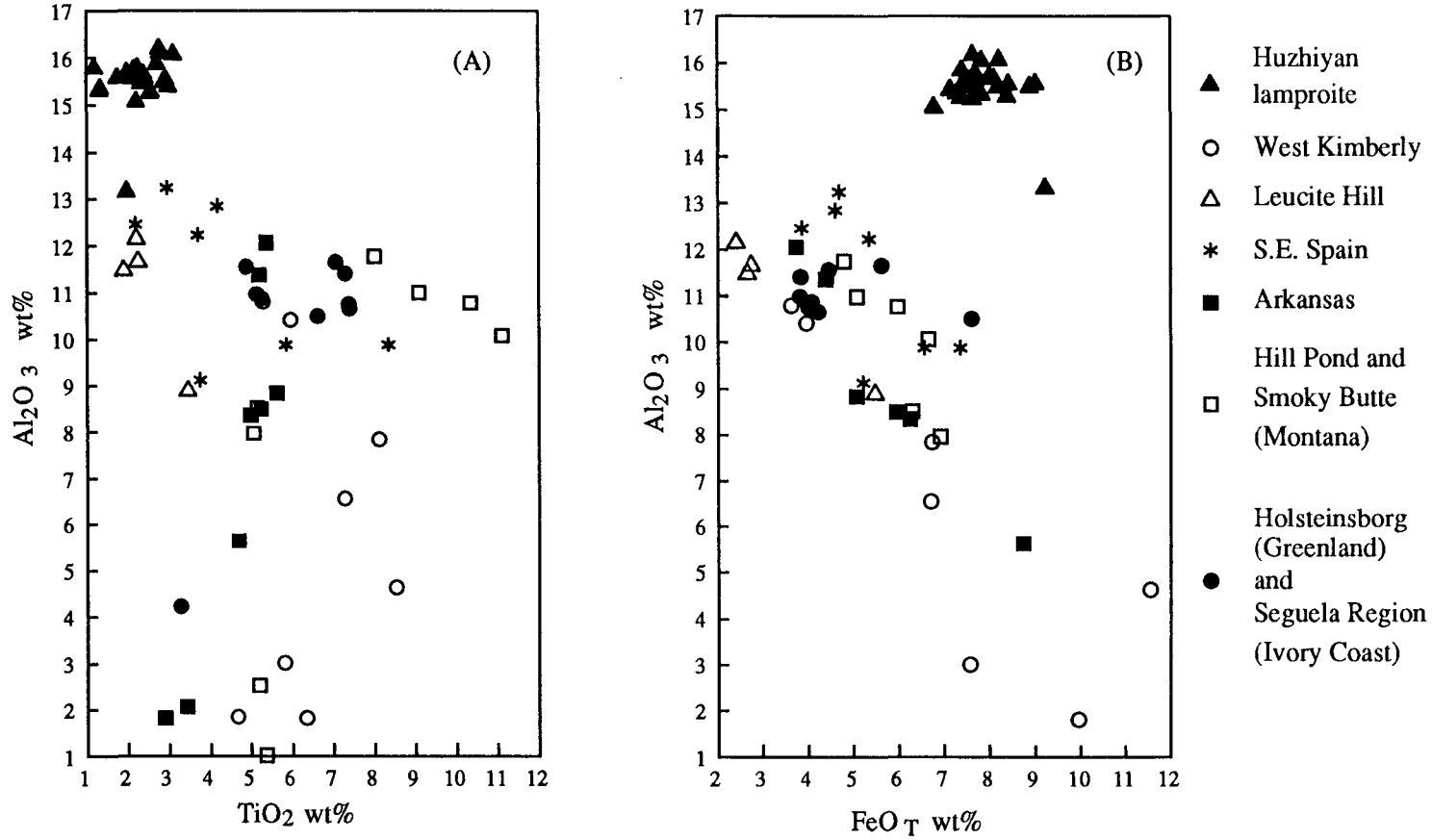

Fig. 3.7 Comparison of the Huzhiyan phlogopites with those from lamproites from around the world (Data other than the Huzhiyan phlogopites are from Mitchell, 1985, and Bergman, 1987).

Table 3.8. Composition of phlogopites in the Huzhiyan lamproites, (#)--# averaged. (sample 1-6 in Lam4, 9-14 in Lam1; c--core, m--margin)

	Phl1	Phl2	Phl3	Phl4 (4)	Phl5c	Phl5m	Phl6c	Phl6m
SiO_2	36.62	37.15	35.55	36.16	37.42	36.32	36.75	36.43
TiO_2	1.79	2.14	2.81	2.23	2.43	2.75	2.38	2.58
Al_2O_3	15.60	15.67	16.21	15.67	15.68	15.89	15.54	15.27
FeO	9.02	7.53	7.64	7.95	7.70	7.40	8.89	7.63
MnO	0.16	0.10	0.12	0.09	0.11	0.10	0.15	0.06
MgO	19.21	20.21	19.45	19.60	19.69	19.44	18.64	19.78
CaO	0.14	0.04	0.10	0.08	0.02	0.08	0.17	0.55
BaO	2.38	1.95	3.24	2.27	2.20	2.82	2.62	2.95
Na_2O	0.45	0.45	0.41	0.41	0.51	0.50	0.36	0.42
K_2O	9.13	9.35	8.48	8.89	9.11	8.76	8.89	8.62
Total	94.50	94.59	94.01	93.35	94.87	94.06	94.39	94.29
Number of Ions Calculated Based on 11 O Atoms								
Si	2.737	2.744	2.667	2.718	2.757	2.711	2.748	2.721
Ti	0.101	0.119	0.159	0.126	0.135	0.154	0.134	0.145
Al	1.374	1.364	1.433	1.388	1.362	1.398	1.369	1.344
Fe^{+3}	0.101	0.119	0.159	0.126	0.135	0.154	0.134	0.145
Fe^{+2}	0.463	0.346	0.321	0.374	0.340	0.308	0.422	0.332
Mn	0.010	0.006	0.008	0.006	0.007	0.006	0.009	0.004
Mg	2.140	2.225	2.175	2.196	2.163	2.163	2.077	2.202
Ca	0.011	0.003	0.008	0.006	0.002	0.006	0.014	0.044
Ba	0.070	0.056	0.095	0.067	0.064	0.082	0.077	0.086
Na	0.065	0.064	0.060	0.060	0.073	0.072	0.052	0.061
K	0.871	0.881	0.811	0.852	0.856	0.834	0.848	0.821
#Mg	0.819	0.863	0.869	0.853	0.862	0.873	0.828	0.868
Fe^{+2}+Mn	0.473	0.353	0.328	0.379	0.347	0.314	0.432	0.335
Mg	2.140	2.225	2.175	2.196	2.163	2.163	2.077	2.202
Ti+Fe^{+3}+Al	0.313	0.346	0.417	0.358	0.388	0.417	0.385	0.354

Table 3.8. Continued

	Phl9c	Phl9m	Phl10	Phl11 (3)	Phl12	Phl13	Phl14c	Phl14m (2)
SiO_2	36.81	37.19	36.16	36.02	36.64	38.24	36.30	37.61
TiO_2	2.37	1.24	2.92	2.93	2.83	0.70	2.01	1.37
Al_2O_3	15.47	15.80	15.51	15.60	16.11	13.36	13.18	15.35
FeO	7.15	7.70	8.19	7.51	8.21	9.22	21.60	8.12
MnO	0.10	0.08	0.10	0.09	0.16	0.12	0.40	0.15
MgO	20.02	20.53	18.52	19.79	19.32	20.72	11.75	20.73
CaO	0.10	0.08	0.08	0.07	0.07	0.00	0.11	0.07
BaO	3.14	2.31	3.29	3.42	3.01	0.62	0.80	1.18
Na_2O	0.60	0.37	0.35	0.43	0.37	0.41	0.30	0.41
K_2O	9.04	9.31	8.80	8.58	8.80	9.90	8.88	8.87
Total	94.80	94.61	93.92	94.44	95.52	93.29	95.33	93.86
Number of Ions Calculated Based on 11 O Atoms								
Si	2.734	2.753	2.724	2.692	2.704	2.865	2.827	2.780
Ti	0.132	0.069	0.165	0.165	0.157	0.039	0.118	0.076
Al	1.354	1.379	1.377	1.374	1.401	1.180	1.210	1.337
Fe^{+3}	0.132	0.069	0.165	0.165	0.157	0.039	0.118	0.076
Fe^{+2}	0.312	0.408	0.351	0.305	0.350	0.538	1.289	0.426
Mg	2.216	2.266	2.080	2.205	2.125	2.314	1.364	2.284
Ca	0.008	0.006	0.006	0.006	0.006	0.000	0.009	0.006
Ba	0.091	0.067	0.097	0.100	0.087	0.018	0.024	0.034
Na	0.086	0.053	0.051	0.062	0.053	0.060	0.045	0.059
K	0.856	0.879	0.846	0.818	0.829	0.946	0.882	0.836
#Mg	0.875	0.846	0.854	0.877	0.855	0.809	0.509	0.840
Fe+Mn	0.318	0.413	0.357	0.310	0.360	0.546	1.316	0.435
Mg	2.216	2.266	2.080	2.205	2.125	2.314	1.364	2.284
$Ti+Fe^{+3}+Al$	0.352	0.270	0.433	0.395	0.420	0.124	0.273	0.269

#Mg stands for Mg number, Fe^{+3}/Fe^{+2} ratio is calculated by charge balance.

show intergrain composition change, especially in Na_2O, CaO and MgO (Table 3.9). The origin of analcime in lamproite is a matter of debate. Velde (1975) suggested that the analcime in the lamproites from Smoky butte, Montana is a low-temperature secondary phase which replaced original leucite. However, neither leucite nor nepheline was found in the Huzhiyan rocks. The analcimes which contain inclusion of other minerals are more likely a late stage magmatic phase. The intergrain change in composition may reflect a small scale inhomogeneity of the magma when the analcimes crystallized. The analcimes around phlogopite (plate 7b) are definitely a secondary phase after the phlogopite.

3.2.2.5 K-feldspar

The K-feldspars in the Huzhiyan rocks are limited mainly to the 2-phase pockets, and are one of the last phases to crystallize. Unlike the analcimes in the rocks, the feldspars show little intergrain change in composition. These feldspars are very potassium-rich, with K_2O greater than 16% (Or > 97.5%), Na_2O+BaO+CaO less than 1% (Fig. 3.8; Table 3.10), typical for the K-feldspars in lamproites (Bergman, 1987). But compared to other lamproite K-feldspars, the Huzhiyan K-feldspars are not as high in FeO_T.

3.2.3 Summary

In conclusion, the mineral assemblage of the Huzhiyan rocks is exotic, different from the basanites and trachybasalts or any ordinary alkaline rocks. It is broadly similar to the mineral assemblages of lamproites from Smoky Butte, Montana (Velde, 1975) and from Kamas & Moon Canyon, Utah (Morris, 1953; Best et al., 1968). The mineral chemistry of the major phases (olivine, clinopyroxene, phlogopite, K-feldspar and analcime) in the rocks show more affinities to lamproites than to any other rock families. The high SiO_2 content (near 50%) of the rocks is incompatible with kimberlite; the absence of plagioclase precludes them to be an ordinary alkaline mafic or ultramafic rocks. Therefore, the Huzhiyan rocks are classifed as madupitic olivine lamproite in this study. The modifier

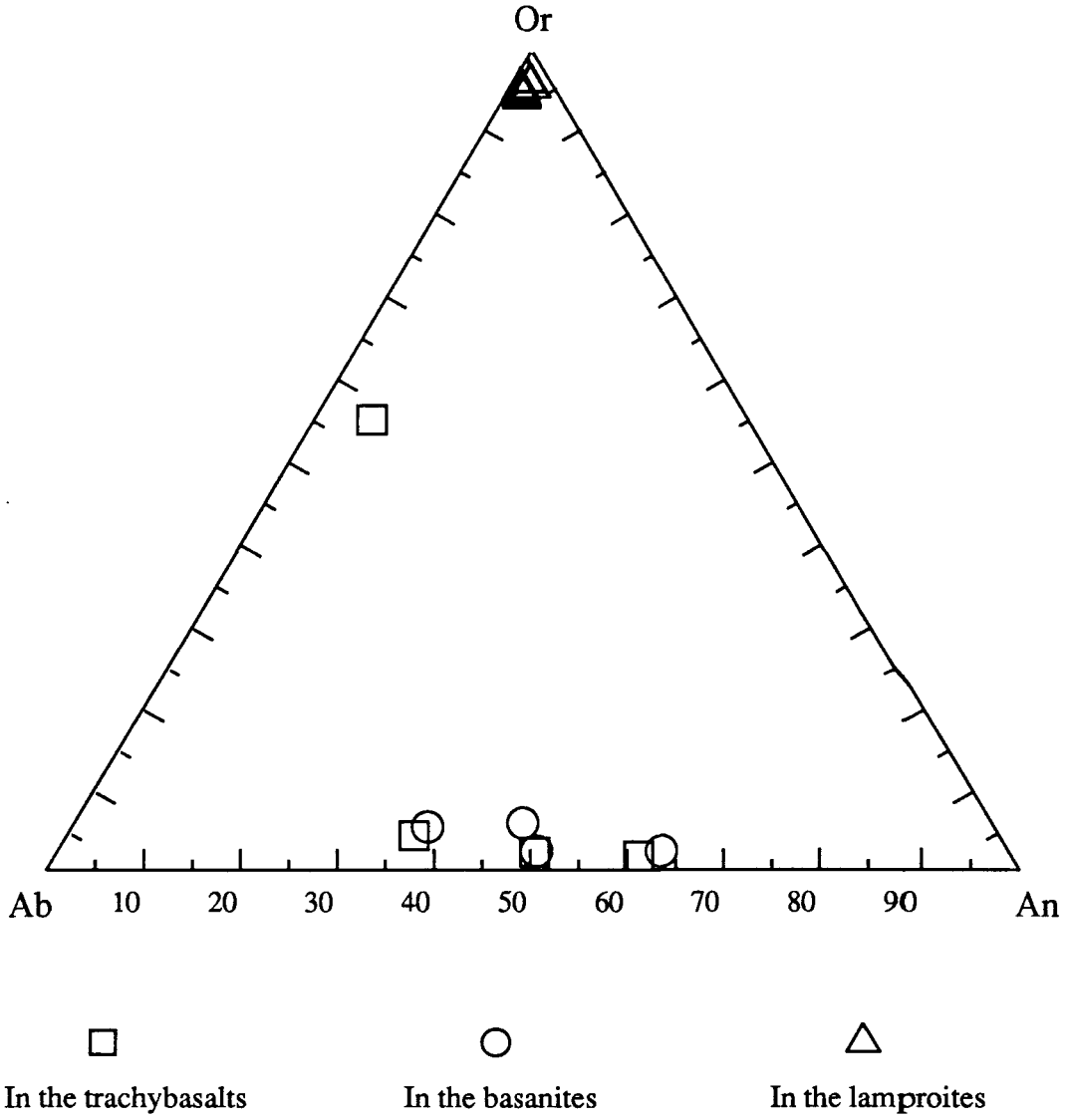

Fig. 3.8 Or-Ab-An diagram showing the range in compostion of the feldspars in the alkaline rocks from the inland subvolcanic belt of southern China.

Table 3.9. Composition of analcimes in the Huzhiyan lamproites (in Sample Lam4)

	Anal1	Anal2	Anal3	Anal4	Anal5	Anal6	Anal7	Anal8
SiO_2	59.19	54.93	53.81	56.03	56.88	57.98	54.26	58.21
Al_2O_3	22.43	22.09	21.21	22.49	21.51	21.95	20.65	22.36
TiO_2	0.03	0.00	0.01	0.00	0.05	0.05	0.09	0.06
FeO	0.62	0.57	1.64	0.13	0.62	0.44	0.63	3.55
MnO	0.04	0.04	0.08	0.00	0.02	0.02	0.06	0.02
Na_2O	4.18	10.58	8.36	11.82	8.56	5.82	7.15	8.71
MgO	1.74	2.87	3.73	0.05	0.13	0.98	3.00	0.81
K_2O	0.50	0.28	1.10	0.28	0.76	0.34	0.46	0.41
CaO	2.78	0.70	0.56	0.78	1.20	2.13	3.13	0.99
Total	91.50	92.07	90.52	91.59	89.73	89.84	89.42	91.93
Cations Based on 6 Oxygen Atoms								
Si	2.107	1.999	1.999	2.044	2.098	2.111	2.025	2.055
Al	0.941	0.947	0.929	0.967	0.935	0.942	0.908	0.930
Ti^{+4}	0.001	0.000	0.000	0.000	0.001	0.001	0.003	0.002
Fe^{+2}	0.018	0.017	0.051	0.004	0.019	0.013	0.020	0.105
Mn	0.001	0.001	0.003	0.000	0.001	0.001	0.002	0.001
Na	0.289	0.747	0.602	0.836	0.612	0.411	0.517	0.596
Mg	0.092	0.156	0.207	0.003	0.007	0.053	0.167	0.043
K	0.023	0.013	0.052	0.013	0.036	0.016	0.022	0.018
Ca	0.106	0.027	0.022	0.030	0.047	0.083	0.125	0.037
Total	3.578	3.907	3.864	3.897	3.757	3.631	3.788	3.786

Table 3.10. Composition of K-feldspars in the Huzhiyan lamproites (in smaple Lam4)

	Feld1	Feld2	Feld3	Feld4	Feld5	Feld6	Feld7	Feld8
SiO_2	64.94	64.61	64.11	64.56	64.35	64.45	63.83	64.04
TiO_2	0.03	0.01	0.01	0.01	0.01	0.01	0.07	0.03
Al_2O_3	17.55	16.99	18.51	17.84	18.02	17.21	18.66	18.64
FeO	0.36	0.75	0.19	0.30	0.25	0.86	0.20	0.10
CaO	0.06	0.05	0.03	0.04	0.03	0.00	0.10	0.02
BaO	0.18	0.30	0.15	0.56	0.11	0.17	0.26	0.12
Na_2O	0.28	0.30	0.13	0.11	0.11	0.24	0.13	0.27
K_2O	16.48	16.32	16.67	16.57	16.67	16.41	16.47	16.44
Total	99.88	99.33	99.80	99.99	99.55	99.35	99.72	99.66
Number of Ions Calculated Based on 8 O Atoms								
Si	3.017	3.027	2.982	3.005	3.000	3.018	2.973	2.979
Ti	0.001	0.000	0.000	0.000	0.000	0.000	0.002	0.001
Al	0.961	0.938	1.015	0.979	0.990	0.950	1.024	1.022
Fe	0.014	0.029	0.007	0.012	0.010	0.034	0.008	0.004
Ca	0.003	0.003	0.001	0.002	0.001	0.000	0.005	0.001
Ba	0.003	0.006	0.003	0.010	0.002	0.003	0.005	0.002
Na	0.025	0.027	0.012	0.010	0.010	0.022	0.012	0.024
K	0.977	0.975	0.989	0.984	0.991	0.980	0.979	0.976
Percentage of End members								
An	0.6	0.8	0.4	1.2	0.4	0.3	1.0	0.3
Ab	2.5	2.7	1.2	1.0	1.0	2.2	1.2	2.4
Or	97.7	97.5	98.9	98.4	99.1	98.0	97.9	97.6

"madupitic olivine" comes from Mitchell's (1985) terminology. It should be pointed out that though the mineral assemblage is consistent with the lamproite family, the phases in the Huzhiyan rocks are not as poor in Al_2O_3, or as rich in TiO_2 as phases in typical lamproites.

3.3 PLAGIOCLASE-BEARING ROCKS

3.3.1 Texture and Mineralogy

3.3.1.1 Basanites

The basanites are porphyritic rocks (plate 8). They consist of subhedral to anhedral olivine megacrysts (0.05-0.8 mm, 10-15%), subhedral clinopyroxene megacrysts (0.2-0.5 mm, less than 1%), tabular labradorite (0.2-0.5 mm 3-5%, see Table 3.11 for chemical composition) and euhedral opaque minerals (ilmenite, ulvöspinel, Table 3.1; 0.05-0.2 mm, 5-8%) set in a very fine groundmass which is composed of prismatic plagioclase (0.03-0.05, 30-35%) intergrown with small subhedral clinopyroxene (0.02-0.1 mm, 25-30%) and interstitial anhedral mineral (0.01 mm, about 10%) with low relief, dark grey bireference color and diffuse boundaries which could be alkali feldspar and/or analcime (plate 9). There are some small euhedral brown biotites and kaersutite (?) (0.02-0.05 mm, 1-2%, plate 10) and minor amounts of euhedral apatite in the matrix.

Olivine phenocrysts have reacted with the groundmass to form a rim of secondary hydrous minerals (plate 11), which indicates that the olivine phenocrysts were not in equilibrium with the magma.

These rocks fall in the phonolitic basanite field in the Alkali-feldspar – Plagioclase – Foid mineral classification diagram (Streckeisen, 1979) using modal phase percentage estimated above (Fig. 3.9). Equal amounts of alkali feldspar and analcime are assumed out of their estimated total of 10%. Analcime is treated as a foid mineral in constructing the diagram. For comparison, the rocks are also projected on the diagram using the normative

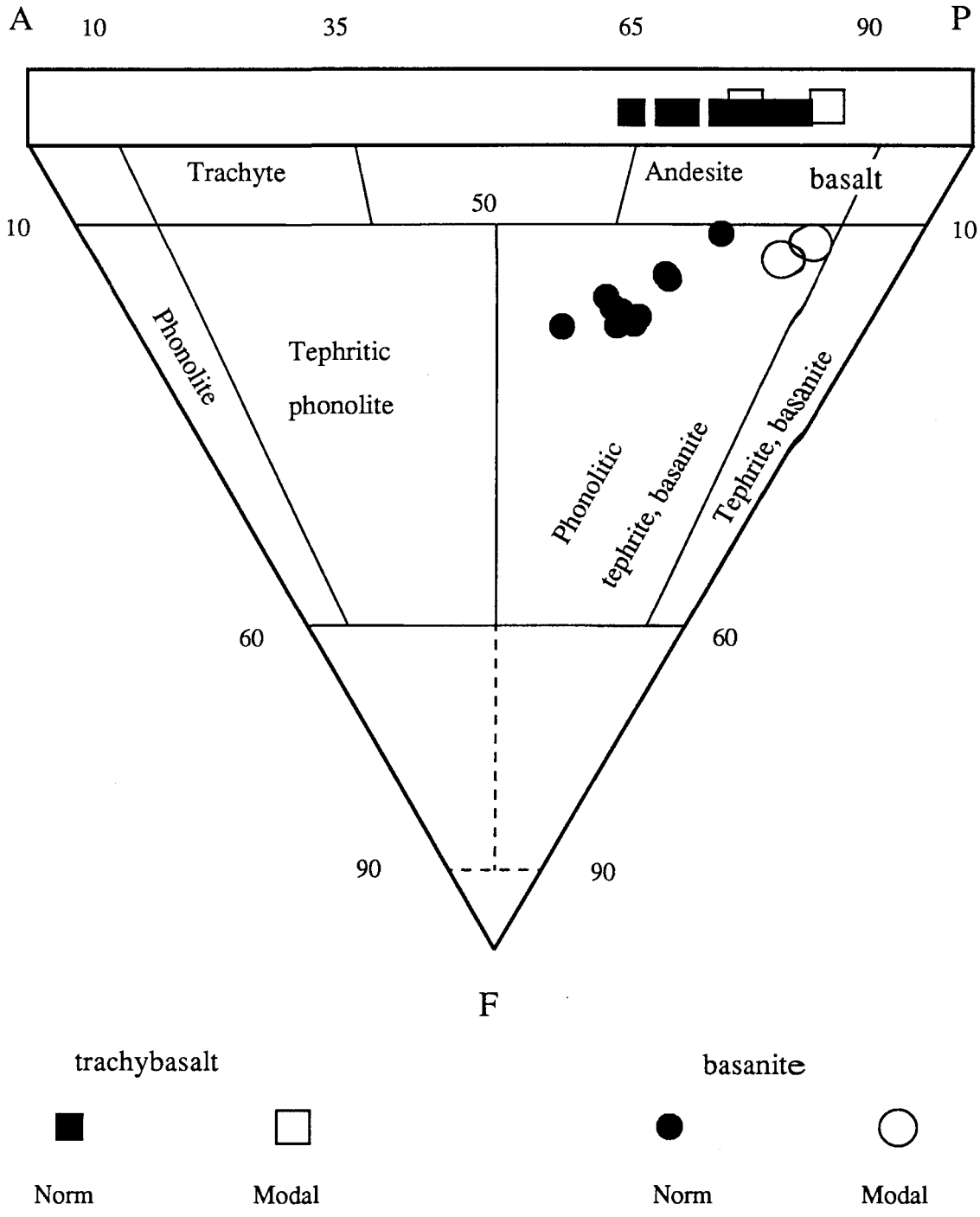

Fig. 3.9 Mineralogical classification of the inland alkaline rocks of southern China (Modal division after Streckeisen, 1979).

Table 3.11. Composition of plagioclases in the trachybasalts and basanites
TBfs--feldspar in TB5 (Tab4.3), BPl--Plag. in Bas4 (Tab4.2)

	TBfs1	TBfs2	TBfs3	TBfs4	Bpl1	Bpl2	Bpl3	Bpl4
SiO_2	57.35	63.90	54.27	52.59	55.06	51.83	58.82	56.31
TiO_2	0.18	0.18	0.11	0.05	0.10	0.17	0.18	0.25
Al_2O_3	25.56	20.12	27.79	29.93	27.33	30.25	25.48	26.73
FeO	0.96	0.24	0.65	0.05	0.82	0.13	0.04	0.07
MgO	0.43	0.10	0.05	0.00	0.09	0.05	0.13	0.08
CaO	7.30	1.10	10.07	12.24	10.13	12.72	7.54	9.57
Na_2O	6.73	4.28	5.44	4.23	5.43	3.96	6.56	5.43
K_2O	0.75	9.61	0.40	0.31	0.42	0.42	0.92	1.02
Total	99.26	99.53	98.78	99.40	99.38	99.53	99.67	99.46
Number of Ions Based on 8 Oxygen Atoms								
Si	2.601	2.913	2.484	2.396	2.506	2.365	2.641	2.551
Ti	0.006	0.006	0.004	0.002	0.003	0.006	0.006	0.009
Al	1.366	1.081	1.499	1.607	1.466	1.627	1.348	1.427
Fe	0.036	0.009	0.025	0.002	0.031	0.005	0.002	0.003
Mg	0.029	0.007	0.003	0.000	0.006	0.003	0.009	0.005
Ca	0.355	0.054	0.494	0.597	0.494	0.622	0.363	0.464
Na	0.592	0.378	0.483	0.374	0.479	0.350	0.571	0.477
K	0.043	0.559	0.023	0.018	0.024	0.024	0.053	0.059
Percentage of End Members								
An	35.5	5.4	49.4	59.7	49.4	62.2	36.3	46.4
Ab	59.2	37.8	48.3	37.4	47.9	35.0	57.1	47.7
Or	4.3	55.9	2.3	1.8	2.4	2.4	5.3	5.9

percentages of plagioclase, orthoclase+albite and nepheline in place of the estimated percentages of these minerals. This also classifies these rocks as phonolitic basanite. The rocks are transitional, however, between basanite and trachybasalt on Le Bas's chemical classification diagram (Le Bas, 1986; Chapter 4 Fig. 4.1). Despite their transitional character, these rocks will be referred to as basanite rather than phonolitic basanite or trachybasalt in this work, because (1) Le Bas's diagram shows the alkali contents of these rocks are not high enough to qualify them as phonolitic basanite; (2) if some of the alkali feldspars are actually analcime, the rocks will shift from the phonolitic basanite field toward the basanite field; (3) these rocks are different petrographically and chemically from trachybasalts described below.

3.3.1.2 Trachybasalts

The trachybasalts are porphyritic rocks with a groundmass having a trachytic texture (plate 12). These rocks contain megacrysts of olivine (0.2-1 mm, 3-5%) and clinopyroxene (0.5-0.1 mm, less than 1%). The groundmass is composed mainly of subparallel laths or tabular crystals of plagioclase (0.05-0.5 mm, 50-55%, plate 12) with interstitial short tabular clinopyroxene (0.02-0.05 mm, 15-20%) and anhedral alkali feldspar (about 0.05 mm, 8-10%, Table 3.11). About 10% opaque minerals (0.05-0.2 mm), which are ilmenite or ulvöspinel (Table 3.1), are dispersed in the groundmass (plate 13). Apatites and biotite occur in minor amounts (less than 1%). Thin calcite veins (<1%) are found along fractures in the rocks (Plate 14). They are interpreted as the result of post-magmatic interaction with wall-rock carbonates.

Most olivine phenocrysts in the trachybasalts reacted with the groundmass around the margin and along the fractures forming H_2O-bearing secondary mineral rims or aggregates (plate 15).

3.3.2 Mineral Chemistry

3.3.2.1 Olivine

The olivine megacrysts in the trachybasalt and basanite are similar in composition (Table 3.4 & 3.5). They can be divided into xenocrysts and phenocryts on the basis of their shape and composition. The phenocrysts are subhedral, and relatively Fe-rich, ranging from Fo_{64} to Fo_{84} (Fig. 3.1, Tables 4 & 5, where p stands for phenocryst). The cores of the phenocrysts have higher Fo and Ni contents and lower Mn and Ca contents than the margins (Fig. 3.1, Tables 3.4 & 3.5). In contrast, the xenocrysts, which are interpreted to come from broken mantle xenoliths, are irregular in shape, homogeneous in composition and more magnesium rich (around Fo_{90}) than the phenocrysts (Fig. 3.1, Tables 3.4 & 3.5, where x stands for xenolith). Actually, the xenocrysts are very similar to olivines in lherzolite xenoliths (compare Tables 3.4, 3.5 and 3.3).

3.3.2.2 Pyroxenes

The pyroxenes, which appear both as megacrysts and as a groundmass phase in the plagioclase-bearing rocks, are mostly diopsidic; but a few megacrysts of orthopyroxene are present in the trachybasalts (1-2%, Fig. 3.3). The orthopyroxene megacrysts are very similar in composition to those orthopyroxenes in mantle lherzolite (Table 3.12, where OpxT stands for opx megacryst in the trachybasalts, OpxLh stands for opx in the lherzolite xenoliths from the rocks). They are very probably xenocrysts, because in alkaline rocks orthopyroxene is generally not present. Clinopyroxene megacrysts in the trachybasalts and basanites are clustered around $Wo_{38\text{-}43}$ $En_{38\text{-}45}$ $Fs_{3.5\text{-}16.5}$ (Table 3.13). Beside quadrilateral components, the megacryst pyroxenes in trachybasalts contain 8.8-12.2 mole% of $NaAlSiO_6$ and/or $NaCrSiO_6$, and those in basanites contain about 5% non-quadrilateral components. Compared to lherzolite diopside (Table 3.6), megacryst diopside in the basanites contains less Cr_2O_3 and Al_2O_3; megacryst diopside in trachybasalt is poorer in Cr_2O_3, but richer in TiO_2 and Al_2O_3 (Fig. 3.4). The groundmass pyroxenes are very small interstitial grains,

Table 3.12. Composition of orthopyroxenes in lherzolites and trachybasalts (OpxLh-- Opx in a lherzolite xenolith in sample TB6; OpxT-- Opx megacryst in TB5)

	OpxLh1	OpxLh2	OpxLh3	OpxLh4	OpxLh5	OpxLh6	OpxT1	OpxT2
SiO_2	56.38	56.28	55.84	55.98	55.57	53.92	54.71	55.86
TiO_2	0.06	0.01	0.06	0.08	0.04	0.14	0.11	0.08
Cr_2O_3	0.44	0.63	0.47	0.47	0.49	0.33	0.28	0.54
Al_2O_3	3.26	3.21	3.46	3.18	3.50	5.18	4.21	3.31
FeO	5.62	5.50	5.55	5.59	5.53	6.10	6.23	5.54
MnO	0.09	0.13	0.18	0.10	0.16	0.17	0.14	0.07
MgO	33.64	33.80	33.75	34.10	32.84	31.88	32.42	32.79
CaO	0.68	0.73	0.64	0.59	0.63	0.66	0.68	0.68
Na_2O	0.10	0.07	0.07	0.07	0.08	0.22	0.15	0.10
Total	100.27	100.36	98.97	100.02	100.15	98.85	98.59	98.91
Calculated Number of Ions Based on 6 Oxygen Atoms								
Si	1.934	1.930	1.922	1.924	1.934	1.889	1.910	1.940
Ti^{+4}	0.002	0.000	0.002	0.002	0.001	0.004	0.003	0.002
Cr^{+3}	0.012	0.017	0.013	0.013	0.013	0.009	0.008	0.015
Al	0.132	0.130	0.140	0.129	0.144	0.214	0.173	0.136
Fe^{+2}	0.161	0.158	0.160	0.161	0.161	0.179	0.182	0.161
Mn	0.003	0.004	0.005	0.003	0.005	0.005	0.004	0.002
Mg	1.720	1.728	1.732	1.747	1.703	1.665	1.687	1.698
Ca	0.025	0.027	0.024	0.022	0.023	0.025	0.025	0.025
Na	0.007	0.005	0.005	0.005	0.005	0.015	0.010	0.007
Percentage of End Members (unnormalized to 100%)								
Fs	8.31	8.10	8.31	8.37	8.34	8.36	9.46	9.52
En	86.02	86.40	84.89	86.58	87.36	85.16	83.23	84.34
Wo	1.25	1.34	1.27	1.18	1.09	1.17	1.24	1.27
Jadeite	0.70	0.50	0.70	0.50	0.50	0.50	1.50	1.00

Table 3.13. Composition of clinopyroxenes in the basanites and trachybasalts.
(CpxBg, Cpxbp in Bas4; CpxTg, CpxTp in TB5)
(Numbers in bracket are the number of analyses averaged, g--groundmass, p--phenocryst)

	CpxBg	CpxBp1	CpxBp2	CpxBp3	CpxTg	CpxTp1	CpxTp2	CpxTp3
	(2)				(3)			
SiO_2	51.70	51.97	51.93	52.44	51.54	50.32	51.24	51.81
TiO_2	0.41	0.10	0.08	0.07	0.71	1.05	0.58	0.56
Cr_2O_3	0.11	0.91	0.81	0.73	0.09	0.33	0.69	0.63
Al_2O_3	2.87	4.50	4.47	4.32	3.14	6.80	6.85	6.79
FeO	8.50	2.21	2.07	2.16	9.47	4.83	2.74	2.58
MnO	0.10	0.01	0.05	0.06	0.09	0.10	0.12	0.10
MgO	15.54	16.40	16.45	16.59	14.51	13.89	14.99	15.04
CaO	18.78	21.85	21.83	22.02	19.31	21.12	20.21	19.73
Na_2O	0.43	0.78	0.73	0.71	0.35	1.23	1.72	1.67
Total	98.44	98.73	98.42	99.10	99.21	99.67	99.14	98.91
Number of Ions Calculated Based on 6 Oxygen Atoms								
Si	1.937	1.906	1.909	1.914	1.927	1.849	1.871	1.888
Ti^{+4}	0.012	0.003	0.002	0.002	0.020	0.029	0.016	0.015
Cr^{+3}	0.003	0.026	0.024	0.021	0.003	0.010	0.020	0.018
Al	0.127	0.195	0.194	0.186	0.138	0.295	0.295	0.292
Fe^{+2}	0.266	0.068	0.064	0.066	0.296	0.148	0.084	0.079
Mn	0.003	0.000	0.002	0.002	0.003	0.003	0.004	0.003
Mg	0.868	0.897	0.901	0.903	0.809	0.761	0.816	0.817
Ca	0.754	0.859	0.860	0.861	0.774	0.832	0.791	0.770
Na	0.031	0.055	0.052	0.050	0.025	0.088	0.122	0.118
Percentage of End Members (unnormalized to 100%)								
Fs	14.35	3.61	3.43	3.53	16.45	9.75	5.56	5.24
En	43.40	44.83	45.06	45.14	40.44	38.04	40.79	40.85
Wo	37.70	42.93	42.99	43.06	38.68	41.58	39.53	38.52
Jadeite	3.1	5.5	5.2	5.0	2.5	8.8	12.2	11.8

and therefore difficult to analyse. The five available analyses indicate that the groundmass clinopyroxene in the basanites is similar in composition to that in the trachybasalts. They are also diopsidic; but contain more FeO. They are poorer in CaO, Al_2O_3, and Cr_2O_3 than megacryst pyroxenes (Fig. 3.4, Table 3.12, where g stands for groundmass, p for phenocryst).

3.3.2.3 Feldspars

Plagioclase is the most important feldspar in the basanites, but alkali feldspars are significant in the trachybasalts. The plagioclases are broadly similar in composition in the basanites and trachybasalts, ranging from labradorite to andesine (Table 3.11), but they differ texturally. In basanite, plagioclases appear as two distinct generations: tabular phenocrysts with labradoritic composition ($An_{49.4}$-$An_{62.2}$) and groundmass thin laths ($An_{36.3}$-$An_{46.4}$). In trachybasalt, plagioclases are gradational in size, shape and twin habit: from larger slender laths with well-developed twins to smaller tabular or subhedral crystals with fewer twins. Accompanying this shape and size change, the composition changes from labradorite (An_{62}) to andesine (An_{35}) (Table 3.11). This compositional change is limited to the zone approaching ideal solid solution of An and Ab (Or < 6 mole%, Fig. 3.8), and is caused by Na_2O increase toward the late magmatic stage. At a late stage of the magma crystallization, plagioclase changed to alkali feldspar with a composition of $Or_{55.9}Ab_{37.8}An_{5.4}$ (Table 3.11, Fig. 3.8).

3.4 XENOLITHS

Two type of xenoliths are found in the inland alkaline mafic subvolcanic rocks: small (less than 8 cm in diameter) mantle-derived peridotite xenoliths and larger (about 10-15 cm in diameter) crustal fragments. Mantle xenoliths collected in this study include lherzolite, harzburgite, and websterite (Fig. 3.10). Lherzolite xenoliths appear in all the subvolcanic rocks and are far more common than the other two types of xenoliths. The basanites in Juxiang carry lherzolite and harzburgite xenoliths which are small (0.5-2 cm) and abundant. The trachybasalts in Ningyuan have lherzolite and websterite xenoliths. The former are larger (2-8 cm) and more common. Besides these peridotite xenoliths, the lamproites in Huzhiyan carry a number of round gabbro xenoliths (usually 10-15 cm in diameter) which are strongly deformed. Some of these gabbros have a layered structure in which thinner clinopyroxene layers are interlaced with plagioclase (plate 16).

Lherzolite xenoliths from Ningyuan are composed of 60-65% olivine (Table 3.3 for composition), 20-25% enstatite (Table 3.12), 10-20% diopside (Table 3.7) and small amount of spinel (Table 3.1) with a granoblastic texture (plate 17). In these lherzolite xenoliths, enstatites are equilibrated with diopsides as indicated by their trilateral boundary (plate 18).

Harzburgite is similar in texture to the lherzolite, except that there is little clinopyroxene, and that olivine is more abundant (upto about 70%). Collected websterite xenoliths are less fresh. They are dark green to black, and contain about 40% clinopyroxene.

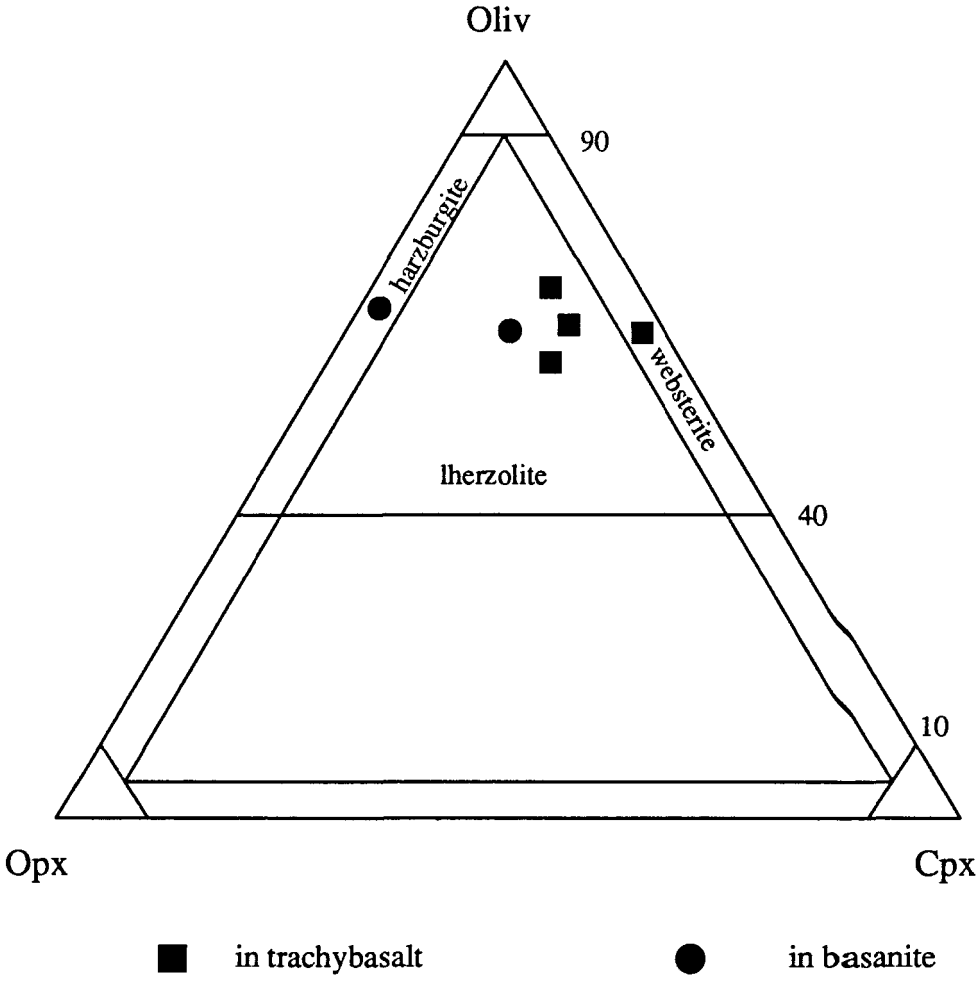

Fig. 3.10 Mineralogical Classification of the mantle-derived xenoliths from the inland subvolcanic rock belt of southern China (Modal division after Streckeisen, 1967)

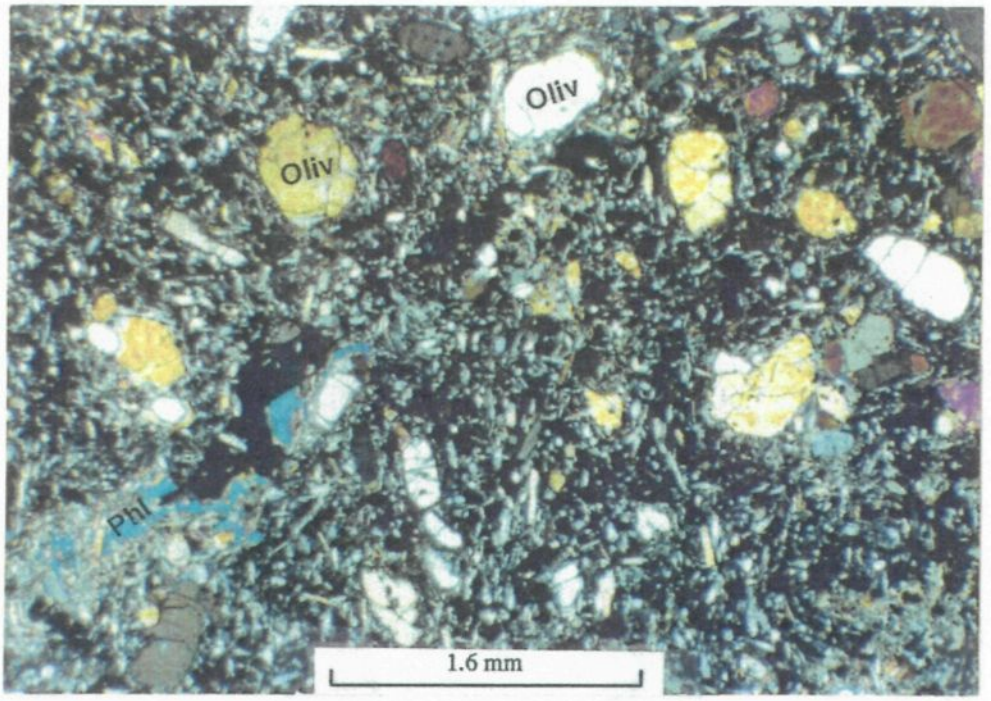

Plate 1a. Porphyritic texture of the Huzhiyan lamproites: olivine megacrysts are set in a fine groundmass composed of mainly clinopyroxenes, poikilitic phlogopites, alkali feldspar, analcimes and opaque minerals. Crossed nicols.

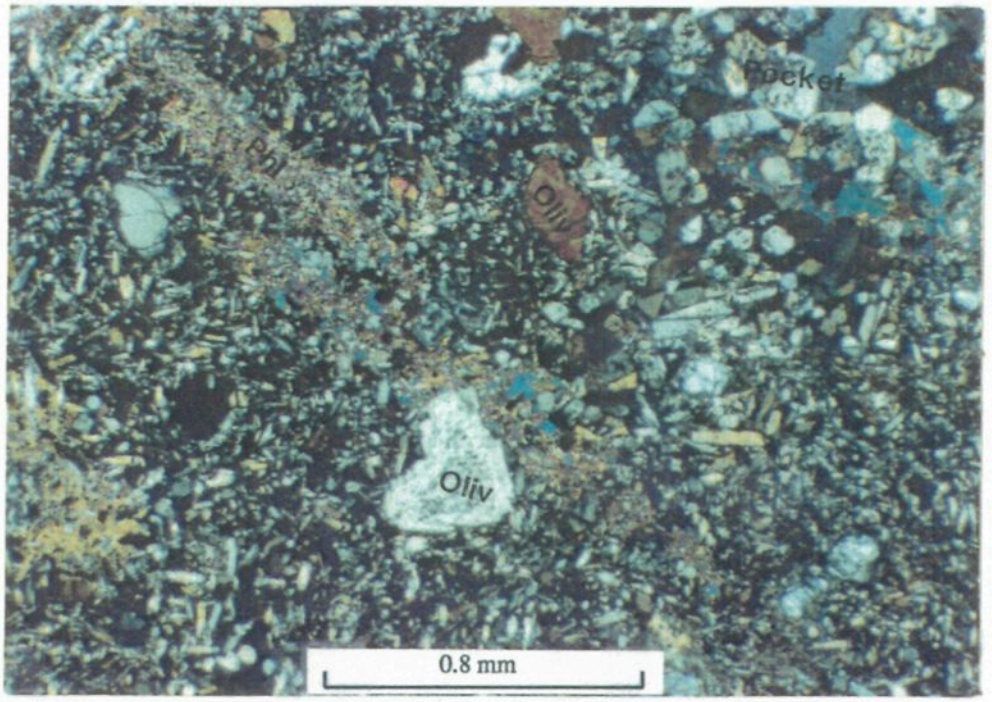

Plate 1b. The lamproite groundmass is very inhomogeneous, a mixture of elongated poikilitic phlogopites (Phl), alkali feldspar-and-clinopyroxene-enriched pocket areas (pocket) and fine 'normal groundmass'. Crossed nicols.

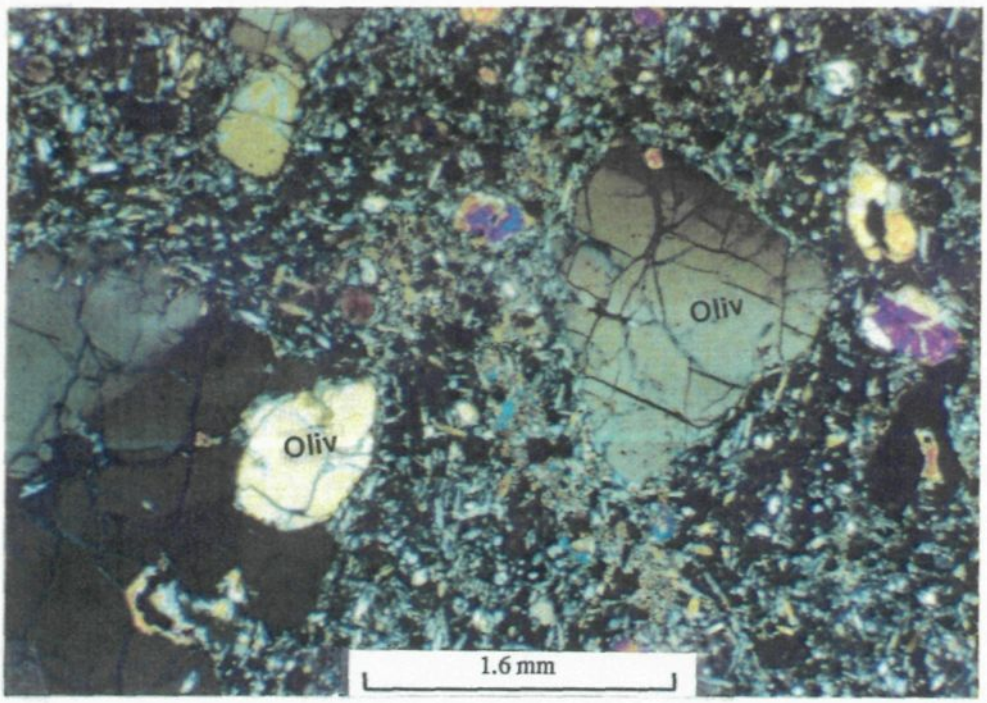

Plate 2. Undulatory extinction of the anhedral olivine xenocrysts in the lamproites indicates that the xenocrystic olivines had been deformed before being included in the lamproites. Crossed nicols.

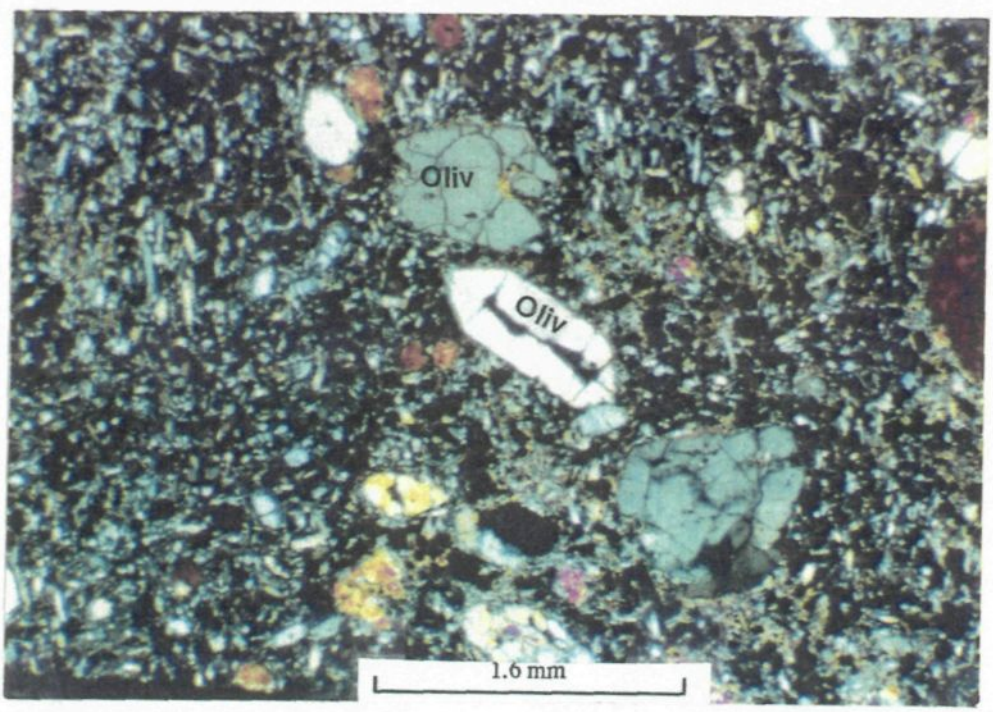

Plate 3. Euhedral olivine phenocrysts in the lamproites are often skeletal crystals. Crossed nicols.

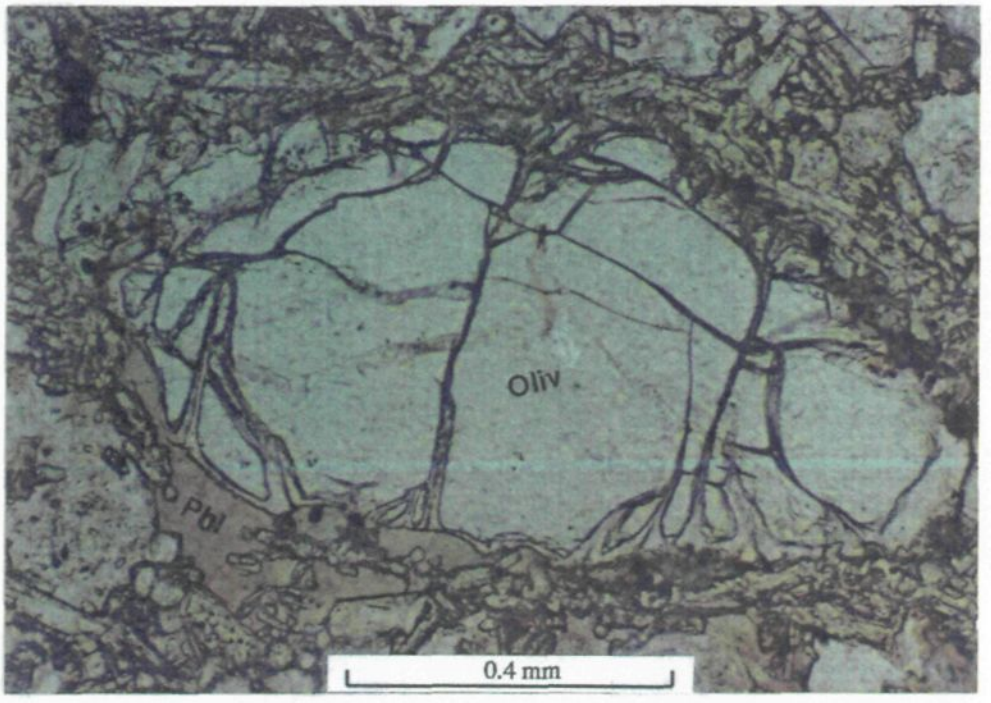

Plate 4. Some olivine megacrysts in the lamproite have been altered around the margin forming secondary phlogopites (phl). Crossed nicols.

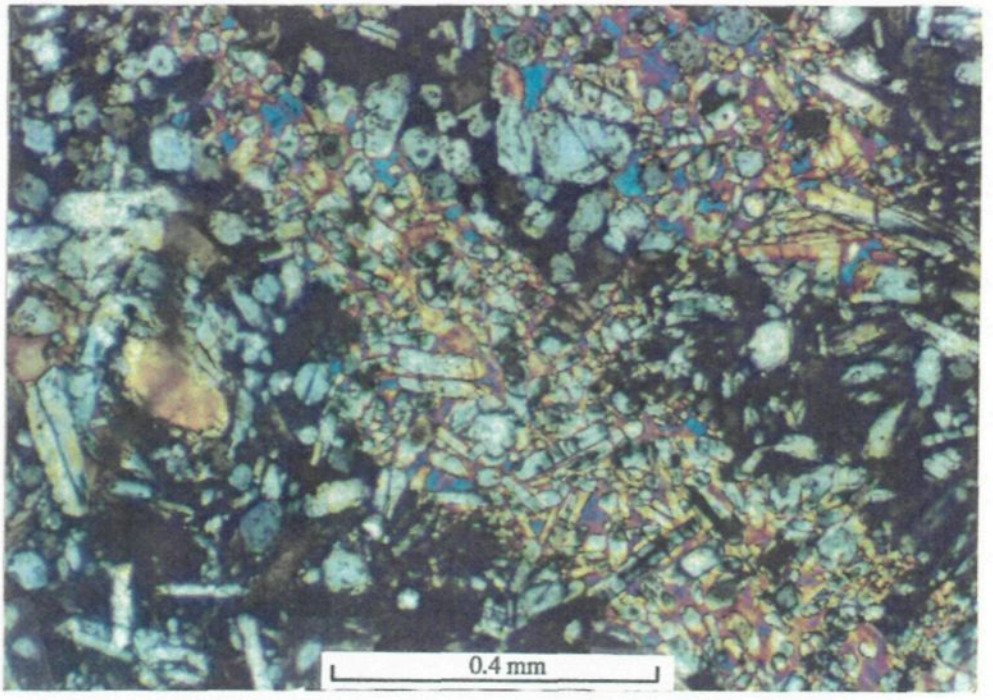

Plate 5. Poikilitic phlogopite crystals in the lamproites contain mainly clinopyroxenes. Most poikilitic phlogopites are very long strips, but some are less elongated subhedral crystals or 'patches'. Crossed nicols.

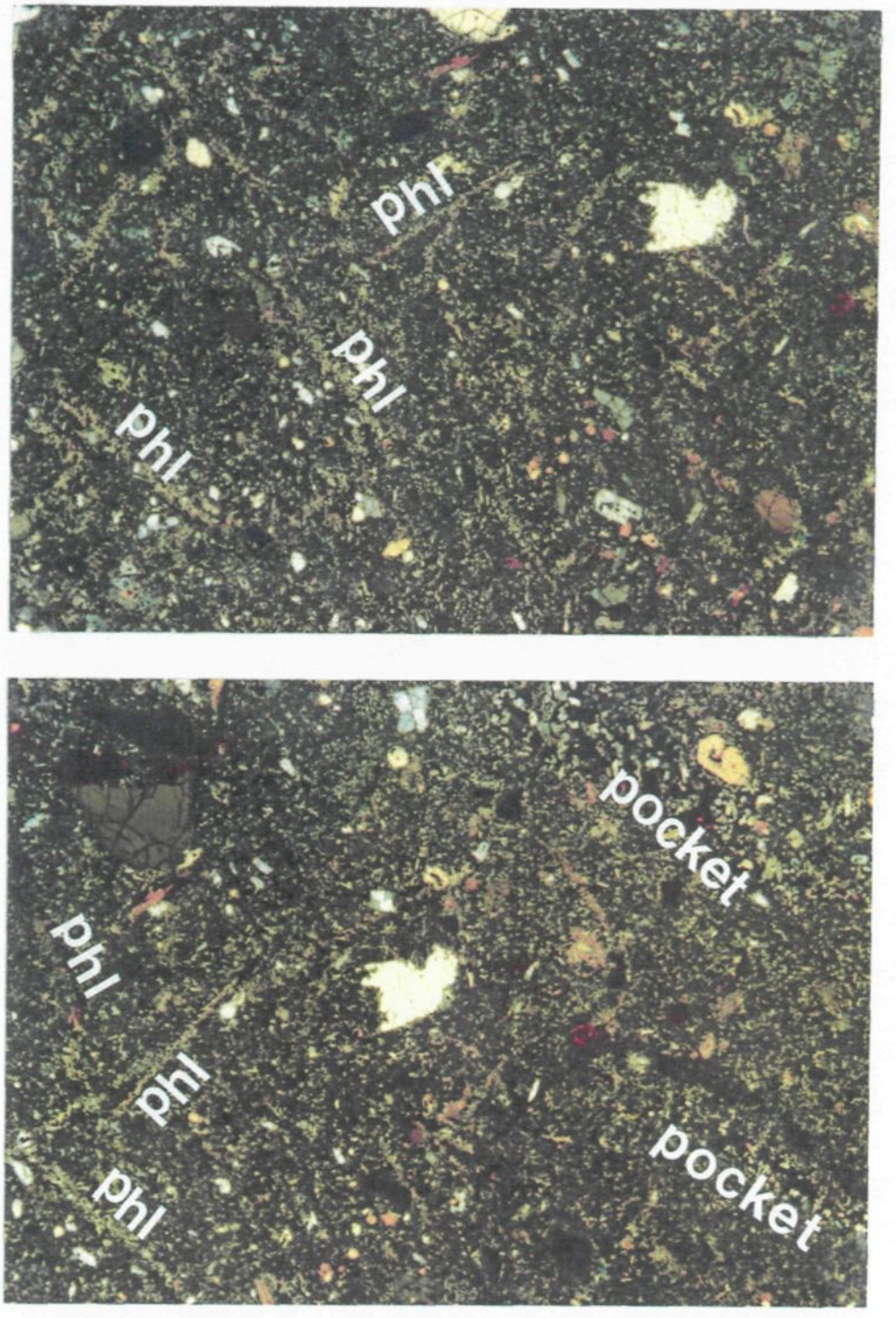

Plate 6. Two linear directions of the poikilitic phlogopite distribution in the lamproites groundmass (above). Alkali feldspar-and-clinopyroxene-enriched pocket areas are parallel to one of the linear directions (below). Photo size is about half a thin section.

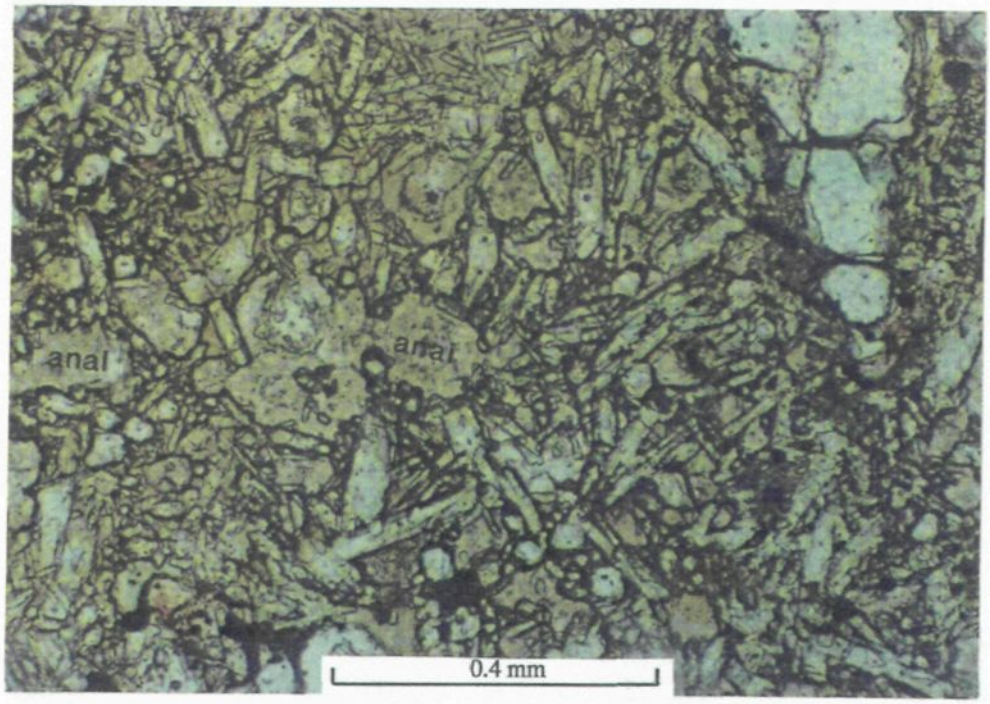

A Parallel nicols.

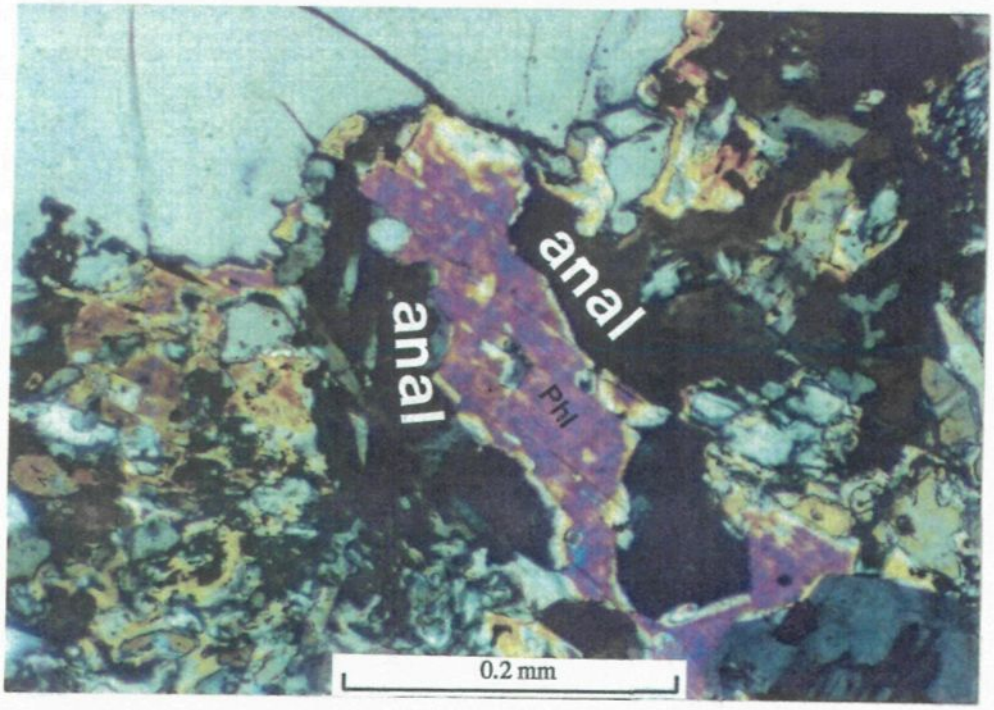

Plate 7. Analcimes appear as round grains in the lamproite groundmass (A) or as a secondary mineral replacing the phlogopites (B). Crossed nicols.

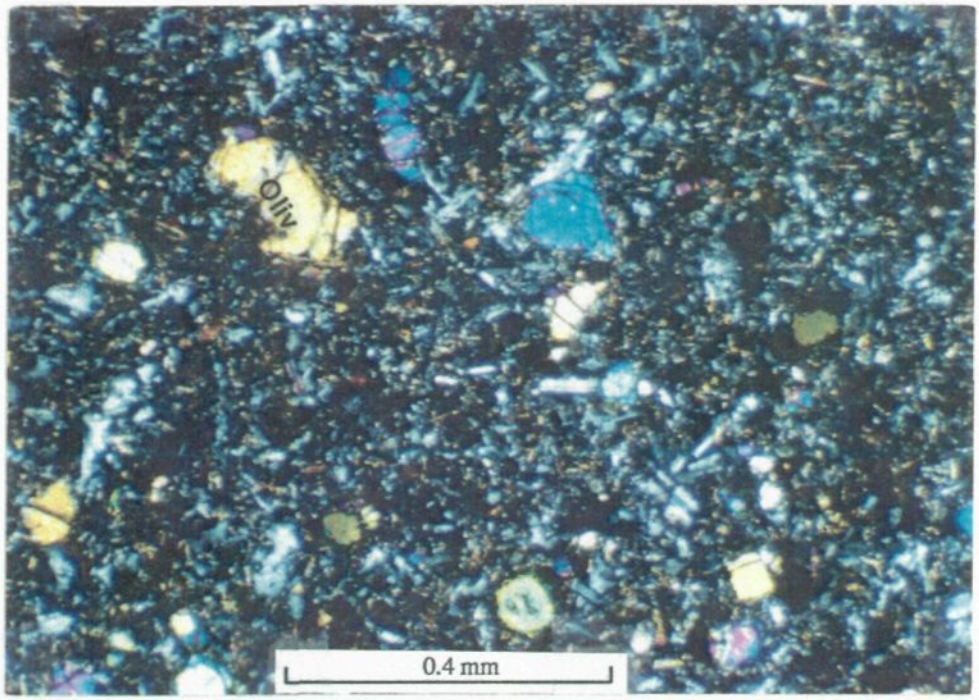

Plate 8a. Porphyritic texture of the Juxiang basanites: olivine and plagioclase megacrysts are set in a fine groundmass. Crossed nicols.

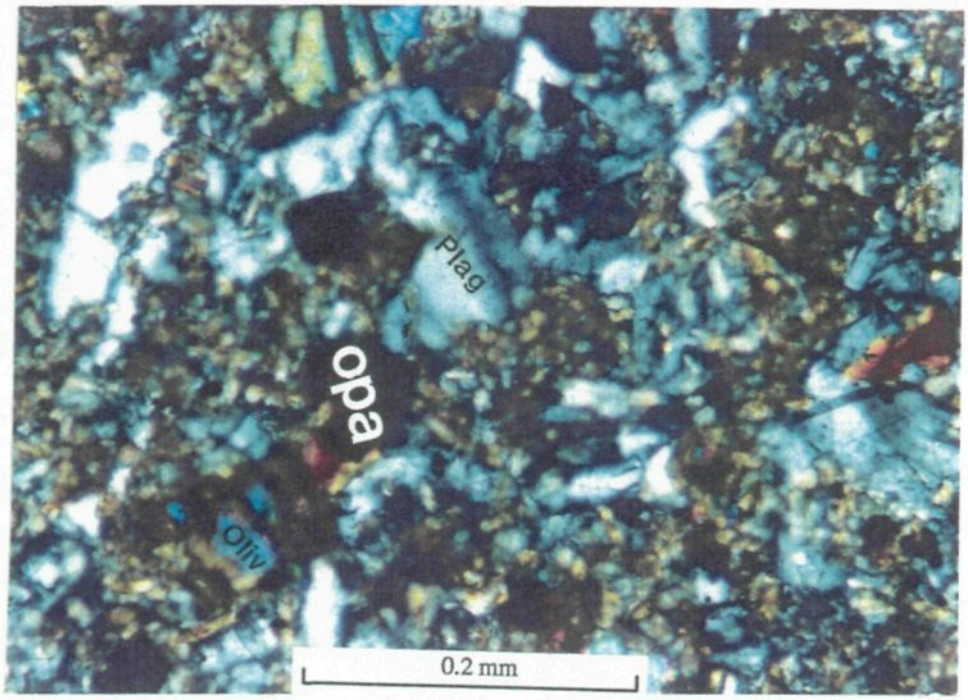

Plate 8b. A closer look of the holocrystalline groundmass, which is composed of plagioclase laths, clinopyroxene, opaque minerals (opa), and minor amounts of olivine, alkali feldspar, phlogopite, and kaesutite. Crossed nicols.

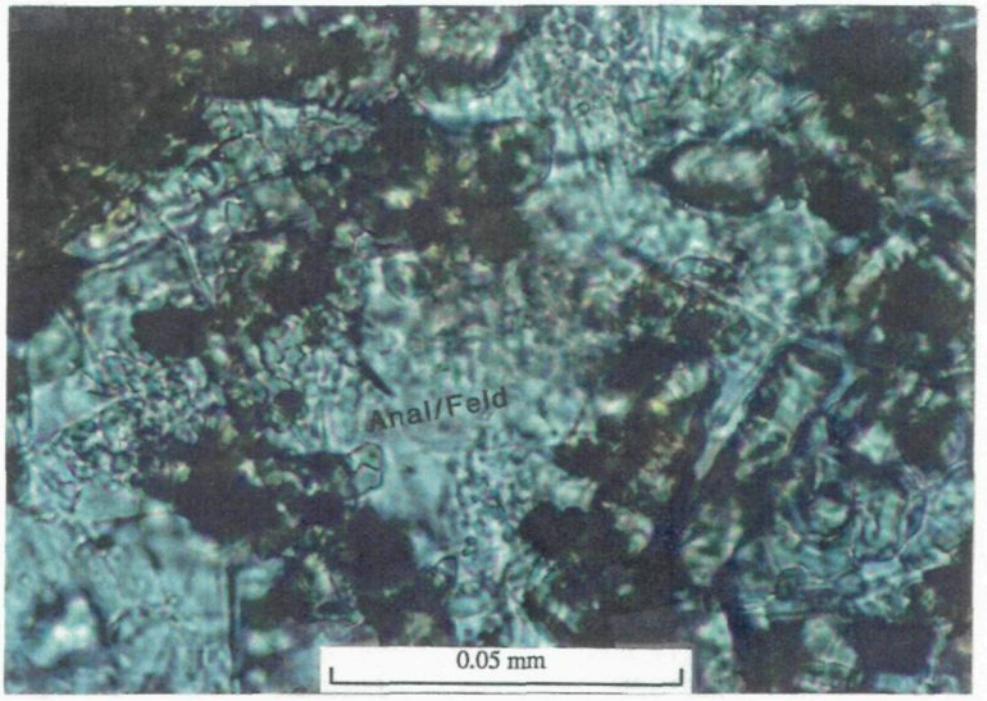

Plate 9a. Anhedral grains of analcime or alkali feldspar (anal/Feld) in the groundmass of the basanites. The mineral is very similar to the alkali feldspar shown below, but looks isotropic. Parallel nicols.

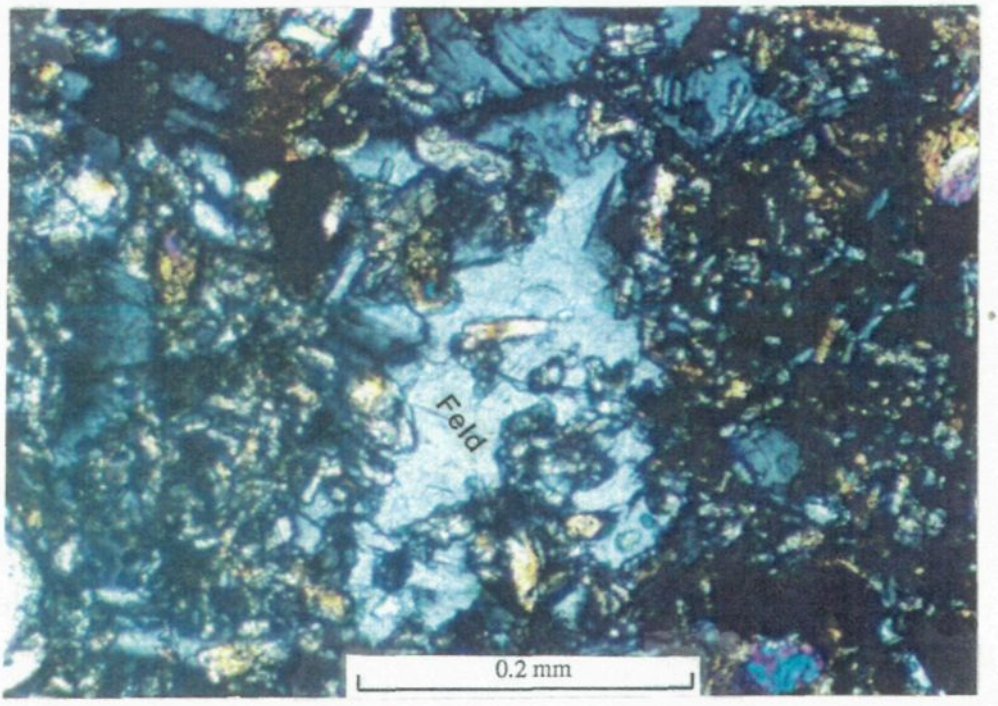

Plate 9b. Anhedral alkali feldspar (Feld) in the basanite groundmass. In some cases, the feldspar contains clinopyroxene or other minerals. Crossed nicols.

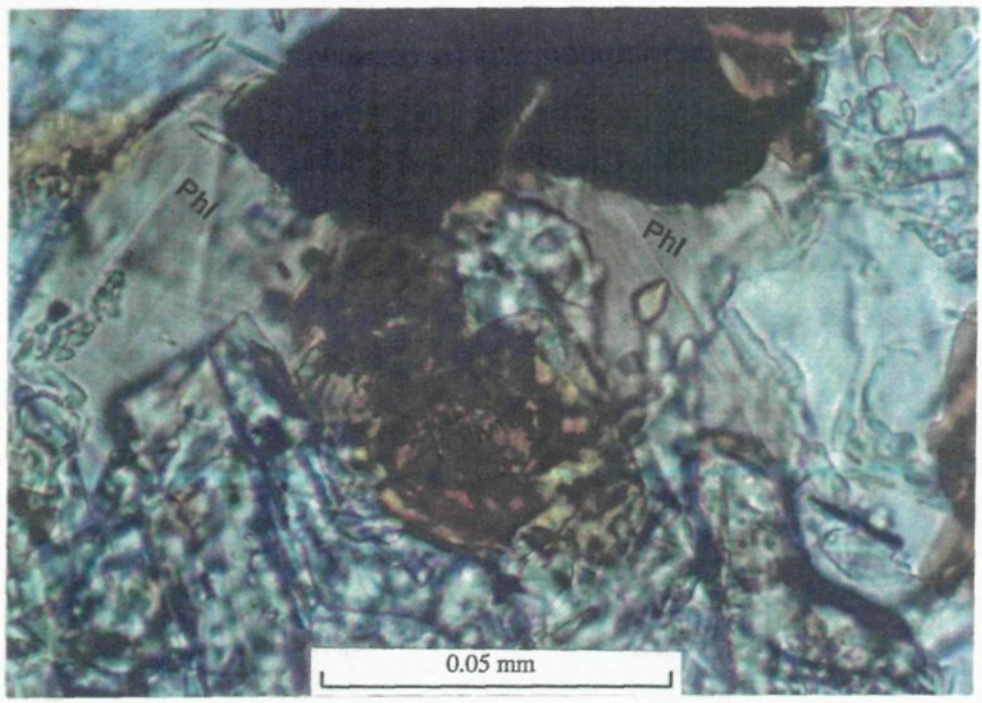

Plate 10a. Phlogopites (Phl) in the groundmass of the basanites. Parallel nicols.

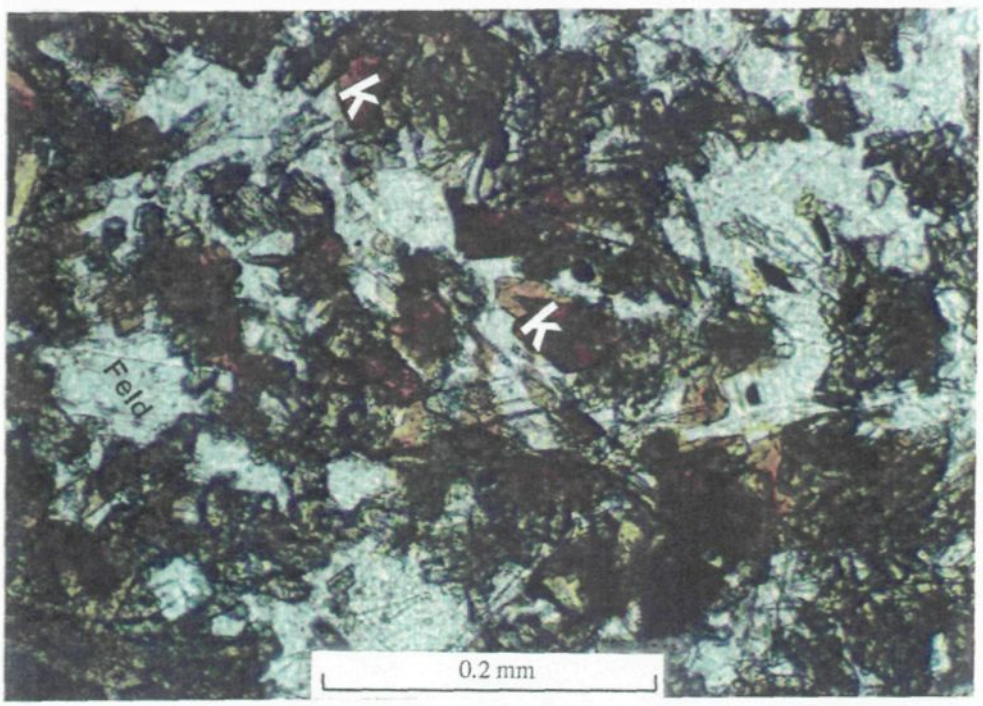

Plate 10b. Kaesutites ? (K) in the groundmass of the basanites. The dark brown subhedral kaesutites are similar to the phlogopites, but with slightly higher relief and without 3rd degree blue to green interference colors. Parallel nicols.

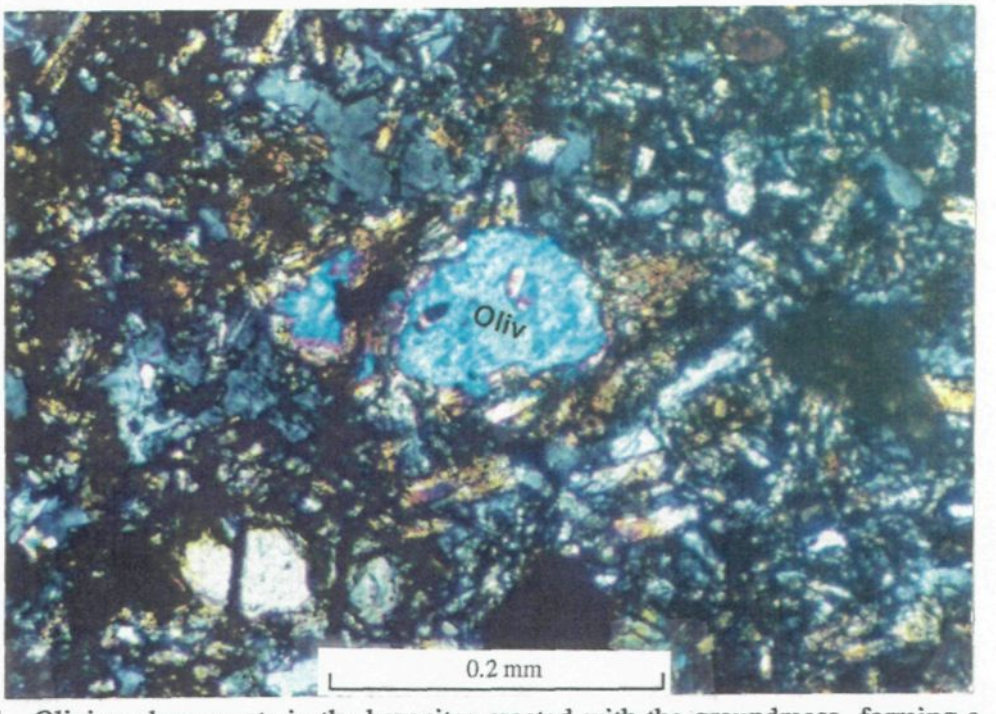

Plate 11. Olivine phenocrysts in the basanites reacted with the groundmass forming a iddingsite rim, which indicates that the olivine was not in equilibrium with the magma. Crossed nicols.

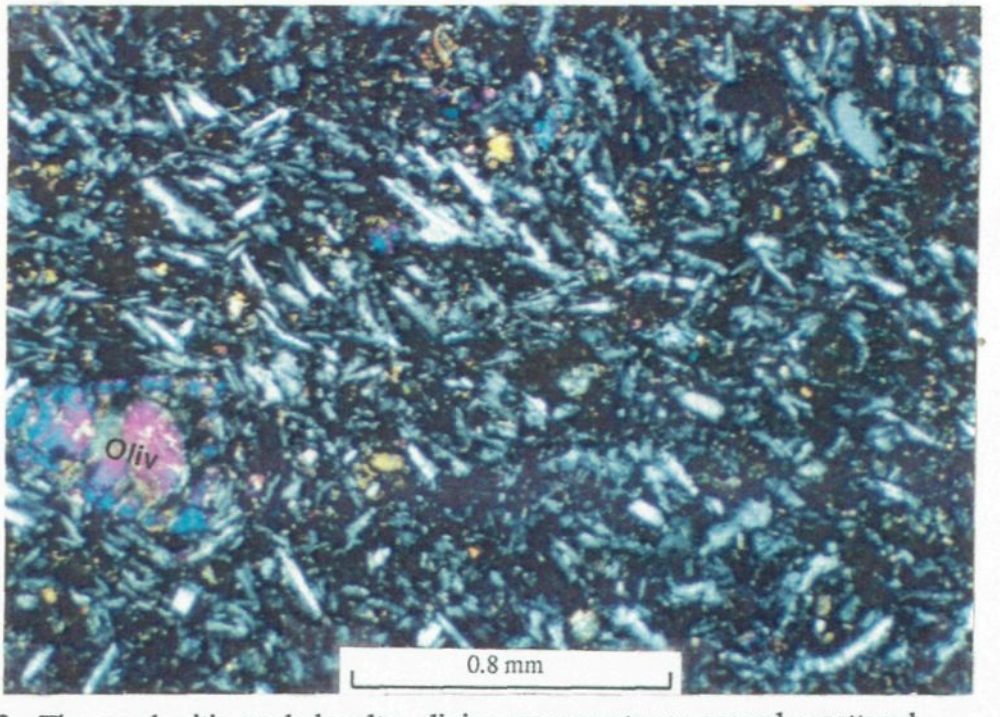

Plate 12. The porphyritic trachybasalts: olivine megacrysts are sparsely scattered in a groundmass with a trachytic texture. The groundmass is composed of plagioclases, alkali feldspars, opaque minerals, and clinopyroxenes. Crossed nicols.

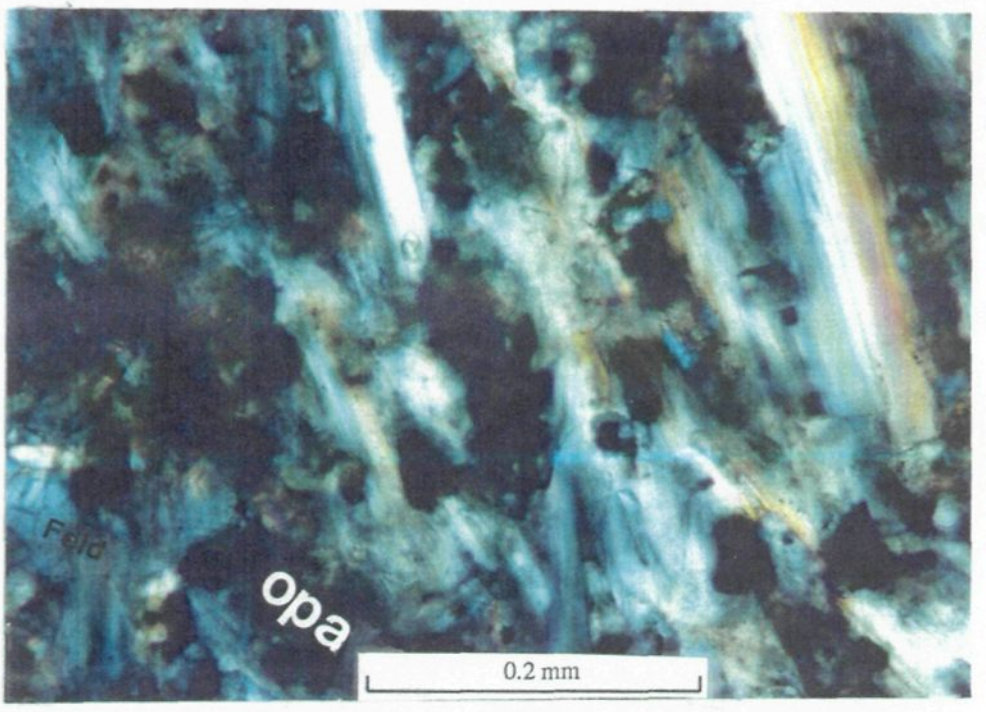

Plate 13. Opaque minerals (opa = ilmenite and ulvöspinel) and alkali feldspars (Feld) in the groundmass of the trachybasalts. Crossed nicols.

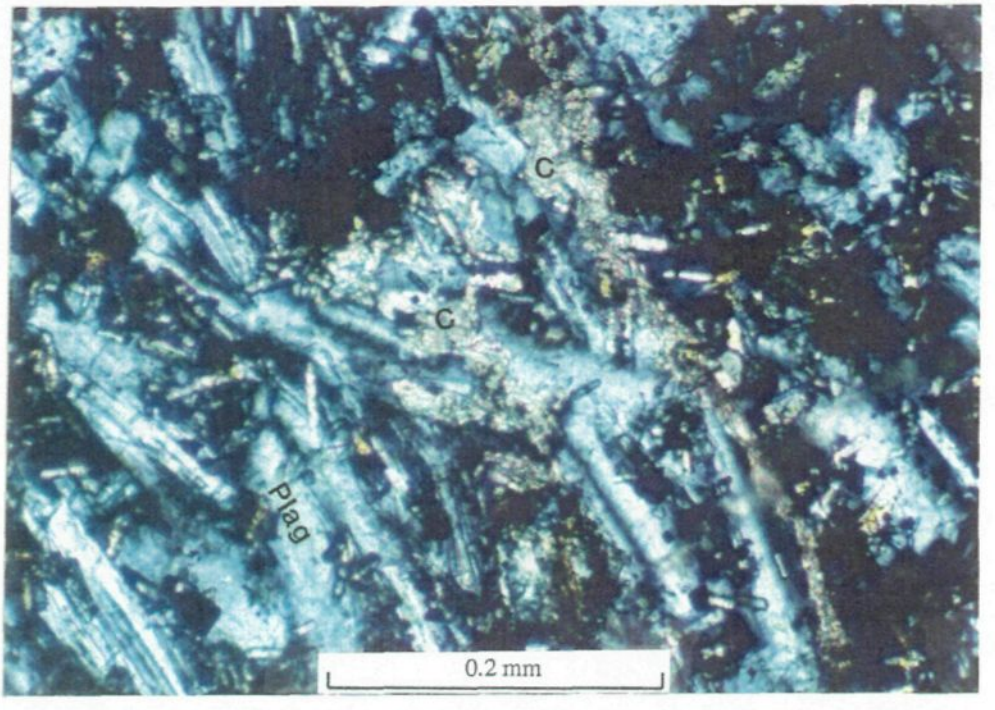

Plate 14. Calcite veinlets in the trachybasalts (C). These calcites appear in the vicinity of fractures, and therefore could be secondary minerals. Crossed nicols.

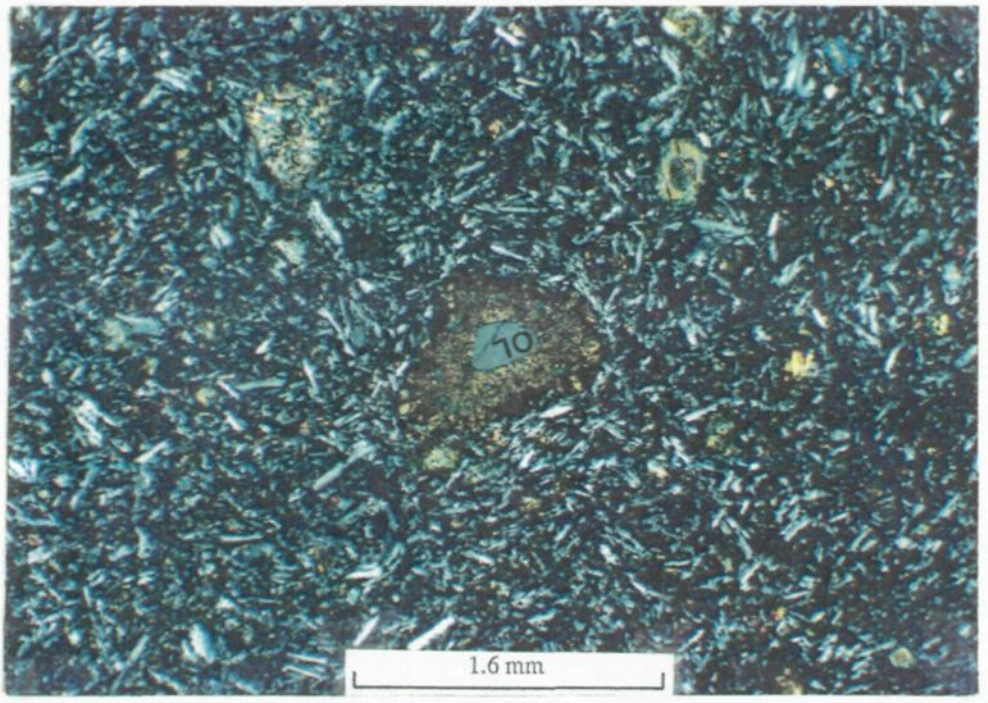

Plate 15a. Olivine megacrysts in the trachybasalts with a reaction rim of very fine minerals around the olivine crystal. Crossed nicols.

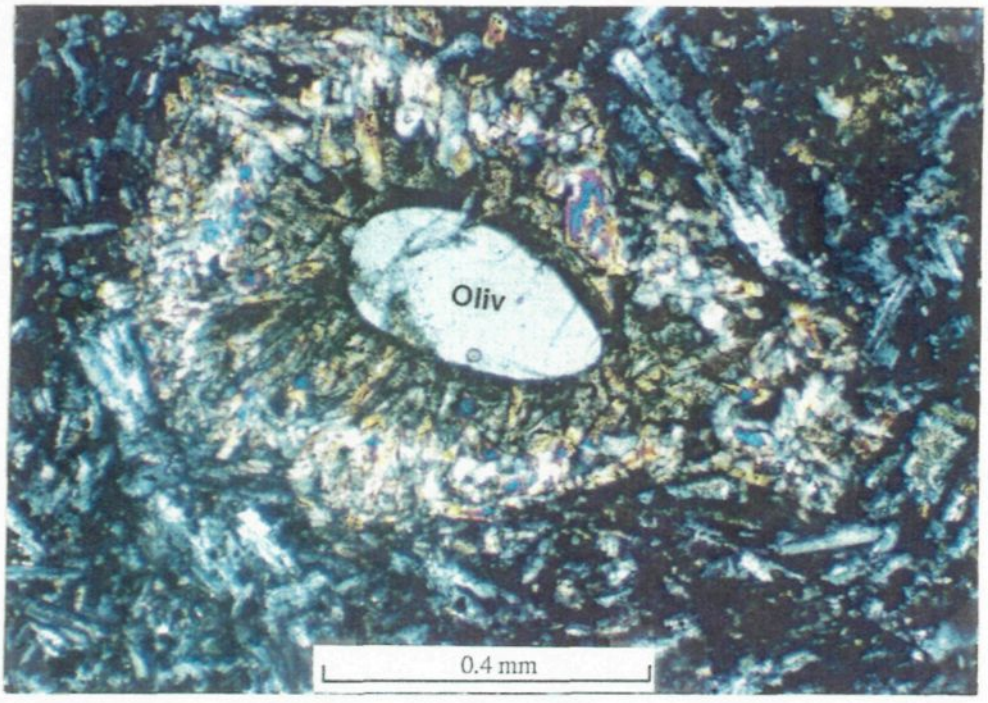

Plate 15b. Olivine megacrysts in the trachybasalts with a corona composed of perpendicular pyroxenes in the inner layer and pyroxenes, micas and unidentified minerals in the outer layer. Crossed nicols.

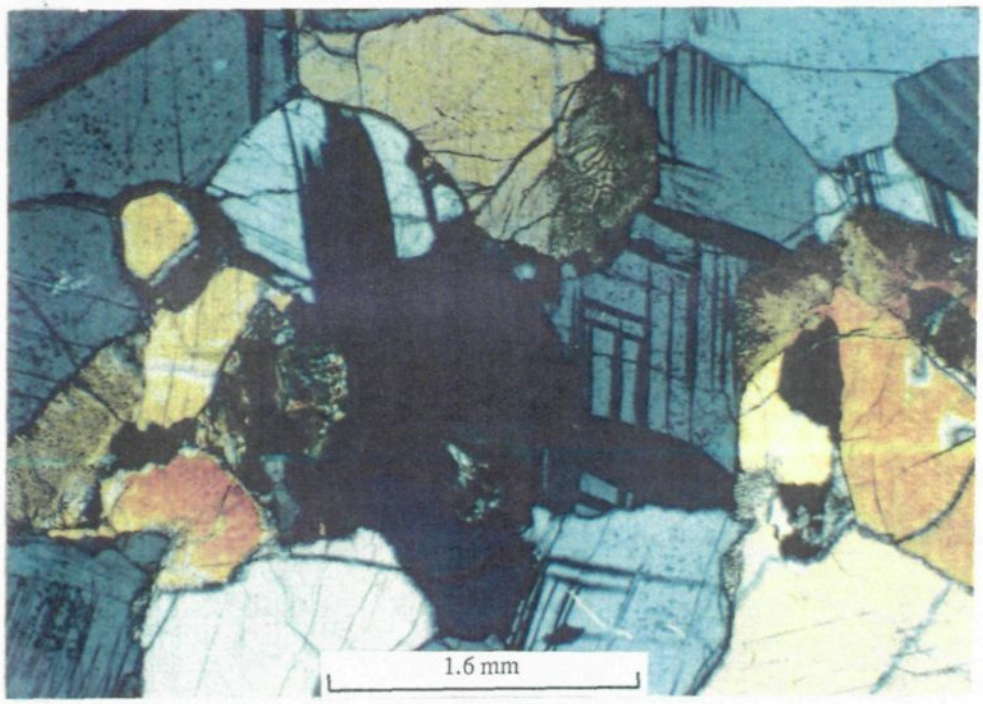

Plate 16. A deformed gabbro xenolith from the lamproites. Pyroxenes are interlayered with plagioclases. Crossed nicols.

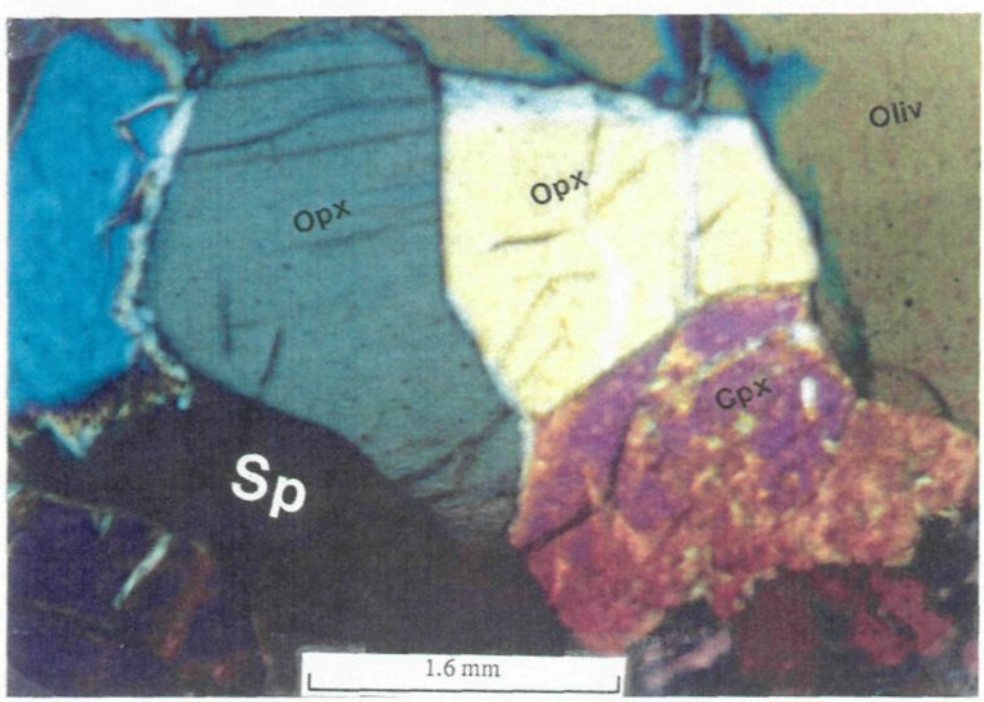

Plate 17. A spinel lherzolite xenolith from the trachybasalts. The lherzolite has a granoblastic texture. Crossed nicols.

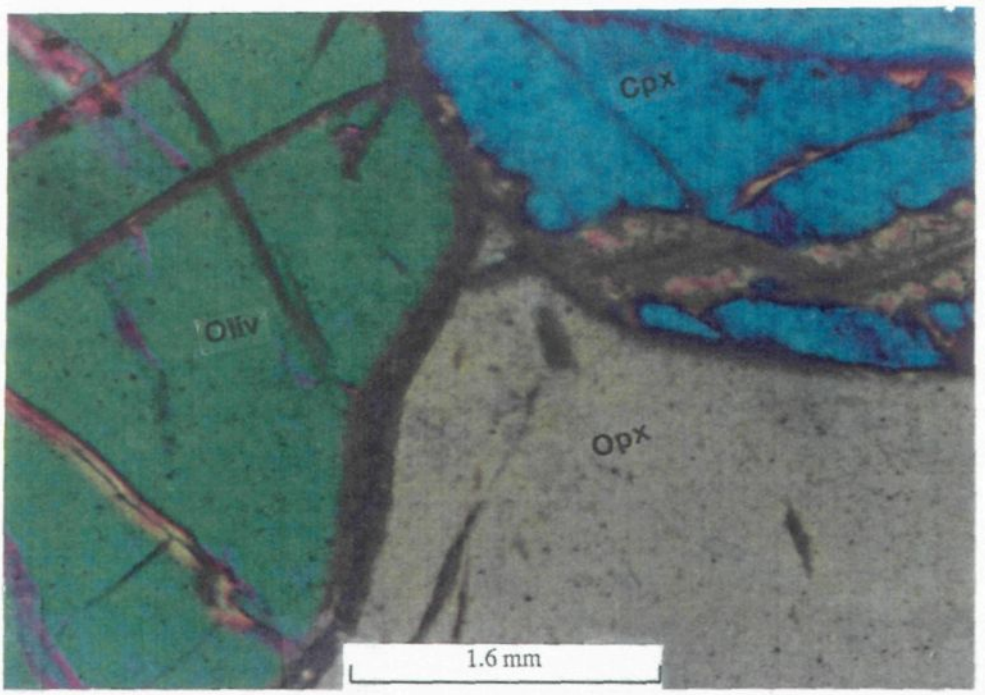

Plate 18. The orthopyroxene, clinopyroxene and olivine meet at a triple junction in a lherzolite xenolith from the trachybasalts, which indicates equilibrium was achieved among the minerals. Crossed nicols.

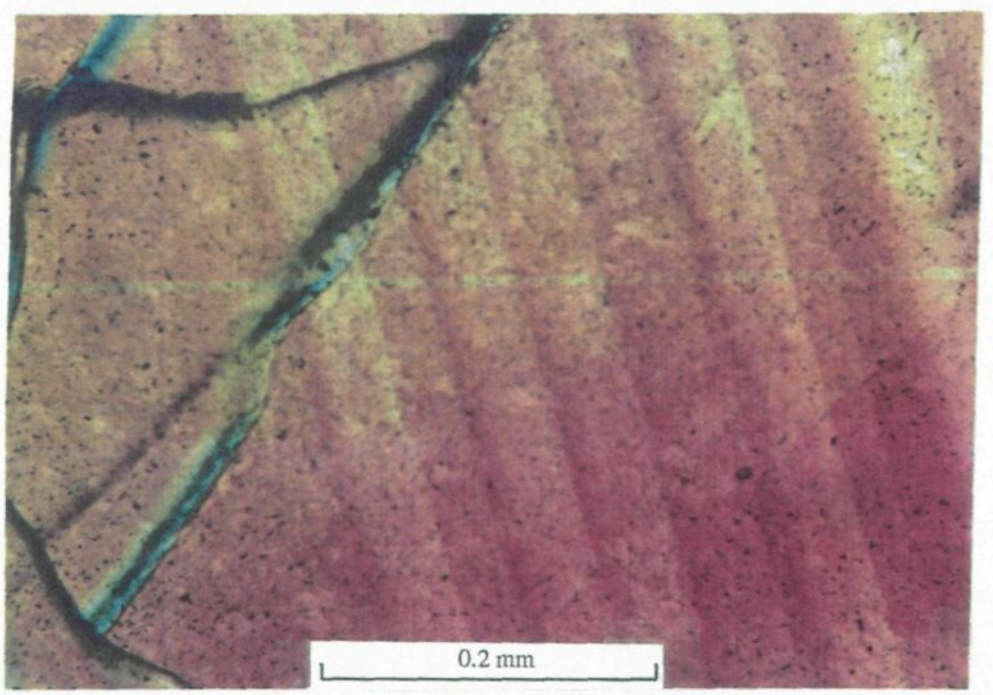

Plate 19. An orthopyroxene in a lherzolite xenolith from the trachybasalts has "kink bands", indicating the lherzolite had been deformed. Crossed nicols.

Chapter IV

CHEMICAL COMPOSITION

4.1 INTRODUCTION

4.1.1 Analytical Methods

Selected samples of the alkaline rocks from the study area were analyzed for their major oxides, trace, rare earth and platinum group elements in different laboratories by different methods. Major oxides were analyzed by wet chemical analysis (in China) and by XRF technique (at McGill University). The XRF results are listed in table 4.1 through 4.3. Wet chemical results are given for reference in appendix A. The analyses from the two laboratories are very similar. Rare earth elements (REEs) were analyzed by ICP-AES (in China) and by INAA (at University du Québec à Chicoutimi--UQAC) using the method of Bédard & Barnes (1990); U, Th, Rb, Ba, Co and Ni were analyzed by INAA (at UQAC) and by XRF (at McGill) techniques; Nb, Zr, Y, Sr, Pb, V and Cu were analyzed by XRF (at McGill); Cs, Ta, Hf, Sc, and Au were analyzed by INAA (at UQAC); platinum-group elements (PGEs) were analyzed by INAA using the method of Robert et al. (1971). All the trace element analyses results are listed in table 4.4 through 4.7. For those elements analyzed more than once, only the INAA result is given. Results by other analytical methods are presented in appendix B for comparison. It is relevant to state that different analytical techniques provide virtually the same results for the rocks in this study. This establishes the reliability of the analyzed data.

4.1.2 Chemical Series and Classification

All rocks collected from the study area are alkaline (Fig. 4.1, Tables 4.1-4.3). They can be divided into two series: the high K/Na (>0.6) ratio series and the low K/Na (<0.5) ratio series (Fig.4.2, Table 4.1-4.3). The high K/Na ratio rocks are exposed in Huzhiyan Daoxian, Hunan Province, the eastern group. They fall in the alkaline basalt field on the total alkali-silica diagram (Fig.4.1), and could be called high-K olivine basalt by Le Bas's chemical classification (Le Bas, 1986). But the high K/Na rocks contain no modal plagioclase, which rules them out as basaltic rocks. A comprehensive consideration of their mineralogy, major and trace element characteristics (see previous chapter and discussion below) suggests that these rocks could be best classified as lamproite.

The low K/Na ratio rock series outcrops in Juxiang, Guangxi Province, the western group, and in Ningyuan, Hunan Province, the eastern group. The rocks from Juxiang fall on the boundary between the basanite and the trachybasalt fields on the total alkali-silica diagram (Fig.4.1). They contain 5.9-11% nepheline and more than 10% olivine in their CIPW norm (Table 4.2), which establishes them as basanite. The rocks in Ningyuan fall across the border line between the trachybasalt and the basaltic trachyandesite fields. They contain no foid minerals; some samples even contain small amount of hypersthene (Table 4.3). They have high alkali (Na_2O+K_2O > 5 wt%) yet basaltic MgO content (5.7-8.4 wt%). These lead to them being classified as trachybasalt in this study, although some of them could termed shoshonite in Le Bas' classification. However, these trachybasalts will fall to the right of the Oliv-Di-Plag plane, if projected on the basalt tetrahedron (Yoder & Tilley, 1962) because of the normative hypersthene. This is unusual for alkaline rocks, which could imply that the rocks have evolved through a path different from low pressure crystal fractionation.

For simplicity, in the following sections, the term lamproitic refers to all alkali rocks having a K/Na > 0.6; the term alkali basaltic refers to all alkali rocks with K/Na ratio <0.6.

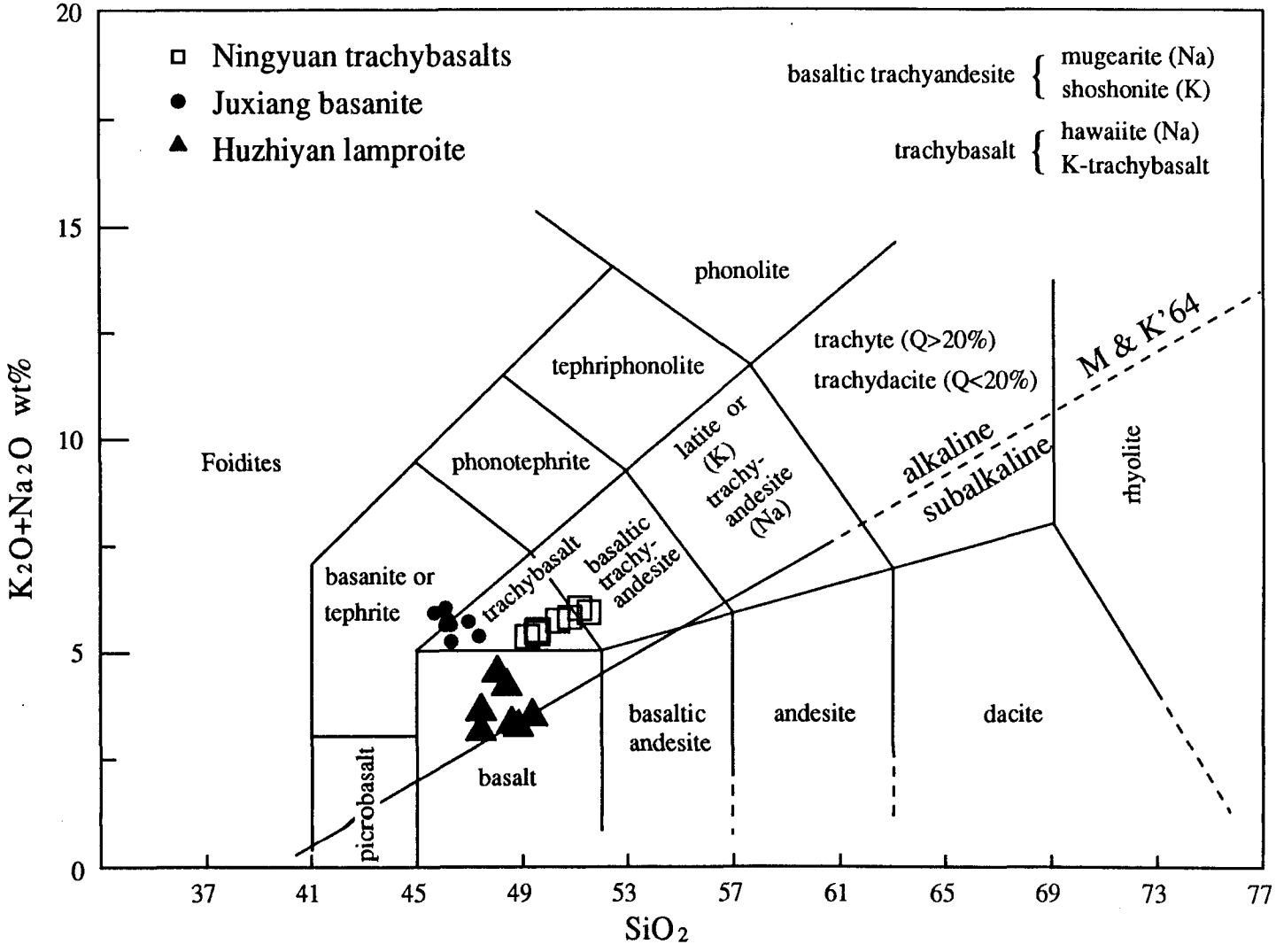

Fig. 4.1 Total Alkali-Silica classification diagram for the alkaline rocks in from the inland subvolcanic belt of southern China (After Le Bas et al., 1986; MacDonald & Katsura, 1964).

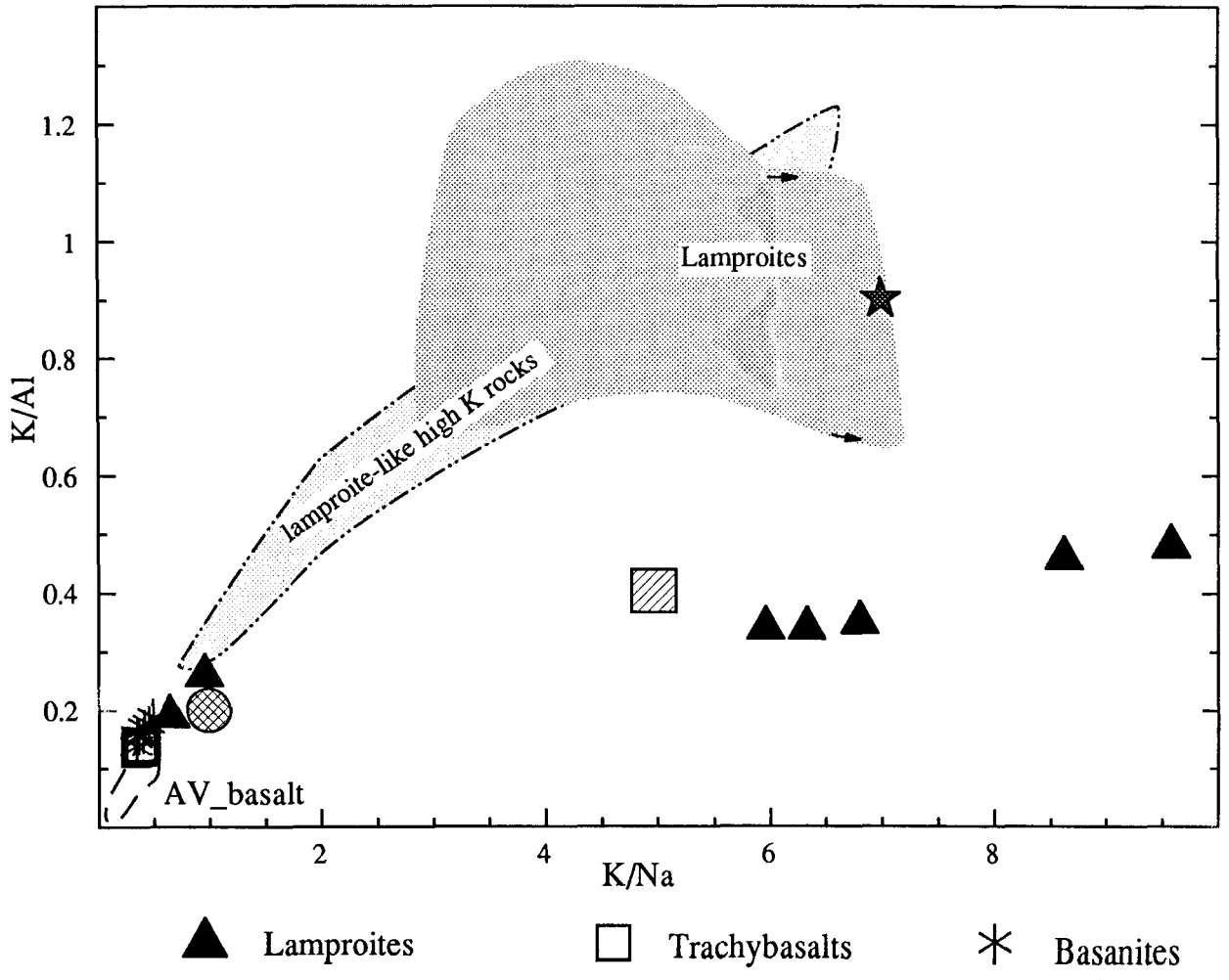

Fig. 4.2 K/Al versus K/Na diagram for the alkaline rocks from inland, southern China. The alkaline rocks are divided into high K/Na(>0.6) and low K/Na(<0.5) series. The high K/Na rocks show similarity to lamproitic rocks. For comparison, average lamprophre ⊗ , kimberlites ▨ , lamproite range(shaded) and lamproite average★ are also ploted (Data source for average rock types from Bergman, 1987).

Table 4.1 Major oxide chemistry (wt%) of lamproites from Hunan, southern China

	Lam1	Lam2	Lam3	Lam4	Lam5	Lam6	Lam7
SiO_2	45.83	45.15	46.37	45.51	46.01	44.43	46.49
TiO_2	0.57	0.61	0.62	0.56	0.61	0.59	0.62
Al_2O_3	8.20	8.25	8.47	8.10	8.50	8.51	8.79
Fe_2O_3	7.36	7.49	7.64	7.44	7.60	7.24	7.34
MnO	0.18	0.17	0.19	0.19	0.20	0.17	0.18
MgO	16.90	16.29	16.40	16.89	16.50	15.33	15.33
CaO	14.08	11.03	11.75	13.42	11.64	11.62	11.68
Na_2O^*	1.50	0.27	0.28	1.38	0.30	0.26	0.28
K_2O	1.43	3.52	2.68	1.97	2.70	3.77	2.88
LOI	3.26	6.60	5.18	3.55	5.64	7.10	4.83
P_2O_5	0.58	0.57	0.59	0.56	0.57	0.55	0.59
Total	99.93	99.78	100.39	99.38	100.31	99.52	99.29
#Mg	0.84	0.84	0.83	0.84	0.84	0.83	0.83
K^+/Al^{+3}	0.19	0.46	0.34	0.26	0.34	0.48	0.35
K^+/Na^+	0.63	8.60	6.31	0.94	5.94	9.56	6.78
NORM in Weight Percent							
Ortho.	8.51	187.70	15.91	8.07	16.01	15.50	17.29
Albite	0.50	0.00	2.38	0.00	2.55	0.00	2.41
Anorth	11.50	10.97	14.00	10.19	13.92	11.03	14.45
Neph	6.65	1.25	0.00	6.39	0.00	1.20	0.00
Leucit	0.00	2.54	0.00	2.90	0.00	9.41	0.00
Diop	43.69	32.06	32.33	42.39	32.01	34.64	32.21
Hypers	0.00	0.00	3.72	0.00	2.03	0.00	4.93
Oliv	21.76	24.64	22.17	22.40	23.61	21.97	19.54
Ilmeni	1.09	1.17	1.18	1.07	1.16	1.13	1.20
Magnet	1.64	1.67	1.70	1.66	1.69	1.62	1.65
Apatit	1.38	1.36	1.40	1.34	1.35	1.32	1.42
H_2O_T	3.28	6.65	5.21	3.59	5.66	7.18	4.91

* Na_2O is analyzed by INAA method; all other oxides by XRF method.

Table 4.2 Chemical composition of basanites from Juxiang, Guangxi, southern China

	Bas1	Bas2	Bas3	Bas4	Bas5	Bas6	Bas7	Bas8
SiO_2	44.32	44.74	44.70	44.56	44.84	44.77	45.78	45.27
TiO_2	2.59	2.60	2.60	2.59	2.60	2.62	2.43	2.47
Al_2O_3	13.42	13.47	13.42	13.44	13.29	13.42	13.96	13.64
Fe_2O_3	11.17	11.26	11.27	11.23	11.33	11.16	11.34	11.19
FeO	nd	nd	nd	nd	nd	nd	nd	nd
MnO	0.18	0.17	0.17	0.18	0.18	0.17	0.18	0.18
MgO	9.52	9.58	9.36	9.46	9.97	9.57	9.05	9.22
CaO	9.85	9.77	9.91	9.78	9.80	9.91	9.02	9.22
Na_2O	3.19	3.62	3.09	3.54	3.14	3.37	3.40	3.54
K_2O	2.20	1.94	2.33	1.93	1.92	2.11	1.78	1.95
LOI	2.72	2.28	2.40	2.32	2.14	2.27	2.44	1.97
P_2O_5	0.76	0.79	0.76	0.78	0.78	0.79	0.77	0.77
Total	99.92	100.22	100.01	99.81	99.99	100.16	100.15	99.42
#Mg	0.66	0.66	0.65	0.67	0.67	0.66	0.65	0.65
Al/K	0.18	0.16	0.19	0.16	0.16	0.17	0.14	0.15
K/Na	0.45	0.35	0.50	0.36	0.40	0.41	0.35	0.36
NORM in Weight Percent								
Ortho.	13.13	11.54	13.89	11.53	11.45	12.56	10.60	11.70
Albite	9.23	10.98	9.39	11.12	12.33	10.20	18.28	14.75
Anorth	15.96	14.88	16.01	15.25	16.65	15.37	17.71	15.80
Neph	9.77	10.76	9.20	10.39	7.84	10.04	5.80	8.48
Diop	22.93	23.22	23.11	23.16	22.01	23.39	18.06	20.65
Oliv	17.35	17.39	17.03	17.26	18.43	17.16	18.30	17.87
Ilmeni	4.97	4.97	4.98	4.97	4.98	5.01	4.65	4.76
Magnet	2.05	2.03	2.08	2.05	2.23	2.04	2.24	2.09
Apatit	1.82	1.88	1.82	1.87	1.86	1.89	1.84	1.85
Chromi	0.05	0.05	0.05	0.05	0.05	0.05	0.06	0.04
H_2O_T	2.75	2.30	2.42	2.35	2.16	2.29	2.46	2.00

Table 4.3 Major oxide chemistry of trachybasalts from Hunan, southern China

	TB1	TB2	TB3	TB4	TB5	TB6	SH1	SH2	SH3
SiO_2	47.45	47.65	47.58	48.17	47.63	47.56	49.40	48.93	49.12
TiO_2	1.99	2.03	2.05	1.95	2.02	2.02	1.90	1.86	1.75
Al_2O_3	14.98	15.23	15.32	15.63	15.14	15.29	15.94	15.56	15.51
Fe_2O_3	11.43	11.42	11.44	11.44	11.70	11.38	10.72	11.25	10.98
FeO	nd	nd	nd	nd	nd	nd	nd	nd	nd
MnO	0.19	0.20	0.19	0.22	0.23	0.19	0.27	0.22	0.22
MgO	8.42	7.33	7.28	6.53	7.17	7.65	5.52	6.71	6.72
CaO	7.13	7.20	7.25	6.58	7.27	6.94	6.67	6.48	6.18
Na_2O	3.26	3.31	3.27	3.51	3.31	3.20	3.58	3.54	3.67
K_2O	1.84	1.92	1.92	1.91	1.92	1.95	2.04	1.99	2.04
LOI	2.91	2.93	2.97	2.86	3.17	2.50	3.24	2.92	2.54
P_2O_5	0.71	0.74	0.73	0.72	0.74	0.73	0.75	0.73	0.72
Total	100.31	99.96	100.00	99.52	100.30	99.41	100.03	100.19	99.45
#Mg	0.63	0.60	0.60	0.57	0.59	0.61	0.54	0.58	0.58
Al/K	0.13	0.14	0.14	0.13	0.14	0.14	0.14	0.14	0.14
K/Na	0.37	0.38	0.39	0.36	0.38	0.40	0.38	0.37	0.37
NORM in Weight Percent									
Ortho.	10.94	11.45	11.45	11.45	11.42	11.70	12.15	11.84	12.23
Albite	27.74	28.27	27.92	30.12	28.19	27.49	30.54	30.16	31.50
Anorth	20.93	21.23	21.65	21.55	20.92	21.92	21.58	20.84	20.11
Diop	8.11	8.12	8.02	5.56	8.60	6.67	5.63	5.51	5.09
Hypers	1.01	2.30	2.52	5.59	1.95	4.36	9.97	7.09	6.42
Oliv	20.38	17.58	17.33	14.95	17.68	17.23	9.19	13.95	14.70
Ilmeni	3.80	3.89	3.93	3.76	3.86	3.89	3.64	3.56	3.37
Magnet	2.39	2.37	2.38	2.35	2.42	2.40	2.20	2.31	2.22
Apatit	1.69	1.77	1.74	1.73	1.76	1.76	1.79	1.74	1.73
Chromi	0.07	0.06	0.04	0.04	0.00	0.04	0.04	0.05	0.04
H_2O_T	2.93	2.96	3.00	2.90	3.19	2.54	3.27	2.94	2.58

4.2 LAMPROITES

The lamproites show a SiO_2 range from ultrabasic to basic, intermediate between the basanites and the trachybasalts. To visualize more clearly the major oxide variation of these rocks, oxide variation diagrams of SiO_2 versus other oxides were constructed (Fig.4.3a); FeO/Fe_2O_3 ratio is adjusted using the Le Bas's (1986) statistical approach. These diagrams demonstrate that the most striking characteristics of the rocks are their high MgO and K_2O, and low Al_2O_3 and TiO_2 contents compared to the basanites or trachybasalts. These chemical traits contrast to normal basaltic rocks. These distinctive features can be further considered on a plot of Al_2O_3 versus MgO and Al_2O_3 versus K_2O plots (Fig.4.4a, b). On the Al_2O_3 - MgO plot, the close affinity of these rocks to the lamproite family is clear. This lamproite affinity is also shown on the K/Al-K/Na diagram (Fig.4.2), where the Huzhiyan rocks plot in a trend parallel to that of lamproites. Though the Huzhiyan rocks are not as K-rich as most lamproites, the K/Na ratios of most samples of the Huzhiyan rocks are much higher than the basanites and trachybasalts in the this study and than any other alkali basaltic rocks in the world. This high K/Na feature is typical for lamproitic rocks. The high K_2O, K/Na and MgO, low Al_2O_3 chemical characteristics of the Huzhiyan rocks are consistent with their phlogopite-rich, plagioclase-free petrographic features. The MgO-Al_2O_3 correlation trend shown on Fig. 4.4a indicates that the high MgO and low Al_2O_3 are related feature of the lamproites. This relation could be explained by increasing degrees of partial melting; but this explanation does not apply to the Huzhiyan lamproites, because the lamproites have high CaO contents, and increasing degrees of partial melting would have decreased the CaO content of the rocks. Progressive mantle metasomatism, however, can explain the trend without disturbing CaO content.

The high Ni (660-850 ppm) and Cr (~1000-1100 ppm) concentrations of Huzhiyan lamproites, together with their high MgO content are consistent with olivine accumulation. The Sc level of the rocks is about 20 ppm (Table 4.4), comparable to that

Table 4.4 Trace element composition of the lamproites in Huzhiyan, southern China (Unit ppm, NA--for No Available value)

	Lam1	Lam2	Lam3	Lam4	Lam5	Lam6	Lam7
Cs	445.4	4.6	10.2	362.2	10.8	4.5	8.9
Rb	96	78	38	100	45	93	46
Ba	2687	1612	1522	2687	1253	1343	1522
Th	10.6	11.6	10.6	10.1	11.5	11.2	11.0
U	4.0	4.0	3.9	3.9	4.2	4.0	3.5
Pb	8	14	NA	9	14	9	16
Ta	0.3	0.6	0.4	0.5	0.5	0.6	0.3
Nb	5	8	NA	5	10	8	9
Zr	106	104	NA	106	107	106	108
Hf	1.9	2.2	2.1	1.9	2.5	2.3	2.2
La	51.3	52.7	52.2	50.6	53.0	50.9	57.9
Ce	93.7	104.6	100.5	97.6	102.4	96.7	97.7
Nd	41	48	48	42	48	45	41
Sm	9.62	10.62	9.72	9.89	10.44	9.75	10.76
Eu	3.18	2.86	2.77	2.96	2.65	2.87	2.90
Tb	1.21	1.19	1.05	1.05	1.19	1.18	1.05
Ho	0.8	0.6	0.7	0.9	0.6	0.6	0.8
Yb	1.26	1.42	1.47	1.22	1.51	1.41	1.47
Lu	0.22	0.25	0.24	0.21	0.25	0.22	0.24
Y	20	23	NA	20	22	21	22
Sr	1143	635	NA	1118	566	806	634
Sc	21.4	22.2	21.6	22.2	21.5	20.9	22.2
V	130	138	138	125	131	121	133
Cr	1163	1163	1094	1163	1094	1026	1094
Ni	847	934	694	819	802	754	659
Co	42	40	38	32	40	39	41
Cu	64	47	61	47	61	51	40
Th/La	0.21	0.22	0.20	0.20	0.22	0.22	0.19
(La/Yb)	27.31	24.89	23.82	27.82	23.54	24.21	23.61

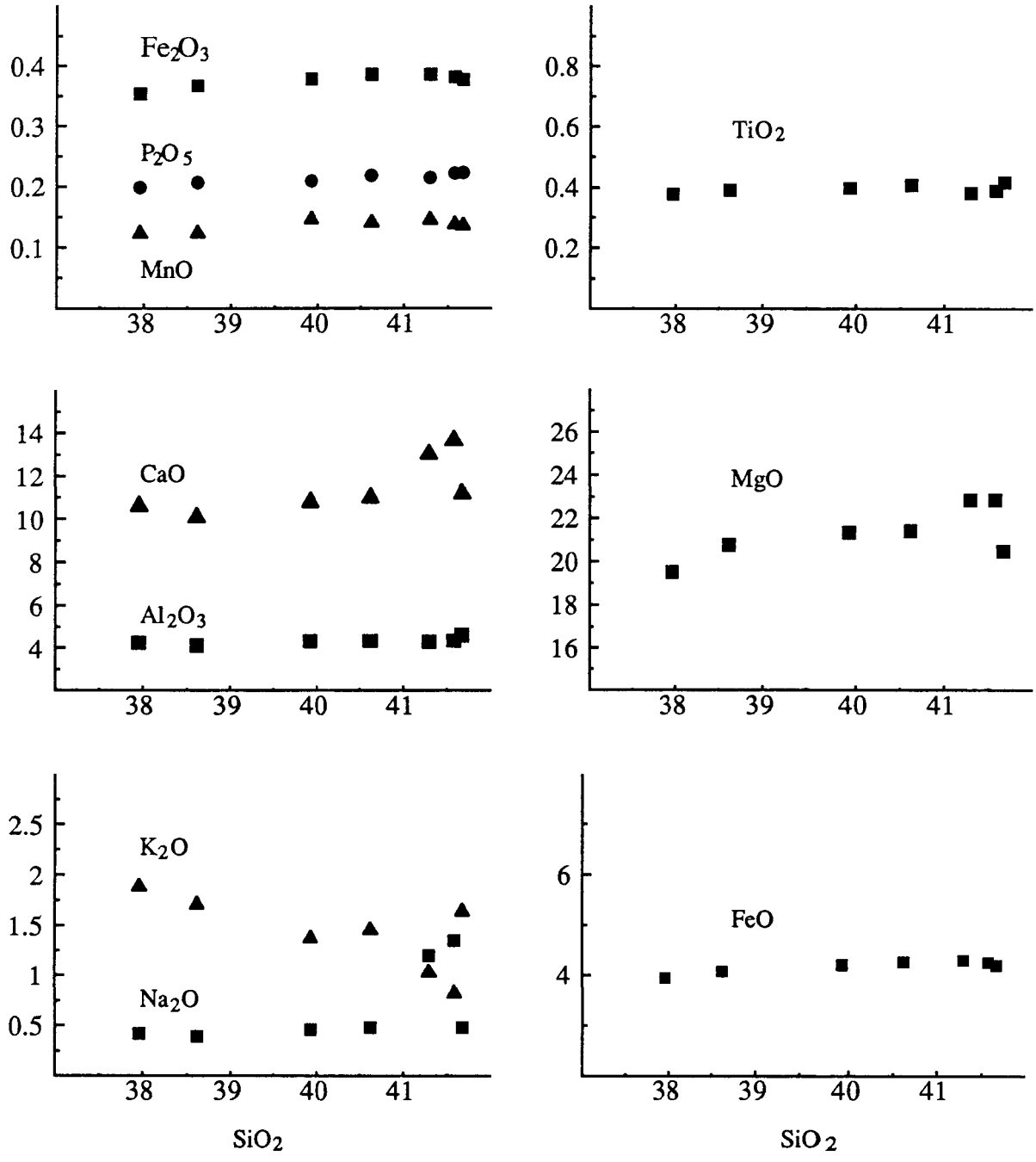

Fig. 4.3a SiO_2- Oxides (in mole unit) variation diagrams for the lamproites

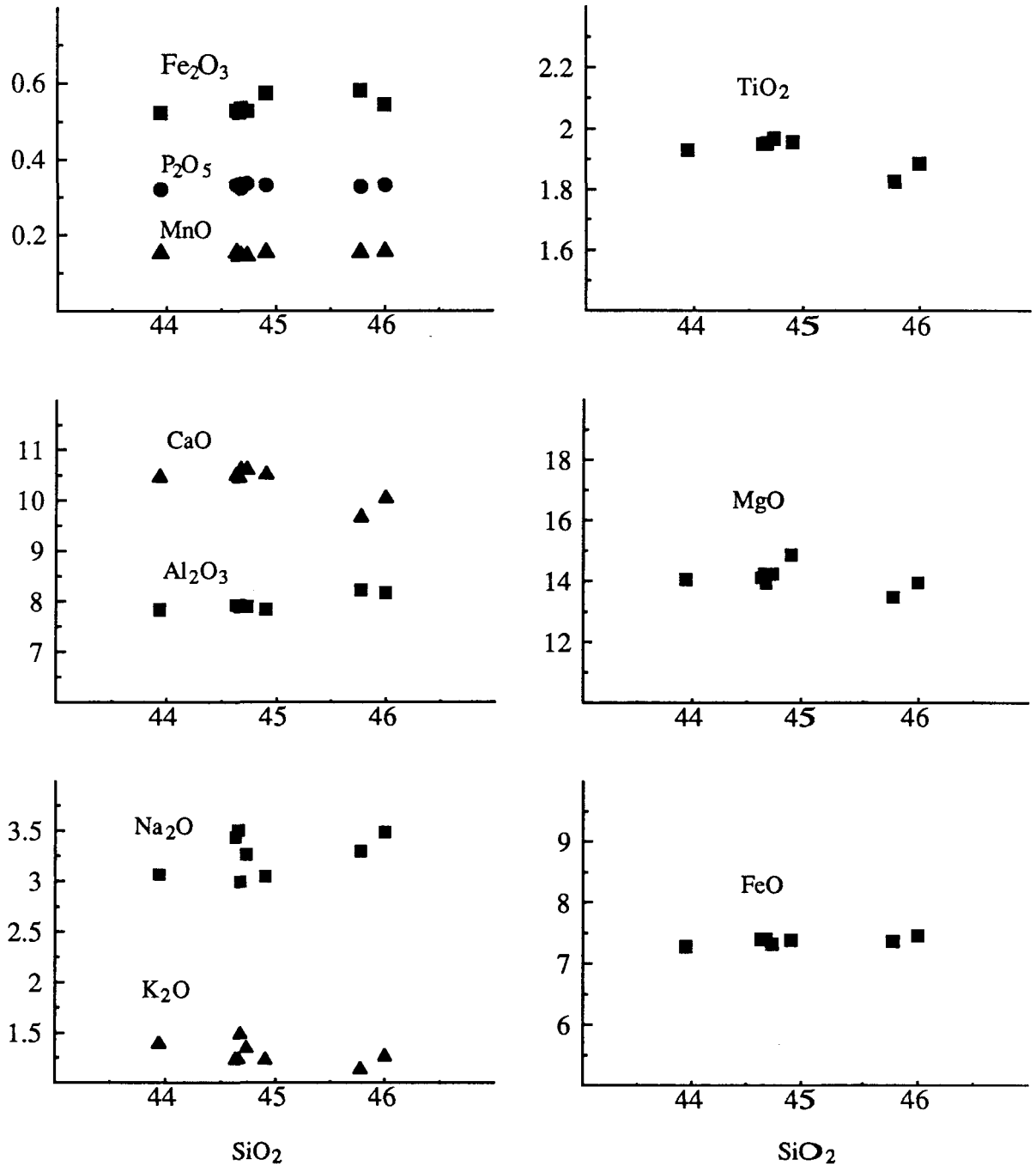

Fig. 4.3b SiO_2- Oxides (in mole unit) variation diagrams for the basanites

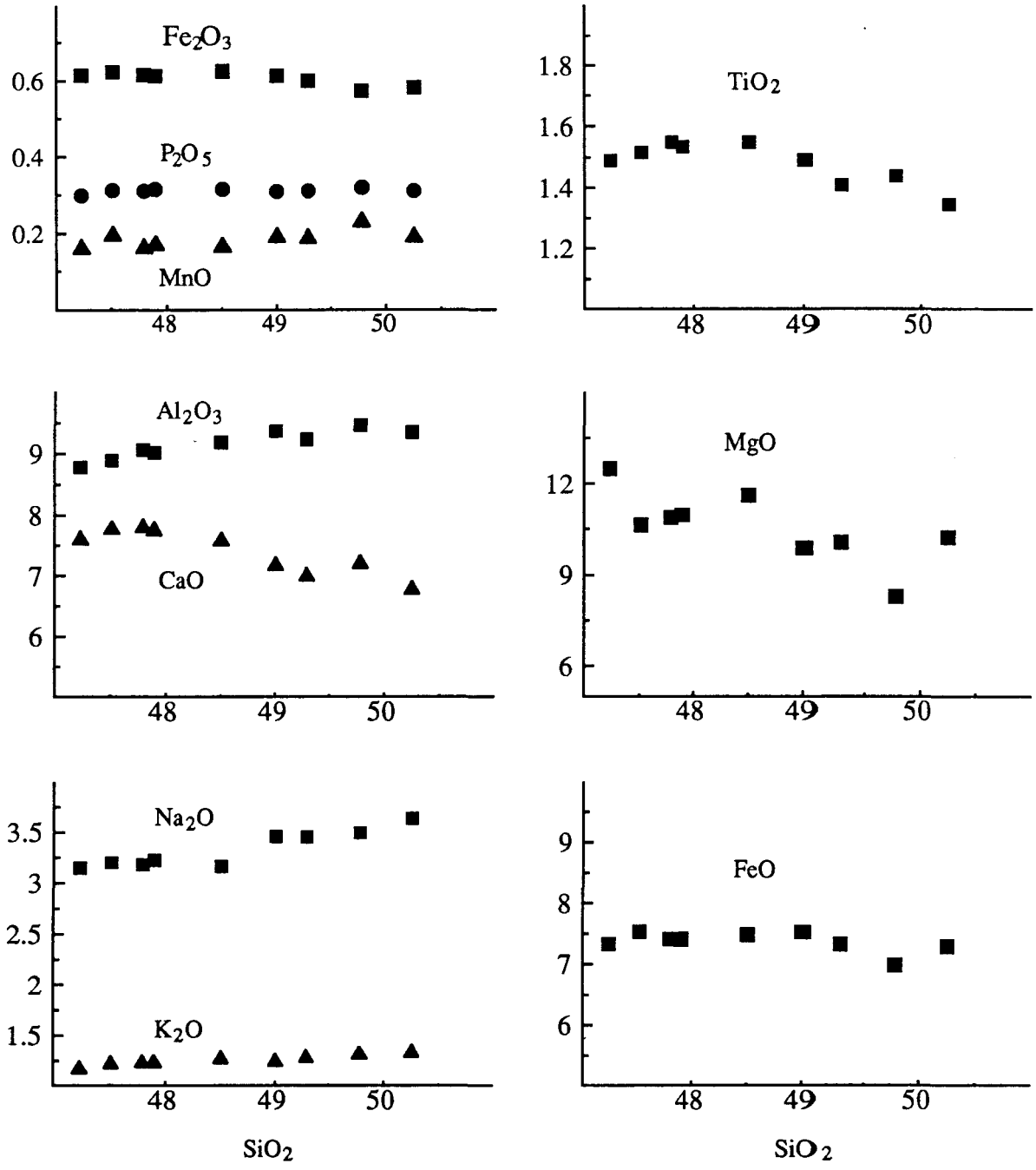

Fig. 4.3c SiO_2- Oxides (in mole unit) variation diagrams for the trachybasalts

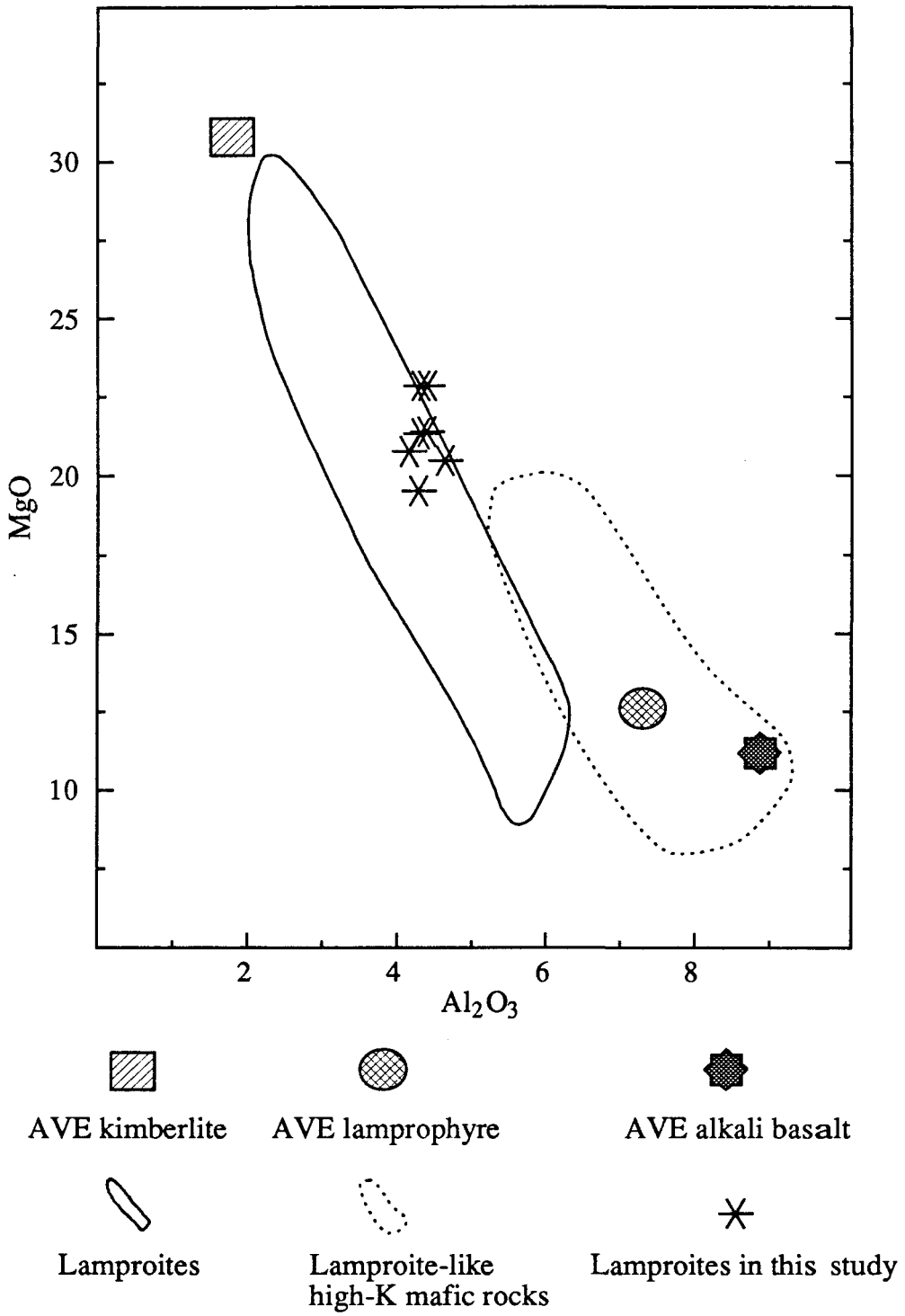

Fig. 4.4a MgO versus Al_2O_3 (in mole unit) plot for the Huzhiyan lamproites. Average rock types from alkali basalts to kimberlites define a linear trend similar to the trend manifested by lamproites (data from Bergmann, 1987)

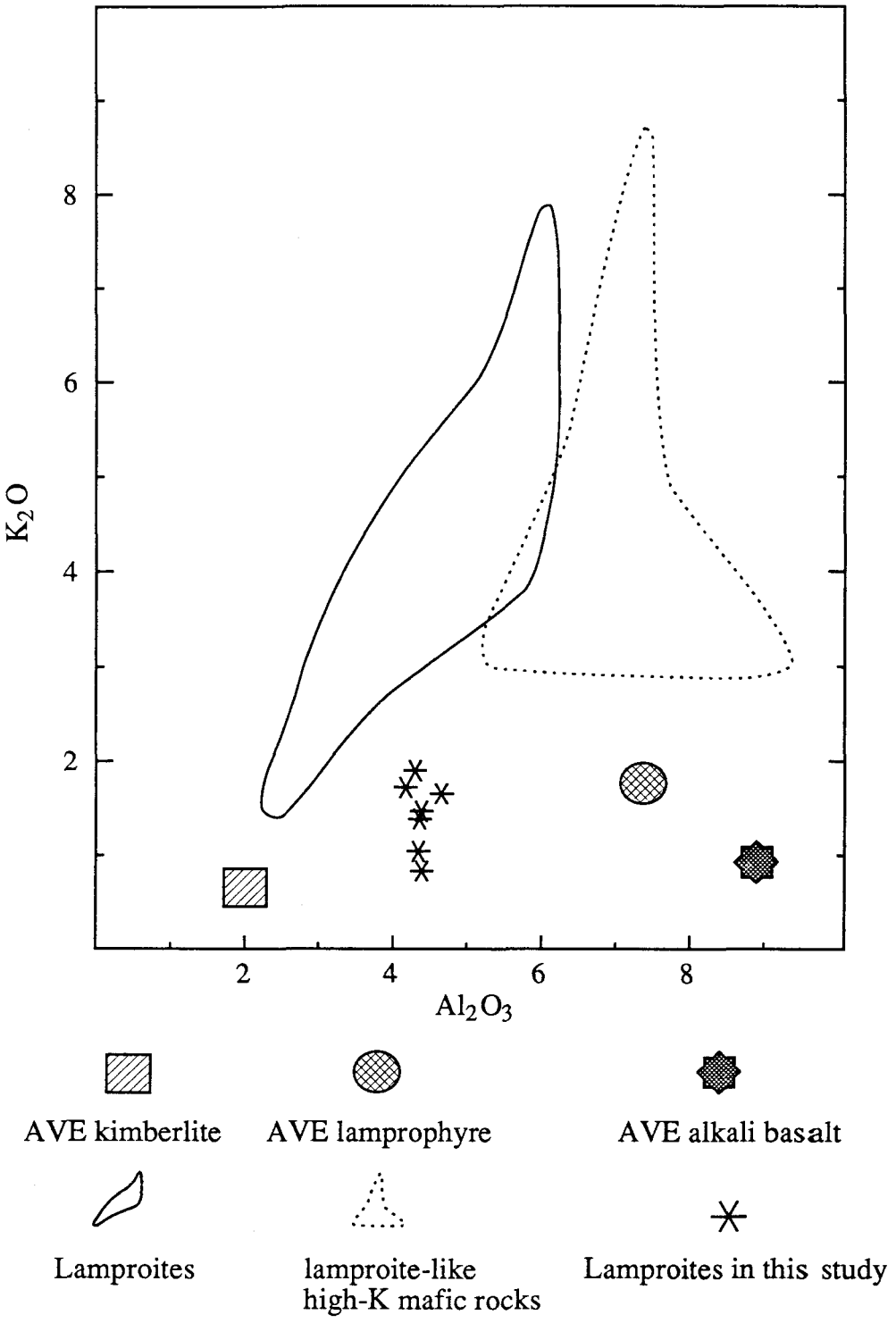

Fig. 4.4b K_2O versus Al_2O_3 (in mole unit) plot for the Huzhiyan lamproites. These Huzhiyan rocks show distinct characters that most resemble those of the lamproite family (data for comparison from Bergmann, 1987).

of the basanites, and within the typical range of this element in all other lamproites (Bergman, 1987). The lamproites are enriched in most incompatible elements (Table 4.4, Fig.4.5). Their REE patterns are differentiated with $(La/Yb)_N$ ratios of 23.8-27.3. On a Thompson spidergram (Thompson, et al., 1984), the Huzhiyan lamproites show a trace element trend very similar in shape but at a lower level compared to lamproites from other places in the world (Fig.4.5). Though less enriched in LILEs (Large Ion Lithophile Elements) than typical lamproites, the Huzhiyan rocks are enriched in K, U, Ba and Rb compared to all other alkaline rocks including kimberlite. The enrichment is about 2 times for Rb, Th, U and K; 3-4 times for Ba relative to the basanites. The LILEs are also enriched relative to the LREEs (Light Rare Earth Elements) in the lamproites. This last character is common to all lamproites; but very rare in alkali basaltic rocks if it exists at all. While the LREEs of the Huzhiyan lamproites are similar in pattern shape and level to the basanites and trachybasalts, the HREEs (Heavy Rare Earth Elements) of the lamproites are relatively depleted, which may suggest garnet retention during partial melting. HREE depletion is another common chemical trait among lamproitic rocks (Bergman, 1987). The trace element chemistry differences between the Huzhiyan lamproites and the basanites and trachybasalts, the former having high LILEs but lower HREEs, reflect two fundamental differences in the source between lamproitic and alkali basaltic rocks. These systematic fundamental differences could be related to the K/Na difference between the two rock series and to the MgO-Al_2O_3 trend demonstrated in Fig. 4.4a.

Another important feature of the trace element chemistry of the lamproites is the strong negative anomalies at Nb-Ta and at Zr-Hf-Ti on the spidergram (Fig. 4.5), a typical feature of subduction-related volcanic rocks (Wilson, 1989). This indicate that the lamproites were derived from a mantle which has retained some ancient subduction feature. Though Nb-Ta and Ti anamolies appear in most lamproites, they are much stronger in the Huzhiyan rocks. At the beginning of this chapter, it was said that the Huzhiyan rocks could be best classified as lamproites. As the detailed major and trace element chemistry demonstrated, these Huzhiyan rocks are similar to lamproites. But the rocks have lower

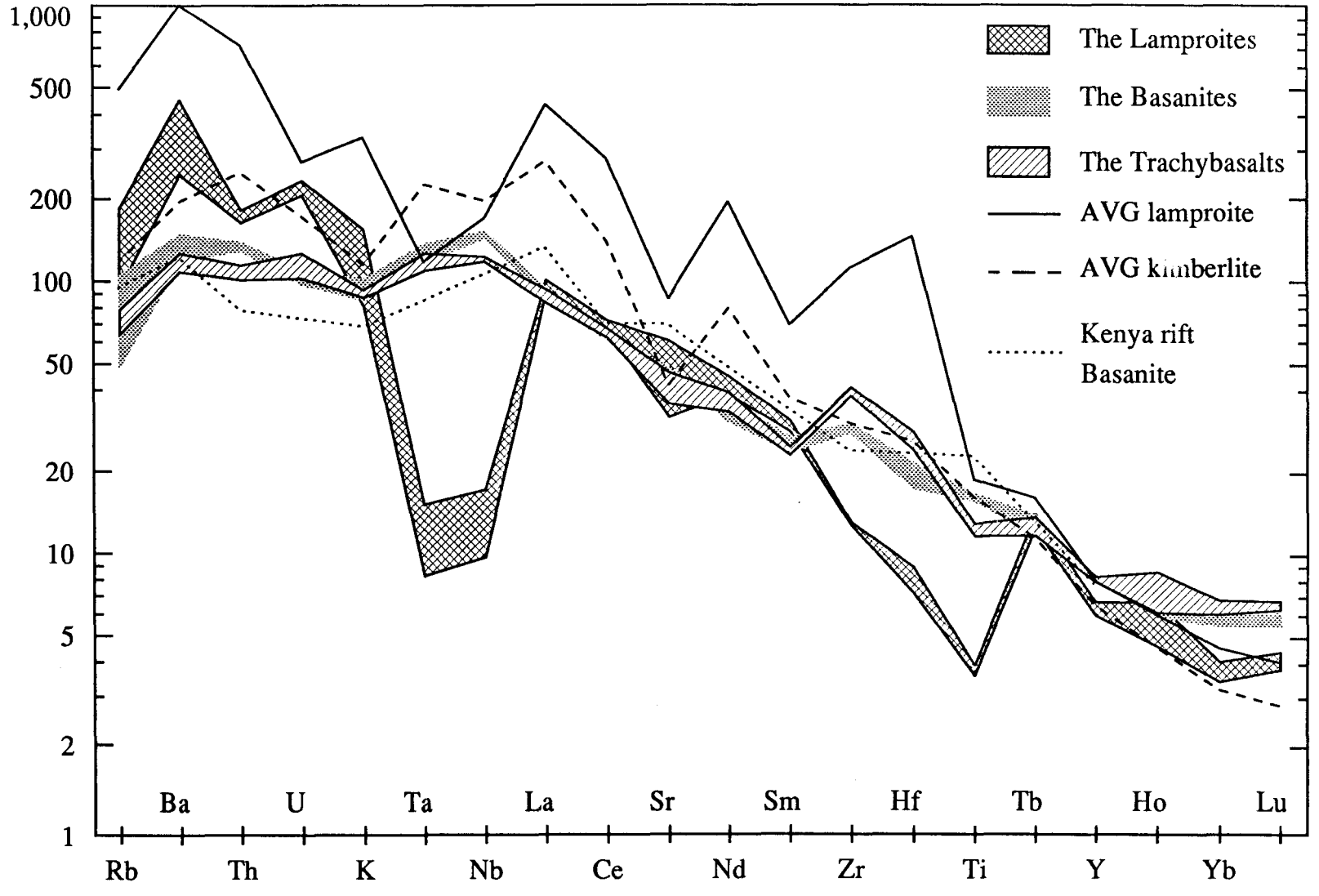

Fig. 4.5 Spidergrams for the alkaline rocks from inland southern China. The basanites and trachybasalts are similar to Kenya continental rift basanites. The Huzhiyan lamproites best resemble average lamproite but have lower incompatible element concentrations (data from Bergman 1987, Wilson 1989).

K_2O and LILE elements contents than typical lamproites. The negative Ta, Nb, Zr, Ti, Hf anomalies are also much stronger than those of most lamproites (Fig.4.5). In these regards, the Huzhiyan rocks are not lamproites *sensu stricto*; but they do fit in the lamproite clan in a broad sense (Bergman (1987).

At this point, it is necessary to examine whether the analyzed rock data could reflect the composition of the liquid magma. It is very hard to estimate the true magma liquid composition because of the presence of numerous olivine megacrysts. As the Ni and Cr contents suggested, the Huzhiyan rocks may have olivine accumulation. The composition of the olivine phenocrysts from the rocks ranges from Fo 92.5 to 95 with an average 92.9. Such olivines would have equilibrated with a magma having #Mg (magnesium number) about 80 (Roeder & Emslie, 1970). This is a little lower than that of the analyzed rocks which have #Mg 83-84.3. Removing 2-3% olivine will lower the #Mg of the Huzhiyan rocks to about 80. By removing 2-3% olivine (Fo 93) the MgO contents of these rocks are lowered to 14-15 wt%, which are still quite high. The high Fe_2O_3/FeO ratio (see wet chemical analyses in Appendix A) and high non-structural H_2O contents indicate that these rocks are somewhat altered. But the fresh olivine and pyroxene mineralogy (Chapter 3 plate 1) of the two low volatile samples (Table 4.1 sample 1 and 4) argues against significant alteration. The close similarity of the low water and high water samples suggests that most of elements were not significantly affected (but Na, K contents may have changed). Allowing for a small amount of olivine accumulation, these data can be considered to reflect the major chemistry of the liquid magma.

4.3 BASANITES

The basanites are the most silica-poor of the rocks studied. They have high alkali contents (Na_2O+K_2O > 5 wt%) and relatively low K/Na (<0.5) ratios compared to the lamproites (Table 4.2). They fall to the left of the olivine-albite joint on (Na+K)-Si diagram, as all basanites in the world do (Fig. 4.6; Francis & Ludden, 1990). They contain

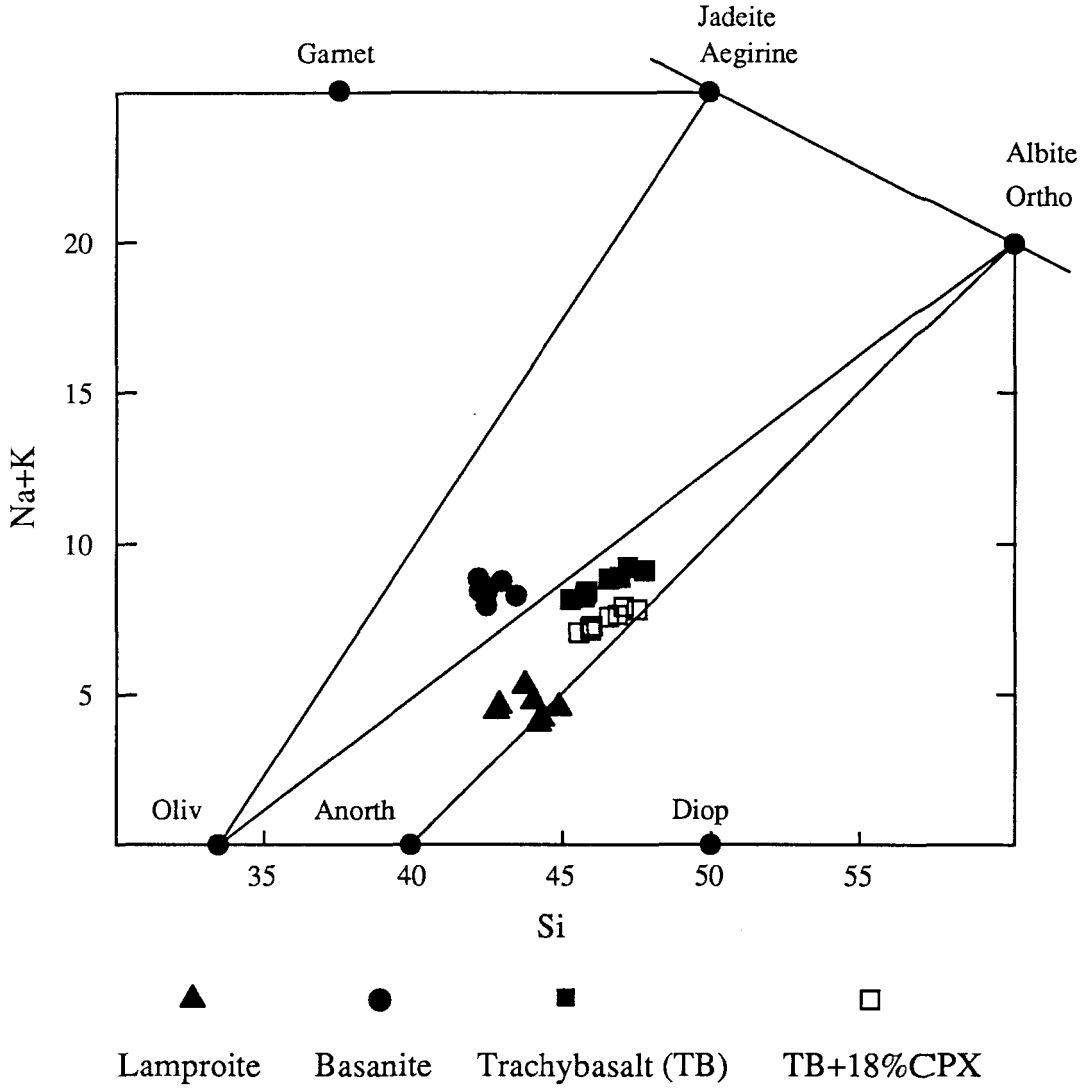

Fig. 4.6 Na+K versus Si (mole %) diagram for classification. It basically shows the same result as Le Bas classification diagram; but it allows analysis of the rocks' chemical trend using mineral joint lines (After Francis & Ludden, 1990).

about 9.5 wt% MgO and about the same amount of CaO. Their Al_2O_3 (13-14 wt%) is a little lower than most basalts. These major oxide contents establish these rocks as basanite. On the total alkali-silica diagram (Fig. 4.1), these basanites are transitional to the trachybasalts. This is consistent with the petrographic observations in which the basanites show a gradual transition to the trachybasalts in texture and mineralogy.

On Harker diagrams (Fig. 4.3b), the basanites show very limited variation. The Cr (212-267 ppm) and Ni (~200 ppm) contents of the basanites are close to the level of the two elements in suggested primitive tholeiitic magma (BVSP, 1981). The magnesium number of the basanites is about 66 (Table 4.2), slightly lower than primitive tholeiitic melts. The most magnesium-rich olivine phenocryst in the basanites has a composition about Fo_{85}, suggesting a equilibrated magma of even lower #Mg (~63).

The Zr, Ti and P of the basanites are about the same level as those of the trachybasalts; but are 4-5 times as much as in the lamproites (Table 4.5). Sc in the basanites is about 20 ppm, similar to that in the lamproites; but is about 1.5 times higher than in the trachybasalts. The Sc content of the basanites, typical for alkaline mafic rocks (Francis & Ludden, 1990; Wilson, 1989), is significantly lower than that of oceanic-floor tholeiites. Incompatible elements are highly enriched in the basanites compared to primitive mantle (Fig. 4.5). The LILEs of the basanites are depleted compared to the lamproites; but are enriched compared to basanites from Kenya (Wilson, 1989) or Hawaii (Macdonald & Katsura, 1968), and about twice as much as in oceanic island or island-arc alkali basalts (BVSP, 1981). REE patterns of the basanites are strongly differentiated with $(La/Yb)_N$ ratios of 14.4-16.7 (Fig. 4.5). The LREEs in the basanites are about 100 times of that in primitive mantle, at about the same level to that in the lamproites. Compared to the lamproites, the apparent difference on spidergram is that the LILEs are depleted relative to La in the basanites. This difference between the basanites and lamproitic rocks is shared by all alkali basaltic rocks. The overall spidergram of the basanites resembles that of Kenya rift basanites, except that the latter are less enriched in LILEs (Fig. 4.5).

Table 4.5 Trace element composition of the basanites in Juxiang, southern China (Unit in ppm, NA--for No Available value)

	Ban1	Ban2	Ban3	Ban4	Ban5	Ban6	Ban7	Ban8
Cs	4.3	2.7	2.0	2.4	3.0	2.7	2.4	2.4
Rb	65	28	65	29	32	41	48	31
Ba	672	654	699	851	654	645	618	645
Th	8.7	8.8	8.1	8.1	8.7	8.5	8.6	8.8
U	1.9	2.0	1.9	1.9	1.7	1.7	1.9	1.9
Pb	<5	<5	<5	<5	<5	<5	<5	<5
Ta	5.4	5.1	4.7	4.5	4.6	5.1	5.4	5.5
Nb	83	84	82	84	83	83	77	81
Zr	232	234	232	233	234	234	258	247
Hf	4.9	5.0	4.6	4.8	5.2	5.2	6.2	5.9
La	48.5	48.6	46.4	47.6	49.7	46.7	52.6	52.6
Ce	87.2	92.5	87.0	89.6	93.8	89.3	91.3	88.4
Nd	32	36	33	34	41	39	36	34
Sm	8.81	8.82	8.06	8.02	8.84	8.46	9.55	9.34
Eu	2.71	2.77	2.56	2.62	2.77	2.63	2.75	2.73
Tb	1.07	1.16	0.96	1.03	1.27	1.19	1.04	1.13
Ho	0.8	0.9	0.8	0.8	1.1	1.1	0.8	0.8
Yb	2.09	2.16	2.00	1.97	2.27	2.17	2.15	2.11
Lu	0.32	0.33	0.32	0.34	0.32	0.30	0.35	0.34
Y	27	27	28	27	28	28	28	27
Sr	840	820	853	805	827	830	863	795
Sc	20.9	21.1	20.2	20.9	22.0	21.2	19.7	20.3
V	191	203	200	206	196	223	183	195
Cr	239	212	253	226	239	226	267	212
Ni	195	207	-	194	230	220	201	221
Co	64	63	62	56	66	75	71	79
Cu	55	42	41	27	48	39	36	44
Th/La	0.18	0.18	0.17	0.17	0.18	0.18	0.16	0.17
(La/Yb)	15.56	15.09	15.56	16.21	14.69	14.43	16.41	16.72

4.4 TRACHYBASALTS

The trachybasalts are the most silica-rich rocks in this study. They are silica-saturated (Table 4.3), which, as mentioned earlier, is unusual. Like the basanites, they have low K/Na ratios though some of them may be called shoshonite in the classification proposed by Le Bas (1986). Compared with the basanites, the trachybasalts have higher SiO_2 and Al_2O_3 contents , lower MgO and CaO contents. The alkali contents of these rocks are at the same level as of the basanites. On Francis & Ludden's (1990) (Na+K)-Si diagram (Fig. 4.6), these rocks plot between the olivine-albite joint and the feldspar joint, similar to alkali olivine basalts, but with higher alkali content. To study the oxide variations, oxides-silica variation diagrams for these rocks are presented in Fig 4.3c. It is interesting to note that the trachybasalts lie on a continuous trend with the basanites toward the SiO_2 rich direction, and most of the oxides show similar trends in the two rock types. To reinforce this point, the trachybasalts are replotted on Harker diagrams together with the basanites (Fig.4.7a, b). The diagrams demonstrate that the trachybasalts and the basanites have collinear oxide variation trends for Al_2O_3, MnO, P_2O_5, K_2O, and Na_2O. In contrast, the MgO and CaO contents have an apparent break between the basanites and the trachybasalts.

Trace element characteristics of the trachybasalts are similar to that of the basanites. Cr, Ni contents in the trachybasalts are at about the same level as in the basanites (Tables 4.5 & 4.6), and are not directly related with the MgO contents of the rocks (Fig. 4.8). Therefore, the Ni and Cr contents could have been buffered by some phases, like small amount of sulphides as suggested by the PGE (platinum-group element) data (see discussion later), and ulvöspinel which is ubiquitous in the trachybasalts and basanites. The REE of the rocks are strongly differentiated with $(La/Yb)_N$ ratio varying between 13.1 and 14.9. All of the incompatible elements in the trachybasalts are enriched relative to primitive mantle (Fig.4.5). The enrichment pattern and level are almost indistinguishable from that of the basanites except the latter have slightly lower HREEs. Like the basanites,

Table 4.6 Trace element composition of the trachybasalts in Ningyuan, southern China (Unit in ppm, NA--for No Available value)

	TB1	TB2	TB3	TB4	TB5	TB6	SH1	SH2	SH3
Cs	1.9	2.1	1.7	1.6	2.3	2.3	0.8	1.2	1.8
Rb	36	40	31	44	38	42	41	37	43
Ba	537	627	627	627	627	627	537	448	537
Th	6.5	6.7	6.4	7.1	6.5	6.8	7.2	6.9	7.7
U	2.3	2.3	2.1	2.1	1.8	1.7	1.9	2.1	2.2
Pb	<5	<5	<5	<5	<5	<5	<5	<5	<5
Ta	4.3	4.4	4.4	4.9	4.4	5.3	4.8	4.6	5.0
Nb	65	66	67	67	66	66	69	67	69
Zr	308	317	319	328	315	324	341	331	342
Hf	6.2	6.5	6.4	7.5	6.9	7.4	7.5	7.1	7.6
La	44.9	46.1	45.2	50.0	47.6	50.5	47.6	50.1	53.0
Ce	89.8	91.5	90.9	96.2	89.2	89.6	89.4	95.0	99.1
Nd	36	36	35	41	40	34	39	41	43
Sm	8.15	8.35	7.97	8.31	8.03	8.81	7.82	8.29	8.28
Eu	2.37	2.59	2.58	2.74	2.60	2.87	2.52	2.72	2.71
Tb	1.03	1.00	1.02	1.19	1.14	0.98	1.12	1.19	1.17
Ho	0.8	0.8	0.8	1.1	1.1	0.7	1.0	1.0	1.1
Yb	2.23	2.26	2.21	2.53	2.43	2.27	2.33	2.49	2.56
Lu	0.37	0.38	0.38	0.37	0.35	0.38	0.34	0.37	0.37
Y	26	27	27	27	27	28	28	27	28
Sr	690	703	713	679	705	972	701	676	684
Sc	13.6	13.6	13.5	13.9	13.8	14.1	13.4	12.9	13.1
V	146	143	160	141	131	143	142	129	128
Cr	342	274	205	205	-	205	205	274	205
Ni	253	227	230	161	207	175	211	205	193
Co	57	57	52	53	62	73	52	62	50
Cu	48	39	39	34	35	37	39	44	39
Th/La	0.14	0.15	0.14	0.14	0.14	0.13	0.15	0.14	0.15
(La/Yb)	13.50	13.68	13.72	13.26	13.14	14.92	13.70	13.50	13.89

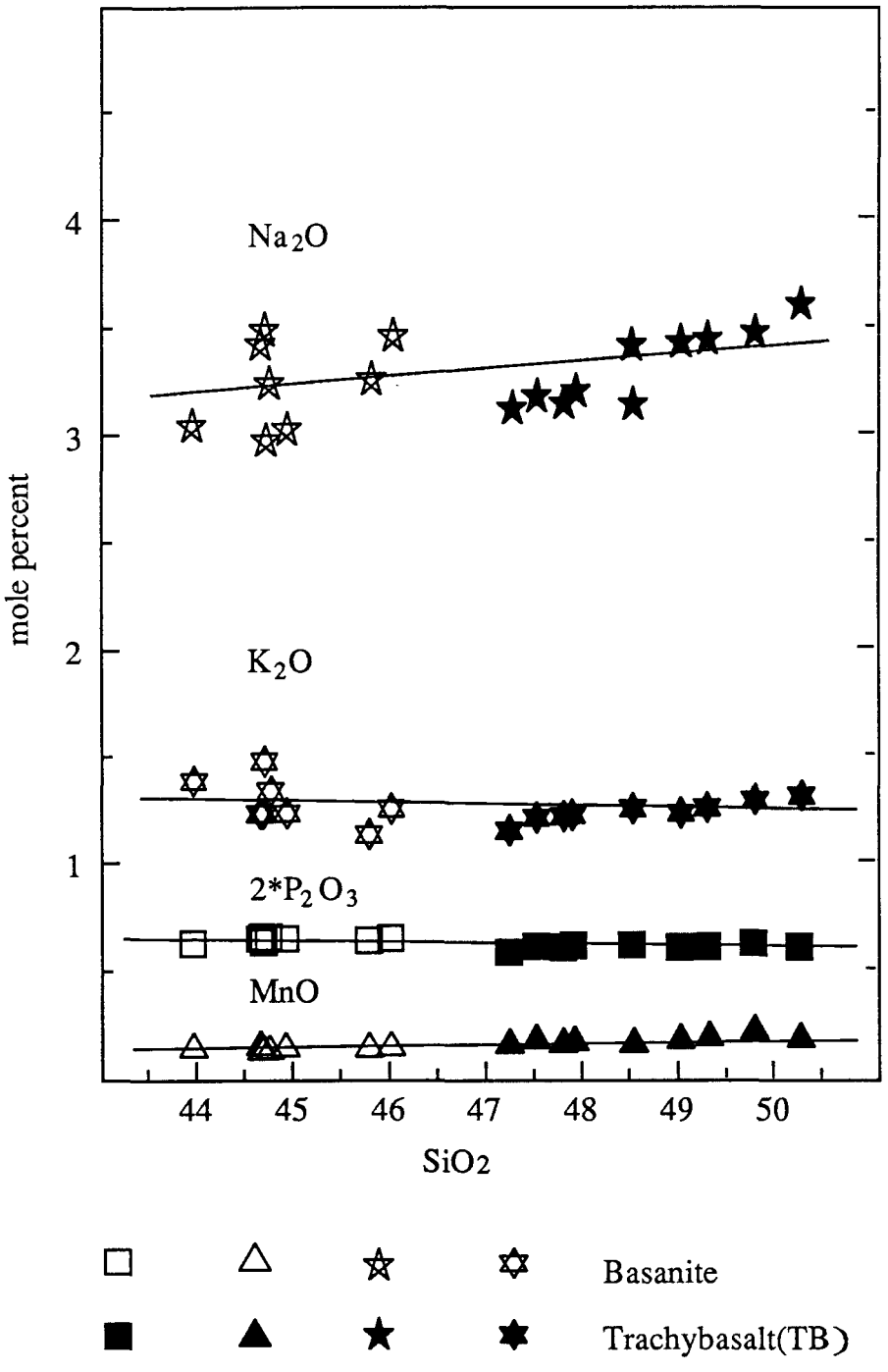

Fig. 4.7a Harker diagrams showing the linear variation trends of oxides defined by the basanites and the trachybasalts.

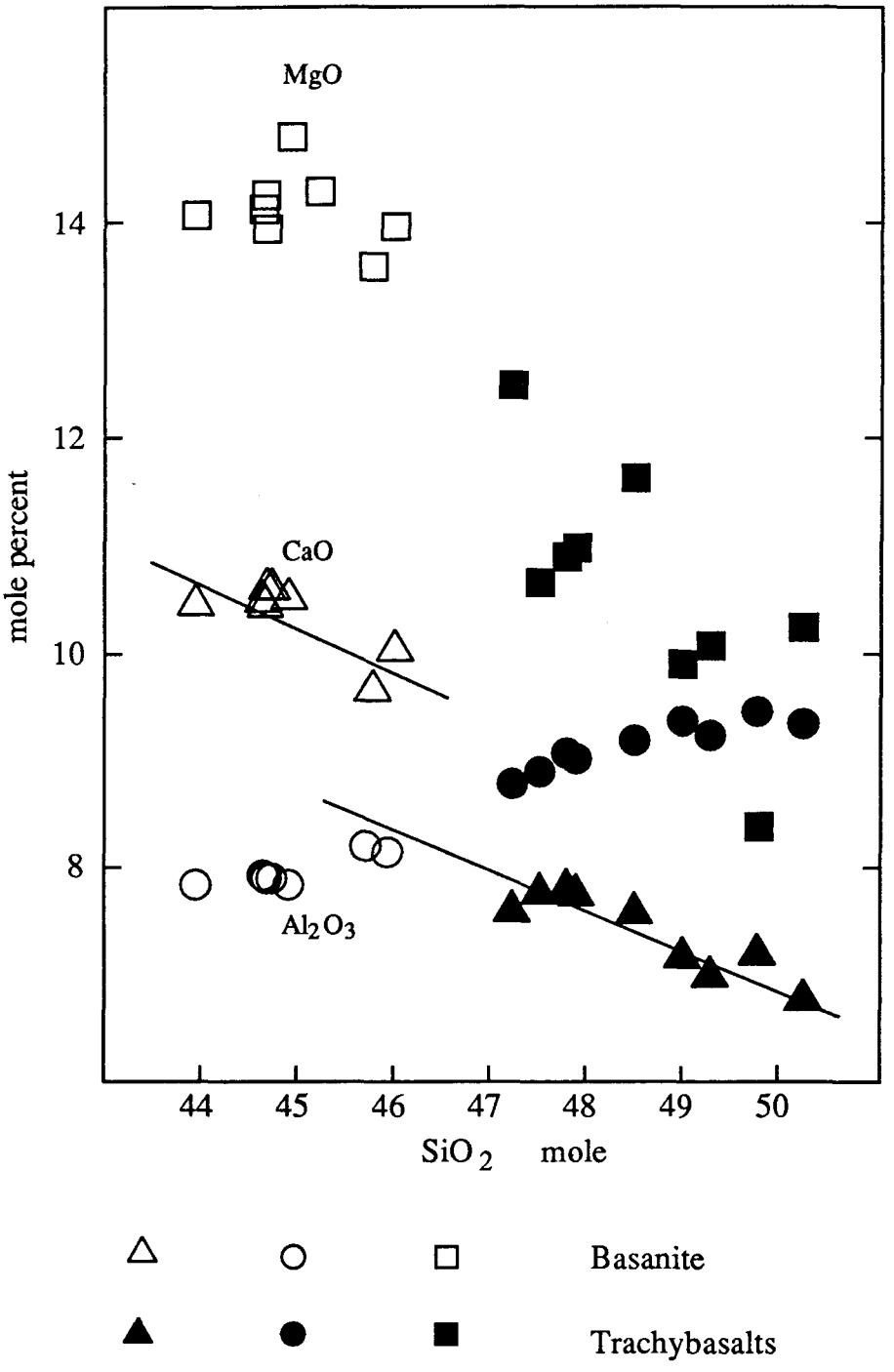

Fig. 4.7b Contrast to figure 4.7a, these Harker diagrams show the oxide trends breaks from the basanites to the trachybasalts.

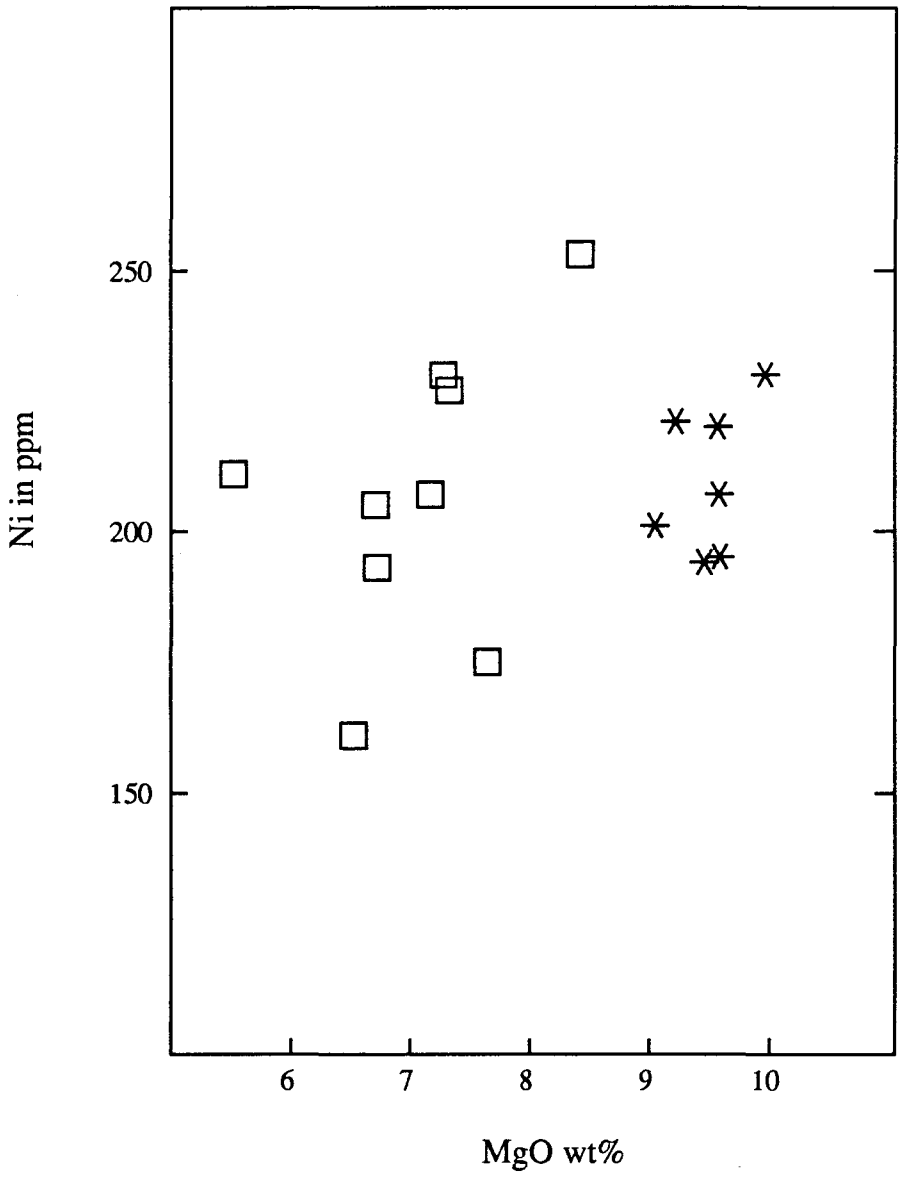

Fig. 4.8 Ni versus MgO plot for the trachybasalts □ and basanites ✳ The lack of correlation between Ni content and MgO content suggests more than one phase (Oliv) control over the Ni in the magma.

the trachybasalts show close affinity to continental rift-related alkaline mafic rocks, especially Kenya basanites (Fig. 4.5). In contrast to the similarity of other trace elements between the two rock types, Sc in the trachybasalts (~13 ppm) is only about two thirds of that in the basanites. This Sc depletion could be related to the CaO and MgO depletion of the trachybasalts relative to the basanites. At first glance, the depletion in Sc and mild enrichment in HREEs of the trachybasalts relative to the basanites are contradictory, it could signify more than one control factor. Considering the control of clinopyroxene and garnet over the HREEs and Sc in magmas may shed some light to the problem. Both HREEs and Sc are strongly partitioned in garnet (K_D is about 4.4-6.1 for the HREEs, 4.3 for Sc, Irving, 1978). Clinopyroxene, however, takes about 6 times more Sc (K_D~3, Wedepohl, 1985) than HREEs (K_D~0.5, Wedepohl, 1985). If the trachybasalts and the basanites have similar mantle source, a small amount of garnet in the residue could account for the weak HREE depletion of the basanites relative to the trachybasalts. The residual garnet, however, would have also retained Sc in source. Therefore, lower Sc in the basanites should be expected. This is opposite to the fact that the basanites have higher Sc than the trachybasalts.

In fact, the source for the basanites and trachybasalts probably does not contain any garnet at all (these rocks most possibly originated in ampibole peridotite zone which is limited to low pressure spinel field. Refer to chpater 5). The trachybasalt magmas may originally have higher HREEs and Sc than the basanites because of a larger degree of partial melting. The strong depletion of Sc in the trachybasalts could be explained by clinopyroxene crystallization. Diopside crystallized from the parental trachybasalt magmas and depleted the magma in Sc. So the resulting trachybasalts have lower Sc than the basanites. Diopside crystallization would have also depleted the magma in CaO and MgO. Because of the similar SiO_2 percentage in diopside and in the trachybasalt magmas, SiO_2 and all other oxides not consumed by diopside precipitation will not change much; but MgO and CaO will become lower and lower as the crystallization continues. This can explain the lower MgO and CaO contents of the trachybasalts than the basanites (Fig. 4.7b).

This clinopyroxene crystallization hypothesis will be tested using high-pressure phase diagrams and by numerical modelling in chapter 5.

4.5 PLATINUM-GROUP ELEMENTS (PGEs)

PGEs could be helpful in studying mafic magma evolution processes. Though little PGE data are available for alkaline mafic rocks, and the behaviour of the PGEs is less well understood in sulphide-poor magmas than in sulphide-rich magmas (Barnes et al., 1988). With the intention to observe further the behaviour of PGEs in alkaline rocks, 4 samples of the basanites, 5 trachybasalts and 3 lamproites were analyzed for their PGE contents (Table 4.7). Because the limitation of available analytical techniques, only an upper limit can be set for Os and Ru. The analytical results for Ir, Pt, Pd, and Rh are reasonably good. Samples with 3 or more data on the PGEs were plotted on mantle normalized diagram (Fig.4.9). Compared to the LILEs (100-500 times of mantle), the Cu, Pt, and Pd contents of all the alkaline rocks in this study are low (~0.5-4 times mantle). This could be explained either by sulphide retention or an earlier partial melting event which depleted the mantle in these elements (see below). The Ir contents of the basanites and trachybasalts are low (~0.03 times mantle) and depleted relative to the Pt. This indicates that Ir is compatible during partial melting, probably because of olivine. The lamproites have higher Ir concentration (~0.1 times mantle), it still behaves as a compatible element but less so than in the basanites and trachybasalts. The high Ir content suggests that either less olivine was retained in the source when the lamproites formed or that the source for this rock type was more olivine rich. The high Ir content is consistent with the high Ni and Cr contents of the lamproites.

The trough-shaped PGE patterns of the alkaline rocks and the very low level of PGEs could have been caused either by (a) sulphide retention in the mantle or (b) sulphide segregation from the system. considering the first possibility it can be argued that, since the basanites and trachybasalts formed from low degree of partial melting (see chapter 5)

Table 4.7 PGE concentrations of the alkaline rocks from the inland subvolcanic belt of southern China (PGEs in ppb; Cu, Ni in ppm; NA--for No Available value)

	Ni	Os	Ir	Ru	Rh	Pt	Pd	Au	Cu
Lam1	847	<0.43	0.35	<2.25	<.54	3.33	2.6	0.61	64
Lam2	934	NA	0.57	<13.91	1.42	<6.29	<10.56	0.62	47
Lam3	694	0.7	0.36	2.55	<0.27	3.03	2.39	0.84	61
Tb1	253	<2.07	0.41	<15.58	0.82	<10.3	<7.01	1.48	48
Tb2	227	<0.56	0.13	<3.84	<0.31	2.79	<4.82	0.2	39
Tb4	161	<1.39	0.13	<8.5	0.5	5.69	8.73	1.1	34
SH1	177	<1.36	0.14	<7.42	<1.23	12.18	<10.05	0.25	39
SH2	319	<1.92	0.16	11.48	<0.8	<7.51	18.4	0.33	44
Ban2	234	<1.26	0.13	<8.32	<0.66	<4.81	<5.68	0.48	42
Ban3	1142	<0.67	0.05	<4.79	<1.26	<2.32	<3.07	0.4	41
Ban4	194	1.05	0.16	<6.0	0.97	3.75	<6.68	0.41	27
Ban5	184	<0.41	0.12	NA	<0.38	<1.65	2.38	0.61	48

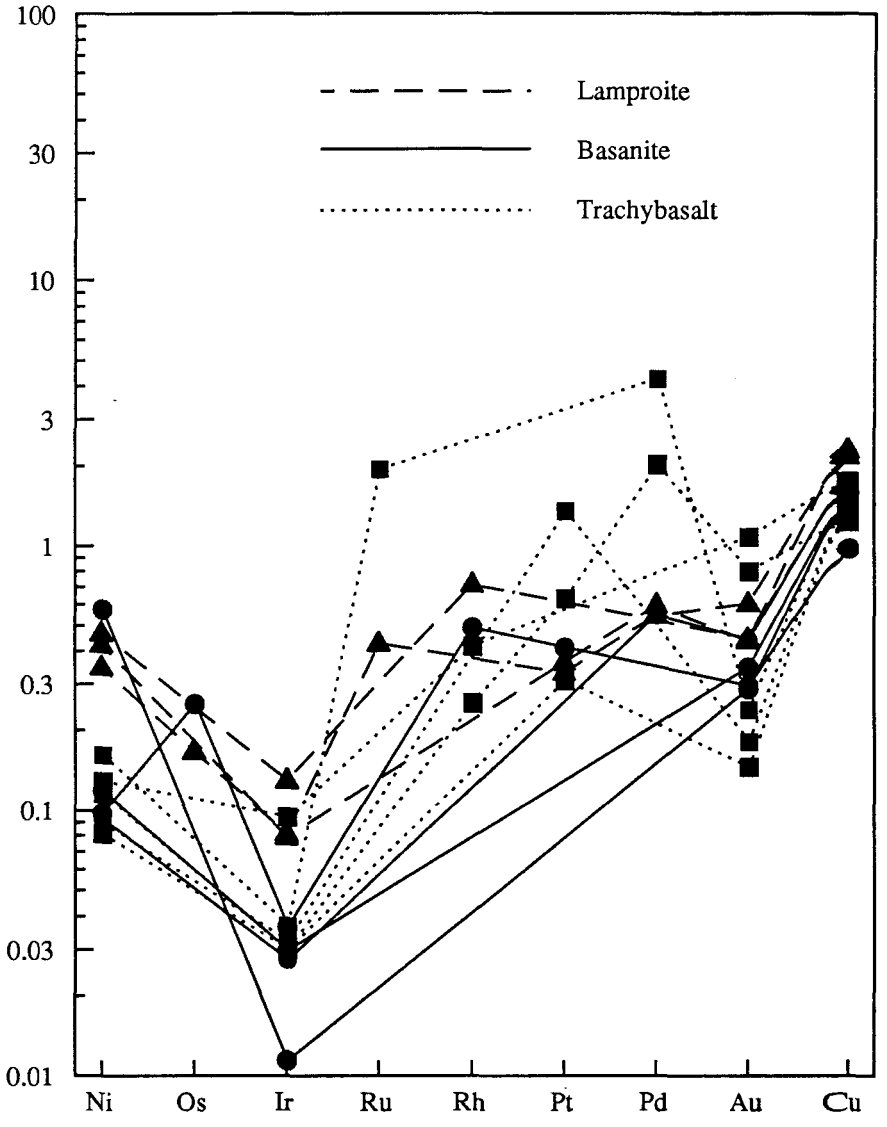

Fig. 4.9 Mantel-normalized PGE distribution diagram (Barnes et al., 1988) for the alkaline rocks from the inland subvolcanic belt of southern China.

and approximately 20% partial melting is required to consume all the sulphides in the mantle (Barnes et al., 1988) it is probable that some sulphides remained in the mantle as restite phase and thus retained the Pt, Pd and Cu. Assuming 1% partial melting the magma should contain 0.5 ppb Pd, 1 ppb Pt and 55 ppm Cu. The point that deserves attention is how did any PGE get into the magma since the PGE have such high K_D into sulphides (>10000, Barnes et al., 1988), the mantle contains approximately 0.1% sulphide so K_D would be at least 10 for the mantle. One way to account for the presence of the Pt and Pd is to suggest that a small amount sulphide was entrained as sulphide droplets with the magma. The second possibility would require that during an earlier melting event or metasomatism of the source most S had been removed form the system so very little or no sulphides remain in the source and Pt and Pd could be released during the second event. The effect of this on the PGE is more difficult to predict, but possibly some Pt and Pd were lost in an earlier partial melting event and the Pt and Pd now present in the rocks represents the remaining Pt and Pd.

To analyze possible phase control over the PGE evolution, the PGE data are plotted on the Pd/Ir versus Ni/Cu and Ni/Pd versus Cu/Ir diagram (Barnes, et al., 1988) with projected mineral control vectors of olivine, chromite and sulphides or platinum group element minerals (PGM) (Fig.4.10). In defining the fields of the rocks under study, half upper limit value of Pd is used for samples without definitely measured Pd datum. Like the metal patterns, these metal ratio diagrams show once again consistency with the major and trace element chemistry about the close relation between the basanites and the trachybasalts. The significant overlap between fields of different rock types suggest that PGEs may not be efficient discriminator of magma evolution processes. However, the positions of the lamproites on Fig. 4.10a and Fig. 4.10b do agree with olivine accumulation suggested by the high #Mg of the rocks. PGEs can be used to study source characteristics and processes of alkali mafic rocks, but it is hard to do so at present. Much more PGE data is needed.

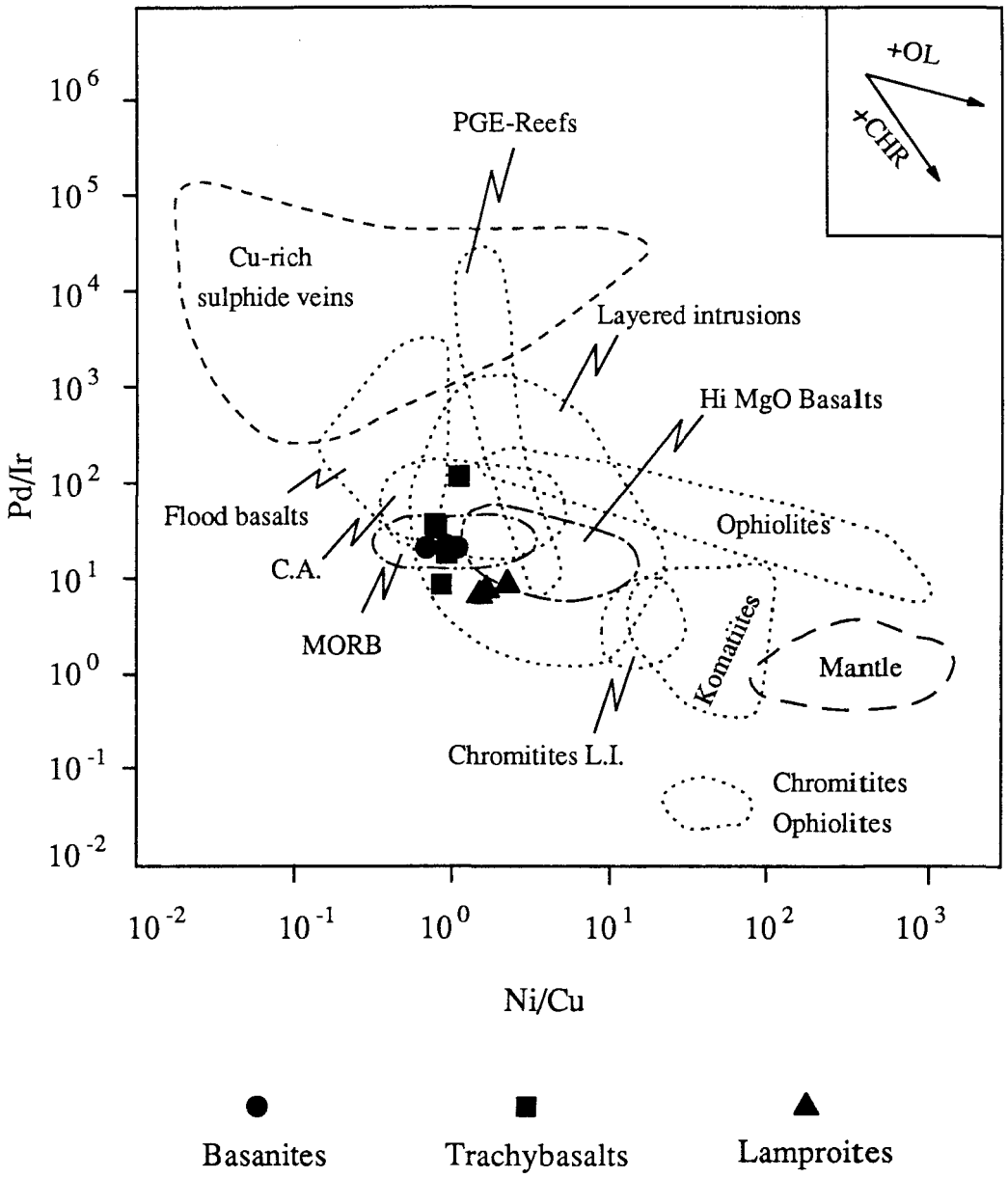

Fig. 4.10A

Pd/Ir versus Ni/Cu plot for the alkaline rocks from the inland subvolcanic rock belt of southern China. The overlapping field of the basanites and trachybasalts suggests a similar origin of the two rock types. The lamproites fall in the High MgO basalts field indicating their high MgO characters (Barnes, et al., 1988).

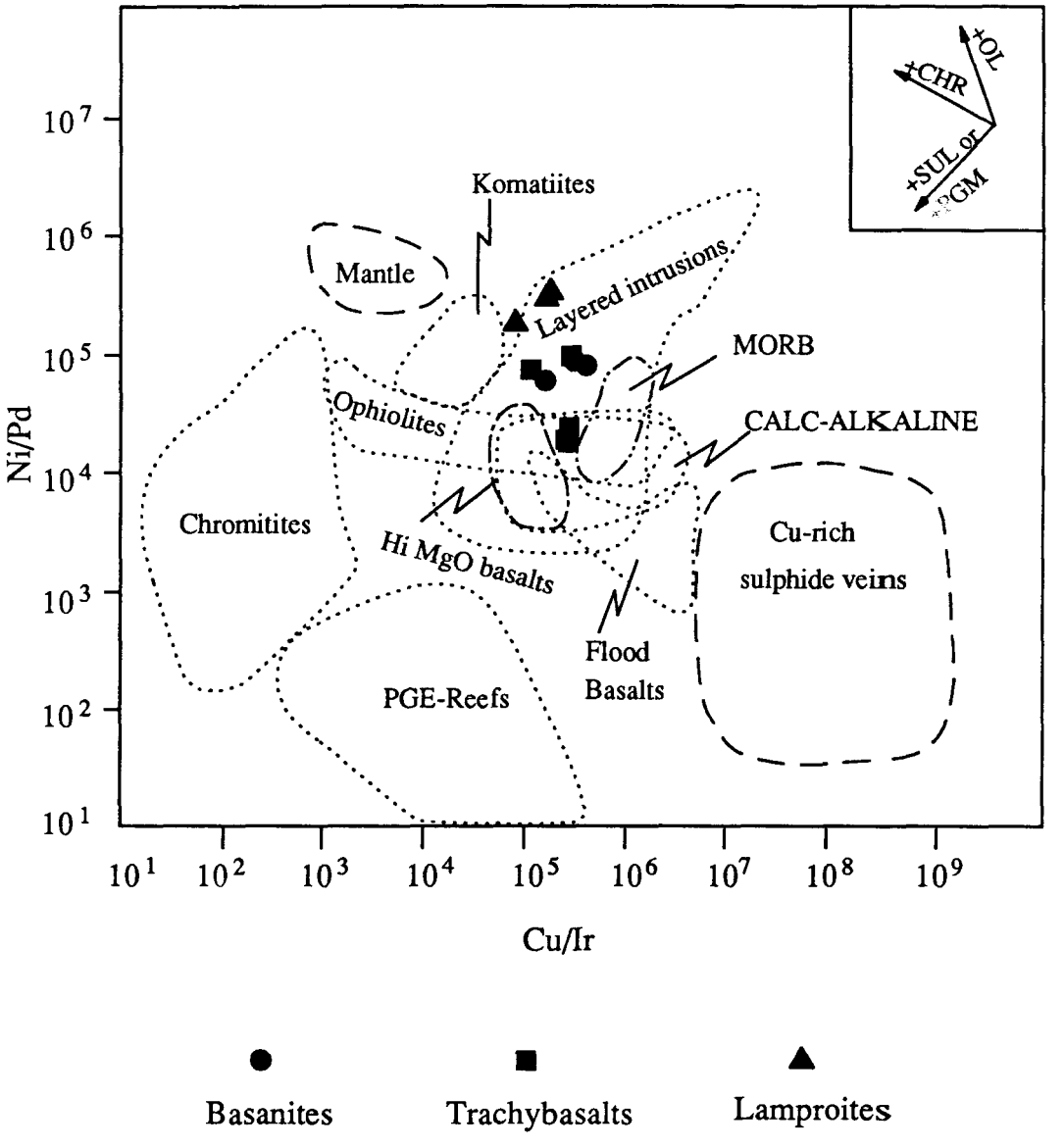

Fig. 4.10B

Ni/Pd versus Cu/Ir plot for the alkaline rocks. The lamproites fall off the trend from primitive mantle to flood basalts indicating some olivine accumulation in the lamproites (Barnes, et al., 1988).

CHAPTER V

PETROGENESIS

5.1 INTRODUCTION

The study of igneous petrogenesis involves answering two questions: What is the origin of the parental magma in a given rock association? How were the individual igneous rocks of the rock association derived from the parent magma? (Hess, 1989). In addressing the first question, the first thing to do is to identify the composition of the parent magma of a given rock association. Once this composition has been estimated, the source composition of the parent magma can be deduced by geochemical constraints.

Ideally, to answer the second question a crystallization sequence must be established (Bowen, 1928), which explains how the parent magma produced the remaining members of a rock association. This step is usually approached through a careful petrographic analysis and confirmed by geochemical data (Hess, 1989). In reality, a rock series is not always derived from a single parent magma, that is the geochemical data of the rock series do not confirm to a simple model. Magma mixing of two or more parent magmas or crustal contamination by assimilation could have occurred. To make the matter more complex, the igneous rocks in a given rock association may have changed their composition through post-magmatic processes.

Therefore, in this study, work proceeds backward; the original composition of each rock type is established through the analysis of post-magmatic processes; parent magmas are identified through the analyses of fractional crystallization and crustal contamination; source chemistry of the parent magmas and the physical processes involved in generating

the parent magmas are discussed by applying the constraints of major and trace element concentrations.

5.2 WEATHERING AND DEUTERIC ALTERATION

5.2.1 Introduction

Weathering and deuteric alteration can change the composition of igneous rocks, and make it difficult to discover the relationship between rock members in a region and to deduce the composition of the parent magma. Therefore, these post-magmatic processes will be considered first for the alkaline rocks in the study area.

5.2.2 Lamproites

The lamproites are the most altered rocks in this study. The alteration is mainly manifested by the hydration of olivine megacrysts. As there is little carbonate in these rocks, the LOI content approximates the H_2O content. Therefore, the elevated LOI contents of these rocks could have resulted from this alteration, and hence the LOI content of a rock could probably indicate the degree of its alteration.

There are two samples which have significantly lower LOI contents than other samples (Table 4.1 sample #1 & #4); they also have higher CaO and Na_2O but lower K_2O contents; the K_2O decrease in the low LOI samples is complemented by about the same amount of increase of Na_2O. One possible explanation for the differences between the high and low LOI samples lies in the origin of the analcime in these rocks. If some or all of the analcime in the lamproites is a replacement of leucite or phlogopite by deuteric alteration (analcime replacing phlogopite has been observed, Plate 15), then samples with more analcime would have higher Na_2O and lower K_2O (e.g. samples #1 & #4 in Table 4.1). The problem with this explanation is that analcime replacement would have also increased the H_2O content of the samples #1 & #4, because of the higher H_2O content of

analcime compared to phlogopite. Another possible explanation for the difference between the high and low LOI samples is that the low LOI samples contain more clinopyroxene and less phlogopite than the high LOI samples. This is possible in view of the heterogeneous character of these hypabyssal lamproite dykes. The two low LOI samples are also coarser-grained than the other samples, and therefore, they could represent an earlier crystallized part of the lamproite dykes. Weathering could cause the loss of K_2O content in the samples #1 & #4, but it cannot increase the Na_2O of the two samples relative to others. Furthermore, the fresh mineralogy of the two low LOI samples suggests little weathering.

No matter what process has caused the differences of the alkali and CaO contents between the two low LOI samples and others, the process would have not affected much the contents of other oxides, because the contents of oxides other than K_2O, Na_2O and CaO are very similar between the low and high LOI samples. Therefore, the major oxide composition of the lamproites, at least for the oxides other than K_2O, Na_2O and CaO, can be considered not significantly affected by weathering or deuteric alteration.

5.2.3 Basanites

The basanites are very fresh rocks. No weathering or significant alteration was observed in thin sections of these rocks except for some iddingsitization. Though they have higher water contents than most recent fresh basaltic rocks, the higher water content may be a magmatic feature in view of the presence of some mica and/or kaersutite in the groundmass.

5.2.4 Trachybasalts

The trachybasalts have a wider compositional range. Though some samples are significantly weathered, most of them are quite fresh. Samples selected for composition analysis were carefully examined using a microscope, and no significant alteration or

weathering was observed. Therefore, the effect of the post-magmatic processes on the trachybasalts is considered to be insignificant.

5.3 CRUSTAL CONTAMINATION

5.3.1 Introduction

Alkaline mafic rocks are mantle derived (Wilson, 1989), but they may not truly reflect the chemistry of their mantle source, because they could have been contaminated as they passed through the crust to the surface. Therefore, it is necessary to evaluate the effects of crustal contamination before proceeding to demonstrate any chemical relationship among the alkaline rocks in this study.

5.3.2 Lamproites

The high MgO and low Al_2O_3 character of the lamproites (Table 4.1) suggests that there has not been significant crustal contamination during magma transportation, at least as far as major elements are concerned. Otherwise higher Al_2O_3 and lower MgO than observed should be expected. The high Ni and Cr contents (Table 4.4) also suggest little crustal contamination. The highly enriched and differentiated incompatible trace element distribution of the Huzhiyan lamproites is similar to all other lamproitic rocks. This trace element character cannot identify itself as being mantle-derived or crustal contamination-related. The related Ta-Nb and Zr-Hf-Ti negative anomalies are consistent with subduction-related mantle origin.

In summary, the major element compositions of the lamproites basically reflect the chemical compositions of their magma. The trace element chemistry is also consistent this argument. However, conclusive remarks about the effect of crustal contamination on the trace element chemistry is impossible without isotopic data.

5.3.3 Basanites

The low SiO_2, high MgO (Table 4.2), and high Ni, Cr (Table 4.5) contents of the basanites argue against any significant crustal contamination. Like the lamproites, the basanites are highly enriched in LILEs and have differentiated REE patterns. In the literature, there is no consensus about the genesis of this type of REE pattern (Hess, 1989; Wilson, 1989). It is tentatively assumed that this type of trace element character of the basanites is mantle-derived based on the major element chemistry. But again it is very difficult to argue definitely about the role of crustal contamination on the trace element chemistry of these rocks without isotopic data.

5.3.4 Trachybasalts

In the same way as is the basanites, the high MgO (5.7-8.3 wt%) and Ni, Cr contents of the trachybasalts suggest little crustal contamination. The low CaO content of these rocks also argues against significant crustal contamination. The incompatible element chemistry of the trachybasalts is almost indistinguishable from that of the basanites. So the same arguments for the basanites apply to the trachybasalts.

5.4 CRYSTAL FRACTIONATION

5.4.1 Introduction

Before discussing the magma source chemistry, there is another step, that is, to identify the primary magma, that is, a magma derived from partial melting of a mantle without undergoing any differentiation (Wilson, 1989). Crystal fractionation and magma mixing can generate a wide variety of derived magmas, and hence a number of rock types that are related to one or more parental magmas. All rock types exposed in a volcanic field do not necessarily represent a single distinct primary magma type. Only those which represent the composition of a primary magma can be used to discuss the chemical

characteristics of the mantle source. Theoretically, magma differentiation is inevitable if magmas come to the surface through a magma chamber (O'Hara, 1968, Wilson, 1989). Therefore, no primary magma could be identified. In practice, parental magma instead of primary magma is identified.

Often the most magnesium-rich rock is thought to represent the parental magma of a series of chemically related rock types. Rocks with very different chemistry in a volcanic field are, in general, hard to relate each other, and are therefore commonly treated as representing different parental magmas.

In the study area, as demonstrated in chapter 4, two distinct rock series have been identified. So at least two distinct primitive magma sources existed. In the following discussion, each of the rock types will be examined to demonstrate their relationship and evolution status.

5.4.2 Lamproites

The lamproites represent a distinct magma type in the study area (see chapter 4), because they are so different in mineralogy, major and trace element concentrations from the other rock types that there is no conceivable way to relate them to the other rocks. The high Ni, Cr, and MgO contents of the lamproites indicate no olivine or pyroxene has been removed; in contrast, they could have a certain amount of olivine accumulation, as discussed in chapter 4.

To study the internal relationships among the lamproites, the rocks were plotted on a Pearce diagram of (Fe+Mg)/Th versus (Ca+Na-K-1/2Al)/Th (Fig.5.1; Pearce, 1968; Stanley & Russell, 1987). It is clear from the diagram that the two low LOI, fresher samples (on top right of the diagram) with high CaO and Na_2O but lower K_2O stand out from other samples. The relation between these two samples and the rest on this Pearce

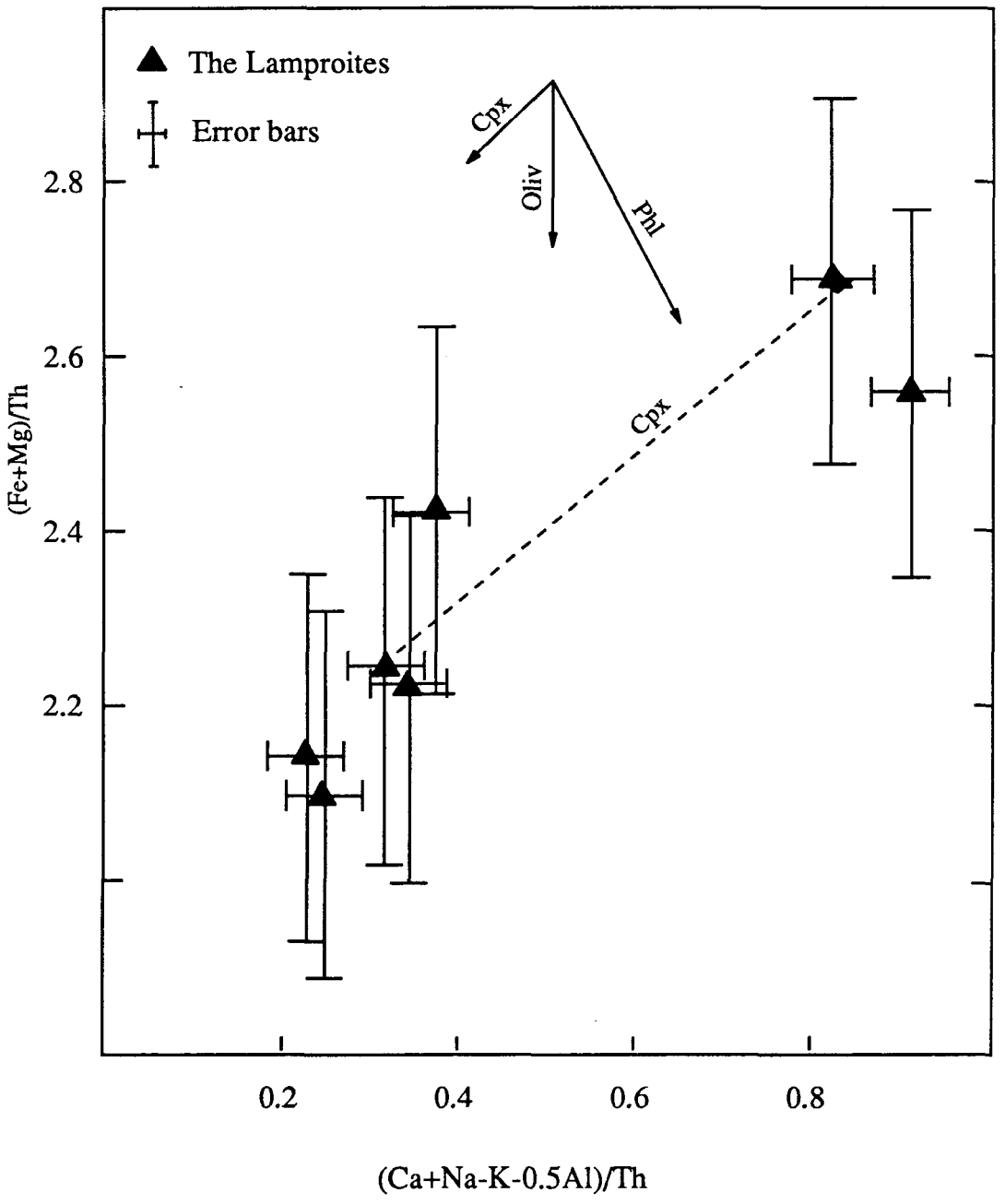

Fig. 5.1 Pearce diagram for exploring Cpx-Olivine control over the Huzhiyan lamproite evolution. The two low LOI (upper right) samples could contain more clinopyroxene and slightly less phlogopite.

diagram is consistent with the explanation that the high Na_2O and CaO samples contain more clinopyroxene than the others. But this diagram does not rule out replacement of leucite by analcime.

The magmatic evolution exhibited by the lamproites is very limited. Neither major nor trace elements show changes significant enough to affect the discussion of the source composition of the lamproites. The high Ni, Cr contents and #Mg (>80) of these rocks suggest some olivine accumulation; but as shown in chapter 4, this olivine accumulation is very limited (2-3%). Therefore, the lamproites could be taken as a good estimate of primary, unfractionated magmas.

5.4.3 Basanites

The basanites have a very narrow composition range. No definite trends could be revealed on Pearce diagrams. For example on the (Fe+Mg)/Th versus (Ca+Na-K-1/2Al) plot, designed to evaluate the effect of olivine and clinopyroxene fractionation (Fig. 5.2), the basanites are scattered randomly. This aspect alone suggests a primary status of the magma, if sampling limitations can be ignored. The major elements, and Ni, Cr contents of the rocks do not suggest significant fractionation either.

5.4.4 Trachybasalts

The trachybasalts have wider internal variation in composition than the basanites. On the same Pearce diagram as for the basanites, the trachybasalts define a good linear trend (Fig.5.2). This trend suggests that the variation in composition of the trachybasalts is controlled by olivine and clinopyroxene. The trend could represent either a crystal fractionation path, or a partial melting path. The difficulty regarding this trend is that it shows no relation with the basanites. This is not consistent with the similar trace element chemistry of the two rock types. It is not even consistent with the major element

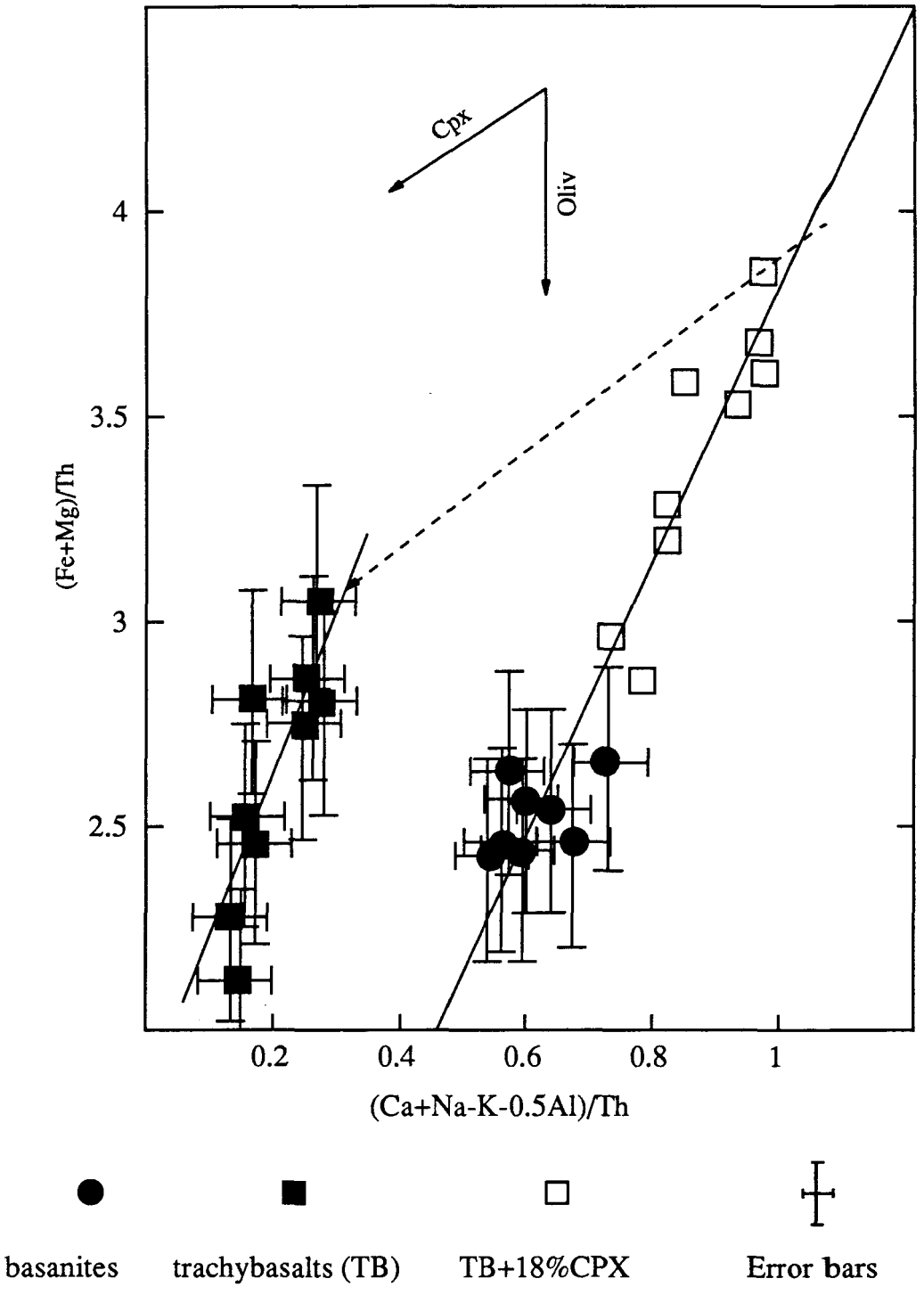

Fig. 5.2 Pearce diagram for exploring Cpx-Olivine control over the low K/Na series rock evolution. The trachybasalts can be related to the basanites by the addition of clinopyroxene.

relationship of the two rock types demonstrated by the Harker diagrams. This apparent contradiction demands an explanation for the relation of the two rock types suggested in the previous chapter that the trachybasalts and the basanites may define a linear compositional array based on the Harker diagrams. It is clear from the Pearce diagram that crystal fractionation of olivines and/or clinopyroxenes cannot derive the trachybasalts from the basanites. However, as mentioned in chapter 4, the discrepancy of MgO, CaO and Sc from the compositional spectrum defined by the basanites and trachybasalts on Harker diagrams does suggest clinopyroxene (CPX) crystallization. To check wether this CPX crystallization process can also establish a relationship between the trachybasalts and basanites on the Pearce diagram, the CPX crystallization was simulated numerically.

A clinopyroxene with highest MgO content of the probed clinopyroxene phenocrysts from the trachybasalts (CpxTp2 in Table 7) was added to each of the trachybasalt analyses. Major oxides were adjusted by mass balance; trace elements were calculated using a Rayleigh crystal fractionation model and Irving's (1978) K_Ds. Numerical results of the calculations with 16, 18 and 20% clinopyroxene added are listed in table 5.1 and represented graphically in figure 5.2 through 5.5. Comparing Fig.5.3 with Fig.4.7, one will see that the discrepancy of MgO, CaO and Al_2O_3 of the trachybasalts from otherwise a good linear composition array could be modelled by adding 18% CPX to the trachybasalts. Using the K_D value 3 of Sc in clinopyroxene (Wedepohl, 1985), 18% CPX crystallization also account for the Sc deficiency in the trachybasalts (Fig.5.4). On the Pearce diagram (Fig.5.2), the modified compositions of the trachybasalts with 18% CPX added plot in a band that is collinear with the basanites. The basanites fit on the evolution trend of the CPX-adjusted trachybasalts (parental trachybasalts hereafter). The parental trachybasalts together with the basanites define a new trend which is parallel to the trend defined by the unadjusted trachybasalts. This new trend defined by the trachybasalts and basanites on the Pearce diagram (Fig.5.2) has restored the relation between the two rock types demonstrated on the Harker diagrams that the two rocks seem to form a linear composition array.

Table 5.1a Composition of the model magma with 20%CPX added to the trachybasalts

	TB1	TB2	TB3	TB4	TB5	TB6	SH1	SH2	SH3
TiO_2	1.71	1.74	1.76	1.68	1.73	1.73	1.64	1.60	1.52
Cr_2O_3	0.18	0.17	0.16	0.16	0.14	0.16	0.16	0.17	0.16
Al_2O_3	13.35	13.55	13.63	13.87	13.48	13.60	14.12	13.82	13.78
Fe_2O_3	1.31	1.30	1.30	1.28	1.33	1.30	1.21	1.26	1.21
FeO	7.60	7.60	7.61	7.63	7.78	7.57	7.18	7.51	7.36
MnO	0.18	0.18	0.18	0.20	0.21	0.18	0.24	0.20	0.20
MgO	9.73	8.86	8.82	8.22	8.73	9.12	7.41	8.37	8.37
CaO	9.75	9.80	9.84	9.31	9.86	9.59	9.38	9.23	8.99
Na_2O	2.95	2.99	2.96	3.15	2.99	2.90	3.21	3.18	3.28
K_2O	1.47	1.54	1.54	1.53	1.54	1.56	1.63	1.59	1.63
H_2O_T	2.33	2.34	2.38	2.29	2.54	2.00	2.59	2.34	2.03
P_2O_5	0.57	0.59	0.58	0.58	0.59	0.58	0.60	0.58	0.58
Ba	430	502	502	502	502	502	430	358	430
Th	5.2	5.4	5.1	5.7	5.2	5.4	5.8	5.5	6.2
U	1.8	1.8	1.7	1.7	1.4	1.4	1.5	1.7	1.8
Ta	3.5	3.6	3.6	4.0	3.6	4.3	3.9	3.8	4.1
Nb	53	54	55	55	54	54	56	55	56
Sr	561	571	579	552	573	790	569	549	556
Zr	252	259	261	268	258	265	279	271	280
Hf	5.3	5.6	5.5	6.4	5.9	6.3	6.4	6.1	6.5
Sc	21.3	21.3	21.1	21.7	21.6	22.0	20.9	20.2	20.5
La	36.5	37.4	36.7	40.6	38.7	41.0	38.7	40.7	43.1
Ce	75.1	76.6	76.1	80.5	74.6	75.0	74.8	79.5	82.9
Nd	30	30	29	34	33	28	33	34	36
Sm	6.91	7.08	6.75	7.04	6.81	7.47	6.63	7.03	7.02
Tb	0.88	0.86	0.87	1.02	0.98	0.84	0.96	1.02	1.00
Ho	0.7	0.7	0.7	1.0	1.0	0.6	0.9	0.9	1.0
Yb	1.95	1.98	1.93	2.21	2.13	1.99	2.04	2.18	2.24
Lu	0.32	0.33	0.33	0.32	0.31	0.33	0.30	0.32	0.32

Table 5.1b Composition of the model magma with 18%CPX added to the trachybasalts

	TB1	TB2	TB3	TB4	TB5	TB6	SH1	SH2	SH3
SiO_2	48.13	48.30	48.24	48.72	48.28	48.22	49.73	49.35	49.50
TiO_2	1.74	1.77	1.78	1.70	1.76	1.76	1.66	1.63	1.54
Cr_2O_3	0.17	0.16	0.15	0.15	0.12	0.15	0.15	0.16	0.15
Al_2O_3	13.51	13.72	13.79	14.05	13.65	13.77	14.30	13.99	13.95
Fe_2O_3	1.34	1.33	1.34	1.31	1.36	1.34	1.24	1.30	1.24
FeO	7.72	7.72	7.73	7.75	7.90	7.69	7.29	7.63	7.48
MnO	0.18	0.19	0.18	0.20	0.21	0.18	0.24	0.20	0.20
MgO	9.60	8.71	8.67	8.06	8.58	8.97	7.23	8.20	8.21
CaO	9.49	9.55	9.59	9.04	9.60	9.33	9.11	8.96	8.71
Na_2O	2.98	3.02	2.99	3.19	3.02	2.93	3.24	3.21	3.32
K_2O	1.51	1.57	1.57	1.57	1.57	1.60	1.67	1.63	1.67
H_2O_T	2.39	2.40	2.43	2.34	2.60	2.05	2.66	2.39	2.08
P_2O_5	0.58	0.61	0.60	0.59	0.61	0.60	0.61	0.60	0.59
Ba	441	514	514	514	514	514	441	367	441
Th	5.3	5.5	5.2	5.8	5.3	5.6	5.9	5.7	6.3
U	1.9	1.9	1.7	1.7	1.5	1.4	1.6	1.7	1.8
Ta	3.6	3.7	3.7	4.1	3.7	4.4	4.0	3.8	4.2
Nb	54	55	56	56	55	55	58	56	58
Sr	574	584	593	564	586	808	583	562	569
Zr	258	265	267	274	263	271	285	277	286
Hf	5.4	5.7	5.6	6.5	6.0	6.4	6.5	6.2	6.6
Sc	20.2	20.2	20.1	20.7	20.5	21.0	19.9	19.2	19.5
La	37.3	38.3	37.6	41.6	39.6	42.0	39.6	41.6	44.1
Ce	76.6	78.1	77.6	82.1	76.1	76.5	76.3	81.1	84.6
Nd	31	31	30	35	34	29	33	35	37
Sm	7.04	7.21	6.88	7.18	6.93	7.61	6.75	7.16	7.15
Tb	0.90	0.87	0.89	1.04	0.99	0.85	0.97	1.04	1.02
Ho	0.7	0.7	0.7	1.0	1.0	0.6	0.9	0.9	1.0
Yb	1.98	2.01	1.96	2.25	2.16	2.02	2.07	2.21	2.27
Lu	0.33	0.34	0.34	0.33	0.31	0.34	0.30	0.33	0.33

Table 5.1c Composition of the model magma with 16%CPX added to the trachybasalts

	TB1	TB2	TB3	TB4	TB5	TB6	SH1	SH2	SH3
SiO_2	48.06	48.23	48.17	48.66	48.21	48.15	49.70	49.30	49.46
TiO_2	1.76	1.80	1.81	1.73	1.79	1.79	1.69	1.65	1.56
Cr_2O_3	0.15	0.14	0.14	0.14	0.11	0.14	0.14	0.14	0.14
Al_2O_3	13.68	13.89	13.96	14.22	13.81	13.94	14.48	14.16	14.12
Fe_2O_3	1.38	1.36	1.37	1.34	1.39	1.37	1.27	1.33	1.27
FeO	7.84	7.84	7.85	7.87	8.03	7.81	7.40	7.74	7.59
MnO	0.18	0.19	0.18	0.20	0.21	0.18	0.25	0.20	0.20
MgO	9.47	8.56	8.52	7.89	8.42	8.83	7.04	8.04	8.05
CaO	9.23	9.29	9.33	8.77	9.35	9.07	8.84	8.68	8.43
Na_2O	3.01	3.06	3.02	3.22	3.06	2.96	3.28	3.25	3.36
K_2O	1.54	1.61	1.61	1.60	1.61	1.64	1.71	1.67	1.71
H_2O_T	2.44	2.46	2.49	2.40	2.66	2.10	2.72	2.45	2.13
P_2O_5	0.60	0.62	0.61	0.60	0.62	0.61	0.63	0.61	0.60
Ba	451	527	527	527	527	527	451	376	451
Th	5.5	5.6	5.4	6.0	5.5	5.7	6.0	5.8	6.5
U	1.9	1.9	1.8	1.8	1.5	1.4	1.6	1.8	1.8
Ta	3.7	3.8	3.8	4.2	3.8	4.5	4.1	3.9	4.3
Nb	56	56	57	57	56	56	59	57	59
Sr	587	598	606	577	599	827	596	575	582
Zr	263	271	273	280	269	277	291	283	292
Hf	5.5	5.8	5.7	6.6	6.1	6.5	6.6	6.3	6.7
Sc	19.3	19.3	19.1	19.7	19.5	20.0	19.0	18.3	18.6
La	38.2	39.2	38.4	42.5	40.5	42.9	40.5	42.6	45.1
Ce	78.1	79.6	79.0	83.7	77.6	77.9	77.7	82.6	86.2
Nd	31	31	30	36	35	30	34	36	37
Sm	7.16	7.34	7.00	7.30	7.06	7.74	6.87	7.28	7.28
Tb	0.91	0.88	0.90	1.05	1.01	0.87	0.99	1.05	1.04
Ho	0.7	0.7	0.7	1.0	1.0	0.6	0.9	0.9	1.0
Yb	2.01	2.04	1.99	2.28	2.19	2.05	2.10	2.24	2.31
Lu	0.33	0.34	0.34	0.33	0.32	0.34	0.31	0.33	0.33

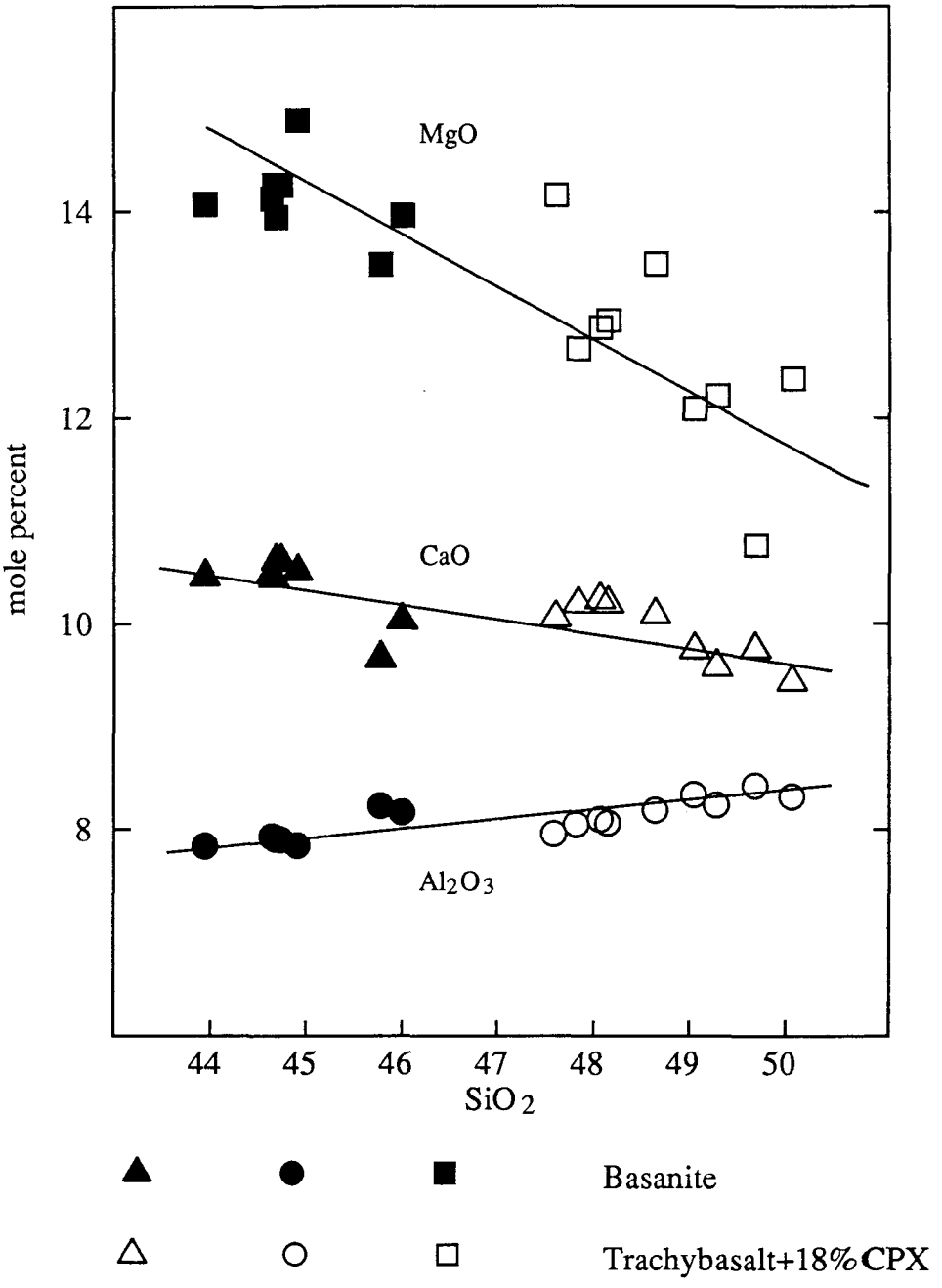

Fig. 5.3 Harker diagrams same as figure 4.7b except that the compositions of the trachybasalts have been adjusted by reversing Cpx crystallization. After this adjustment, the linear composition spectrum demonstrated in figure 4.7a is restored.

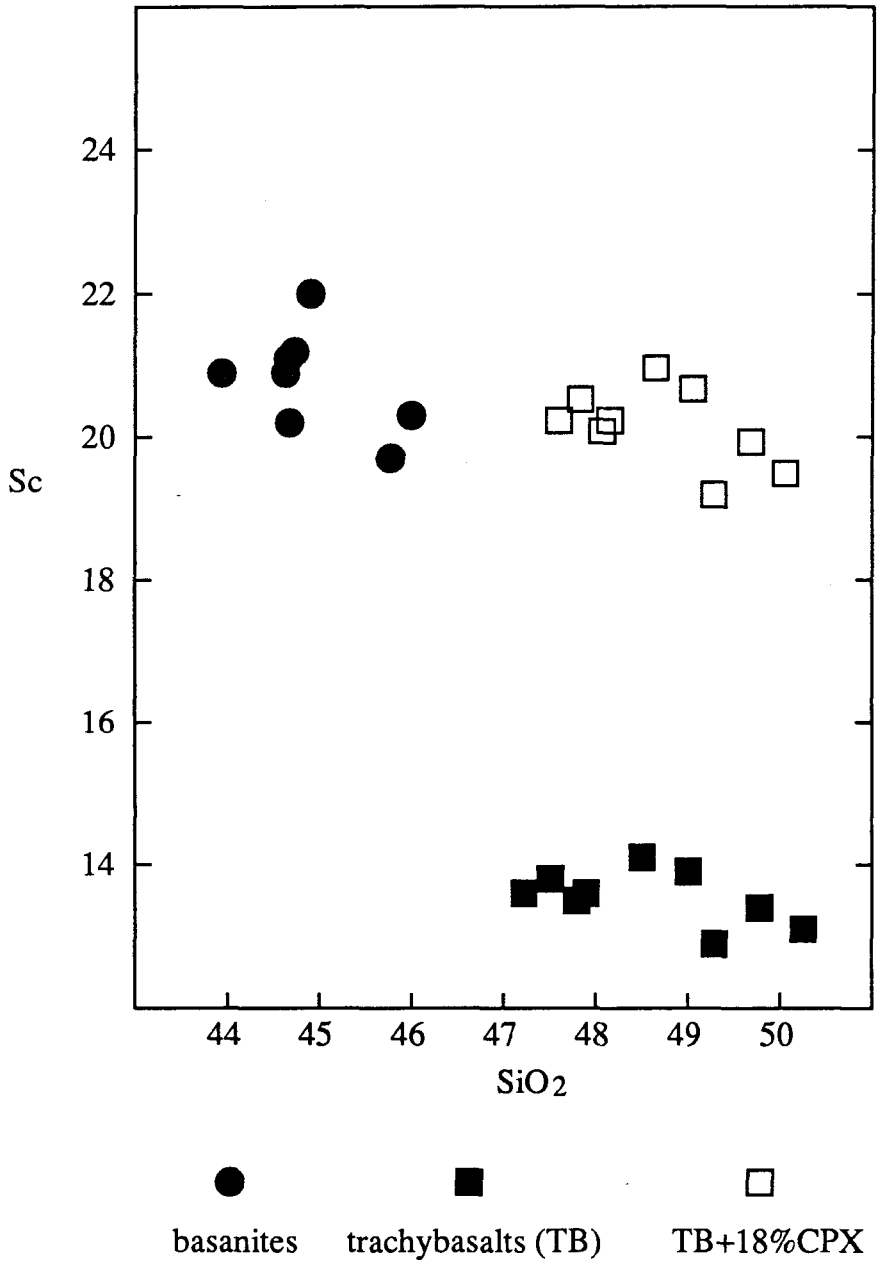

Fig. 5.4 Sc - SiO_2 diagram showing the Sc change after the trachybasalts being adjusted by reversing Cpx crystallization.

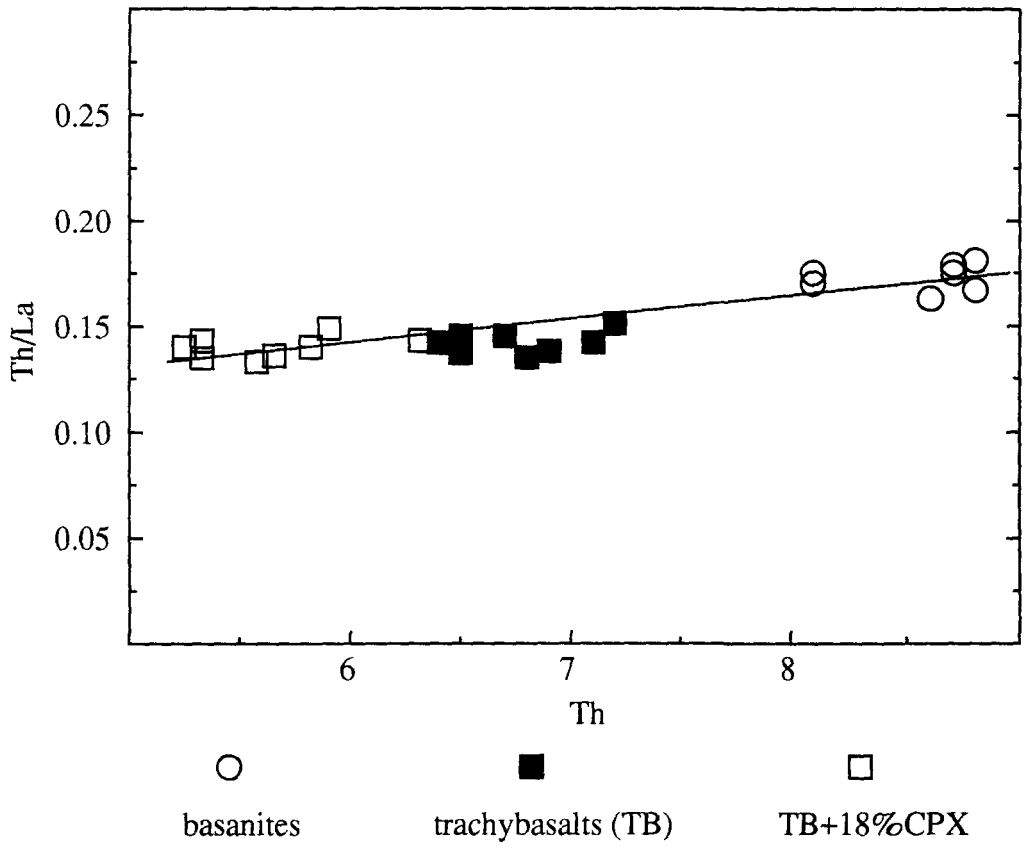

Fig. 5.5 Th/La versus Th diagram for magma processes identification. The basanites and the parental trachybasalts lie on a straight line which can be best interpreted by batch partial melting (Minster & Allegre 1977)

There are two possible interpretations for the relationship between the parental trachybasalts and the basanites: (1) the basanite magmas were derived from the parental trachybasalt magmas by crystal fractionation of olivines and clinopyroxenes. (2) the parental trachybasalt magmas were derived from the basanite magmas by the addition of melts from melting an olivine-clinopyroxene assemblage. Crystal fractionation is unlikely in this case, because it is impossible for the saturated trachybasalt magmas to get across the thermal divide and evolve to the undersaturated basanites. By contrast, a partial melting model can easily explain the basanite-trachybasalt trend in figure 5.2. For example, an amphibole veined mantle source could have generated the basanites by melting the easy-to-melt vein materials (Merrill & Wyllie, 1975). To the basanite magmas formed this way, melts from further melting of pyroxene and olivine were added to form the parental trachybasalt magmas. In this scenario, both the basanites and the parental trachybasalts are primary magmas.

The partial melting model also gets support from trace elements. On the Th/La-Th diagram (Fig.5.5), the parental trachybasalts define a linear trend that passes through the basanites which themselves show a less definite trend collinear with the parental trachybasalts trend. This linear trend has a non-zero intercept and a positive slope. As Treuil and Joron (cited from Minster & Allègre, 1978) demonstrated, the trace element path of a melting process on a diagram of type Fig. 5.5 can be analytically expressed as,

$$\frac{C^{Th}}{C^{La}} = \frac{D_o^{La} - D_o^{Th}\,\dfrac{1-P^{La}}{1-P^{Th}}}{C_o^{La}} C^{Th} + \frac{C_o^{Th}}{C_o^{La}} \frac{1-P^{La}}{1-P^{Th}}$$

where Co^{Th} and Co^{La} stand for the Concentration of Th and La respectively in the initial solid, C^{Th} and C^{La} stand for the concentration of Th and La respectively in the magma;

Do^{Th} and Do^{La} stand for the bulk partition coefficient of Th and La respectively for the initial solid phase assemblage; P^{Th} and P^{La} stand for the bulk coefficient of Th and La respectively for the phase assemblage entering into the liquid magma.

It is clear from the above equation that if both P^{Th} and P^{La} are constant during the melting process, the equation defines a straight line with a positive slope and a positive intercept on the Th/La axis. Batch partial melting meets this condition. In fact, apart from batch partial melting no other simple processes can produce a straight line on a diagram of type Fig. 5.5 (Minster & Allègre, 1978). Therefore, the trend is most likely to reflect a batch partial melting process.

If the parental trachybasalt magmas were formed by larger degrees of partial melting of a amphibole-veined mantle peridotite and which would have also generated the basanite magmas by a smaller degree of partial melting, then the Al/Ca ratios of the parental trachybasalts should not differ much from the basanites (Fig.5.6), because the melting process proceeding from the basanites to the parental trachybasalts involves mainly olivine plus some clinopyroxene. On the other hand, if the basanites were derived from the parental trachybasalts, the Al/Ca constraint requires that a substantial amount of olivine was crystallized. Such a fractionation path is different from the path required to deduce the trachybasalts which, as demonstrated, involves mainly clinopyroxene. It is difficult to imagine the same parental magmas will take two different crystallization paths under high pressures (low pressure fractionation has been shown to be impossible) to form the basanites and the trachybasalts in a single volcanic province at about the same time.

The above discussions demonstrate that trachybasalts are evolved magmas; they were derived from their parent magmas by clinopyroxene fractionation. The parental trachybasalt magmas are different from the basanite magma; but they may originate from a similar mantle source. By invoking a clinopyroxene crystallization model for the trachybasalts, a number of seemingly contradictory facts can be reconciled, and the

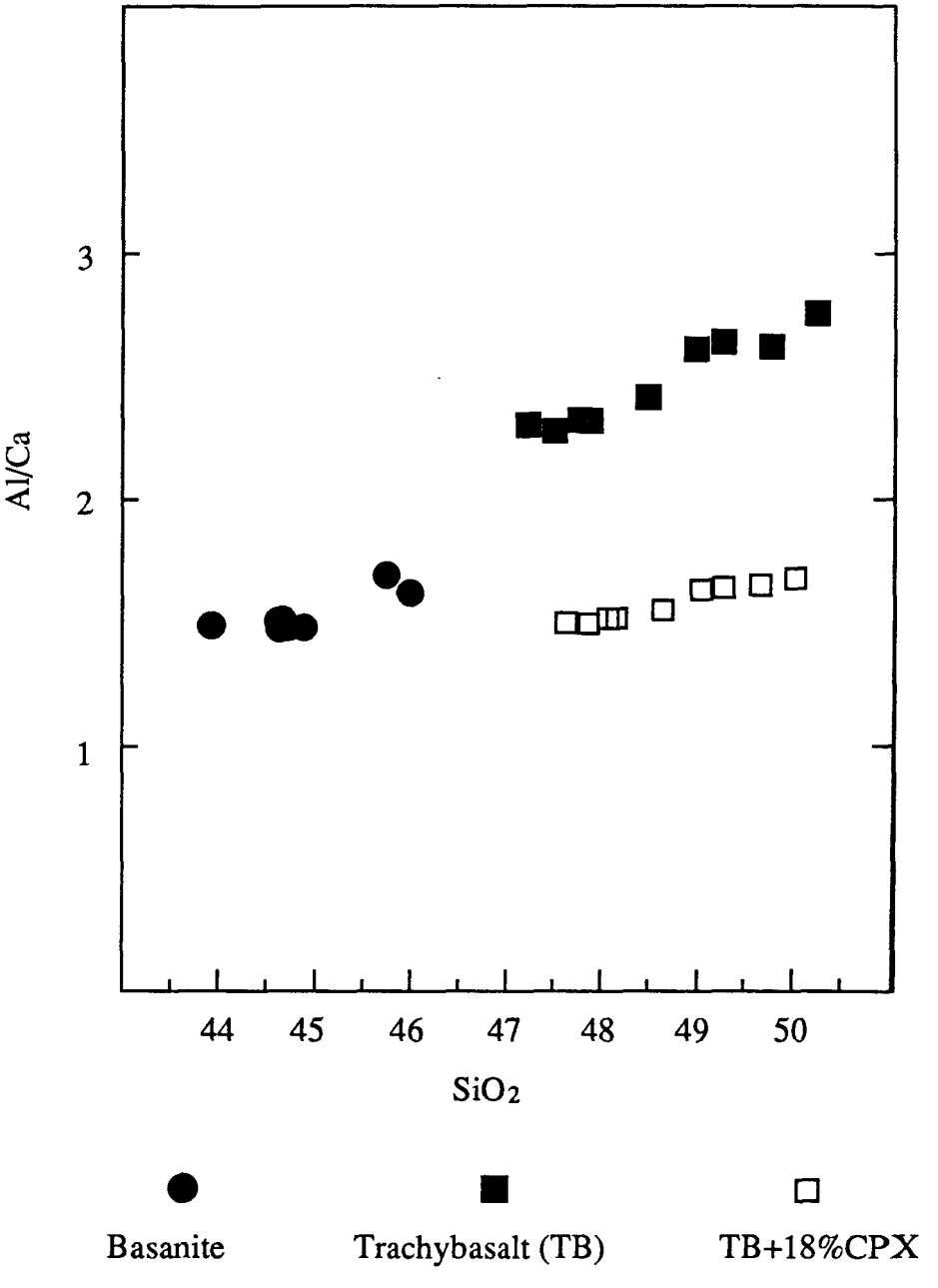

Fig. 5.6 Al/Ca versus SiO_2 plot showing the Al/Ca relation between the basanites and trachybasalts before and after Cpx adjustment.

chemically similar trachybasalts and basanites can be genetically related. However, these discussions do not sufficiently qualify the clinopyroxene model. Because (1) invoking a clinopyroxene crystallization is not the only possible way to relate the basanites and the trachybasalts and to explain their trace element similarity; (2) The plausibility of clinopyroxene crystallization must be confirmed by the phase relations of the system under the conditions of crystallization.

To check the possibility of crystallizing clinopyroxene from the assumed parental trachybasalt magmas, the trachybasalts (TB) and computed rocks (TB+18%CPX) were projected on the olivine-clinopyroxene-nepheline triangle phase diagram (Fig. 5.7) following the manner of Sack et al. (1987). It is evident from the phase diagram that a magma with the composition of the computed parental trachybasalts will crystallize clinopyroxene first under elevated pressure. Clinopyroxene crystallization continues until the magma reaches the cotectic line of clinopyroxene and olivine. The position of the cotectic line labelled 5-30 Kbar in Fig. 5.7 is a key control factor for the trachybasalts to be derived from the computed parental magmas by clinopyroxene fractionation. Unfortunately, the position of the cotectic line under high pressures is uncertain. More experimental data are needed to get better control of the line. But one thing is sure with available experimental data, as pressure goes higher, the line will shift itself toward the olivine apex (Sack, et al. 1987). For example, the cotectic line labelled 5-30KB could shift to somewhere near the dashed line on the diagram. So it is quite plausible that the trachybasalts were derived from more primary melts by clinopyroxene crystallization.

5.5 MANTLE SOURCE CHEMISTRY AND METASOMATISM

5.5.1 Chemical Characteristics of the Sources of the Basanites and the Trachybasalts

In the previous discussion, it has been shown that the trachybasalts and basanites are genetically related, and that they have close affinity to continental rift basanites from

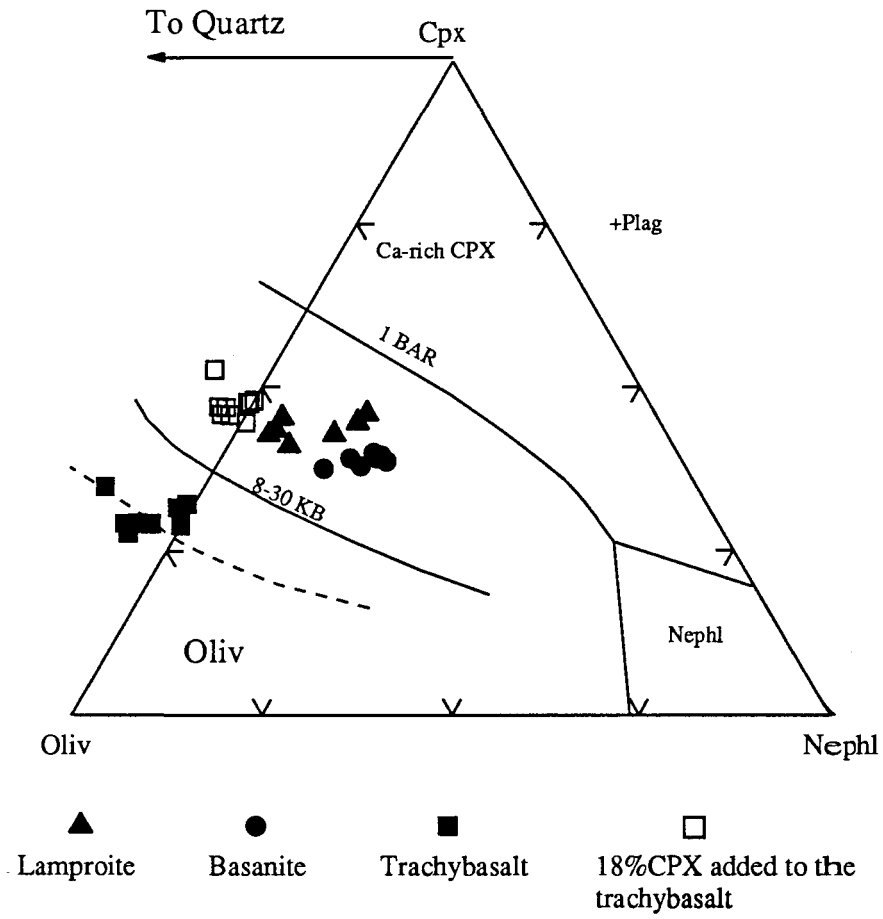

Fig. 5.7 Olivine-Nepheline-Clinopyroxene phase diagram. The position of the cotectic labelled 8-30KB is uncertain. What is certain is that it will shift toward the Oliv end when pressure goes high (Sack et al., 1988). For example, it could be at a position near the projections of the trachybasalts (indicated by the dashed line). Therefore, magmas with a composition of the basanites or the parent trachybasalts would crystallize clinopyroxene when they were at depth (Modified after Sack et al.,1988).

Kenya (eastern Africa) in their trace element patterns. The geological setting of these rocks is consistent with the interpretation of their trace elements. Therefore, it can be assumed that the basanites and trachybasalts originate in the subcontinental lithospheric mantle in the study region. It is difficult to estimate what exactly this mantle was; instead, primitive mantle was chosen as the starting material to which modifications are applied based on the chemistry of the basanites and trachybasalts.

A classical problem in generating alkali basaltic magmas from a primitive mantle is the difficulty in obtaining the high level of LREE and the degree of differentiation of the REE patterns of the magmas (Wilson, 1989). A very small degree of partial melting is required.

For the basanites and parental trachybasalts in this study, it is possible to generate their high incompatible trace element concentration by about 1% partial melting of a mantle with primitive trace element signature (Taylor, 1986), if the K_Ds of the highly incompatible elements such as U, Th and La are assumed to be zero (Table 5.2). However, searching for the residual mineralogy for such a partial melting process using real non-zero K_Ds of those highly incompatible elements proves to be very difficult. No satisfactory mantle mineral assemblage was found in this study. As a matter of fact, any substantial amounts of clinopyroxene in the residue (which is normally the case for a very small degree partial melting of the primitive mantle) will make it impossible to get the elevated concentrations of the incompatible elements of the basanites by any conceivable degree (say 0.5%) of partial melting. To demonstrate this point, residual Cpx is plotted against the degrees (F in percent) of partial melting needed in generating magmas with different enrichment factors of trace elements (Fig. 5.8). To simplify the calculation, zero K_D is assumed for all minerals except clinopyroxene. For the basanites, the enrichment factors of La and U are about 130 therefore if the minimum degree of partial melting is 0.5% (Meen et al., 1990) then the maximum amount of clinopyroxene in the restite would be 6%.

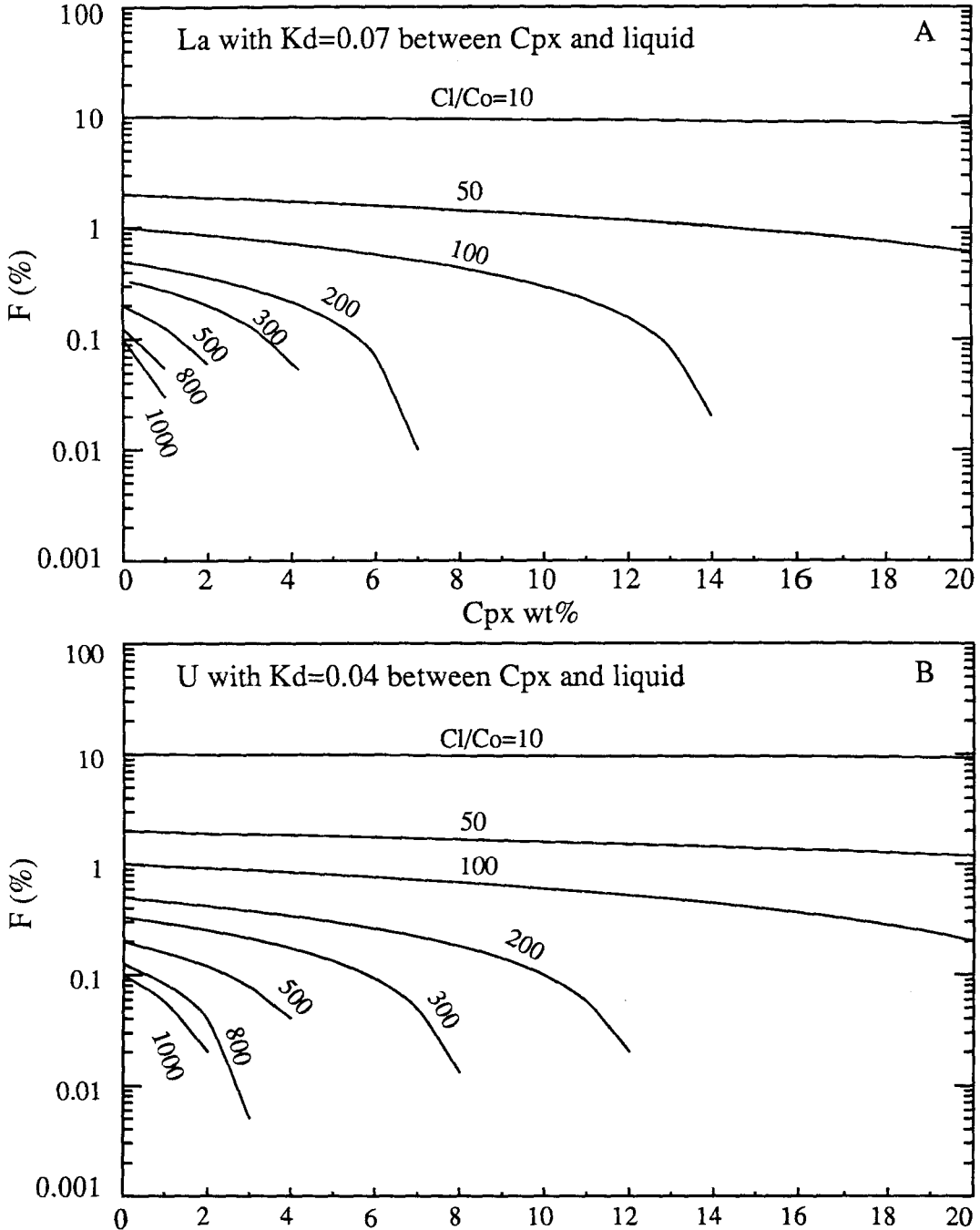
La with Kd=0.07 between Cpx and liquid
A
Cl/Co=10
50
100
200
300
500
800
1000
F (%)
Cpx wt%
U with Kd=0.04 between Cpx and liquid
B
Cl/Co=10
50
100
200
300
500
800
1000
F (%)

Table 5.2 Degree of partial melting calculated for the alkaline rocks in the study area based on a primitive mantle source. Zero KD is assumed for Rb, Ba, Th, U and La

Lamproites	Lam1	Lam2	Lam4	Lam5	Lam6	Lam7
Rb	0.57	0.70	0.55	1.22	0.59	1.19
Ba	0.19	0.31	0.24	0.39	0.37	0.33
Th	0.60	0.55	0.63	0.56	0.57	0.58
U	0.45	0.45	0.46	0.43	0.45	0.51
La	1.07	1.04	1.09	1.04	1.08	0.95

Basanites	Ban1	Ban2	Ban3	Ban4	Ban5	Ban6	Ban7	Ban8
Rb	0.85	1.96	0.85	1.90	1.72	1.34	1.14	1.77
Ba	0.76	0.78	0.73	0.60	0.78	0.79	0.82	0.79
Th	0.74	0.73	0.79	0.79	0.73	0.75	0.74	0.73
U	0.95	0.9	0.95	0.95	1.06	1.06	0.95	0.95
La	1.14	1.13	1.19	1.16	1.11	1.18	1.05	1.05

Trachy-basalts	Tb1	Tb2	TB3	TB4	TB5	TB6	SH1	SH2	SH3
Rb	1.53	1.37	1.77	1.25	1.45	1.30	1.34	1.49	1.28
Ba	0.95	0.81	0.81	0.81	0.81	0.81	0.95	1.14	0.95
Th	0.98	0.95	1.0	0.90	0.98	0.94	0.89	0.93	0.83
U	0.78	0.78	0.86	0.86	1.0	1.06	0.95	0.86	0.81
La	1.23	1.19	1.22	1.10	1.16	1.09	1.16	1.11	1.04

	trachybasalts		plus	20%CPX					
	TB1	TB2	TB3	TB4	TB5	TB6	SH1	SH2	SH3
Rb	1.91	1.72	2.22	1.56	1.81	1.64	1.68	1.86	1.60
Ba	1.19	1.02	1.02	1.02	1.02	1.02	1.19	1.42	1.19
Th	1.22	1.19	1.24	1.12	1.22	1.17	1.10	1.15	1.03
U	0.97	0.97	1.06	1.06	1.24	1.31	1.17	1.06	1.01
La	1.51	1.47	1.50	1.36	1.42	1.34	1.42	1.35	1.28

Furthermore, partial melting of a primitive mantle cannot explain the depletion in LILEs relative to La of the basanites and trachybasalts, or indeed of almost all alkaline basaltic rocks. Alternatively, the elevated incompatible element concentration of the basanites and trachybasalts could be caused by selective enrichment of incompatible elements in the mantle source, in other words, the source was not a primitive mantle but was enriched in incompatible trace elements by metasomatism. A metasomatized mantle could easily explain the elevated incompatible element concentration of the basanites and the parental trachybasalts without resorting to extremely small degrees of partial melting. It can also explain the relative depletion of LILEs compared to La content of these rocks by arguing that the LILEs were less enriched than La during metasomatism.

The existence of mantle metasomatism itself is beyond doubt. A large number of mantle xenoliths from a wide variety of localities and alkaline rock types have been observed to be metasomatized (Boyd & Nixon 1973; Lloyd & Bailey, 1975; Francis, 1976; Erlank & Richard, 1977; Jones, 1982; Haggerty et al 1983; Harte, 1983; Menzies, 1983; Menzies et al. 1985; Erlank et al., 1987; Harte, et al., 1987). The model that mantle metasomatism as an integrated part of alkaline magmatism has been widely studied and accepted in the last decade (Allègre, 1982; Allègre, et al., 1982, 1983; Bailey 1982; Holm & Munksgaard, 1982; O'Reilley & Griffin, 1984; Sun, 1984; Roden & Murthy 1985; Hawkesworth et al. 1984, 1987; Davidson, 1987; Menzies, et al., 1987; Woodhead, et al., 1987; Dupuy, et al., 1989; Haggerty, 1989; Meen et al. 1989; Francis & Ludden 1990).

The attraction of source metasomatism to this study is not only because it offers a simple, easy-to-understand explanation of incompatible trace element chemistry of the basanites and trachybasalts. It is also required by the major element chemistry of these rocks. Magmas originating from primitive mantle peridotite (e.g. pyrolite) with a olivine composition of about Fo_{90} should fall in the shaded area on the Hanson-Langmuir FeO-MgO diagram (Fig. 5.9; Hanson & Langmuir, 1978), if equilibrium partial melting process and Roeder & Emslie's (1970) partition coefficients for Fe and Mg between olivine and

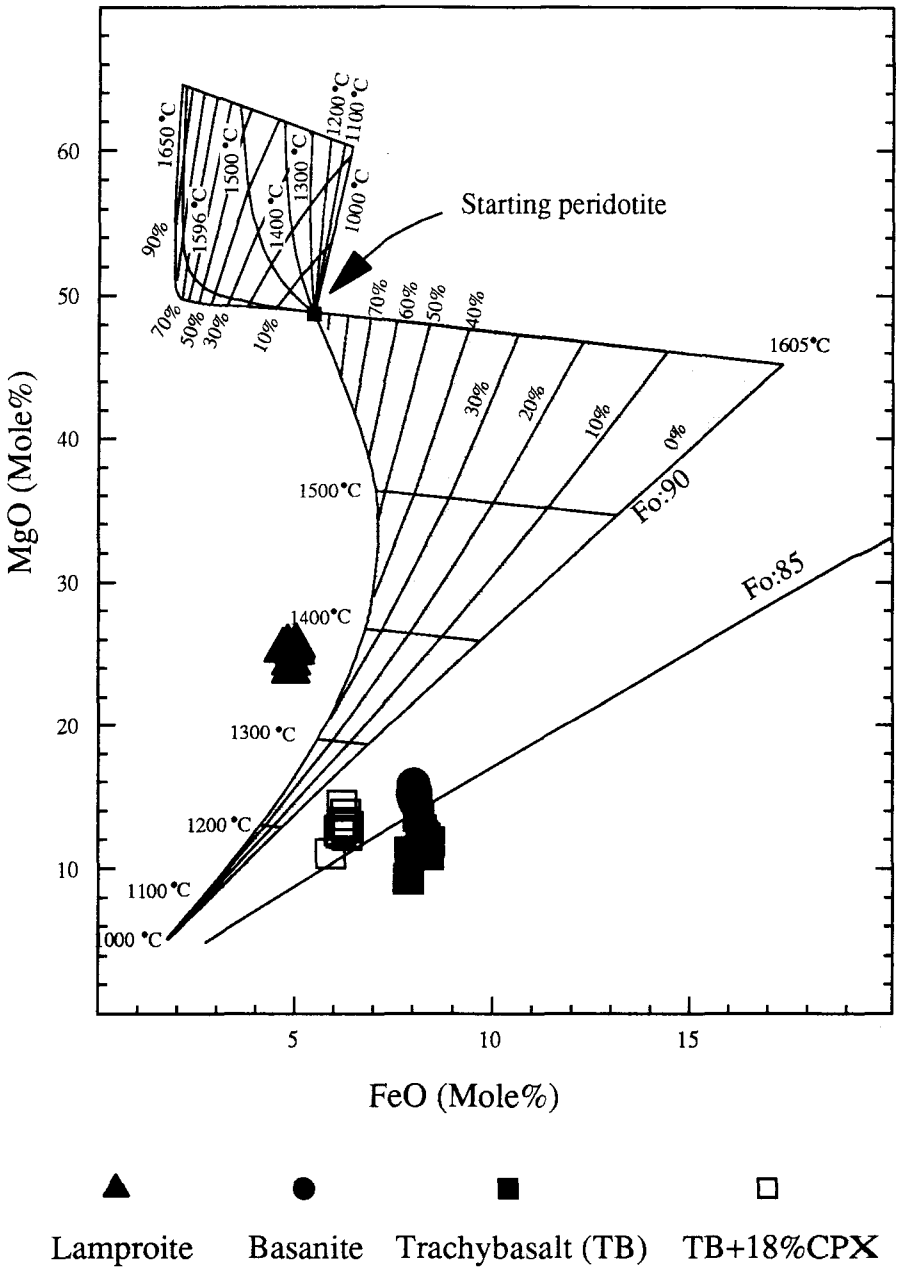

Fig. 5.9 MgO-FeO diagram showing the possible composition range (shaded area) of magmas originated from a melting of a primitive mantle source with Fo_{90}. The lines with percent label indicate degrees of partial melting; the lines with temperature label indicate the temperatures at which the melting takes place. (Calculated after Hanson and Langmuir, 1977).

liquid magma are assumed. The basanites and trachybasalts fall below the line of zero degree of partial melting on the diagram. This could indicate one of three possibilities: (1) the mantle source of these rocks contained Fe-rich olivine; (2) the magmas had never equilibrated with olivine in the source; (3) olivine-liquid Fe/Mg K_D in the system of this study is lower than Roeder & Emslie's value (1970).

Considering the first possibility, the Mg # of the basanites and parental trachybasalt imply that the fosterite content of olivine in source was 85 (Fig. 5.9). This is much lower than that observed in mantle xenoliths. Though the third case is possible in view of recent experimental evidence for a decrease in the olivine-liquid Fe/Mg K_D in very alkaline magmas (Gee & Sack, 1988), petrographic characteristics support the second case. In many samples reactions between xenocrystic olivines and their host alkali magma were observed in these rocks (Chapter 3 plate 11 & 15; also Francis & Ludden, 1990). This suggests that these rocks may never have been in equilibrium with mantle olivine. Disequilibrium between magma and mantle olivine is expected if the magma have been generated by disequilibrium melting of a mantle peridotite. Though disequilibrium mantle melting is very likely in many cases (Bédard, 1989; Prinzhofer & Allègre, 1985), it cannot generate magmas with #Mg as low as those of the basanites from a normal mantle peridotite, because magmas with lowest #Mg which can be generated by disequilibrium melting will approach the line of 0% partial melting in figure 5.9. Alternatively, the basanite magmas might have been confined to some special portion of the mantle source during partial melting, so that their interaction with olivine in the residue would have been kept at a minimum level, and no equilibrium was achieved.

The basanites and parental trachybasalts in this study define a linear trend in an olivine liquidus projection (Fig. 5.10). This trend was also demonstrated for the Fort Selkirk alkaline rocks and for many other alkaline volcanic suites by Francis and Ludden (1990). To explain this trend, amphibole-veined peridotite source was proposed for the Fort Selkirk alkaline rocks by Francis and Ludden (1990). The MgO/FeO ratios of mantle

amphiboles resemble those of basanites (Francis & Ludden 1990). It is proposed that selective melting of alkaline amphiboles in an amphibole-veined peridotite could have generated alkaline melts as rich in iron as basanites (Merrill & Wyllie, 1975). This model implies that melting could have begun with the vein material and the melt may have been kept along the veins. In this way the magma interaction with the mantle olivine would have been kept at a very low level.

The above model may be applied to the basanites and trachybasalts in this study as follows. The melts formed by melting of only the amphibole veins were transported directly to surface to form the basanites. As the degree of partial melting increased, in addition to the vein material some of the mantle surrounding the veins melted, this mixed source formed the trachybasalts.

5.5.2 Chemical Characteristics of the Sou of the Lamproites

The lamproites have very high #Mg and Ni, Cr contents, but very low Al_2O_3 content. This could suggest that either they came from a refractory source, probably harzburgite or dunite, or they formed by very high degree of partial melting. On the other hand, these rocks have extremely high concentration of incompatible elements, which suggests an enriched mantle source. This contradictory behaviour is common to all lamproitic rocks (Bergman, 1987). A number of hypotheses have been proposed to explain this enigma. These hypotheses can be outlined as three broad groups:

1. Crustal contamination of otherwise normal mantle derived ultramafic melts. This is an efficient way to explain the contradiction. It was proposed as early as in 1910 (Daly 1910), and does not conflict with recent isotopic studies (Vollmer & Norry 1983; Taylor & Cundari, 1984).

2. Zone refining (Harris 1957; Harris & Middlemost 1969).

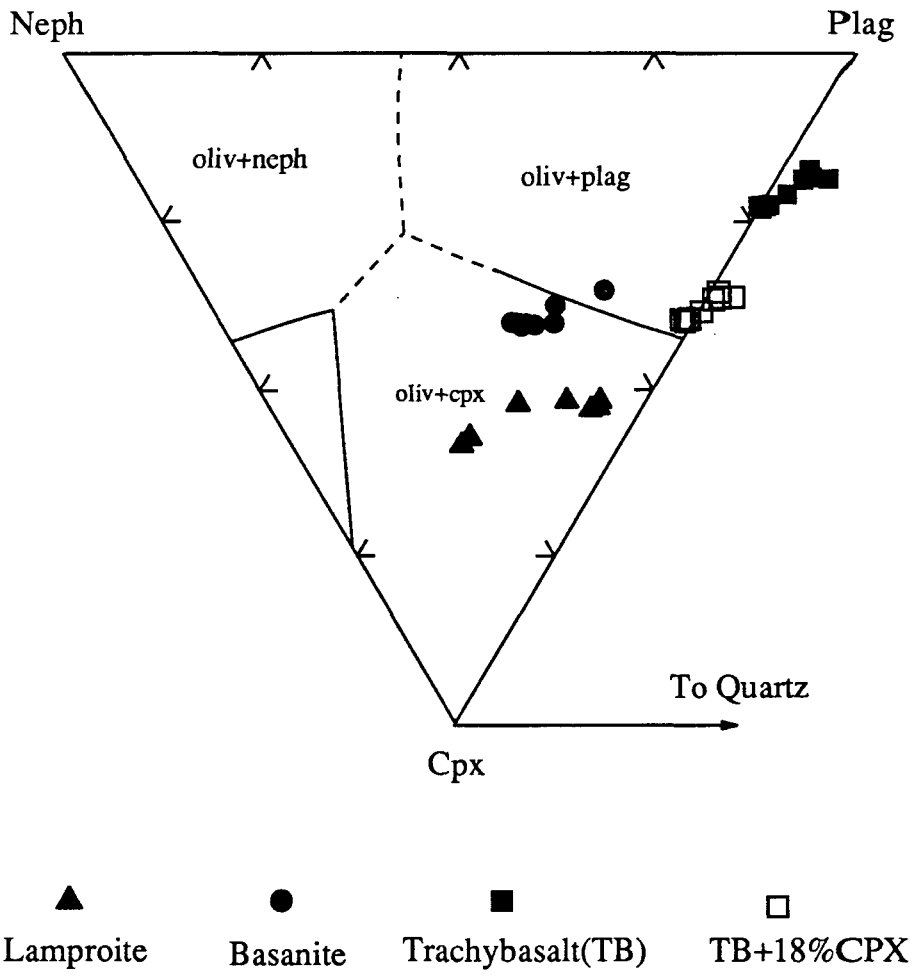

Fig. 5.10 Olivine liquidus projection of the basalt tetrahedron. The basanites and the parental trachybasalts define a linear trend near the cotectic between plagioclase and clinopyroxene. This trend is shared by many alkaline volcanic suites from foidite to hypersthene end members (see figure 15 in Francis & Ludden 1990).

3. Source metasomatism or selective enrichment in certain elements (Gupta et al., 1976; Bergman 1987; Haggerty 1989; Jones 1989; Meen et al. 1989).

It is difficult to argue for an unique genetic model for the lamproites. Magma evolution through zone refining is not considered in this study, because of the difficulty in explaining the similar LILEs/LREEs ratios of rocks with quite different level of these elements (Hanson 1977) and because they are theoretical rather than practical in this author's view. Crustal contamination can explain the trace element enrichment of the lamproites, therefore, it is a possible model. However, the high MgO, low Al_2O_3 and TiO_2 (Table 4.1) character of the Huzhiyan rocks is not consistent with crustal contamination. Instead of crustal contamination, mantle metasomatism will be considered as mechanism to explain both the trace and major element chemistry of the Huzhiyan lamproites. The high MgO low Al_2O_3 feature of the Huzhiyan rocks could be better explained by mantle metasomatism when the rocks are considered in the context of all alkaline rocks. Considering alkaline mafic rocks as a whole Al_2O_3 shows a negative correlation with MgO (Fig. 4.4a), while CaO shows a positive correlation. This combination of major element behaviour can not be explained by increasing the degree of partial melting or crustal contamination since in both of these cases CaO would be expected to correlate positively with Al_2O_3.

The trend can be explained, however, by a progressive metasomatic process of mantle peridotites described by Erlank et al. (1987). In the progressive metasomatic process, garnet peridotite (GP) is metasomatized by replacing some of it's garnets with phlogopite, forming garnet phlogopite peridotite (GPP). The GPP is in turn metasomatized to phlogopite peridotite (PP) by more phlogopite replacement. In this stage some chromium spinel may form and will be further replaced by phlogopite and/or "LIMA" minerals (lindsleyite and mathiasite). As the metasomatic process approaching its highest level, an extremely Al-poor phase, K-richterite is formed, and the rock turns to phlogopite K-richterite peridotite (PKP). During this whole metasomatic process, aluminum-rich

phases gradually decrease till they disappear, at the same time Mg-rich phlogopite increases. Mineral chemistry studies show that from GP to PKP, clinopyroxene becomes poorer and poorer in Al (Erlank, et al. 1987). This explains why Al_2O_3 decrease is correlated with MgO increase without disturbing CaO. This progressive metasomatic process would also make the source peridotite more and more enriched in incompatible trace elements if an incompatible-element-rich metasomatic agent is assumed. If lamproitic rocks result from more advanced source metasomatism, it is possible, in this way, to explain the general lower Al_2O_3, and stronger incompatible elements enrichment of lamproitic rocks relative to alkali basaltic rocks.

The #Mg (>80) of the Huzhiyan lamproites indicates that these rocks can not be generated by primitive mantle using Hanson & Langmuir's major element modelling model (Fig. 5.9; Hanson & Langmuir, 1978). More Mg-rich mantle source is needed to generate the high #Mg of the rocks. Though any harzburgite or dunite will meet this need, a particular rock type, the phlogopite peridotite (PP) given by Erlank et al.(1987) was chosen as a possible source for the lamproites in this study. The Hanson & Langmuir diagram is recalculated using the PP as a starting material which has an average olivine composition of $Fo_{91.5}$. The lamproites can be generated by 30-40% partial melting of such a PP source (Fig. 5.11). In view of the fact that the lamproites have 2-3% olivine accumulation, the actual partial melting degree may be lower. That the lamproites may originate from a PP source also gets support from the pyroxene chemistry of the rocks. The FeO content is plotted against the Al_2O_3 content for the clinopyroxene in the lamproites along with clinopyroxenes from different mantle sources (Fig. 5.12). It is clear from the diagram that the clinopyroxene of the lamproites fall into two populations, similar to that of a PP source. The Al_2O_3 contents of the two populations are coincident with the two corresponding populations of a PP source, but the clinopyroxenes in the lamproite have higher FeO content than the PP clinopyroxenes.

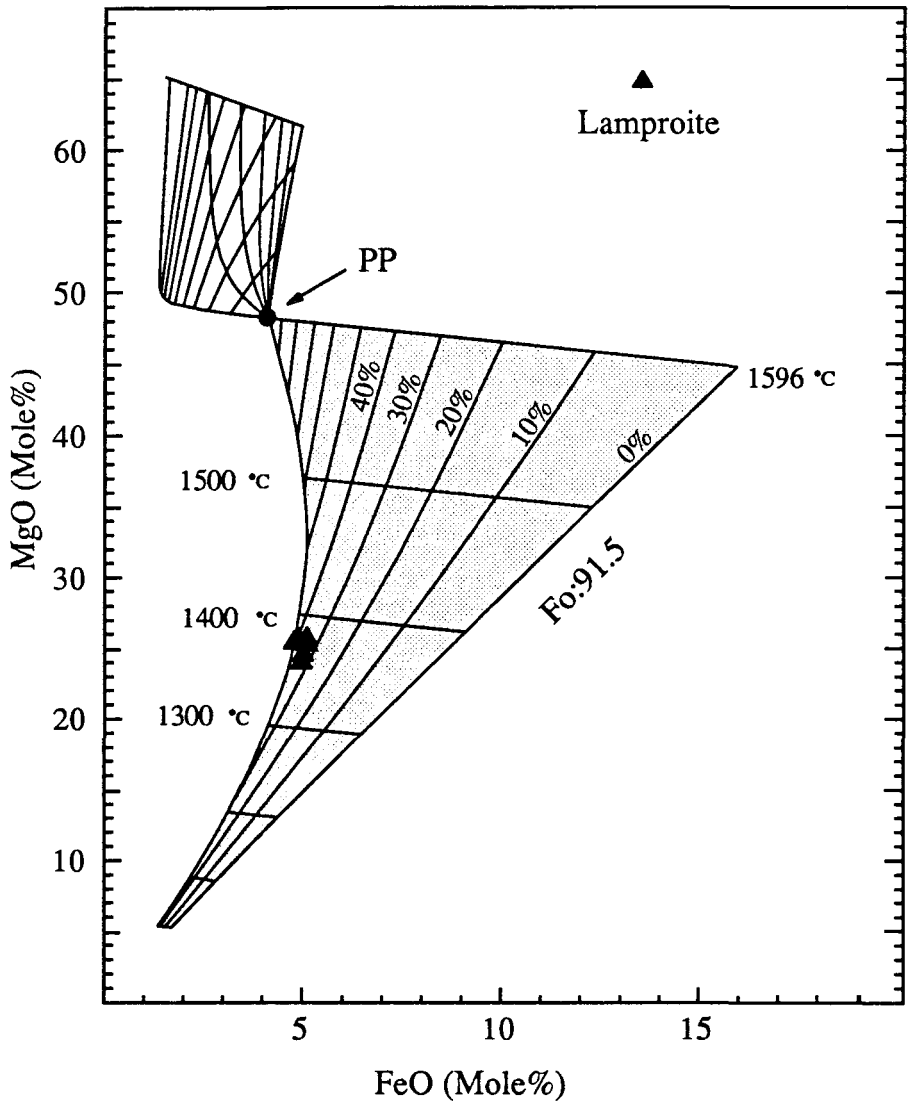

Fig. 5.11 Same as figure 5.9 except the initial source in this calculation is a phlogopite peridotite ($Fo_{91.5}$) rather than a primitive lherzolite. The lamproites can be generate by 30-40% melting of such a source.

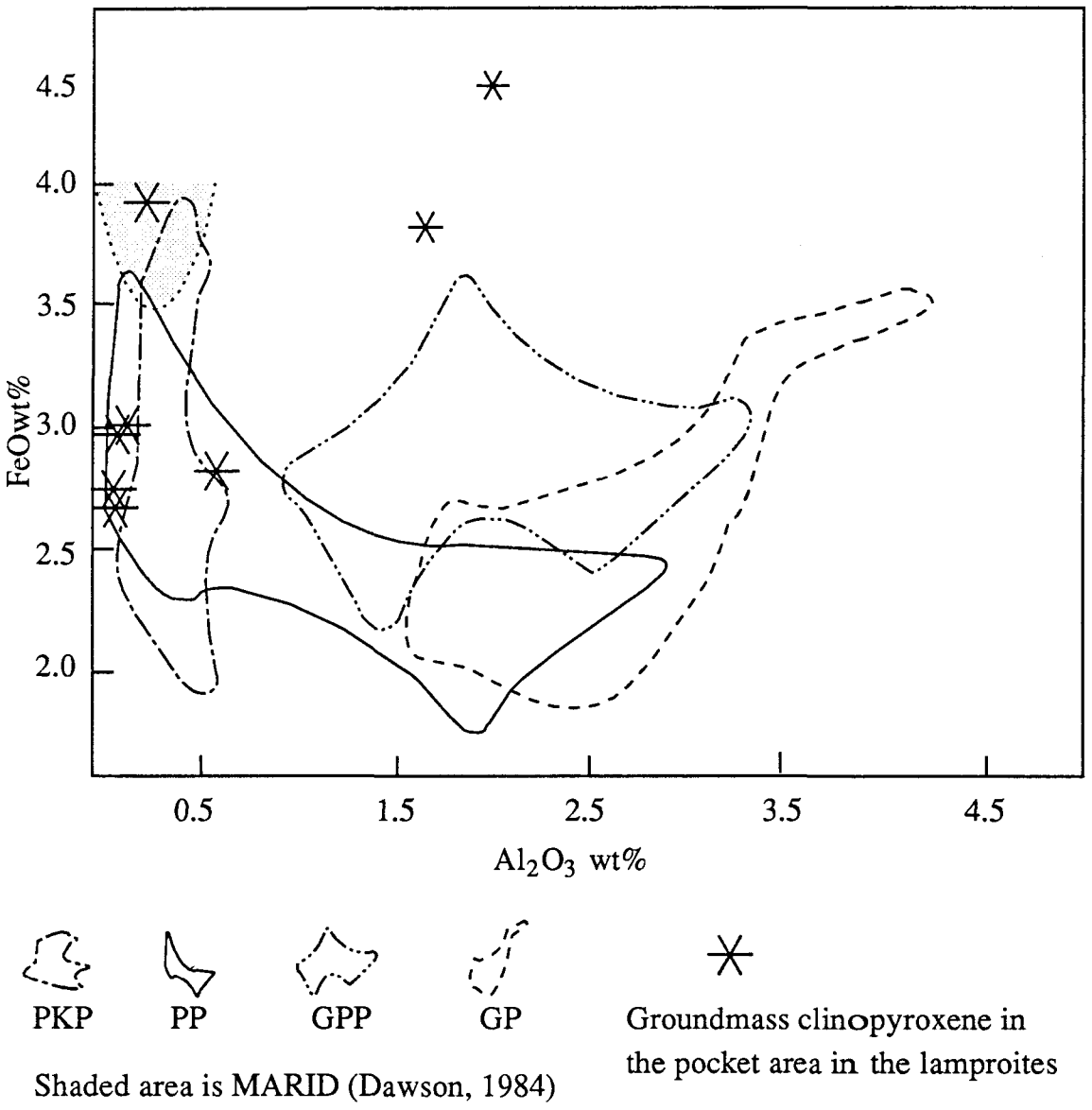

Fig. 5.12 FeO versus Al_2O_3 variation plot for clinopyroxenes from the lamproites and metasomatized mantle peridotites. The clinopyroxene in the lamproites falls in two population, similar to the case of phlogopite peridotites (PP) (abbreviation see text; modified after Erlank etal. 1987).

The most persistent characteristics of the REE patterns of all lamproitic rocks is their depletion in HREEs relative to alkali basaltic rocks. The REEs could have been lost during an earlier melting episode and then LREEs were added. Another possibility is that the HREEs could have been retained by garnet. Yet another possibility is that the HREEs might have been lost during metasomatic processes due to the replacement of garnet. In any case, the lamproitic rocks originate in garnet peridotite field in the mantle, deeper than alkali basaltic rock source. So a metasomatized garnet peridotite source is also required by REE distribution of the lamproites.

The high and variable K/Na ratios of the Huzhiyan lamproites are a character shared by all other lamproites. There are three different ways to explain the K-enrichment relative to Na: (1) fractional crystallization of phases with a high K/Na ratio such as leucite and phlogopite. This mechanism could be the major process that differentiates K/Na ratios of a rock series which originate from a single parental magma; (2) source metasomatism by precipitating more phlogopite than Na-rich phase like amphiboles; (3) selective transfer of K via volatile phases. Experiments show that the K/Na ratio in a liquid is strongly affected by the $H_2O/(H_2O+CO_2)$ ratio (Olafsson & Eggler 1983; Schneider & Eggler 1984), which indicates that selective transfer of K volatile-phase could be very effective. In view of the wide K/Na variations among lamproites in general both intrasuite and intersuite, all the three mechanism could contribute to the K/Na differentiation process. However, source metasomatism may be the key factor that differentiate K/Na among different lamproite suites and between lamproitic rocks and alkali basaltic rocks. Because first of all, K-rich phase crystallization requires that the magma be K-rich initially.

Crustal contamination can raise the K/Na ratio of primitive mantle-derived magma. However the K/Na ratios of crustal materials (<1) are just not high enough to produce the high K/Na ratios observed in most lamproites by contamination. The source metasomatism, on the other hand, can be very effective in differentiating K from Na, seeing that the selective volatile phase transfer mechanism may actually act as part of a metasomatic

process. To consider this, the alkaline rocks from the study area were plotted on a K/Na versus $(La/Yb)_N$ diagram along with other mantle derived rocks (Fig.5.1 3). It is interesting to find that all mantle derived rocks lie on a linear band. This trend indicates that the K/Na ratios of mantle derived rocks are proportionally related to their $(La/Yb)_N$. While La can be differentiated from Yb during partial melting by retaining garnet or clinopyroxene in the source, K can not be differentiated from Na in this manner. A possible way to explain this trend is source metasomatism in which K is preferentially enriched relative to Na by the precipitation of phlogopite and other potassium-rich phases like mathiasite. Accompanying the K-enrichment, is LREEs enrichment relative to HREEs. If the enrichment process is related to the metasomatic process that caused the Al_2O_3-MgO negative correlation suggested in Fig.4.4a, then progressive metasomatic process was responsible for both the major and trace element characteristics observed in the alkaline rocks.

All the above discussion argue for a phlogopite peridotite enriched in LILEs and LREEs as the mantle source of the lamproites. Can such a source generate lamproite? Available experiments on the phlogopite peridotites can partly answer this question. At pressures above 30 Kbar in the presence of magnesite, phlogopite peridotite melts to produce carbonatitic liquids which become more and more SiO_2 and K_2O rich as pressure increases (Wendlandt & Eggler 1980). The experiment of Wendlandt & Eggler also shows that melt composition in such melting process is controlled by pressure, H_2O/CO_2 ratio and equilibrium mineralogy. So it is possible to generate lamproite from a phlogopite peridotite under proper conditions. Lamproites could also represent the selective melting of phlogopite in such a peridotite source diluted by small amounts of pyroxene and/or olivine (Bergman, 1987).

A very prominent feature of the Huzhiyan lamproites is the Ta-Nb and Zr-Hf-Ti negative anomalies on the spidergram (Fig. 4.5). This feature is usually regarded as "Island-arc signature" (Wilson, 1989). Most lamproites have negative Nb, Ta anomalies, though usually not as strong as in the Huzhiyan lamproites. Bergman (1987) stated in his

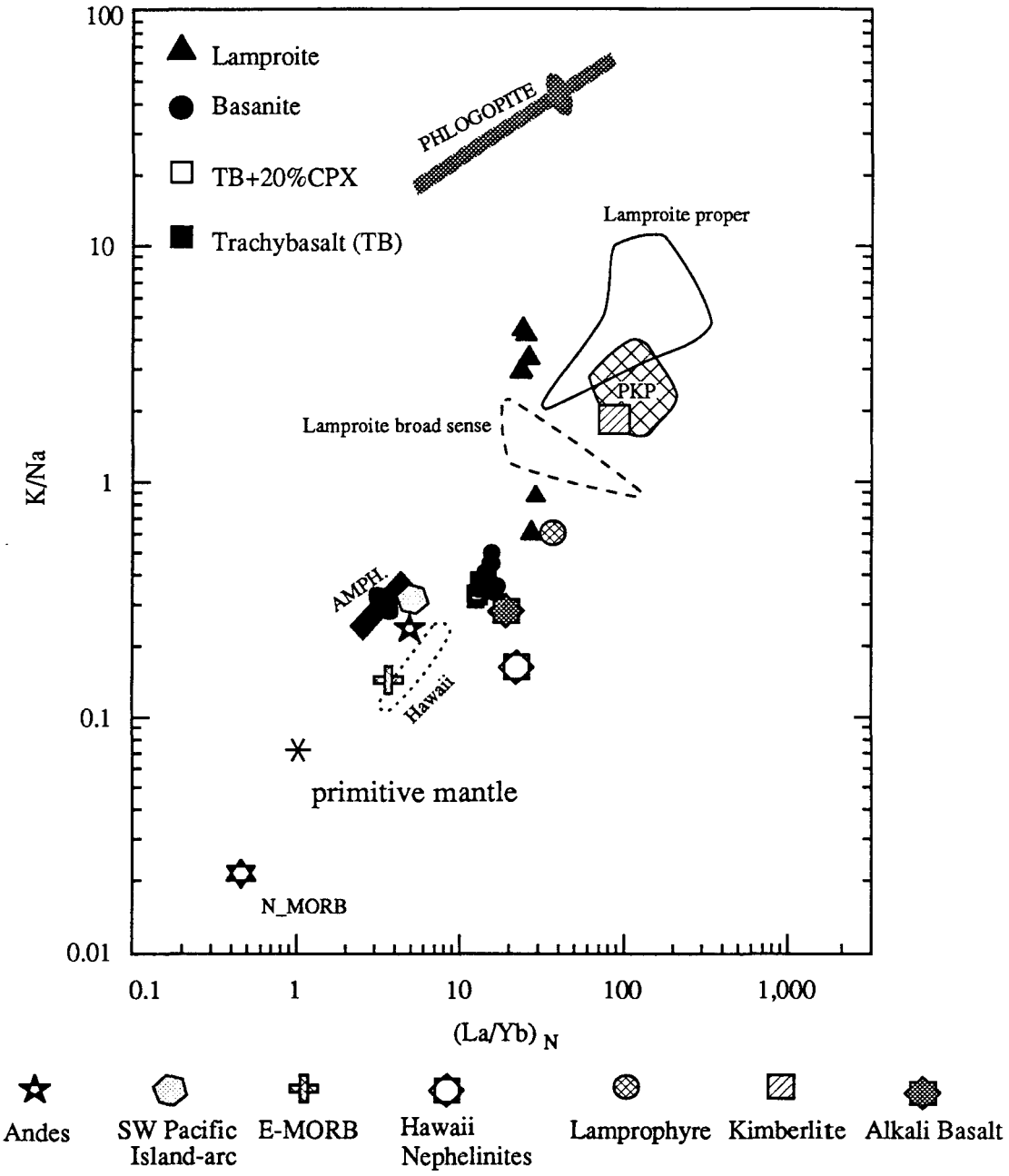

Fig. 5.13 K/Na versus $(La/Yb)_N$ diagram showing the correlation between K/Na differentiation and incompatible element enrichment. The correlation suggests a common process that differentiate K from Na and the REE distribution (Data sources: Bergman, 1987; BVSP, 1981; Taylor, 1986; Wilson, 1989; Erlank, et al., 1987).

review article that lamproites are, in general, the result of post-orogenic magmatic products in regions that have experienced collisional orogenesis several tens to hundreds million years prior to their eruption. Such regions often have fossil Benioff zone (Bergman, 1987). The Huzhiyan lamproites are exposed in an ancient subduction zone (Fig 1.2 & Fig. 2.2). The subduction ceased in late Triassic (~200 Ma), about 70 Ma prior to the lamproite formation which was about 130 Ma ago. The subduction-related feature of the lamproites indicates that a fossil Benioff zone was present in the source of the rocks. Such a fossil Benioff zone can be preserved at least for 70 million years. Subducted material is also helpful in explaining oxygen isotopic data of some lamproites (Bergman, 1987).

5.5.3 Metasomatism and Relationship between the High K/Na and Low K/Na rock series

The close spacial relationship and similar REE chemistry of the high and low K/Na rock series in the study area lead the author to believe that there might be some sort of relationship between them. The correlation trends of Al_2O_3-MgO and K/Na-$(La/Yb)_N$ shown in Fig. 4.4a and Fig.5.13 support this idea. This possible relationship deserves further exploration because it could affect views toward mantle processes and alkaline rock genesis in general.

Ever since Gast's (1968) work, numerical modelling of igneous rock geochemistry has contributed tremendously to our knowledge about the chemistry and structure of the mantle. The prevalence of MORB leads to the consensus that a MORB-like depleted mantle source is prevalent in the upper mantle. The higher incompatible element concentration of the oceanic island basaltic rocks is thought to originate from mantle plume which brings primitive mantle or some recycled crustal material from lower mantle (Sun 1984; Zindler & Hart 1986; Frey & Roden 1987). The geochemical coherence of oceanic island basalts and the island-arc basalts has suggested a "pudding-structure" mantle (Morris & Harte 1983). However, the numerical modelling of magma genesis also encountered some problems, notably the difficulty to generate the high REE contents of some oceanic

island alkali basalts from a primitive mantle source. A direct inference from Schilling's partial melting model is to use very small degrees of partial melting in order to get high REE concentrations (Feigenson, et al. 1983). Although the very small degrees (often <1%) of partial melting required to generate some oceanic island alkali basaltic rocks are acceptable, it is very difficult or impossible to get a reasonable degree of partial melting for generating lamproitic, kimberlitic and some continental rift-related alkaline rocks. For these cases, crustal contamination has been invoked by some researchers (Powell & Bell 1970; Taylor & Turi 1976). While crustal contamination may occur in some cases, it is not consistent with the isotopic data and/or major element chemistry for a large number of alkaline volcanic suites. Alternatively, mantle source contamination by incompatible element rich agents including, in some cases, recycled old subducted materials can explain the incompatible element enrichment feature of all alkaline rocks, from oceanic island alkali basalts to continental rift alkaline rocks to lamproites and kimberlites. Furthermore, this source contamination model, usually called metasomatism, does not have the problem being inconsistent with major and/or isotopic chemistry.

Patent metasomatism (a type of mantle metasomatism with visible metasomatic minerals which are not common to normal mantle peridotite) has been observed widely in mantle xenoliths from kimberlites/lamproites and alkali basaltic rocks (Menzies et al. 1987 and cited therein). In addition to patent metasomatism, there are numerous records of 'cryptic metasomatism' in which only trace elements were enriched (Dawson 1984; Roden & Murthy 1985). Some patent metasomatism may not be recognized when phlogopite or amphibole or alkali-bearing titanate were not present. However, patent metasomatism does not necessarily involve non-typical peridotite constituents. Some diopsides have metasomatic origin (Frey & Roden 1987). So metasomatism may be more widely spread in space and time than it is thought to be. Metasomatism as a mantle process is accepted by most geochemists. The question is how to evaluate it's role and envisage it's relation with alkaline magmatism.

Therefore, the origin of metasomatism needs to be considered. It has been proposed that metasomatism is caused by carbonatitic, kimberlitic or basanitic melts or carbonated alkaline melts (Frey & Roden 1987; Harte et al. 1987; Jones 1989; Meen et al. 1989). Some metasomatized mantle xenoliths have experienced pervasive alteration by their host magma. It is very likely that alkaline magmas will alter the wall rocks in their passage when they were transported to the surface. However, alkaline melts themselves require a enriched source. Although some mantle xenoliths have been metasomatized by their host magma, the author believe that most metasomatic processes in the mantle are not caused by alkaline magma; on the contrary, the author share Bailey's view that mantle metasomatism is a precursor of alkaline magmatism (Bailey, 1982).

For a long time, people treated the metasomatism associated with alkali basaltic rocks (including nephelinite, basanite) as a totally different process from that associated with lamproitic magmatism, because the second type of metasomatism usually results in a more K-rich product with higher La/Yb and H_2O/CO_2 ratios (Kramers, et al. 1983; Bergman 1987). Studies of fluid inclusions in spinel lherzolite xenoliths have shown CO_2 to be a very important component in mantle fluids at relatively shallower depths (Bergman & Dubessy 1984). So the differences between the two types of metasomatism might be only the consequence of a pressure difference. Such differences do not necessarily indicate that the two types of metasomatism are unrelated: They might be merely different manifestations of a related process at different depths in the mantle. The phase relations of peridotite in the presence of small amount of H_2O and CO_2 (Fig. 5.14) established by the experiments of Olafsson & Eggler (1983) can be used to explain the related metasomatic process. Metasomatic fluids rising from below would interact with mantle peridotite. At pressures higher than 22 Kbar (about 70 km), phlogopite and carbonate can precipitate resulting in high K/Na ratio metasomatic products. As the fluids rises higher, it can precipitate amphibole and carbonate at pressures between 22 and 17 Kbar. Because of the earlier phlogopite precipitation, the metasomatic fluid at this stage will be less K-rich, plus the precipitation of amphibole in the place of phlogopite, metasomatic products

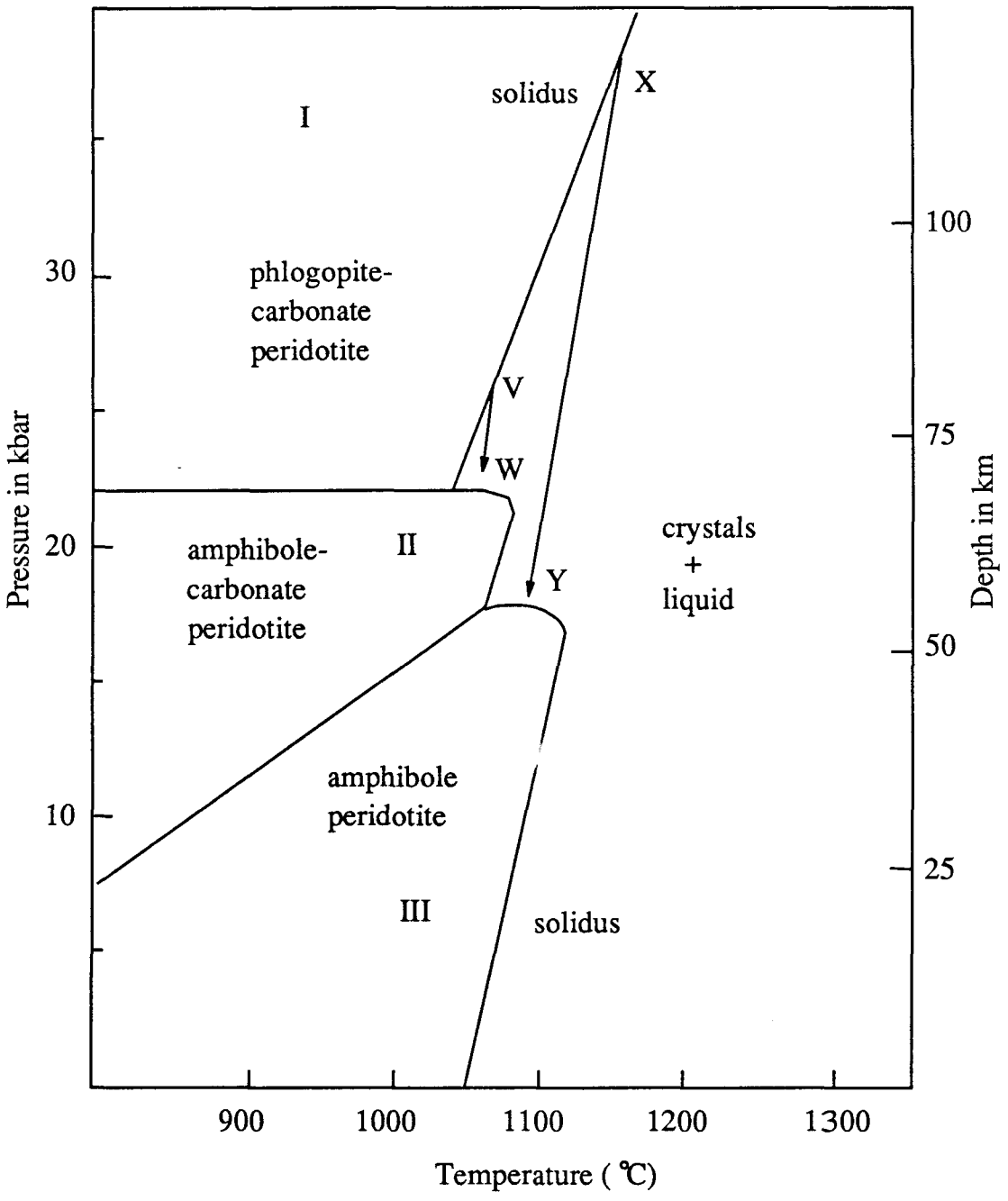

Fig. 5.14 Phase relations of peridotite in the presence of small amounts of H_2O and CO_2 (from Meen et al.,1989, after Olafsson & Eggler 1983). Low degree partial melts formed at depths in excess of 70 km cross the peridotite-H_2O-CO_2 solidus at low pressure (eg. X→Y, V→W). After crossing the solidus, the melt would metasomatize the wall-rocks.

will be less K-rich. As the metasomatic liquid rises to even shallower depths (<17 Kbar), carbonate becomes unstable, only amphibole precipitates. This leads the fluid phase to become more CO_2 rich, therefore less K precipitation, resulting an even lower K/Na product. Because the metasomatic agents come from below, a stronger metasomatism might be expected in the phlogopite zone than in the amphibole zone, therefore, magmas generated by melting the phlogopite zone would have higher REE and LILE level and more differentiated pattern. Amphibole is usually more aluminous than phlogopite, therefore, the phlogopite-zone would have a lower Al_2O_3 content. So from the carbonate-free zone to phlogopite-zone, a progressive metasomatic process, conceptually similar to the one described by Erlank et al (1987), is effectively developed. Such a progressive metasomatic scenario is depicted in Fig. 5.15. Mantle metasomatism thus developed may be widely spread in the upper mantle on a time-integrated scale. An ideal model speculated for the lithospheric mantle is presented in Fig 5.16. Melts originate in the phlogopite zone will be lamproitic; that originate in the amphibole zone will be alkali basaltic. Because the thinner (normally <75 km) and younger lithosphere in oceanic area, no phlogopite zone might have been developed and the metasomatism is weaker than in continental area. This is probably why no lamproitic magmatism occur in oceanic areas.

Using the lithosphere model presented in Fig.5.16, the high and low K/Na series of alkaline rocks in the study area is related by a time-integrated metasomatic process. The lamproites represent melts from the phlogopite zone which was formed earlier in the mantle after the ancient southern China Ocean (Banxi Ocean) was closed. The basanites and the trachybasalts represent melts from the amphibole zone which might be formed later than the phlogopite zone. The low K/Na magmatism in the area were triggered by the rifting process in eastern China during the Cenozoic. The lamproite magmatism could have been triggered by post-orogenic extension during the Mesozoic.

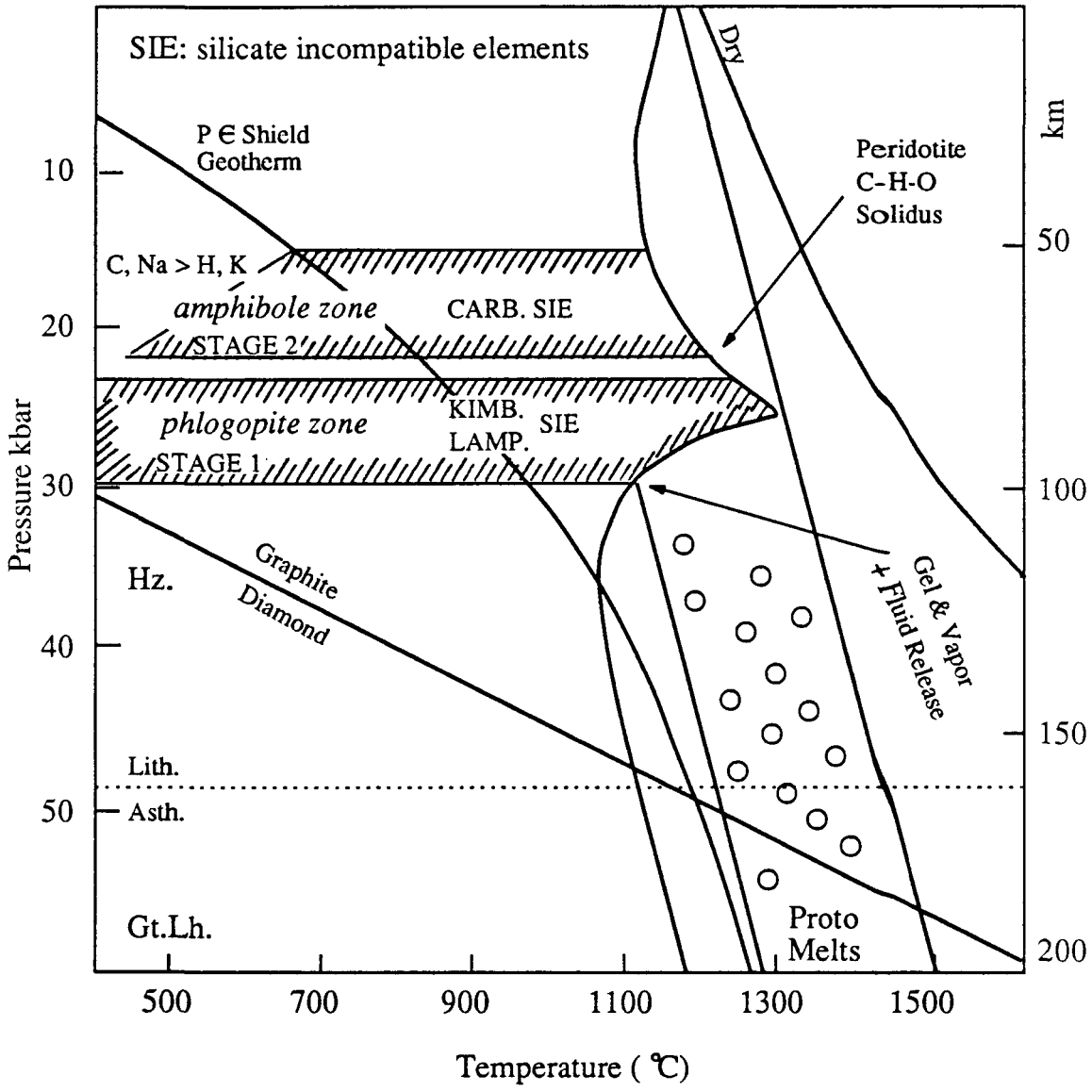

Fig. 5.15 P-T schematic for the development of metasomes in the interval of ~60-100 km in the subcratonic upper mantle lithosphere. Proto melts originating in the asthenosphere (Asth.) from garnet lherzolite (Gt.Lh.) may gel on the intersection with the C-O-H peridotite solidus. Crystallization and fluid release take place, metasomatizing previously depleted lithosphere (Lith.) which is composed of harzburgite (Hz.). Phlogopite metasomatic zone forms at depth >70 km; on top of it amphibole zone is formed (Modified after Haggerty, 1989).

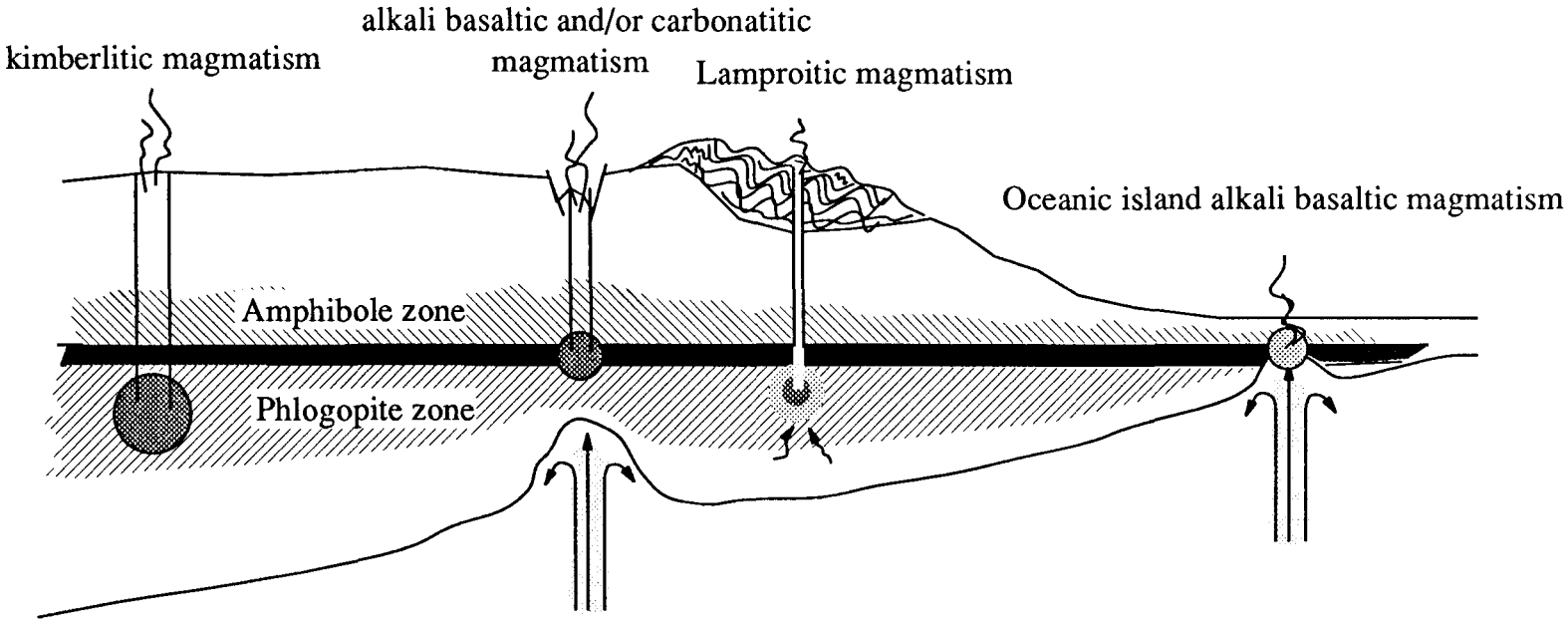

Fig. 5.16 A model for the mantle structure for the study area:
The lithosphere in the study area was suggested by this author to have time -integrated veined metasomatic layers corresponding to the stable zones of phlogopite and amphibole under high pressures. In continental area, lithosphere has a longer history and has reached more advanced stage of metasomatism. Lamproitic (under high P_{H2O} condition) and kimberlitic rocks generate in this area at locations of extension. In rift region, because of mantle plume, melting can occur at shallower depth forming alkali basaltic and/or carbonatitic magmatisms. In oceanic area, lithosphere is rarely thicker than 75 km, especially when a plume is present, therefore there is no phlogopite zone in this region. That could explain why lamproitic and carbonatitic magmatisms are lacking in oceanic region.

Chapter VI

CONCLUSIONS

The petrography, chemical characteristics of the alkaline rocks in southern Hunan and Guangxi Provinces and of the mantle sources of these rocks, magma genesis and evolution processes for these rocks have been systematically studied for the first time. Detailed discussions have been presented in the previous chapters. In this chapter, main points of the previous discussions will be summarized and highlighted.

The alkaline mafic subvolcanic rocks exposed in the inland area from southern Hunan to Guangxi Provinces, southern China fall into two major categories: lamproitic rocks and alkaline basaltic rocks which include basanites and trachybasalts. The lamproitic rocks are distributed in Daoxian area, Hunan Province. The most remarkable petrographic characteristics of these lamproitic rocks are plagioclase-free and phlogopite-rich. These characteristics make the rocks distinct from all other alkaline rocks in the area. Chemically, these lamproitic rocks are MgO and CaO rich, Al_2O_3 poor. They are extremely enriched in LILEs and LREEs. This trace element chemistry is contrast with the MgO rich major element chemistry, a typical character of lamproitic rocks. This contradiction can be best explained by invoking source enrichment in incompatible trace elements. The lamproitic rocks also show a 'Island-arc signature' on their Thompson's spidergram, that is the related Ta-Nb and Zr-Hf-Ti negative anomalies. This feature indicates that the source of the lamproitic rocks may have some involvement of ancient Benioff zone materials.

The alkaline basaltic rocks vary from basanites to trachybasalts as the silica content increases. These rocks have plagioclase and clinopyroxene as their major constituents.

Olivine megacrysts are usually less than 10-15%. Pyroxene megacrysts appear in minor amounts. These rocks also contain alkali feldspar and/or analcime, indicating their high alkali chemistry. Chemically, these rocks are FeO, TiO_2 and MgO rich, but with low #Mg (0.54-0.67). Such low #Mg make it very difficult to generate the basanites and trachybasalts by melting an ordinary mantle peridotite. However, the #Mg of these rocks resemble that of most mantle amphiboles. In fact, the oxide variations of the basanites and trachybasalts define a linear composition array from silica poor to silica saturated end. Such a composition array can be explained by melting an amphibole veined lherzolite. The basanites and trachybasalts are strongly enriched in incompatible trace elements relative to primitive mantle. The enrichment factor of LREEs relative to primitive mantle for these rocks is similar to that for the lamproites; but for LILEs, the basanites and trachybasalts are less enriched than the lamproites. In other word, the LILEs are depleted relative to the LREEs for the basanites and trachybasalts. Such a inconsistent trace element enrichment pattern is difficult to explain by melting a primitive mantle source or by zone refining. Crustal contamination can explain such enrichment pattern; but selective enrichment of incompatible elements in a veined peridotite source can best explain both the trace and major element chemistry of these rocks.

This study provides, for the first time, a detailed petrographic description and reliable systematic geochemical data (major elements, trace elements and PGEs) for the Mesozoic-Cenozoic alkaline rocks from the inland area of southern China. Major points or contributions achieved in this study are:

(1) The first discovery of lamproite in southern China area.

(2) Clarification of terminology used for the alkaline rocks from the study area: classifying the rocks as lamproitic (plagioclase free, phlogopite rich) and alkaline basaltic which are further classified using Le Bas' chemical classification.

(3) The revelation and explanation of a linear composition array defined by the basanites and the trachybasalts from the study area: an amphibole veined lherzolite mantle enriched in incompatible trace elements might have generated the basanite magmas and the parental trachybasalt magmas which evolved to the trachybasalts by crystallizing about 18% clinopyroxene in depth.

(4) The confirmation of a Tertiary subduction zone in the study area by the trace element chemistry of the lamproites.

(5) The demonstration of two chemical trends: the negative correlation between MgO and Al_2O_3 for alkaline rocks from average alkali basalts, mafic lamprophres to lamproitic rocks (including kimberlite); the logarithmic correlation between K/Na and $(La/Yb)_N$ for almost all mantle derived mafic and alkaline rocks.

(6) A progressive metasomatic model is provided for the lithospheric mantle in which a phlogopite peridotite zone was formed by metasomatism in depths greater than 70 km which is overlain by a metasomatism-generated amphibole peridotite zone. This model treats the alkaline basaltic and lamproitic magmatism as source process related events, and which explains the trends mentioned in point 5.

Appendix A

Chemical composition of the alkaline rocks in the study area analyzed by wet chemical methods in the Institute of Geochemistry, Academia Sinica by Liang Fong Xian and Dai Fong Fu.

Table 4.1* Wet chemical analyses for the the lamproites

#	Lam1	Lam2	Lam3	Lam4	Lam5	Lam6
##	HZYB8	HZYB10	HZYB5	HZYB2	HZYB3	HZYB4
SiO_2	46.49	44.84	45.90	45.76	45.33	44.90
TiO_2	0.28	0.27	0.26	0.28	0.26	0.24
Al_2O_3	8.65	8.53	8.56	7.94	8.36	8.50
Fe_2O_3	2.38	2.62	2.62	2.29	2.25	2.82
MgO	15.92	15.58	15.59	16.74	15.84	14.64
FeO	4.29	4.25	4.52	4.65	4.88	4.08
MnO	0.17	0.16	0.18	0.19	0.19	0.17
CaO	13.92	10.99	11.69	13.88	11.48	11.50
Na_2O	1.48	0.24	0.30	1.36	0.28	0.28
K_2O	1.46	3.38	2.89	1.98	2.86	3.93
P_2O_5	0.58	0.57	0.60	0.58	0.59	0.57
H_2O+	3.24	4.41	4.52	3.35	5.52	4.90
H_2O-	1.03	2.53	1.60	0.60	1.79	1.87
Total	99.89	98.37	99.23	99.60	99.63	98.40

\# Sample codes used in the text of this thesis.
Original sample codes used during the field work.

Table 4.2&3* Wet chemical analyses for the trachybasalts and basanites

#	SH1	SH2	SH3	TB4	TB5	Bas4	Bas5
##	TYSB3	TYSB1	TYSB4	TYSB9	TYSB7	JB4	JB5
SiO_2	49.17	47.81	50.12	48.53	47.80	44.10	44.35
TiO_2	1.80	1.56	1.64	1.70	1.89	2.58	2.59
Al_2O_3	15.55	15.37	15.10	15.62	14.75	12.69	12.93
Fe_2O_3	4.59	4.24	4.05	4.20	3.85	2.08	2.37
MgO	5.43	6.54	6.50	6.11	7.02	9.34	9.53
FeO	5.74	6.55	6.20	6.63	7.02	8.64	8.42
MnO	0.27	0.21	0.21	0.22	0.22	0.20	0.19
CaO	6.45	5.96	5.77	6.37	6.93	9.56	9.73
Na_2O	3.86	3.77	3.88	3.75	3.40	3.29	3.68
K_2O	2.18	2.09	2.20	1.86	1.95	2.46	2.04
P_2O_5	0.76	0.73	0.73	0.73	0.73	0.72	0.75
H_2O+	2.77	3.70	2.52	2.72	2.70	2.91	2.23
H_2O-	1.07	0.71	0.57	1.11	0.60	0.45	0.60
Total	99.64	99.24	99.49	99.55	98.86	99.02	99.41

Appendix B

Rare earth elements data for the alkaline rocks in the this study analyzed by ICP-AES technique in the Institute for Geological Survey of Hubei Province, China.

Table 4.4* REE data for the lamproites analyzed by ICP-AES technique

#	Lam1	Lam2	Lam3	Lam4	Lam5	Lam6
##	HZYB8	HZYB10	HZYB5	HZYB2	HZYB3	HZYB4
La	51.14	54.71	55.07	48.76	55.02	53.61
Ce	92.05	100.79	100.42	91.49	100.76	98.73
Pr	10.27	11.11	10.94	9.89	10.96	10.71
Nd	43.26	49.70	47.99	43.10	47.29	47.27
Sm	9.19	10.13	9.82	9.04	9.90	9.97
Eu	2.54	2.81	2.73	2.52	2.73	2.74
Gd	7.67	8.77	8.33	7.80	8.44	8.29
Tb	1.16	1.21	1.23	1.15	1.24	1.24
Dy	4.61	5.22	5.06	4.66	5.07	4.93
Ho	0.80	0.91	0.84	0.81	0.87	0.86
Er	1.74	2.07	1.89	1.78	1.97	1.97
Tm	0.29	0.29	0.30	0.29	0.33	0.32
Yb	1.28	1.57	1.36	1.37	1.57	1.50
Lu	0.18	0.22	0.18	0.19	0.22	0.22
Y	19.50	23.12	20.92	20.23	22.09	21.91

\# Sample codes used in the text of this thesis.
Original sample codes used during the field work.

Table 4.5&6* REE data for the trachybasalts and basanites analyzed by ICP-AES technique

#	SH1	SH2	SH3	TB4	TB5	Bas4	Bas5
##	TYSB3	TYSB1	TYSB4	TYSB9	TYSB7	JXB4	JXB5
La	47.57	50.12	53.00	50.00	47.60	46.65	49.72
Ce	89.39	95.02	99.06	96.03	89.17	87.58	92.14
Pr	9.13	9.70	9.91	9.63	9.32	8.95	9.39
Nd	39.39	41.07	43.22	41.07	39.66	38.73	41.00
Sm	7.82	8.29	8.28	8.31	8.03	8.46	8.84
Eu	2.52	2.72	2.71	2.74	2.60	2.63	2.77
Gd	6.89	7.19	7.47	7.44	7.16	7.55	8.05
Tb	1.12	1.19	1.17	1.19	1.14	1.19	1.27
Dy	5.23	5.60	5.82	5.76	5.68	5.78	6.01
Ho	1.01	1.08	1.10	1.10	1.08	1.07	1.13
Er	2.59	2.74	2.82	2.87	2.73	2.63	2.79
Tm	0.43	0.46	0.46	0.45	0.44	0.41	0.43
Yb	2.33	2.49	2.56	2.53	2.43	2.17	2.27
Lu	0.34	0.37	0.37	0.37	0.35	0.30	0.32
Y	25.23	27.04	27.44	27.18	26.07	26.49	27.72

湘南--桂北中新生代碱性次火山岩成因

刘俊所 （一九九二）

博士论文摘要

在湘南宁远、道县至桂北平乐、平南西折至马山县局巷一带，分布有许多次火山岩脉和/或岩筒。这些次火山岩体距福建海滨约千余公里，因而称为内陆次火山岩带，以便与东部环太平洋广泛发育的滨海火山岩带区别。这些岩石可分为钾镁煌斑岩质和碱性玄武质（函碱性超基性）两大类，包括碧玄岩、粗玄岩和钾镁煌斑岩。

碧玄岩和粗玄岩是新生代岩浆活动产物（52-28Ma）。它们的 #Mg 小于66，相对富铁。碧玄岩含较高的 MgO（9-10 wt%）和 Ni（约 200 ppm），并含有丰富的二辉橄榄岩捕掳体，表明其相对原始的、基本未分异的状态。粗玄岩的 MgO（5.5-8.4 wt%）和 Ni（163-251 ppm）变化稍大，其低 CaO（6.5-7.3 wt%）贫 Sc（约 13 ppm），同时又含较高的 Al_2O_3（约15wt%）。表明这种岩石可能经受过富钙单斜辉石结晶分异。在多元素联合配分图上（Thompson's spidergram），碧玄岩和粗玄岩的不相容元素呈现为富集度向元素不相容性增强方向逐渐增大的强分异趋势，但 LILEs 的富集度和 LREEs 相似或略低：La-Nb-Ta-K-U-Th-Ba 高出原始地幔岩 100-130 倍，相当于洋岛或弧--沟系碱性玄武质岩石的 2-3 倍。这种配分图式与东非裂谷带中 Kenya 碧玄岩的图式很相似。Ba, Th, U 等强不相容元素相对于 La 略显亏损，故这种图式难以用原始地幔极低度部分熔融解释；逐区萃取精化过程（zone refining）同样也不适用。再说，原始地幔橄榄岩部分熔融也难以形成 #Mg < 66 的岩浆。然而，大多数地幔角闪石具有和这种碱性岩浆相似的 #Mg。闪石网脉穿插的地幔橄

榄岩捕掳体在碱性火山岩中常见，并且这种捕掳体往往是不相容元素富集了的。这样的闪石网脉化的富集了不相容元素的橄榄岩是可能的岩浆源。

钾镁煌斑岩是中生代岩浆活动产物(约 135 Ma)。它们极富MgO (15.5-16.9 wt%) 与 CaO(11-14 wt%), 贫 Al_2O_3 (8.1-8.8 wt%), K/Na 比值及 K/Al 比值高，与前述的碱性玄武质岩石(碧玄岩和粗玄岩)迥异。这类岩石的多元素联合配分图表现出比前述碧玄岩及粗玄岩更强的分异图式：Ba 是原始地幔岩的 210-450 倍，La 的富集度与该区碧玄岩相似，而 HREEs 却仅有碧玄岩的约二分之一。HREEs 的相对亏损表明，在其源区可能有石榴石残存或石榴石组分被早期亏损事件所移去。这样强烈分异富集的多元素联合配分图极难用原始地幔岩部分熔融解释。地壳物质混染可以解释不相容元素的富集，然而无法同时解释富镁贫铝的主元素特征。钾镁煌斑岩的高 #Mg (>80) 也与原始地幔岩的部分熔融产物不一致。考虑到橄榄石斑晶的聚积，这个问体可以得到缓和；然而橄榄石斑晶高的 Fo (平均93) 表明高#Mg 是钾镁煌斑岩液态岩浆固有特征。钾镁煌斑岩的多元素联合配分图上有很突出的 Ta-Nb 和 Zr-Hf-Ti 负异常，很可能表明其源区与古俯冲带有一定联系。

虽然主元素迥异，但研究区的钾镁煌斑岩与碧玄岩及粗玄岩的微量元素化学有很大相似之处：它们都很富集微量元素，特别是 MREE-LREE 在两种岩石中的富集程度和趋势基本相同。另外它们在空间上密切相关。迄今为止的文献中都把钾镁煌斑岩质火山活动和碱性玄武质火山活动看成是互不相关的事件，因它们在化学上相差甚远。然而，K/Na 比值在各类幔源岩中的分布可能对这一传统看法产生强烈振撼：在 $K/Na-(La/Yb)_N$ 对数坐标图上，几乎所有幔源火成岩都投影到一条正相关的线性带上，这可能表明幔源火成岩的 K/Na 分异与不相容元素的分异是相关过程。与此相关的是，从平均碱性玄武岩至钾镁煌斑岩至金伯利岩，MgO逐渐增高，Al_2O_3 逐渐降低，MgO 和 Al_2O_3 成负相关关

系；而CaO 在上述岩石序列中却无系统变化。部分熔容过程难以解释上述的两个相关趋势，它们不可避免地要求源区物质的外来组分加入。

综上所述，本文的主要结论是：(1) 碧玄岩和粗玄岩由选择富集了微量元素的闪石网脉化的二辉橄榄岩部分熔融所形成，粗玄岩是原始岩浆经辉石结晶分异后的产物。部分熔融过程由新生代中国东部的区域大陆涨裂活动引发，是新生代滨海火山活动向内陆的延申。(2) 钾镁煌斑岩是中生代初大陆碰撞后的后造山岩浆活动产物，源于比碧玄岩的角闪石橄榄岩源更深的层位。源区物质应是亏损了玄武质组分又在后期交代过程中选择地富集了不相容元素并沉淀有高K/Na比矿物的金云母橄榄岩。这种源区岩石很可能涉及古老俯充带物质。(3) 金云母橄榄岩与闪石橄榄岩构成岩石圈的双层交代结构。作者认为，这种双层交代结构是地幔递进交代作用产物，是交代剂从深部向上运移时，在不同压力带累积交代上地幔橄榄岩所形成。

Appendix D Abbreviations used in this thesis

Anal	Analcime
AVE	Average
B, Bas	Basanite
c	Center of a crystal
CPX, Cpx	Clinopyroxene
Feld, fs	Feldspar
g	Groundmass
IL	Ilmenite
Lam	Lamproite
Lh	Lherzolite
m	Margin of a crystal
OL, Ol, Oliv	Olivine
OPX, Opx	Othorpyroxene
p	Phenocryst
Phl	Phlogopite
Pl	Plagioclase
SH	Shoshonite
SP	Spinel
T, TB	Trachybasalt
x	Xenocryst

References

Allègre, C.J., 1982. Chemical geodynamics. Tectonophysics, **81**, pp. 109-132.

—— , Dupré, B., Richard, P., Rousseau, D. and Brooks, C., 1982. Subcontinental versus suboceanic mantle. II: Nd-Sr-Pb isotopic comparison of continental tholeiites with mid-ocean ridge tholeiites and the structure of the continental lithosphere. Earth and Planetary Science Letters, **57**, pp. 25-34.

—— , Hart, S.R. and Minster, J.F.,1983. Chemical structure and evolution of the mantle and continents determined by inversion of Nd and Sr isotopic data. I: Theoretical methods. Earth and Planetary Science Letters, **66**, pp. 177-190.

—— , Hart, S.R. and Minster, J.F.,1983. Chemical structure and evolution of the mantle and continents determined by inversion of Nd and Sr isotopic data. II: Numerical experiments and discussion. Earth and Planetary Science Letters, **66**, pp.191-213.

—— , and Minster, J.F., 1978. Quantitative models of trace element behaviour in magmatic processes. Earth and Planetary Science Letters, **38**, pp. 1-25.

Bailey, D.K., 1982. Mantle metasomatism -- continuing chemical change within the Earth. Nature, **269**, pp. 525-530.

Barnes, S.-J., Boyd, R., Korneliussen, A., Nilsson, L-P., Often, M., Pedersen, R.B., and Robins, B., 1988. The use of mantle normalization and metal ratios in discriminating between the effects of partial melting, crystal fractionation and sulphide segregation on Platinum-Group Elements, Gold, Nickel and Copper: examples from Norway. In Geoplatinum-87, edited by H. M. Prichard, et al. pp. 113-143, Elsevier London.

Bédard, J. H., 1989. Disequilibrium mantle melting. Earth and Planetary Science Letters, **91**, pp. 359-366.

Bergman, S. C., 1987. Lamproites and Other potassium-rich igneous rocks: a review of their occurrence, mineralogy and geochemistry. Geological Society of America Special Publication, No.30, pp. 103-190.

Bergman, S. C., and Dubessy, J., 1984. CO_2-CO fluid inclusions in a composite peridotite xenolith: implications for upper mantle oxygen fugacity. Contributions to Mineralogy and Petrology, **85**, pp. 1-13.

Bowen, N.L., 1928. The Evolution of the Igneous Rocks. Princeton University Press, Princeton, New Jersey, 332pp.

Boyd, F.R. and Nixon, P.H., 1973. Origin of the ilmenite-silicate nodules in kimberlites from Lesotho and South Africa. In Lesotho Kimberlites edited by P.H. Nixon, pp. 254-268, Maseru Lesotho: Lesotho National Development Corporation.

Cao, R. and Zhu, S., 1987. Mantle xenoliths and alkali-rich rocks in eastern China. In Mantle Xenoliths, edited by P.H. Nixon, pp. 167-180, John Wiley and Sons Ltd, New York.

Chen, J.,1973. Geochemistry of basalts from Penghu islands. Proceedings of the Geological Society of China, **16**, pp. 23-36.

Cong, B., Zhang, W., and Yie, D., 1979. A study of Cenozoic basalts in North China faulting block. Transaction of the Geological Society of China, **2**, pp. 112-124.

Daly, R.A., 1910., Origin of alkaline rocks. Bulletin of the Geological Society of America, **21**, pp. 87-118.

Vollmer R., and Norry M.H., 1983. Possible origin of K-rich volcanic rocks from Virunga, East Africa, by metasomatism of continental crustal material: Pb, Nb and Sr isotopic evidence. Earth and Planetary Science Letters, **64**, pp. 374-386.

Davidson, J.P., 1987. Crustal contamination versus subduction zone enrichment: examples from the Lesser Antilles and implications for mantle source compositions of island arc volcanic rocks. Geochimica et Cosmochimica Acta, **51**, pp. 2185-2198.

Dawson, J.B., 1984. Contrasting types of upper-mantle metasomatism? In Kimberlites II: The mantle and crust-mantle relations. edited by J. Kornprobst, pp. 289-294. ELSEVIER Amsterdam.

Dupuy, C., Barsczus, H.G., Dostal, J., Vidal, P. and Liotard, J.-M., 1989. Subducted and recycled lithosphere as the mantle source of ocean island basalts from southern Polynesia, Central Pacific. Chemical Geology, **77**, pp. 1-18.

Eggler D.H., 1977. The principle of the zone of invariant vapour composition: an example in the system CaO-MgO-SiO_2-CO_2-H_2O and implications for the mantle solidus. the Year-book of Carnegie Institute in Washington, **76**, pp. 428-433.

Engle, A.E.J. and Engle, C. G., 1960. Progressive metamorphism and granitization of the major paragneiss, northwest Adirondack Mountains, New York. Part II: Mineralogy. Bulletin of the Geological Society of America, **71**, pp. 1.

Erlank, A.J. and Rickard R.S. 1977. Potassic richterite bearing peridotites from kimberley and the evidence they provide for upper mantle metasomatism. Extended Abstract, International Kimberlite Conference, 2nd, Santa Fe, New Mexico, USA, unpaged.

—— , Waters, F.G., Hawkesworth, C.J., Haggerty, S.E., Allsopp, H.L., Rickard R.S., and Menzies, M., 1987. Evidence for mantle metasomatism in peridotite nodules from the kimberley pipes, South Africa. In Mantle Metasomatism. edited by M. A. Menzies and C.J. Hawkesworth. pp. 221-311. Academic Press London.

Ernst, R.E., Fowler, A.D. and Pearce, T.H. 1988. Modelling of igneous fractionation and other processes using Pearce diagrams. Contributions to Mineralogy and Petrology, **100**, pp. 12-18.

Feigenson, M.D., Hofmann, A.W., and Spera, F.J., 1983. Case studies on the origin of basalts II: the transition from tholeiitic to alkalic volcanism on Kokala volcano, Hawaii. Contributions to Mineralogy and Petrology, **84**, pp. 390-405.

Francis, D., 1976. The origin of amphibole in lherzolite xenoliths from Nunivak Island, Alaska. Journal of Petrology **17**, pp. 357-378.

—— , and Ludden, J., 1990. The mantle source for olivine nephelinite, basanite, and alkaline olivine basalt at Fort Selkirk, Yukon, Canada. Journal of Petrology **31**, pp. 371-400.

Frey, F.A., Green, D.H. and Roy, S.D., 1978. Integrated models of basalt petrogenesis: a study of quartz tholeiites to olivine melilitites from South Australia utilizing geochemical and experimental petrological data. Journal of Petrology, **19**, pp. 463-513.

Frey, F.A., and Roden, M.F., 1987. The mantle source for the Hawaiian Islands: constraints from the lavas and ultramafic inclusions. In mantle metasomatism. edited by M.A. Menzies and C.J. Hawkesworth, pp. 423-463. Academic Press London.

Gast, P.W., 1968. Trace element fractionation and the origin of tholeiitic and alkaline magma types. Geochimica et Cosmochimica Acta, **32**, pp. 1057-1086.

Gee, L.L. and Sack, R.O., 1988. Experimental petrology of melilite nephelinites. Journal of Petrology **29**, pp. 1233-1256.

Green, D.H., 1970. A review of experimental evidence on the origin of basaltic and nephelinitic magmas. Physics of the Earth Planet Interiors, **3**, pp. 221-235.

Green, D.H., 1980. Island arc and continent building magmatism -- a review of petrogenic models based on experimental petrology and geochemistry. Tectonophysics, **63**, pp. 367-385.

Gupta, A.K., Yagi, K., Hariya, Y., and Onuma, K., 1976. Experimental investigation of some synthetic leucite rocks under water processes. Proceedings of Japan Academy of Sciences, **52**, pp. 469-472.

Gupta, S., 1989. Comment on "Mesozoic overthrust tectonics in South China". Geology, **17**, pp. 669-670.

Haggerty, S.E., 1989. Mantle metasomatism and the kinship between carbonatites and kimberlites. In Carbonatites: genesis and Evolution. edited by K.Bell, pp. 546-560. UNWIN HYMAN London.

—— , 1983. The mineral chemistry of new titanates from the Jagersfontein kimberlites, South Africa: implications for metasomatism in the upper mantle. Geochimica et Cosmochimica Acta, **47**, pp. 1833-1855.

Hanson, G.N., 1977. Geochemical evolution of the suboceanic mantle. Journal of the Geology Society of London, **134**, pp. 235-253.

—— , and Langmuir, C.H., 1978. Modelling of major elements in mantle-melt systems using trace elements approaches. Geochimica et Cosmochimica Acta, **42**, pp. 725-741.

Harte, B., 1983. Mantle peridotites and processes -- the kimberlite sample. In continental Basalts and Mantle Xenoliths, edited by C.J. Hawkesworth, M.J. Norry, pp. 46-91, Cheshire, England: Shiva.

——, Winterburn, P.A., and Gurney, J.J., 1987. Metasomatism and enrichment phenomena in garnet peridotite facies mantle xenoliths from the Matsoku kimberlite pipe, Lesotho. In Mantle Metasomatism edited by M.A. Menzies and C.J. Hawkesworth, pp. 145-221. Academic Press, Orlando, Florida.

Hawkesworth C.J., Calsteren, P.V., Rogers, N.W., and Menzies, M.A. 1987. Isotope variations in recent volcanics: a trace-element perspective. In Mantle Metasomatism. edited by M.A. Menzies and C.J. Hawkesworth. pp. 365-388. Academic Press London.

Hawkesworth C.J., Rogers, N.W., van Calsteren, P.W.C. and Menzies, M.A., 1984. Mantle enrichment processes. Nature, **311**, pp. 331-335.

Hekinian, R., Bonté, P., Pautot, G., Jacques, D., Labeyrie, L., Mikkelsen, N. and Reyss, J.L.,1989. Volcanics of the South China Sea ridge system. Oceanology Acta, **12**, pp. 101-116.

Holm, P.M. and Munksgaard, N.C., 1982. Evidence for mantle metasomatism: an oxygen and strontium isotope study of the Vulsinian District, Central Italy. Earth and Planetary Science Letters, **60**, pp. 376-388.

Hsü, K.-J., Sun, S. Li, J. Chen, H., Pan H. and Sengör, A.M.C., 1983. Mesozoic overthrust tectonics in South China. Geology, **16**, pp. 418-427.

——, Sun, S. and Li, J., 1987. South China be an orogenic zone not a platform. Chinese Sciences **10B**, pp. 1107-1115. (in Chinese).

——, Sun S., Li, J., Chen, H., Pan H. and Sengör, A.M.C.,1989. Reply on "Mesozoic overthrust tectonics in South China". Geology, **17**, pp. 672-673.

——, Li, J., Chen, H., Wang, Q. Sun S., and Sengör, A.M.C.,1990. Tectonics of South China: key to understanding the West Pacific. Tectonophysics, **183**, pp. 9-39.

Huang, W., Xu, J., Gao, Z. and Nan, J., 1982. A mineralogical study of spinel lherzolite xenoliths in basalts from southeastern China. Acta Mineralogica Sinica., **3**, pp. 175-187. (in Chinese).

IGAS, 1979. Geochemistry of granites in South China. Sciences Press, Beijing, pp508.

Irving, A. J., 1978. A review of experimental studies of crystal/liquid trace element partioning. Geochimica et Cosmochimica Acta, **42**, pp. 743-770.

Ito, K. and Kennedy, G.C., 1967. Melting and phase relations in a natural peridotite to 40 kilobars. American Journal of Sciences, **265**, pp. 519-538.

Geeks, A.L. and Green, D.H., 1980. Anhydrous melting of peridotite at 0-15 kb pressures and the genesis of tholeiitic basalts. Contributions to Mineralogy and Petrology, **73**, pp. 287-310.

Jones, A.P., 1989. Upper mantle enrichment by kimberlitic or carbonatitic magmatism. In Carbonatites: genesis and Evolution. edited by K.Bell, pp. 448-463. UNWIN HYMAN London.

Jones, A.P., Smith, J.V., and Dawson, J.B., 1982. Mantle metasomatism in 14 veined peridotites from Bultfontein Mine, South Africa. Journal of Geology, **90**, pp. 435-453.

Kramers, J.D., Roddick, J.C.M. and Dawson, J.B., 1983. Trace element and isotope studies on veined metasomatic and "MARID" xenoliths from Bultfontein, South Africa. Earth and Planetary Science Letters, **65**, pp. 90-106.

Kushiro, I., Syono, Y. and Akimoto, S.-I., 1968. Melting of a peridotite nodule at high pressures and high water pressures. Journal of Geophysical Research, **73**, pp. 6023-6029.

Liu, G., 1980. A discussion on the petrology and origin of the alkaline basalts and their lherzolite xenoliths from Guangxi Province. Bulletin of Chinese Academy of Geological Sciences, Series VIII, **1**, pp. 61-72. (in Chinese).

Liu, G., 1982. The alkaline basaltic rocks and their xenoliths from Hunan and Guangxi Provinces. Journal of Yichang Institute of Geology, Academia Sinica, No.1, pp. 1-36.(in Chinese).

Lloyd, F.E., and bailey, D.K., 1975. Light element metasomatism of the continental mantle: the evidence and the consequences. Phys. Chem. Earth, **9**, pp. 381-416.

Maalfe, S. and Johnston,A.D., 1986. Geochemical aspects of some accumulation models for primary magmas. Contributions to Mineralogy and Petrology, **93**, pp. 449-458.

MacDonald, G. A. and Katsura, T., 1964. Chemical composition of Hawaiian lavas. Journal of Petrology, **5**, pp. 82-133.

Marsh, J.S., 1989. Geochemical constraints on coupled assimilation and fractional crystallization involving upper crustal compositions and continental tholeiitic magma. Earth and Planetary Science Letters, **99**, pp. 70-80.

Meen, J.K., Ayers, J.C., and Fregeau, E.J., 1989. A model of mantle metasomatism by carbonated alkaline melts: trace element and isotopic compositions of mantle source regions of carbonatite and other continental igneous rocks. In Carbonatites: genesis and Evolution. edited by K.Bell, pp. 464-499. UNWIN HYMAN London.

Menzies, M., 1983. Mantle ultramafic xenoliths in alkaline magmas: evidence fro mantle heterogeneity modified by magmatic activities. In Continental Basalts and Mantle Xenoliths. edited by C.J. Hawkesworth and M.J. Norry, pp. 92-110. Cheshire, England shiva.

Menzies, M., Kempton, P., and Dungan M., 1985 Interaction of continental lithosphere and asthenospheric melts below the Geronimo Volcanic Field, Arizona, USA. Journal of Petrology, **26**, pp. 663-693.

—— , Rogers, N., Tingle A., and Hawkesworth C., 1987. Metasomatic and Enrichment Processes in lithospheric peridotites, an effect of Asthenosphere-lithosphere interaction. In Mantle Metasomatism. edited by M.A. Menzies and C.J. Hawkesworth. pp. 313-361. Academic Press London.

Merril, R.B. and Wyllie. P.J., 1975. Kaesutite and kaesutite eclogite from Kakanui, New Zealand — water-excess and water-deficient melting to 30 kilobars. Bulletin of the Geological Society of America, **86**, pp. 555-570.

Minster, J.F. and Allègre, C.J., 1978. Systematic use of trace elements in igneous processes. Part III: Inverse problem of batch melting in volcanic suites. Contributions to Mineralogy and Petrology, **68**, pp. 37-52.

Mitchell, R. H., 1985. A review of the mineralogy of lamproites. Transaction of the Geological Society of South Africa, **88**, pp. 411-437.

—— , 1986. Kimberlites: mineralogy, geochemistry, and petrology. Plenum, New York.

Morris, J.D. and Hart, S.R., 1983. Isotopic and incompatible element constraints on the genesis of island arc volcanics from Cold Bay and Amak Island, Aleutians, and implications for mantle structure. Geochimica et Cosmochimica Acta, **47**, pp. 2015-2030.

Mysen, B.O. and Boettcher A.L. 1975. Melting of a hydrous mantle: I. phase relations of natural peridotite at high pressures and temperatures with controlled activities of water, carbon dioxide and hydrogen. Journal of Petrology, **16**, pp. 520-548.

O'Hara M. J., 1968. The bearing of phase equilibrium studies in synthetic and natural system on the origin and evolution of basic and ultrabasic rocks. Earth Science Review, **4**, pp. 69-13.

—— and Mathews, R.E., 1981. Geochemical evolution in an advancing petrologically tapped continuously fractionated magma chamber. Journal of the Geological Society of London, **138**, pp. 237-278.

Olafsson, M. and Eggler, D.H., 1983. Phase relation of amphibole-carbonate, and phlogopite-carbonatite peridotite: petrologic constraints on the asthenosphere. Earth and Planetary Science Letters, **64**, pp. 305-315.

O'Reilly, S.Y. and Griffin, W.L., 1984. Sr isotopic heterogeneity in primitive basaltic rocks, southern Australia: correlation with mantle metasomatism. Contributions to Mineralogy and Petrology, **87**, pp. 220-230.

Pearce, T.H., 1987. The identification and assessment of spurious trends in Pearce-type ratio variation diagrams: a discussion of some statistical arguments. Contributions to Mineralogy and Petrology, **97**, pp. 529-534.

——, 1968. A contribution to the theory of variation diagrams. Contributions to Mineralogy and Petrology, **19**, pp. 142-157.

Powell, J.L. and Bell, K., 1970. Strontium isotopic studies of alkaline rocks. Localities from Australia, Spain, and western United States. Contributions to Mineralogy and Petrology, **27**, pp. 1-10.

Prinzhofer, A. and Allègre, C. J., 1985. Residual peridotites and the mechanisms of partial melting. Earth and Planetary Science Letters, **74**, pp. 251-265.

Roden, M.F. and Murthy, V.R., 1985. Mantle metasomatism. Annual Review of Earth and Planetary Sciences, **13**, pp. 269-296.

Roeder P.L. and Emslie, R.F., 1970. Olivine-liquid equilibrium. Contributions to Mineralogy and Petrology **29**, pp. 275-289.

Rogers, J., 1989. Comment on "Mesozoic overthrust tectonics in South China". Geology, **17**, pp. 671-672.

Sack, R.O., Walker D. and Carmichael I.S.E., 1987. Experimental petrology of alkaline lavas: constraints on cotectics of multisaturation in natural basic liquids. Contributions to Mineralogy and Petrology, **96**, pp. 1-23.

Schneider, M. E. and Eggler, D.N., 1984. Compositions of fluids in equilibrium with peridotite: implications for alkaline magmatism - metasomatism. In Kimberlites I: kimberlites and related rocks. edited by J. Kornprobst, pp. 383-394. Elsevier Amsterdam.

Shen, Y. and Pan, Z., 1951. The Tertiary basalts from the Black Hill of Jurongse, Jiangshu Province. Comments on Geology, vol.6, No.2, pp. 94-99. (in Chinese).

Smith, B.H., Danchin, R.V., Harris J.W. and Stracke, K.J., 1984. Kimberlites near Orroroo, South Australia. In Kimberlites I: Kimberlites and Related Rocks, edited by J. Kornprobst, pp. 121-142. Elsevier New York.

Stanley, C. R. and Russell, J. K., 1989. Petrologic hypothesis testing with Pearce element ratio diagrams: derivation of diagram axes. Contributions to Mineralogy and Petrology, **103**, pp. 78-89.

Streckeisen, A.L., 1967. Classification and nomenclature of igneous rocks. Neues. Jahrb. Min. Abh., **107**, pp. 144-240.

—— , A.L.,1979. Classification and nomenclature of volcanic rocks, lamprophyres, carbonatites, and melilitic rocks: Recommendations and suggestions of the IUGS subcommission of the systematics of Igneous rocks, Geology, **7**, pp. 331-335.

Sun, S.-S.,1984. Some geochemical constraints on mantle evolution models. Proceedings of the 27th International Geological Conference. Vol.1, pp. 475-508.

Sun, W. and Lai, Zh., 1980. Discussions on the relations of petrochemical characteristics of the Cenozoic volcanic rocks from Fujian Province with tectonic environments. Geochemistry, **2**, pp. 134-147. (in Chinese).

Takahashi, E. and Kushiro, I., 1983. Melting of a dry peridotite at high pressures and basalt magma genesis. American Mineralogist, **68**, pp. 859-879.

Taylor, H.P. and Cundari, A., 1984. $^{18}O/^{16}O$ and the chemical relationships in K-rich volcanic rocks from Australia, East Africa, Antarctica and San Venanzo, Cupaello, Italy. Earth and Planetary Science Letters, **69**, pp. 263-276.

—— , and Turi, B., 1976. High ^{18}O igneous rocks from the Tuscan Magmatic Province, Italy. Contributions to Mineralogy and Petrology, **55**, pp. 34-54.

Turner, J. S. and Campbell, I.H., 1986. Convection and mixing in magma chambers. Earth Science Review, **23**, pp. 255-352.

Velde, D., 1975. Armalcolite-Ti-phlogopite-diopsdie-analcite-bearing lamproites from Smoky Butte, Garfield County, Montana. American Mineralogist, **66**, 566-573.

Wedepohl, K. H., 1985. Origin of the Tertiary basaltic volcanism in the northern Hessian depression. Contributions to Mineralogy and Petrology, **89**, pp. 122-143.

Wendlant, R.F. and Eggler, D.H., 1980. The origin of potassic magmas: I. melting relations in the system $KAlSiO_4$-Mg_2SiO_4-SiO_2 and $KAlSiO_4$-MgO-SiO_2-CO_2 to 30 kb. American Journal of Sciences, **280**, pp. 385-420.

Wetzel, K.,Remer,M. and Hirsh, K., 1989. Minor element effects of combined fractional partial melting and crystallization. Earth and Planetary Science Letters, **93**, pp. 142-150.

Wilson, M., 1989. Igneous Petrogenesis: A Global Tectonic Approach, UNWIN HYMAN, London.

Woodhead, J. D., Harmon, R. S. and Fraser, D. G., 1987. O, S, Sr and Pb isotopic variations in volcanic rocks from the Northern Mariana Islands: implications for crustal recycling in intra-oceanic areas. Earth and Planetary Science Letters, **83**, pp. 39-52.

Yoder, H.S. and Tilley, C.E., 1962. Origin of basalt magmas: an experimental study of natural and synthetic rock systems. Journal of Petrology, **3**, pp. 342-532.

Zhang, R. and Cong, B., 1983. Petrogenesis and implication for tectonics of basanites and their peridotite xenoliths from the Nu Hill, Anhui Province. Petrological Studies, No.3, pp. 111-127. Geology Press, Beijing. (in Chinese).

—— and Cong, B., 1984. Mineralogical studies of the peridotite xenoliths, xenocrysts and phenocrysts in basalts from Xilong, Fujian Province. Geosciences, **1**, pp. 58-72. (in Chinese).

—— and Cong, B., 1987. Cenozoic volcanic rock series and their ultramafic xenoliths in South China. In Cenozoic basalts and Xenoliths from Depth in the East China, edited by M. É and D. Zhao, pp. 349-475. Science Press, Beijing. (in Chinese).

Zhang, W., 1986. A Geotectonic Map of Continental and Oceanic areas of China and its Neighborhood. Science Press, Beijing, 400pp. (in Chinese)

Zhao, Z., 1956. Chemical petrology studies of the Cenozoic basaltic rocks of eastern China. Chinese Bulletin of Geology, **36**, pp. 315-367. (in Chinese).

Zheng, X., Cong, B., Zhang, W. and Yan, Z., 1978. Discussions of chemical petrology of the Cenozoic basalts from eastern China. Geosciences, **3**, pp. 254-264. (in Chinese).

Zhou, X. and Chen, T., 1981. Compositions and their evolution trend of the Cenozoic basalts from the eastern coast of China. Bull. Gael., **55**, pp. 29–39. (in Chinese).

Zhou, X. and Armstrong, R.L., 1982. Cenozoic volcanic rocks of eastern China -- secular and geographic trends in chemistry and strontium isotopic composition. Earth and Planetary Science Letters, **58**, pp. 301-329.

Zindler,A. and Hart, S., 1986. Chemical geodynamics. Ann. Rev. Earth Planet Sci., **14**, pp. 493-571.